

**Development of Magnesium Aluminate
and Gallate Chemistry Incentivised by
Potential in Rechargeable Battery
Technology**

by

Etienne Volcan Brouillet

A thesis submitted to the Department of Pure and Applied Chemistry, University of Strathclyde, in part fulfilment of the regulation for the degree of Doctor of Philosophy.

April 2018

This thesis is the result of the author's original research. It has been composed by the author and has not been previously submitted for examination which has led to the award of a degree.

The copyright of this thesis belongs to the author under the terms of the United Kingdom Copyright Acts as qualified by University of Strathclyde Regulation 3.50. Due acknowledgement must always be made of the use of any material contained in, or derived from, this thesis.

Etienne Volcan Brouillet

April 2018

My first and most sincere thanks are going to my supervisor and friend Dr Stuart Robertson who gave me the privilege of being the first PhD journey student of his academic career. I thoroughly appreciated his support along my PhD but especially the trust he put in me and the freedom he gave me in developing my project. In times outside from the lab I also enjoyed his friendship, which for me truly started during our trip to Germany. During this project I had the opportunity to collaborate with three other research groups, who integrated me very easily in their teams. For this I would like to express my gratitude to Prof. Duncan Graham, from the University of Strathclyde for the Raman spectroscopy experiments, to Prof. Konrad Koszinowski from Georg-August Universität, who accepted me within his group and personally introduced me to ESI-MS and Dr Serena Corr from the University of Glasgow who gave me access to the world of battery testing, the application of my research.

Apart from Stuart, two people had a huge impact on my work, ex-“team handsome” member Dr Ross McLellan for his training in crystallography and many bright ideas, and Marco Amores for introducing me to the basic principles of rechargeable battery research but also for his genuine interest in my project and help in the lab.

I must also express a special thank you to Prof. Robert Mulvey for sharing his huge expertise during the Mulvey-Robertson’s mini group meetings. And also Dr Alan Kennedy for refining and finalising the crystallographic data of my compounds.

My PhD would not have been the same without the presence of Prof. Robert Mulvey, Prof. Eva Hevia and Dr Charlie O’Hara’s groups members with whom I shared the lab and office space. For the good times I would like to recognize Ross again, Laia, Andy, Sam, Marina, Lewis, Marco, Alberto, Anto, Anna, Maria, Michael, Vicky, Richard, Leonie, Stephen, Callum, Pasquale, Sonia and Janie-Anne. Whether we are in the lab, in the pub, or bruising each other at paintball I had a great time with all of you.

Out of the lab I need to express very special thanks to Alex Girard! For being my partner in crime during the Six Nations games, or any time we spend in the pub really. And Lyndsay for the time we spent together, never talking about chemistry.

Je voudrais aussi remercier mes parents, Dominique et Jean-Paul et mon frère Numa, pour leur soutien, pour me rappeler que je suis bien français en m’envoyant des boîtes pleines de bonnes choses de la maison.

The cationic magnesium moiety of charged-separated magnesium organohaloaluminate complexes, relevant to rechargeable Mg battery electrolytes, typically takes the thermodynamically favourable dinuclear $[\text{Mg}_2\text{Cl}_3]^+$ form in the solid-state. This thesis reports that judicious choice of Lewis donor allows the deliberate synthesis and isolation of the previously putative mononuclear $[\text{MgCl}]^+$ and trinuclear $[\text{Mg}_3\text{Cl}_5]^+$ modifications, hitherto only postulated as existing within electrolytic solutions, forming a comparable series with a common aluminate anion $[(\text{Dipp})(\text{Me}_3\text{Si})\text{NAlCl}_3]^-$.

Battery prototypes using these magnesium aluminates possessing different cationic aggregation as electrolytes were built in order to study the effect of the aggregation state on their performances. Despite early decomposition hindrance of some of the studied electrolytes, surprising behaviour was observed with the stability of the mononuclear species, which is highly enhanced compared to the higher aggregates. Rationally, this increased stability was attributed to the presence of the tetradentate Lewis donor, Me_6TREN , used to control the aggregation of the mononuclear complex.

Rechargeable batteries using magnesium organohaloaluminate electrolytes suffer from unwanted corrosion of the components of the battery cell (e.g., stainless steel parts), which is attributed to the presence of chloride ions. We devised a procedure to prepare sought-after magnesium compounds possessing the “naked magnesium” dication $[\text{Mg}\cdot 6\text{THF}]^{2+}$, by simply transmetallating the organic moieties from a magnesium reagent MgR_2 to an aluminium reagent AlR_3 ($\text{R} = \text{Ph}$ or pyrrolyl). Irrespective of how successful the method is, these types of compound were revealed to be insoluble in ethereal solvents, presumably due to the strong opposite charge attraction emanating for the dication. By using a β -diketiminato ligand, the magnesium cation $[(^{\text{Dipp}}\text{Nacnac})\text{Mg}\cdot 2\text{THF}]^+$ was created, reducing the opposite charge attraction to give a soluble complex. These synthetic advances, alongside preliminary battery tests, give an insight into where the problems lie in the applicability of chloro-free compounds as electrolytes.

Finally, as a potential alternative to aluminate complexes reported in the literature, the synthesis and characterization of analogous group 13 gallate complexes was successfully carried out.

Publication in a Peer Reviewed Journal

Exposing elusive cationic magnesium–chloro aggregates in aluminate complexes through donor control, E. V. Brouillet, A. R. Kennedy, K. Koszinowski, R. McLellan, R. E. Mulvey and S. D. Robertson, *Dalton Trans.*, **2016**, 45, 5590-5597.

Conference Presentations (Oral)

Donor Controlled Cation Aggregation in Magnesium Aluminates for Rechargeable Battery Electrolytes, Dalton 2016, 29th-31st March 2016, University of Warwick, Coventry.

Donor Controlled Cation Aggregation in Magnesium Aluminates for Rechargeable Battery Electrolytes, Universities of Scotland Inorganic Chemistry Conference, 11th-12th August 2016, University of Strathclyde, Glasgow.

Conference Presentation (Poster)

Donor Controlled Cation Aggregation in Magnesium Aluminates for Rechargeable Battery Electrolytes, Royal Society of Chemistry Energy Symposium 2016, 16th February 2016, Burlington House, London.

Donor Controlled Cation Aggregation in Magnesium Aluminates for Rechargeable Battery Electrolytes, Electrochemical Society Student Chapter, 2nd March 2016, University of St Andrews.

Organometallic Magnesium Aluminate Electrolytes for Mg-Ion Rechargeable Batteries: from Design to Performance, 4th EuCheMS Inorganic Chemistry Conference, 2nd-5th July 2017, University of Copenhagen.

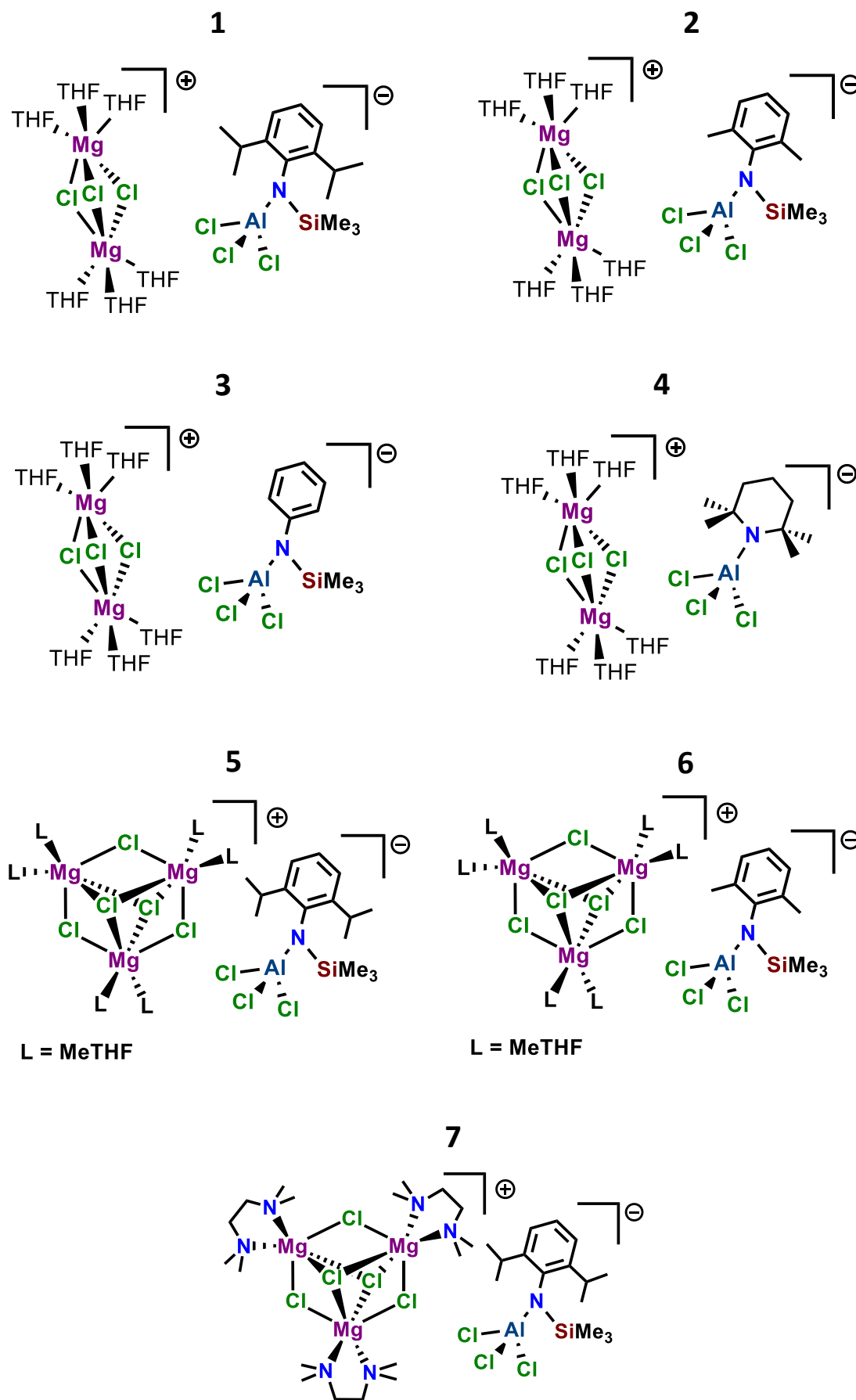
Organometallic Magnesium Aluminate Electrolytes for Mg-Ion Rechargeable Batteries: from Design to Performance, Universities of Scotland Inorganic Chemistry Conference, 29th-30th August 2017, University of St Andrews.

°	Degree
Δ	Heat
ΔE	HOMO-LUMO energy gap
μ	mu (denoting a bridging atom)
π	Pi (denoting a pi bond)
σ	Sigma (denoting a sigma bond)
Å	Ångstroms
An	Anion
APC	All-phenyl-complex ([AlPh ₄] ⁻ [Mg ₂ Cl ₃] ⁺)
aq.	Aqueous
Ar	Aromatic group
BArF	tetrakis(3,5-bis(trifluoromethyl)-phenyl)borate)
BEC	Butylethyl complex
Bn	Benzyl
C ₆ D ₆	Deuterated benzene
CCDB	Cambridge Crystallographic Database
Cp	Cyclopentadienyl
CV	Cyclic voltammogram
CSI-MS	Coldspray Ionisation Mass-Spectrometry
D ₆ -DMSO	Deuterated dimethylsulfoxide
d ₈ -THF	Deuterated THF
DFT	Density Functional Theory
Dipp	2,6-diisopropylphenyl
Dipp-BIAN	1,2-bis[(2,6-diisopropylphenyl)imino]acenaphthene
DME	1,2-dimethoxyethane
Dmp	2,6-dimethylphenyl
DMSO	Dimethylsulfoxide
DPS	Dipropylsulfone
DTBP	2,6-di- <i>tert</i> -butylphenolate
EMIM-TFSI	1-Ethyl-3-methylimidazolium bis(trifluoromethylsulfonyl)imide
ESI-MS	Electrospray Ionisation Mass-Spectrometry
Et	Ethyl

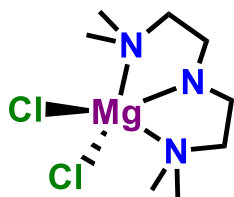
<i>fac</i> -	Facial isomer
hfip	Tetrakis(hexafluoroisopropoxy)
HMDS	1,1,1,3,3,3-hexamethyldisilazide
HMPA	hexamethylphosphoramide
HOMO	Highest occupied molecular orbital
ⁱ Bu	<i>iso</i> -butyl
IL	Ionic liquid
ⁱ Pr	<i>iso</i> -propyl
IR	Infra Red
K	Kelvin
LIB	Lithium-ion battery
Li/S	Lithium-sulphur batteries
LUMO	Lowest unoccupied molecular orbital
MACC	Magnesium aluminium chloride complex
Me	Methyl
Me ₆ TREN	tris[2-(dimethylamino)ethyl]amine
Mes	Mesityl, 1,3,5-trimethylphenyl
MeTHF	2-methyltetrahydrofuran
MIB	Magnesium-ion battery
^{Dipp} NacnacH	β -diketimine
ⁿ Bu	<i>n</i> -butyl
NMR	Nuclear Magnetic Resonance
Ph	Phenyl
PhD	Doctor of Philosophy
ppm	Parts per millions
PMDETA	<i>N,N,N',N'',N''</i> -pentamethyldiethylenetriamine
PYR14-TFSI	1-Butyl-1-methylpyrrolidinium bis(trifluoromethane-sulfonyl)imide
R	Generic alkyl group
RMgX	Generic Grignard reagent
R ₂ NMgX	Generic Hauser base
(R ₂ N) ₂ Mg	Magnesium bisamide
rt	Room temperature
SCXRD	Single Crystal X-Ray Diffraction

TBACl	Tetrabutylammonium chloride
^t Bu	<i>tert</i> -butyl
term	Terminal bond
TFSI	bis(trifluoromethane)sulfonimide
THF	Tetrahydrofuran
TMEA	tris[2-(2-methoxyethoxy)ethyl]amine
TMEDA	<i>N,N,N',N'</i> -tetramethylethylenediamine
TMS	Trimethylsilyl
TMP	2,2,6,6-tetramethylpiperidide
V _{exc}	Excitation voltage
viph	<i>o</i> -vinylphenyl
X	Halogen

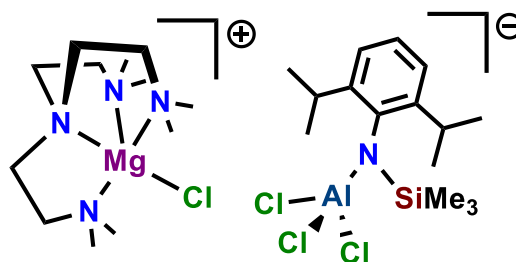
- 1:** [(Dipp)(SiMe₃)NAlCl₃]⁻ [Mg₂Cl₃·6THF]⁺
- 2:** [(Dmp)(SiMe₃)NAlCl₃]⁻ [Mg₂Cl₃·6THF]⁺
- 3:** [(Ph)(SiMe₃)NAlCl₃]⁻ [Mg₂Cl₃·6THF]⁺
- 4:** [(TMP)AlCl₃]⁻ [Mg₂Cl₃·6THF]⁺
- 5:** [(Dipp)(SiMe₃)NAlCl₃]⁻ [Mg₃Cl₅·6MeTHF]⁺
- 6:** [(Dmp)(SiMe₃)NAlCl₃]⁻ [Mg₃Cl₅·6MeTHF]⁺
- 7:** [(Dipp)(SiMe₃)NAlCl₃]⁻ [Mg₃Cl₅·3TMEDA]⁺
- 8:** [MgCl₂·PMDETA]
- 9:** [(Dipp)(SiMe₃)NAlCl₃]⁻ [MgCl·Me₆TREN]⁺
- 10:** [(Dmp)(SiMe₃)NAlCl₃]⁻ [MgCl·Me₆TREN]⁺
- 11:** [(Ph)(SiMe₃)NAlCl₃]⁻ [MgCl·Me₆TREN]⁺
- 12:** [(HMDS)AlCl₃]⁻ [MgCl·Me₆TREN]⁺
- 13:** [(Dipp)(SiMe₃)NAlCl₃]⁻ [Mg₃Cl₄(OⁿBu)·6MeTHF]⁺
- 14:** [(Dipp)(SiMe₃)NAlCl₃]⁻ [Li·4THF]⁺.
- 15:** [(Dipp)(SiMe₃)NAlCl₃]⁻ [Li·3DME]⁺
- 16:** [Al(pyrrolyl)₄]⁻ [Li·4THF]⁺
- 17:** Al(pyrrolyl)₃·OEt₂
- 18:** Mg(pyrrolyl)₂·4THF
- 19:** 2[Al(pyrrolyl)₄]⁻ [Mg·6THF]²⁺
- 20:** 2[Al(pyrrolyl)₄]⁻ [Mg·TMEA]²⁺
- 21:** 2[Al(Ph)₄]⁻ [Mg·6THF]²⁺
- 22:** Al(C₅H₁₀N)₃
- 23:** GaPh₃·OEt₂
- 24:** 2[Ga(Ph)₄]⁻ [Mg·6THF]²⁺
- 25:** [^{Dipp}Nacnac]Mg(pyrrolyl)·THF
- 26:** [Al(pyrrolyl)₄]⁻ [[^{Dipp}Nacnac]Mg·2THF]⁺
- 27:** [^{Dipp}Nacnac]Mg(Ph)·THF
- 28:** [(Al(pyrrolyl)₃)₂O]²⁻ [Mg·6DMSO]²⁺
- 29:** Mg(TFSI)₂·4THF
- 30:** [GaCl₄]⁻ [MgCl·5THF]⁺
- 31:** [GaPh₄]⁻ [Mg₂Cl₃·6THF]⁺



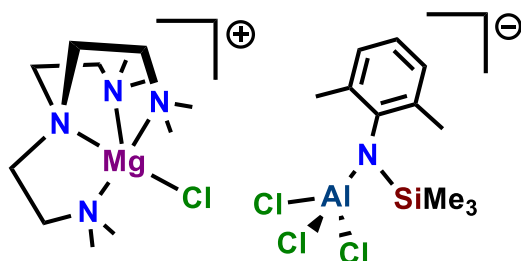
8



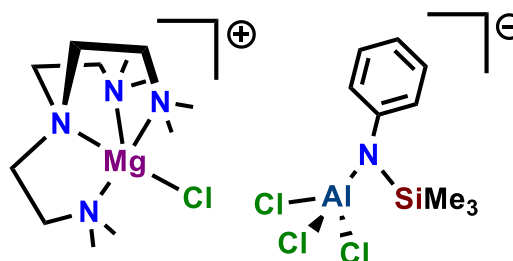
9



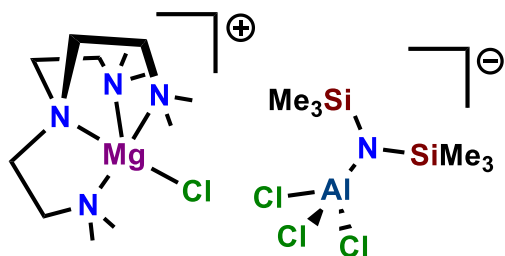
10



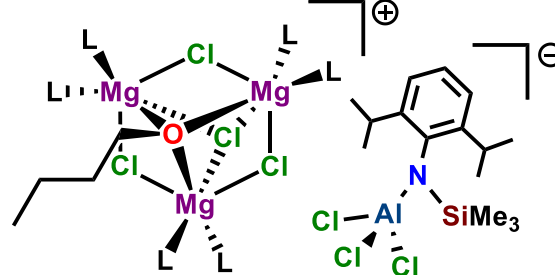
11



12

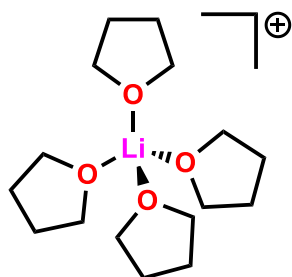


13

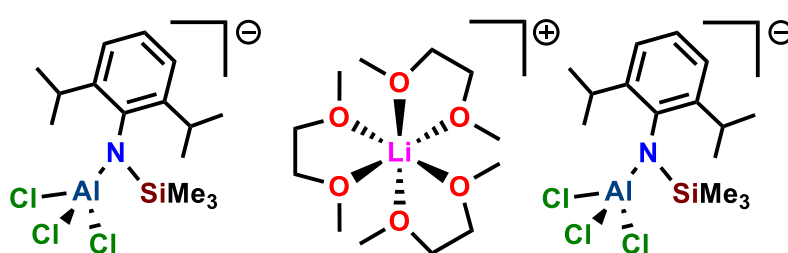


L = MeTHF

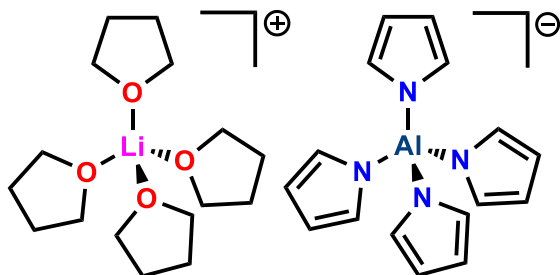
14



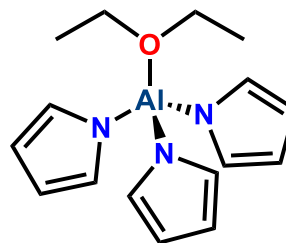
15



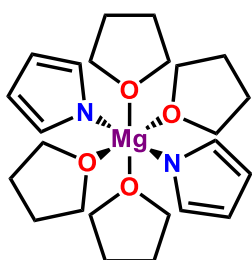
16



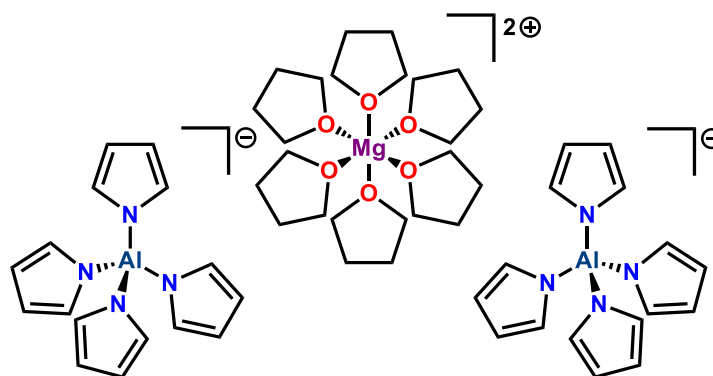
17



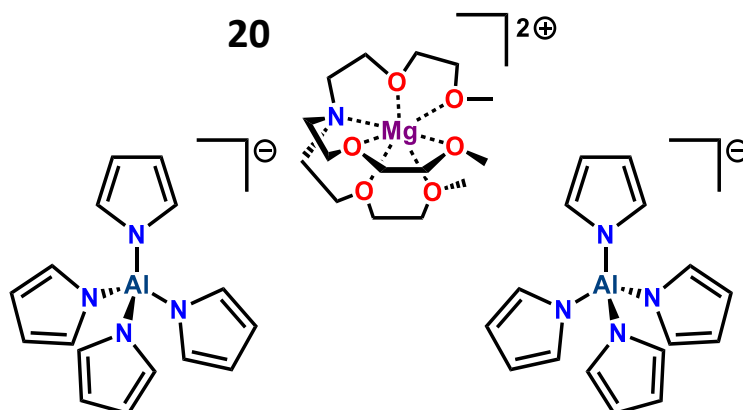
18



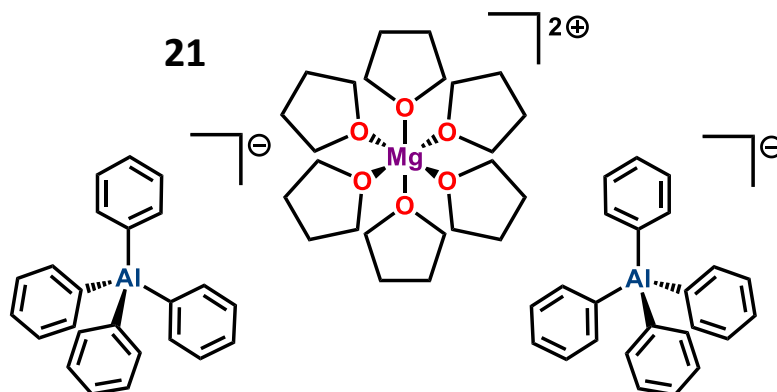
19

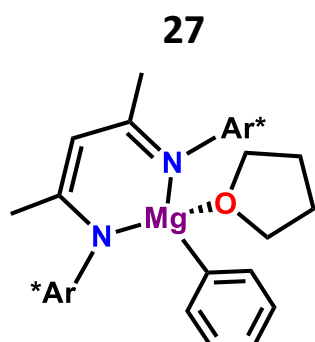
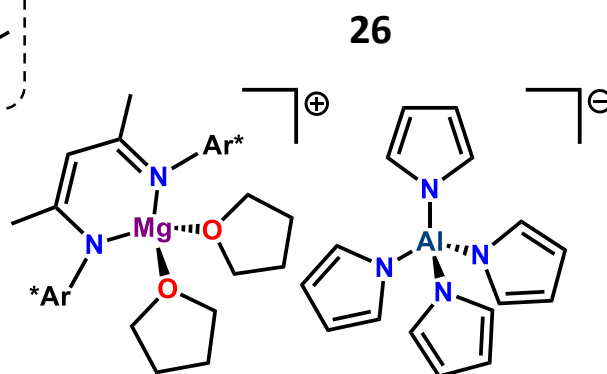
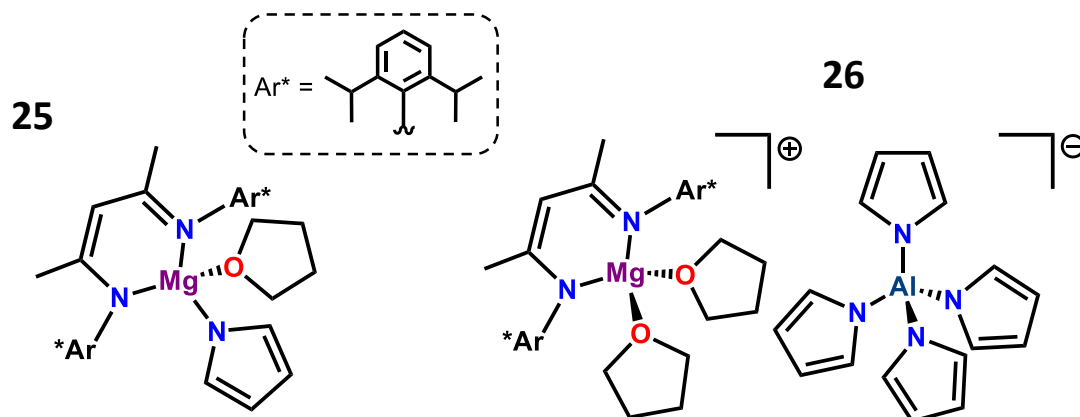
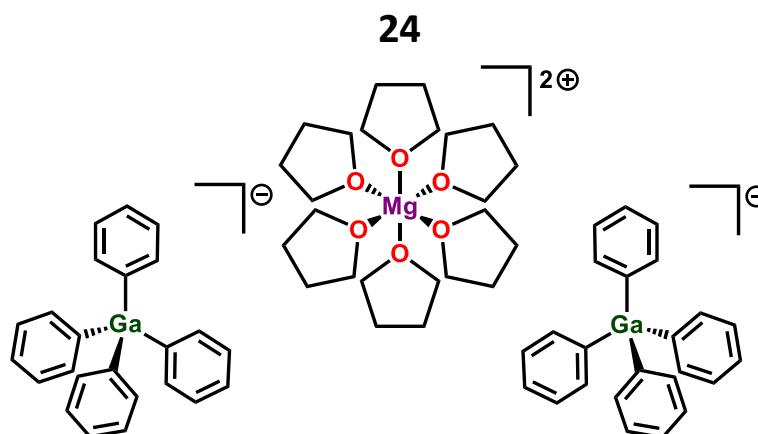
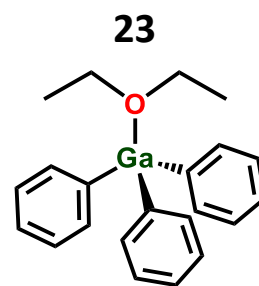
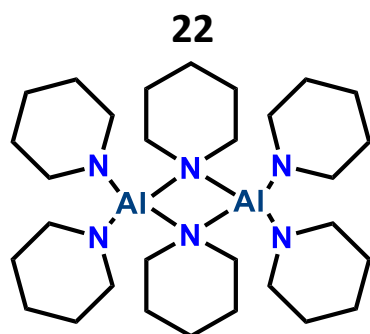


20

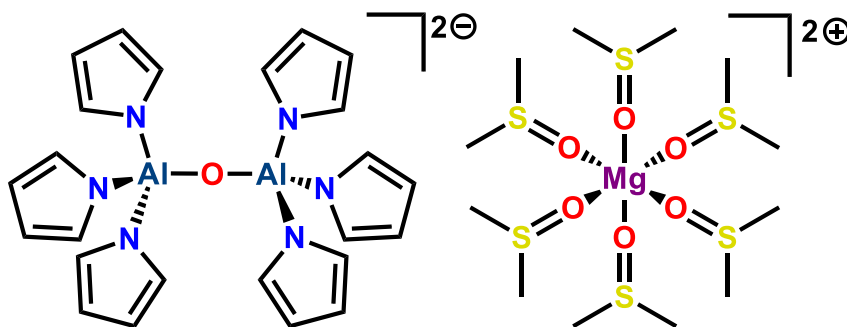


21

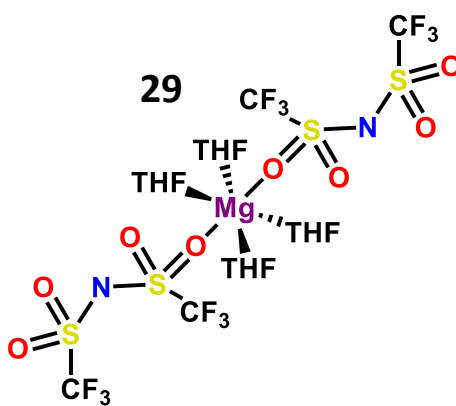




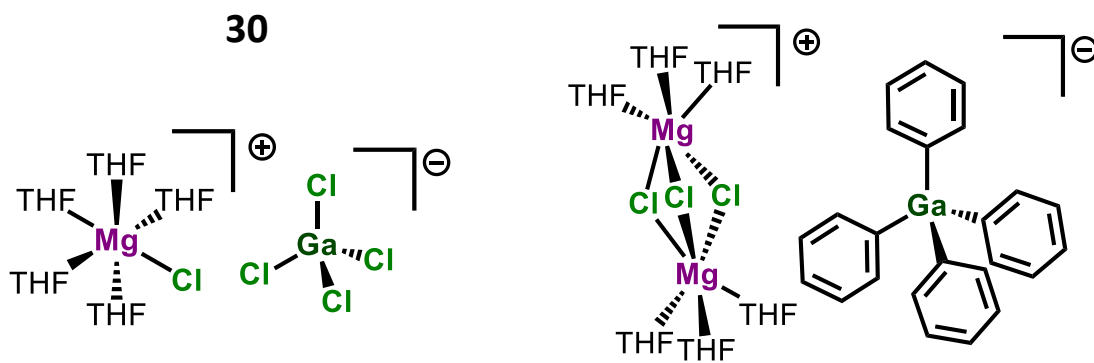
28



29



31



Acknowledgements	i
Abstract	ii
Publication and Conference Presentations	iii
Abbreviations	iv
List of Numbered Compounds	vii
Table of Contents	xiii
<u>Chapter 1: Introduction</u>	1
1.1. Metals of interest	1
1.1.1. Magnesium	2
1.1.1.1. Preparation of magnesium reagents	3
1.1.1.2. Structures of Grignard reagents and magnesium salts	4
1.1.2. Aluminium	9
1.1.2.1. Uses of aluminium reagents in chemistry	10
1.1.2.2. Weakly coordinating anions	12
1.1.2.3. Aluminium containing heterobimetallic reagents	14
1.2. Advances in magnesium batteries	15
1.2.1. Basic principles of a rechargeable battery	16
1.2.2. Simple rechargeable battery scheme	19
1.2.3. Arguments for magnesium batteries	20
1.2.4. Early studies and first issues	21
1.2.5. Magnesium aluminates as battery electrolytes	21
1.2.5.1. Multinuclear NMR spectroscopy studies of magnesium aluminate solutions	22

1.2.5.2. Raman Spectroscopy studies of magnesium aluminate electrolytes	24
1.2.5.3. Crystallographic studies of magnesium battery electrolytes	27
1.2.5.4. Electrochemistry of magnesium aluminate electrolytes	29
1.2.5.5. Investigating the operating mechanism of chlorinated magnesium battery electrolytes	32
1.2.6. Non-corrosive, non-chlorinated magnesium electrolytes	33

Chapter 2: Synthesis, Structure and Solution Characterisation of Different Magnesium Cation Aggregates **43**

2.1. Introduction	43
2.2. A note to the reader	45
2.3. Synthesis of new magnesium amidohaloaluminates	45
2.3.1. Synthesis of magnesium aluminate compounds possessing a dinuclear cation	47
2.3.2. Synthesis of magnesium aluminate compounds in MeTHF: Formation of a trinuclear cation	53
2.3.3. Use of multidentate Lewis donor ligands	56
2.3.4. Use of TMEDA: Formation of a trinuclear cation	57
2.3.5. Use of PMDETA	59
2.3.6. Use of Me ₆ TREN: Formation of a mononuclear cation	61
2.4. X-Ray crystallographic comparison of magnesium aluminate complexes	64
2.4.1. Crystallographic study of the aluminium anion	64
2.4.1.1. Effect of the magnesium cation on the aluminium anion	65
2.4.1.2. Effect of the amide on the aluminium anion	66

2.4.2. Crystallographic study of the magnesium chloride cation	68
2.4.3. Further crystallographic studies	71
2.5. Introduction: Characterisation techniques for the solution study of magnesium aluminates	73
2.5.1. Raman spectroscopy	73
2.5.2. Electrospray ionisation mass spectrometry	75
2.6. Raman spectroscopy results	76
2.6.1. Raman spectroscopy studies in solid state	76
2.6.2. Raman spectroscopy studies in solution	77
2.6.3. Raman spectroscopy summary	79
2.7. Electrospray ionisation mass spectrometry studies	80
2.7.1. ESI-MS of the aluminium anions	80
2.7.2. ESI-MS of the different magnesium cations	82
2.7.3. ESI-MS study of structurally uncharacterised crystals of a magnesium aluminate compound in MeTHF	88
2.8. NMR studies	90
2.9. Conclusions of the solution-state characterisation	93
2.10. Conclusions of the solid-state characterisation	93

Chapter 3: The Influence of Cation Aggregation State on Battery Performance on Magnesium Amidohaloaluminate Electrolytes **100**

3.1. Introduction	100
3.2. Experimental results	103

3.2.1. Battery test: [(HMDS)AlCl ₃] ⁻ [Mg ₂ Cl ₃ ·6THF] ⁺ electrolyte	104
3.2.2. Battery test: [(Dipp)(SiMe ₃)NAlCl ₃] ⁻ electrolyte series	106
3.2.3. Investigating the low oxidative stability of the [(Dipp)(SiMe ₃)NAlCl ₃] ⁻ series	110
3.2.4. Battery test: [(Dmp)(SiMe ₃)NAlCl ₃] ⁻ electrolyte series	114
3.2.5. Battery test: [(Ph)(SiMe ₃)NAlCl ₃] ⁻ electrolyte series	117
3.2.6. Battery test: [(TMP)AlCl ₃] ⁻ [Mg ₂ Cl ₃ ·6THF] ⁺ electrolyte	120
3.3. Discussion	121
3.4. Conclusions and future work	126
<u>CHAPTER 4: Synthetic Design of Novel Chloro-Free Electrolytes</u>	132
4.1. Introduction	132
4.2. Synthesis of novel chloro-free magnesium aluminates	133
4.2.1. Attempted preparation of chloro-free magnesium aluminates using aluminium hydride starting materials	136
4.2.2. Synthesis and characterisation of 2[Al(pyrrolyl) ₄] ⁻ [Mg·6THF] ²⁺ by transmetallation reaction	139
4.2.3. Changing the solvation shell of the Mg ²⁺ dication in 2[Al(pyrrolyl) ₄] ⁻ [Mg·6THF] ²⁺	144
4.2.4. Changing the organic group around the Al anion in 2[AlR ₄] ⁻ [Mg] ²⁺ compounds	146
4.2.5. Changing the metal of the anionic group	150
4.2.6. Synthesis of 1+:1- separated ion pair chloro-free magnesium aluminates	154
4.3. Electrochemistry of chloro-free magnesium aluminates	158

4.3.1. Battery behaviour using “naked magnesium” aluminate compounds in DMSO as electrolyte	159
4.3.2. Battery behaviour of “naked magnesium” aluminate compounds in Ionic liquids/THF	163
4.3.3. $[\text{Al}(\text{pyrrolyl})_4]^- [[^{\text{Dipp}}\text{Nacnac}]\text{Mg}\cdot 2\text{THF}]^+$ as a rechargeable magnesium battery electrolyte	165
4.4. Conclusions and future work	166
<u>CHAPTER 5: Conclusions and Future Work</u>	172
5.1. Conclusions	172
5.2. Future work	174
<u>CHAPTER 6: Experimental Section</u>	179
6.1. General Techniques	179
6.1.1. Schlenk techniques	179
6.1.2. Use of a glove box	180
6.1.3. Solvent purification	181
6.2. Synthetic Protocols	181
6.2.1. General experimental	181
6.2.2. Preparation of starting materials	182
6.2.2.1. Synthesis of DippNHSiMe_3 , DmpNHSiMe_3 and PhNHSiMe_3	182
6.2.2.2. Synthesis of Me_6TREN	183
6.2.3. Preparation of products	183

6.2.3.1. Synthesis of 1 : [(Dipp)(SiMe ₃)NAlCl ₃] ⁻ [Mg ₂ Cl ₃ ·6THF] ⁺ ; 2 : [(Dmp)(SiMe ₃)NAlCl ₃] ⁻ [Mg ₂ Cl ₃ ·6THF] ⁺ ; 3 : [(Ph)(SiMe ₃)NAlCl ₃] ⁻ [Mg ₂ Cl ₃ ·6THF] ⁺ and 4 : [(TMP)AlCl ₃] ⁻ [Mg ₂ Cl ₃ ·6THF] ⁺	183
6.2.3.2. Synthesis of 5 : [(Dipp)(SiMe ₃)NAlCl ₃] ⁻ [Mg ₃ Cl ₅ ·6MeTHF] ⁺ ; 6 : [(Dmp)(SiMe ₃)NAlCl ₃] ⁻ [Mg ₃ Cl ₅ ·6MeTHF] ⁺	185
6.2.3.3. Synthesis of 7 : [(Dipp)(SiMe ₃)NAlCl ₃] ⁻ [Mg ₃ Cl ₅ ·3TMEDA] ⁺	186
6.2.3.4. Synthesis of 8 : MgCl ₂ ·PMDETA	186
6.2.3.5. Synthesis of 9 : [(Dipp)(SiMe ₃)NAlCl ₃] ⁻ [MgCl·Me ₆ TREN] ⁺ and 10 : [(Dmp)(SiMe ₃)NAlCl ₃] ⁻ [MgCl·Me ₆ TREN] ⁺ , 11 : [(Ph)(SiMe ₃)NAlCl ₃] ⁻ [MgCl·Me ₆ TREN] ⁺ and 12 : [(HMDS)AlCl ₃] ⁻ [MgCl·Me ₆ TREN] ⁺	187
6.2.3.6. Synthesis of 14 : [(Dipp)(SiMe ₃)NAlCl ₃] ⁻ [Li·4THF] ⁺	188
6.2.3.7. Synthesis of 15 : [(Dipp)(SiMe ₃)NAlCl ₃] ⁻ [Li·3DME] ⁺	188
6.2.3.8. Synthesis of 16 : [Li·4THF] ⁺ [Al(pyrrolyl) ₄] ⁻	189
6.2.3.9. Synthesis of 17 : Al(pyrrolyl) ₃ ·OEt ₂	189
6.2.3.10. Synthesis of 18 : Mg(pyrrolyl) ₂ ·4THF	190
6.2.3.11. Synthesis of 19 : 2[Al(pyrrolyl) ₄] ⁻ [Mg·6THF] ²⁺	190
6.2.3.12. Synthesis of 20 : 2[Al(pyrrolyl) ₄] ⁻ [Mg·TMEA] ²⁺	191
6.2.3.13. Synthesis of 21 : 2[Al(Ph) ₄] ⁻ [Mg·6THF] ²⁺	191
6.2.3.14. Synthesis of 23 : GaPh ₃ ·OEt ₂	191
6.2.3.15. Synthesis of 24 : 2[Ga(Ph) ₄] ⁻ [Mg·6THF] ²⁺	192
6.2.3.16. Synthesis of 25 : [^{Dipp} Nacnac]Mg(pyrrolyl)·THF	192
6.2.3.17. Synthesis of 26 : [Al(pyrrolyl) ₄] ⁻ [^{Dipp} Nacnac]Mg·2THF] ⁺	193
6.2.3.18. Synthesis of 27 : [^{Dipp} Nacnac]Mg(Ph)·THF	193
6.2.4. Raman spectroscopy	194

6.2.5. Electrospray ionisation mass-spectroscopy	194
6.2.6. Electrochemistry	195
6.2.6.1. Battery cell	195
6.2.6.2. Electrochemical measurements	196
6.2.7. X-ray crystallography	196
6.2.7.1. Selected crystallographic and refinement parameters	197
6.2.8. Appendix	204

Chapter 1: Introduction

This chapter is an introduction covering the most useful aspects of organometallic chemistry required to have a basic understanding in the synthesis of complexes which can potentially be used as rechargeable magnesium batteries electrolytes. It will start with a general view of the two major metals involved in this study, namely magnesium and aluminium. The introduction will then continue with chemistry more related to the battery area, which is extremely wide and requires a broad knowledge in a variety of chemistry's numerous fields. This chapter will hence mostly approach the essential basics in electrochemistry and material chemistry to give an overview of the full process, but it will cover more in-depth the advances in the hunt for the perfect electrolyte featuring, the fundamental and current issues encountered, the evolutions leading to the first prototype and the novelties that led to the results presented in this thesis.

1.1. Metals of interest

Throughout this PhD projects thesis a few metals were continuously used in the laboratory under different forms and for different purposes. As introduced earlier the two metals of interest, magnesium and aluminium, will be presented first and so in a relevant fashion to frame the context of this thesis and make the reader familiar with the previous advances judged important. It is however worth mentioning that despite not being introduced, organolithium reagents were used to prepare a variety of starting materials in classical synthetic ways. For more information, a review by Rathman and Schwinderman provides useful accounts on the "Preparation, properties, and safe handling of commercial organolithiums: alkyllithiums, lithium sec-organoamides, and lithium alkoxides".¹

1.1.1. Magnesium



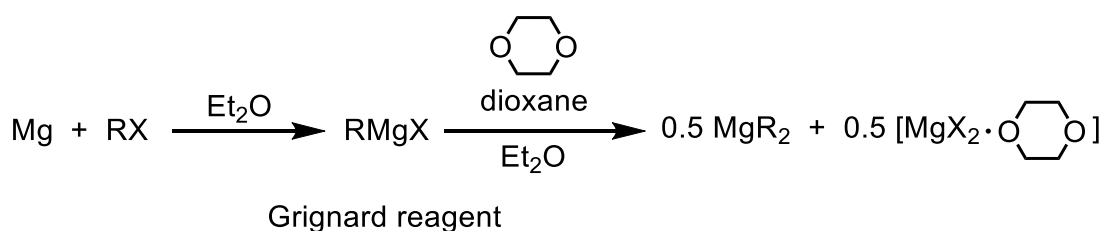
Group 2: Alkaline earth metal
Atomic mass: 24.305 g/mol
Density: 1.738 g/cm ³
Oxidation state: +2, +1, 0
Orbital: [Ne] 3s ²
Price: 1.41 GBP/kg
Production: 800 000 tonnes/year

Magnesium is the second lightest element of group 2 of the Periodic Table which are collectively known as alkaline earth metals. On Earth it is assumed to be the fourth most abundant metal (13.9% of earth's mass).^{2,3} It is a metal that was already used in ancient times under the form of talc and soap stones [Mg₃Si₄O₁₀(OH)₂] which were found in the Magnesian district of Thessaly situated in Greece.⁴ The discovery of elemental magnesium was however attributed to the Scottish scientist Joseph Black who studied the effect of magnesium carbonate for the treatment of kidney diseases back in 1755 at the University of Glasgow, but we had to wait some 50 years before observing magnesium in its pure form thanks to Sir Humphry Davy.

Since then, magnesium found its use in a variety of ways due to its promising properties; being one of the lightest metals it was a popular constituent for aircrafts during the Second World War, its ionic properties improves disease prevention and one's overall health and finally it became a very important element in chemistry with the example of the widely used organometallic Grignard reagents in synthetic chemistry (of empirical formula RMgX, R: alkyl, aryl, vinyl, X: Cl, Br, I).⁵⁻⁷ However its potential is not yet fully exploited and magnesium is already making its way to its next breakthrough in energy storage with the development of rechargeable magnesium batteries which in theory outclasses the recent powerful Li-ion batteries.^{8,9}

1.1.1.1. Preparation of magnesium reagents

In the world of chemistry, Grignard reagents have been one indispensable tool in the formation of numerous element-carbon bonds for more than 100 years. In comparison with its other commercially available organometallic competitors, such as organolithiums or organoaluminiums, organomagnesiums offer a few notable advantages. The solvent of choice both for preparation and utilisation of Grignard reagents has been diethyl ether (Et₂O) for many years before being gradually replaced by tetrahydrofuran (THF), in contrast, organolithiums are known to react at room temperature with ethers and therefore hydrocarbons are usually favoured. The relatively easy preparation of Grignard reagents and related compounds (Scheme 1.1) with elemental magnesium and organohalogen compounds generally offers a good flexibility for the choice of the R group, either for its nature (alkyl, amine) but also for its steric bulk (^tBu, CH₂SiMe₃).¹⁰



Scheme 1.1: Preparation of Grignard and other organomagnesium reagents.

A noticeable number of recent breakthroughs in organomagnesium chemistry originate from Knochel and co-workers since he first reported a route for the preparation of functionalised Grignard reagents via halogen-metal exchange reaction, this overcoming the synthesis of organomagnesium reagents using poorly activated functionalised groups.^{11,12} Other efficient preparation methods were later achieved by insertion of magnesium (this method was also extended to zinc chemistry) into C-Cl and C-Br bonds in the presence of LiCl.¹³⁻¹⁷ In 2004 Knochel developed the “turbo-Grignard reagent”, an enhanced Grignard obtained by the addition of one equivalent of LiCl to ⁱPrMgCl.¹⁸ This enhanced reactivity is obtained by the cooperation between both metals within the molecule to form an ‘ate’ complex leading to synergic metallation of aromatic compounds. Whereas Knochel pioneered the salt supported approach,¹⁹ Kondo,²⁰ Uchiyama,²¹ Mongin,^{22,23} Hevia^{24,25} and Mulvey²⁶⁻²⁸ focused

on the mixed organic anion approach, but also applied this new generation of organometallic reagents to other metals.²⁹ These bases are commonly made up of an alkali metal such as Li, Na or K and a secondary metal such as Mg¹⁹, Mn³⁰, Zn³¹, to form a contacted ion pair ‘ate’ complex (Figure 1.1).

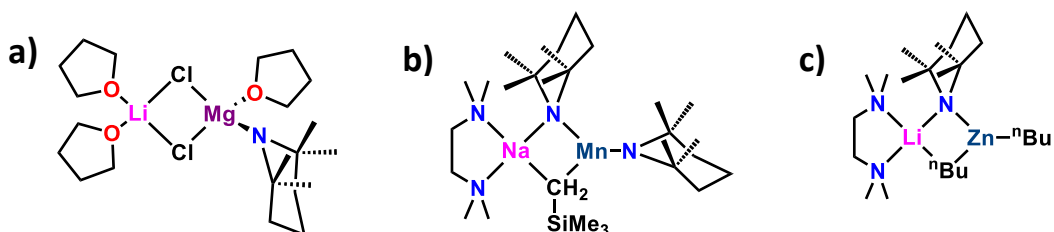


Figure 1.1: Representatives examples of bimetallic bases **a)** $(\text{THF})_2\text{Li}(\text{Cl})_2\text{Mg}(\text{THF})(\text{TMP})$, **b)** $(\text{TMEDA})\text{Na}(\text{TMP})(\text{CH}_2\text{SiMe}_3)\text{Mn}(\text{TMP})$, **c)** $(\text{TMEDA})\text{Li}(\text{TMP})\text{Zn}(\text{}^n\text{Bu})_2$.

1.1.1.2. Structures of Grignard reagents and magnesium salts

This thesis reports the constitutional behaviour of Grignard reagents and magnesium chloride in both the solid state and solution. In the literature a few studies showed that the investigation of these compounds in solution was very challenging and although the solid state can provide useful information, the solution state often involves complicated equilibria. Yamaguchi and Imamoto decided to use coldspray ionisation mass spectrometry (CSI-MS) and X-ray crystallography to study Grignard reagents in tetrahydrofuran (THF). Their solid-state studies on different recrystallised Grignard reagents (RMgCl , R: Bn, Ph, ^tBu, Me) in THF showed three dominant constitutions of MgCl_2 and RMgCl (Figure 1.2). The neutral dimer **A** which possesses two tetracoordinated magnesium atoms with the organic moiety, two chloride atoms and one THF and two hexacoordinated magnesium with four chloride atoms bridging the Mg atoms together. The molecules **B** and **C** are both magnesium magnesiate separated ion pairs which possess the same solvated dinuclear cation where three Cl atoms are bridging two Mg atoms ($[\text{Mg}_2\text{Cl}_3 \cdot 6\text{THF}]^+$). The anion of **B** is a solvated monomer $[\text{RMgCl}_2 \cdot \text{THF}]^-$ whereas **C** has a an unsolvated dianionic dimer $[\text{R}_4\text{Mg}_2\text{Cl}_2]^{2-}$.³²

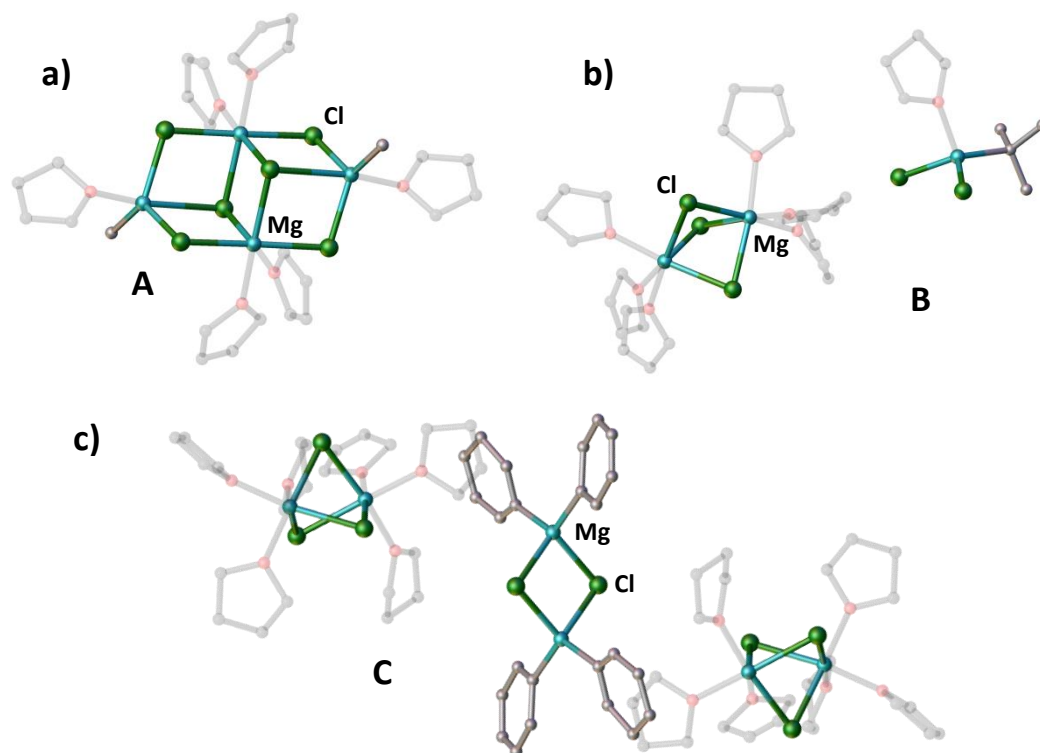


Figure 1.2: Molecular structures of **a)** $\text{Bz}_2\text{Mg}_4\text{Cl}_6(\text{THF})_6$, **A** (phenyl rings are omitted for clarity); **b)** $[\text{tBuMgCl}_2\cdot\text{THF}]^- [\text{Mg}_2\text{Cl}_3\cdot 6\text{THF}]^+$ **B**; **c)** $[\text{Ph}_4\text{Mg}_2\text{Cl}_2]^{2-} 2[\text{Mg}_2\text{Cl}_3\cdot 6\text{THF}]^+$, **C**.

The solution study of Grignard reagents with CSI-MS supported the importance of the $[\text{Mg}_2\text{Cl}_3]^+$ cation observed in the solid state which is believed to be a key component in the reagent's reactivity. The study of a solution of MeMgCl in THF shows three main ion peaks at m/z 457, 529 and 601 corresponding to $[\text{MeMg}_2\text{Cl}_3\cdot n\text{THF}\text{-H}]^+$ where $n = 4, 5$ and 6 respectively (Figure 1.3). Ionisation mass spectrometry is known to induce ionisation of neutral species by adding hydrogen atoms to a metal, hence these results support the presence of the neutral species $\text{MeMg}_2\text{Cl}_3\cdot n\text{THF}$ ($n = 4\text{-}6$).³³ In addition to this study, the most observed form of cationic magnesium chloride in the literature is $[\text{Mg}_2\text{Cl}_3\cdot 6\text{THF}]^+$ with a large variety of counter anions.³⁴⁻³⁶

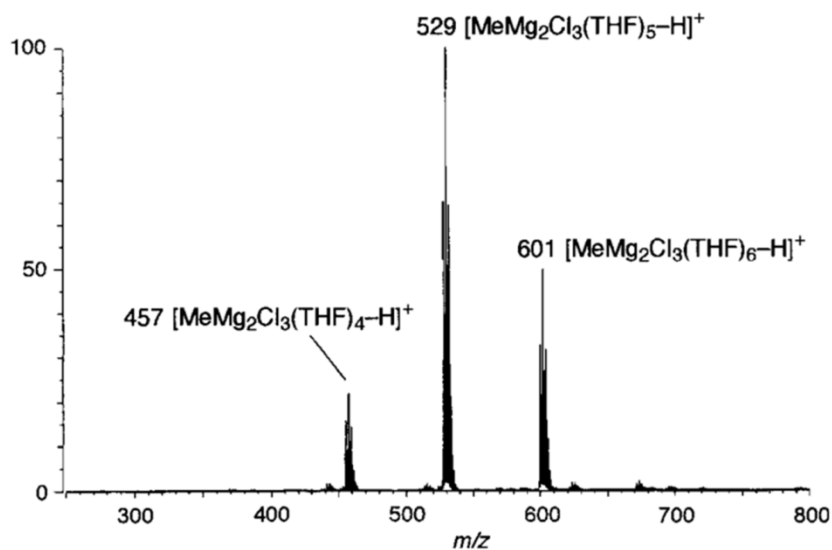


Figure 1.3: CSI-MS spectrum of a solution of MeMgCl in THF.

Many more aggregation levels of neutral and cationic “MgCl” were observed and showed dependence upon the counter anion, the sterics of the donor solvent and the reaction stoichiometry. It is interesting to start with Mg^{2+} , the simplest form of Mg cation often found in aqueous solution but also observed in ethereal solvents. Studies by Harder show that no aggregation related to mononuclear “MgCl” is observed when certain counter anions are used, a rare case as the relatively strong electrostatic bonding shared by the doubly charged alkaline metals of Group 2 and the anions tend to induce a kinetic stabilization of the contacted ion pair. However the separated ion pair can be readily formed if both the cation and anion are stabilized. The two examples in Figure 1.4 show how six molecules of the strong polar donor solvent THF coordinates to obtain a nearly perfect octahedral geometry enhancing this stabilization effect. Harder et al. believed that the coordination effect of the donor solvent is not the only factor involved, and that the packing of the counter anion plays a massive role by encapsulating the $[\text{Mg}\cdot 6\text{THF}]^{2+}$ dication “in a box” which itself implies interactions between the THF ligands and the counter anion through “C–H···C” hydrogen bonds.^{37,38}

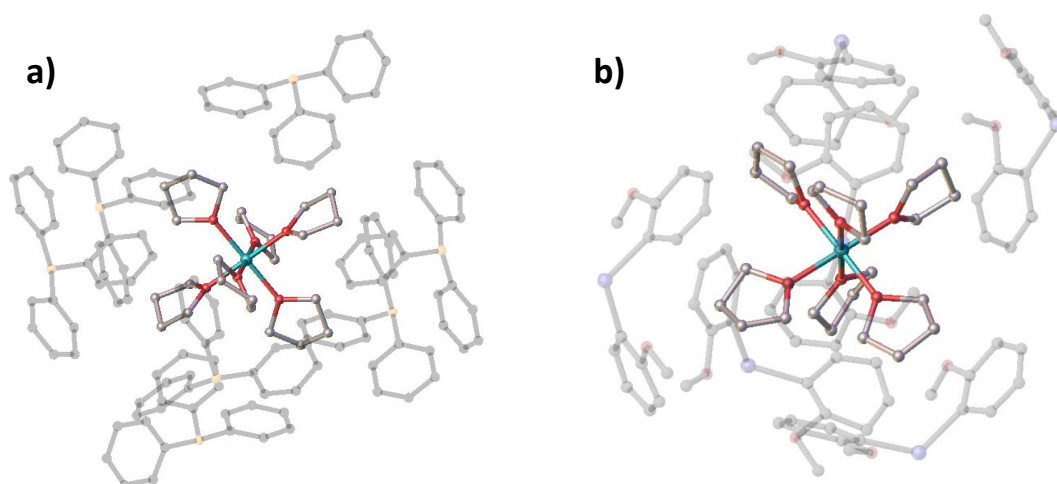


Figure 1.4: Molecular structure of **a)** $[\text{Mg}\cdot 6\text{THF}]^{2+} 2[\text{Ph}_4\text{B}]^-$ and **b)** $[\text{Mg}\cdot 6\text{THF}]^{2+} 2[\text{Zn}(\text{o}-\text{C}_6\text{H}_4\text{OMe})_3]^-$. One Ph and one (o-C₆H₄OMe) per anion were omitted to show the encapsulation with more clarity.

In the case of the mononuclear cation $[\text{MgCl}]^+$, it was observed only a handful of times by X-Ray crystallography. In order to preserve this cationic form the Mg atom requires a significant bulk with at least five THF molecules as represented in Figure 1.5. Other examples reported include a $[\text{MgCl}]^+$ monomer using more sterically demanding ligands such as crown ethers which still need an extra coordinated water molecule to occupy the other axial position trans to the chloride and prevent the formation of the neutral MgCl_2 species.³⁹ The reason why the cation adopts this aggregation level in bulk THF instead of the more commonly observed $[\text{Mg}_2\text{Cl}_3\cdot 6\text{THF}]^+$ has not been investigated. And the rational explanation behind the stabilization of $[\text{Mg}\cdot 6\text{THF}]^{2+}$ by the “in a box” effect does not seem to be applied in this case. With only four examples with different counter anions ($[\text{AlCl}_4]^-$, $[\text{FeCl}_4]^-$, $[\text{Fe}(\text{CH}_2\text{Ph})_4]^-$ and $[\text{Cu}_5(\text{viph})_4\text{Br}_2]^-$, viph = *o*-vinylphenyl) the most probable supposition is that being not often observed in solid state it is thought to be a less favoured aggregation state, but it nevertheless shows evidence of its existence in solution.^{40–43}

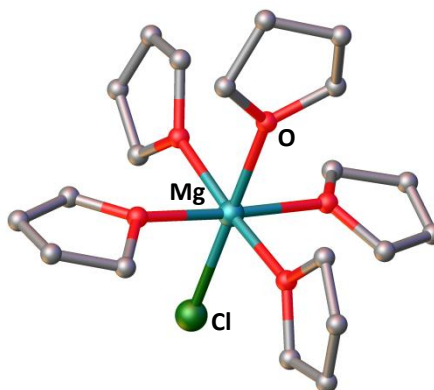


Figure 1.5: Molecular structure of the cation $[\text{MgCl}\cdot 5\text{THF}]^+$.

The dicationic dimer $[\text{Mg}_2\text{Cl}_2\cdot 4\text{DME}]^{2+}$ was reported when 1,2-dimethoxyethane (DME also traditionally known as glyme), was used as the Lewis donor solvent. The difference of bulk and denticity of two glyme molecules compared to the three THF molecules seems to prevent a third chloride bridging atom.^{44,45} Moving to the even higher denticity of diglyme [bis(2-Methoxyethyl) ether], a neutral dimeric form of MgCl_2 is favoured as there is space for only one tridentate solvent molecule coordinating the Mg atom hence not covering the area around the Mg atom enough to prevent Mg-Cl terminal bonds.⁴⁶ Finally a bidentate donor ligand or a donor solvent with a moderate bulk such as TMEDA or diethyl ether was shown to favour the trinuclear $[\text{Mg}_3(\mu_3\text{-Cl})_2(\mu_2\text{-Cl})_3\cdot \text{donor}]^+$ cation (counter ion $[\text{Fe}(\text{Bn})_3]^-$). This aggregation represents a cluster where each Mg atom is surrounded by four Cl atoms, where three of the Cl atoms are bridging two Mg atoms to form a Mg_3Cl_3 ring. The two remaining Cl atoms coordinate to three Mg atoms to give a trigonal bipyramid.^{42,47} These different studies show how diverse forms of magnesium chloride can be observed by X-ray crystallography and how difficult it can be to predict which aggregation state it would adopt during a reaction. The structure of a compound in solid state is also dependent on the packing which is also related to the lattice energy, expressed by the Born-Landé equation (Equation 1). Moreover, in solution the behaviour of the species is often complicated due to equilibria and redistributions hence no definite conclusions can be made only based on the solid state structures (Figure 1.6).

$$E = \frac{N_A M z^+ z^- e^2}{4\pi\epsilon_0 r_0} \left(1 - \frac{1}{n}\right) \quad \text{Equation 1}$$

N_A : Avogadro constant

M : Madelung constant

$z^{+/-}$: numeric charge number of cation/anion

e : elementary charge

ϵ_0 : permittivity of free space

r_0 : distance closest to ion

n : Born exponent

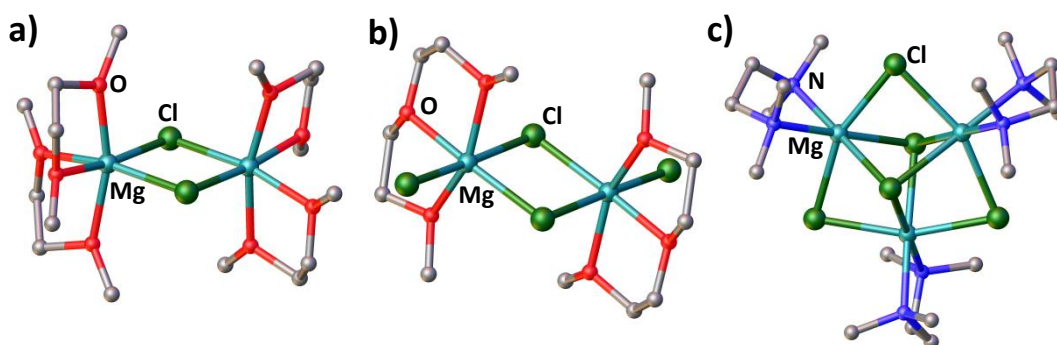


Figure 1.6: Molecular structures of **a)** $[\text{Mg}_2\text{Cl}_2 \cdot 4\text{DME}]^{2+}$ **b)** $[\text{Mg}_2\text{Cl}_4 \cdot 2\text{diglyme}]$ **c)** $[\text{Mg}_3\text{Cl}_5 \cdot 3\text{TMEDA}]^+$.

1.1.2. Aluminium

<p>Group 13: Post transition metal Atomic mass: 26.982 g/mol Density: 2.700 g/cm³ Oxidation state: +3, +2, +1, 0 Orbital: $[\text{Ne}] 3s^2 3p^1$ Price: 1.06 GBP/kg Production: 45 million tonnes/year</p>



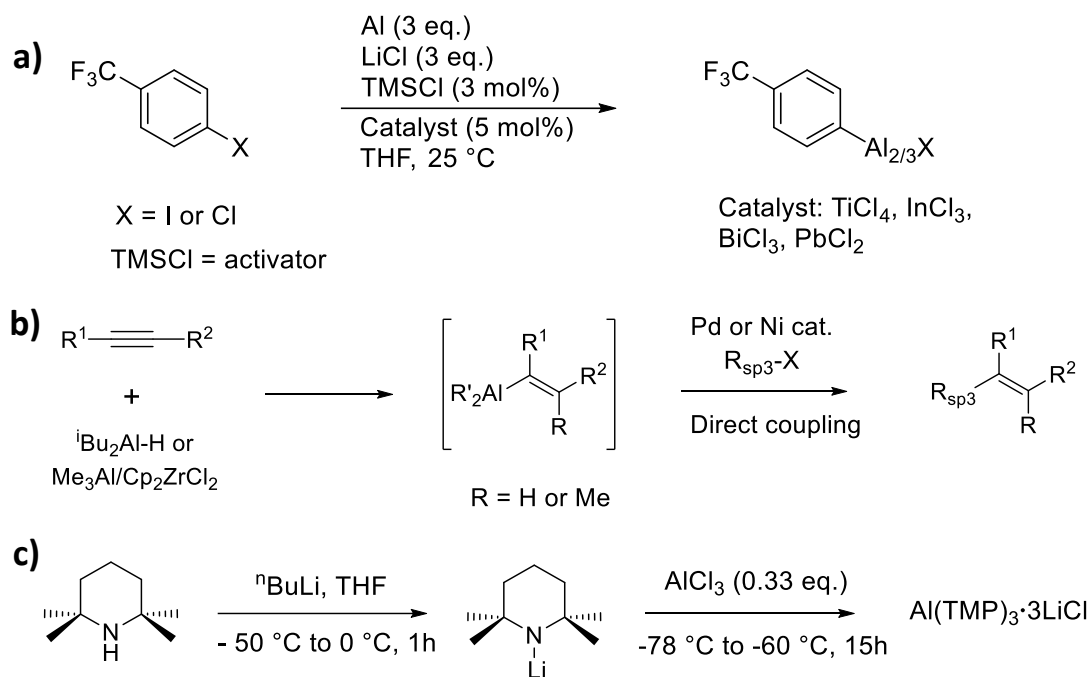
Aluminium is the second lightest element of group 13 and is the first post transition metal of the periodic table. The natural abundance of aluminium is even more notable than magnesium, being the third most abundant element on earth and the most abundant metal in the earth's crust. Aluminium salts were already used by the Greeks and the Romans during the antiquity period in the dyeing process as a mordant.⁴⁸ Since its first partial elemental isolation in 1825 by the Danish scientist Hans Christian Oersted, aluminium rapidly became an extremely popular metal in

everyday life due to its advantageous properties; lightweight metal, resistant to oxidation and corrosion, malleable, ductile, non-toxic and non-magnetic.

If aluminium is notoriously popular as a material, in chemistry organoaluminium reagents do not have the notoriety organomagnesium reagents have. Nevertheless it still is a huge actor in the organometallic world, with the example of trimethylaluminium known as a chloride abstractor co-catalyst for the Ziegler-Natta reaction in the polymerisation of alpha-olefins, chemistry that was rewarded with the Nobel Prize in 1963.⁴⁹ Since then, aluminium grew in popularity in synthetic chemistry as a strong Lewis acid catalyst for the Friedel-Craft reaction, a reducing and alkylating reagent or in synthetic organic chemistry.⁵⁰⁻⁵² In the last five years, Nakamura et al. developed the first Negishi cross-coupling variant using cheaper iron-catalyst and aryl aluminium reagents, and even more recently a direct cross coupling using organoaluminium reagents in the absence of any co-catalysts was reported by Uchiyama.⁵³⁻⁵⁵

1.1.2.1. Uses of aluminium reagents in chemistry

Organoaluminium and related compounds are relatively easy to synthesise and various routes have been developed. A quick highlight would include direct insertion of aluminium powder into alkyl halides and more recently into aryl halides in the presence of LiCl salt, an extremely useful method leading to an efficient functionalisation of aromatic and heteroaromatic aluminium compounds.⁵⁶ Another method involves the reaction of aluminium powder with alkenes in the presence of hydrogen leading to hydro- or carbo- alumination which can further react with alkenes or alkynes; a method often used for cross coupling reactions.⁵⁷⁻⁵⁹ And finally a classical transmetallation method with more electropositive organolithium reagents leads to efficient metathesis reaction with aluminium halides (Scheme 1.2).⁶⁰



Scheme 1.2: Different methods of preparation of organoaluminium reagents, **a)** direct insertion of Al powder into aryl halides, **b)** hydro- or carbo- alumination of alkynes, **c)** transmetalation of bulky 2,2,6,6-tetramethylpiperidine (TMP).

In the solid state aluminium appears in various types of compound, for example as aluminium hydrides (alanes), organoaluminium compounds or salts. Each form can occur as clusters, contacted ion pairs or separated ion pair complexes.^{61–63} Simple trialkylaluminium or aluminium amide reagents usually exist as dimers at room temperature where for trialkylaluminium reagents two alkyls are bridging the two aluminium centres leading to an electron-deficient compound according to the 3-centre 2-electron bond rule. However ¹H NMR studies show evidence of an association-dissociation of the dimer with exchanges between a dimer and the bridging or terminal groups of another dimer which is too fast on the NMR scale, leading to a single resonance hence suggesting a monomer intermediate. This issue is easily overcome using bulky ligands on the aluminium to form exclusively the monomer.^{64–66}

1.1.2.2. Weakly coordinating anions

Aluminium halides are frequently used in both organic and inorganic chemistry as strong Lewis acids and fairly soft anions to form salt adducts with Lewis bases such as NMe_3 or from a multitude of halide containing reagents such as ${}^t\text{BuBr}$ (forming $\text{Me}_3\text{N}\cdot\text{AlX}_3$ and $[\text{Al}_2\text{Br}_7]^- [{}^t\text{Bu}]^+$ respectively and where $\text{X} = \text{Cl}, \text{Br}, \text{I}$).^{67,68} Krossing and co-workers are working extensively with aluminium halide based anions as a tool to stabilise and isolate organic cations in a crystalline solid salt and characterise them by X-ray crystallography. This ingenious technique led to the characterisation of very sensitive carbocations of different size and stability with the particularly interesting examples of $[{}^t\text{Bu}]^+$,⁶⁸ $[\text{Cl}_3]^+$,⁶⁹ $[\text{C}_6\text{H}_7]^+$,⁷⁰ $[\text{C}_7\text{H}_9]^+$ ⁷¹ and finally the first pentacoordinated carbon in the nonclassical 2-norbornyl cation $[\text{C}_7\text{H}_{11}]^+$ ⁷². In his studies Krossing evaluated the ability of different aluminium anions to pair and stabilise a variety of cations using different aluminium halides and its derivatives. By moving from the simple salt AlBr_3 to the less common alkoxyaluminate superacid $\text{LiAl}(\text{OR})_4$ [when $\text{R} = \text{C}(\text{CF}_3)_3$] he controls the coordinating strength of the corresponding anion, ideal to avoid the formation of contacted ion pairs. Figure 1.7 shows three carbocations which possess different counteranions. The more delocalised $[\text{Al}_2\text{Br}_7]^-$ anion will stabilise the norbornyl cation as its lower aggregate form $[\text{AlBr}_4]^-$ seems to be not as efficient. The stabilization of such an unstable cation with $[\text{Al}_2\text{Br}_7]^-$ however requires diffraction with controlled temperatures to avoid cracks, hydride shifts and rearrangements (slow cooling down to 40 K) in order to obtain usable data. $[\text{AlX}_4]^-$ are generally weak enough coordinating anions to stabilise a large number of cations most of which possess metal centres or easily polarised groups. The last example cation was stabilised by the customised superacid $[\text{Al}(\text{OR})_4]^-$, which is one of the weakest nonoxidising coordinating anions developed hence it is used to stabilise the most challenging cations.^{73,74}

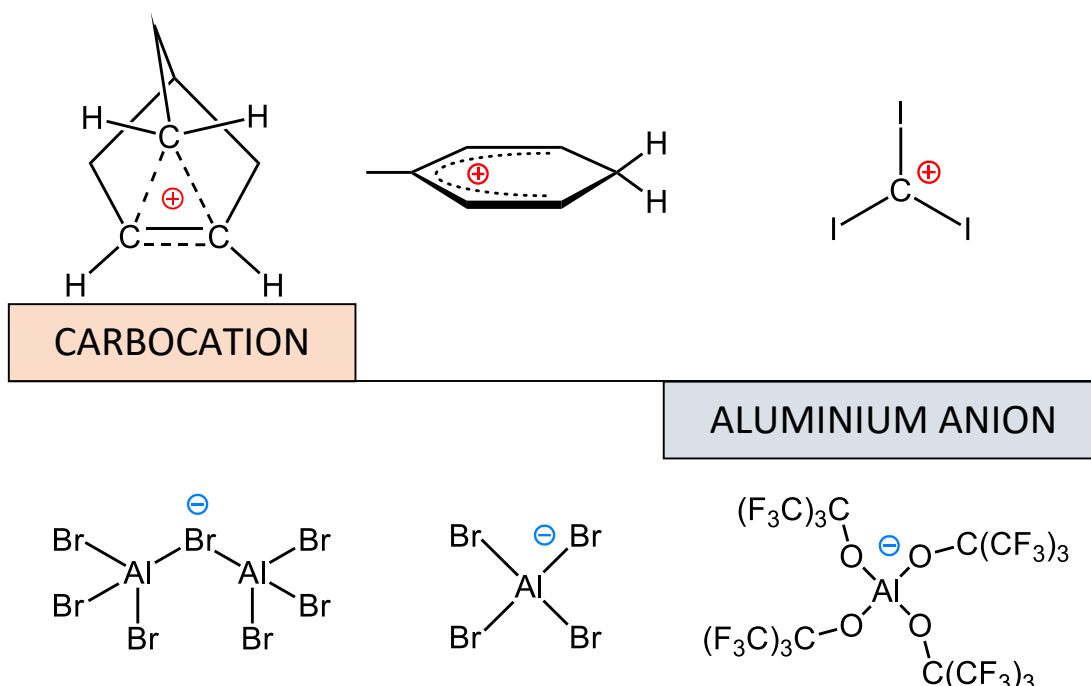


Figure 1.7: Carbocations (top) and their counter aluminium anions (bottom); (left) nonclassical 2-norbornyl cation $[\text{Al}_2\text{Br}_7]^- [\text{C}_7\text{H}_{11}]^+$; (middle) carbocation of toluene $[\text{AlBr}_4]^- [\text{C}_7\text{H}_9]^+$; (right) triiodocarbon carbocation $[\text{Al}(\text{OR})_4]^- [\text{Cl}_3]^+$.

In the literature many other aluminium reagents are used both simultaneously for chemical transfer (transmetallation or halogen transfer) and to improve the stabilisation of the organometallic compounds by forming a separated ion pair salt. Common aluminium reagents of this type include organoaluminium anions such as $[\text{AlMe}_2\text{Cl}_2]^-$,⁷⁵ $[\text{AlEtCl}_3]^-$ ⁷⁶ or $[\text{AlPh}_4]^-$;⁴¹ but also aluminium amide and aluminium alkoxide anions $[\text{AlCl}_2(\text{N}^i\text{Pr}_2)_2]^-$,⁷⁷ $[\text{AlCl}_3(\text{OC}_6\text{H}_4\text{CF}_3)]^-$.⁷⁸ Due to the alkyl, aryl, amide, alkoxide and other substituents on the aluminium, the corresponding anion's coordinating properties are increasing (Figure. 1.8) and its overall stability is reduced compared to its halide equivalent $[\text{AlX}_4]^-$, it however shows advantages in terms of solubility in organic solvents.⁷⁹

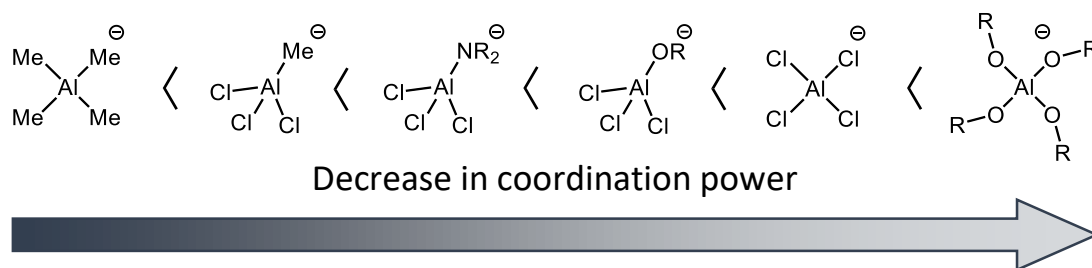
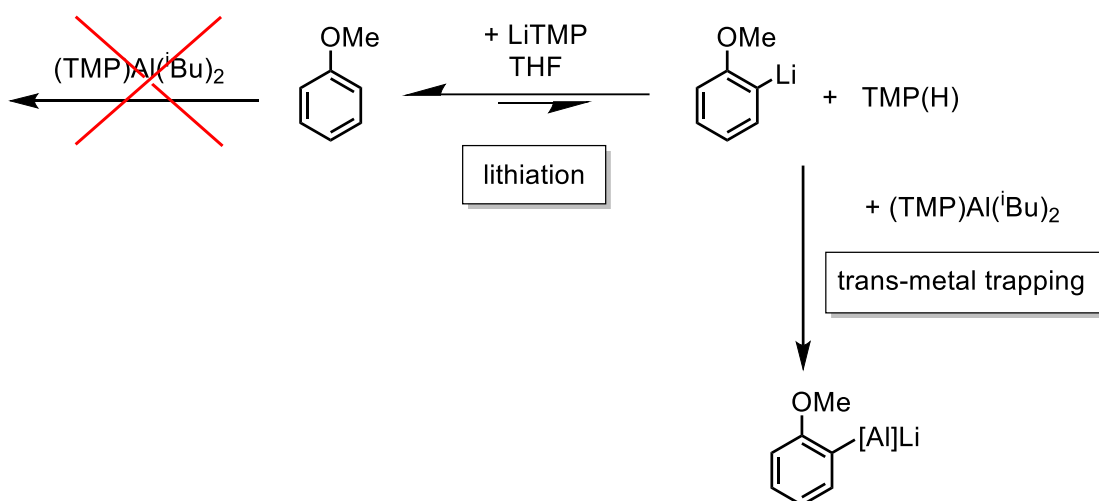


Figure 1.8: Influence of substituents on the aluminium anion's coordination power.

1.1.2.3. Aluminium containing heterobimetallic compounds

Section 1.1.1.1. mentioned the existence of heterobimetallic complexes containing aluminium. This referred to two reagents dominating the alkali-metal-mediated aluminations chemistry, $\text{LiTMP}\cdot\text{Al}(\text{iBu})_3$ developed by Uchiyama and $\text{LiTMP}\cdot\text{Al}(\text{TMP})(\text{iBu})_2$ developed by Mulvey.^{80,81} Recent studies show conflicting evidence of the initial hypothesis on their functionality, where the metallation of a substrate was believed to be the work of the lithium aluminate contacted ion pair. The study demonstrates that neither of the bimetallic bases are able to aluminates a substrate through a cooperative lithium aluminate species, but it is in fact a lithiation reaction which induces the formation of a carbanion which is rapidly trapped by the alkylaluminium reagent leading to an aluminate product in high yield even when the lithiation occurs in only low yield since it removes lithiated substrate and alters the position of equilibrium (Scheme 1.3).^{82,83}



Scheme 1.3: Proposed two-step pathway for the aluminations of anisole.

1.2. Advances in magnesium batteries

The world of batteries has known quite an evolution since the first battery invented by Volta in 1800. The first major battery commercially available and still topical is the lead-acid battery (invented in 1859) which is still used worldwide to start the engine of automobiles fuel, due to its supply of high surge current. However their drawback comes from their low energy to weight and volume ratio, but also for the very toxic properties of some lead compounds. The still widespread nickel batteries (Ni-Cd, in 1898, and more recent Ni-MH in 1967) are generally used for small devices but rarely found their applications for larger, more demanding apparatus. Moreover nickel metal requires an intensive industry as its extraction is difficult and unsustainable.^{84,85} Lithium-ion batteries are the latest innovation in commercially available batteries, imposing their domination in the energy storage market and maintaining a constant evolution. However being today's ultimate battery, it does not mean that it possesses all the characteristics for the perfect battery, and many undesirable features still exist; namely the dangerous dendrite formations, flammability and possible explosions, cost and environmental impact. The search for a powerful, environmentally friendly, cheap battery is therefore still on and many scientists are pursuing it by developing sodium, aluminium, proton and finally magnesium batteries; whose advances are introduced in this chapter.⁸⁶

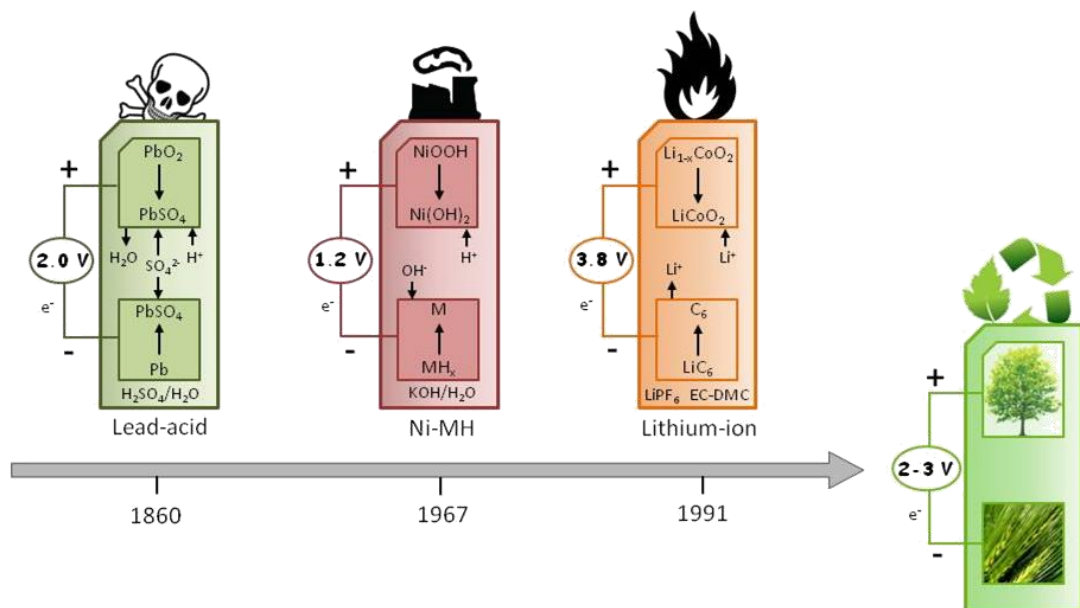


Figure 1.9: Evolutions through the years of useable rechargeable batteries to a utopian green model.

1.2.1. Basic principles of a rechargeable battery

The current knowledge in the operational mechanism of rechargeable batteries was mostly acquired from the large efforts furnished in the development of Li-ion batteries (LIB). This section discusses what is known so far for LIB to give a basic understanding on how metal-ion rechargeable batteries run in general. This gives insight into the processes leading to the electron transfer responsible for the supply of energy, the different components of a battery system and the features more specific to LIBs which enhance their performances but which are not transferable to Mg batteries.

Figure 1.10 displays a simplified explanation in what happens to the Li ions within a battery during the discharging process. When a LIB is fully charged Li ions are intercalated within one of the electrodes only. During the discharge this electrode is the negative electrode known as the anode, the Li^+ ions start to migrate toward the positive electrode known as the cathode until the anode is left empty and the cathode is now full. The electrons are passing through an external circuit, simultaneously producing a current. During the charging process the opposite phenomenon occurs.

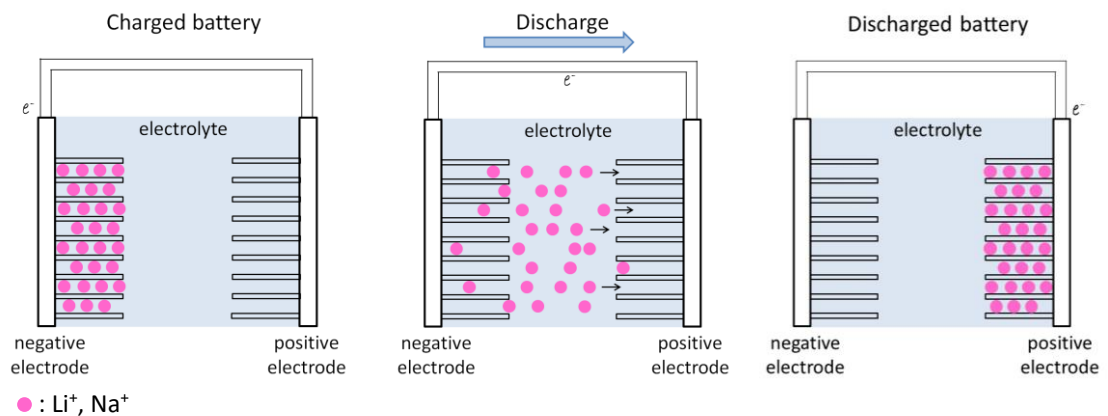


Figure 1.10: Ion transfer during the discharge of an LIB.

Ideally, in rechargeable batteries the anode is simply a sheet of elementary metal of the ions used to produce this current, hence in the case of LIB the use of lithium metal is desirable. In practice however the use of a Li metal anode is hindered by undesired properties during the deposition process. More precisely the Li ions deposit onto the anode in a specific way, giving barbed branch formations called dendrites. Figure 1.11 shows that if these dendrites grow too large and manage to pierce through the separator holding the electrolyte, they can come into contact with the cathode

producing a short circuit path. This will create a thermal runaway situation leading to a large increase of temperature, and in an LIB which contains flammable components, such malfunction can clearly lead to dangerous situations. Instead of using a Li metal anode, efforts were made to produce a material capable of intercalating Li ions within the structure of the material. Often a material as simple as graphite is used in commercially available LIB.^{87,88}

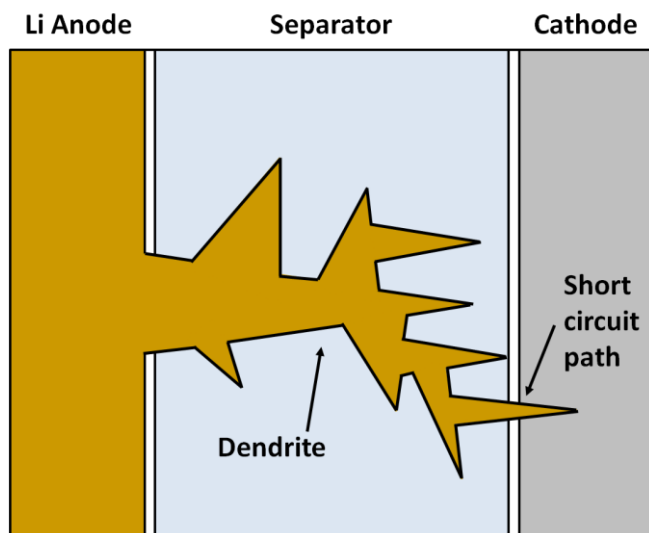


Figure 1.11: Diagram showing the formation of dendrite following the deposition of Li using a Li anode in a lithium battery.

Developing new cathode materials for LIB is the most widely focused research in this area, as the need for a high energy cathode is increasing with the need for more energy.^{89–92} The cathode materials used in currently commercially available LIB are a type called insertion cathodes (Figure 1.12a). These materials are most commonly made using metal oxides, where the metal of choice must have a versatile oxidation state number. When the Li ions are intercalated within the cathode the metal used is reduced by one oxidation state, liberating 1 electron in the process generating the current supply. The most frequently used metals for this type of cathode material are Mn, Fe, Ni or Co and can form porous composites with different morphologies. Figure 1.12b shows a few typically observed morphologies where the pores within the material can be found as straight or distorted channels or layers which can intercalate Li ions but also de-intercalate them.⁹¹ It is the reversibility of the intercalation process which dictates the ability of a battery to be rechargeable and the intercalation/de-

intercalation kinetics which dictates its discharge/charge rate. For the case of magnesium batteries, the metal from the cathode must be able to undergo a 2 electron oxidation state change to be able to intercalate the divalent Mg ions. Although efforts invested in finding different compatible cathode materials were rewarded with a variety of cathodes now available, the cathode of choice for benchmark battery performance test regarding the other components of the battery is the Chevrel phase Mo_6S_8 introduced by Aurbach et al. which was the cathode proposed for the first Mg rechargeable prototype.⁹³

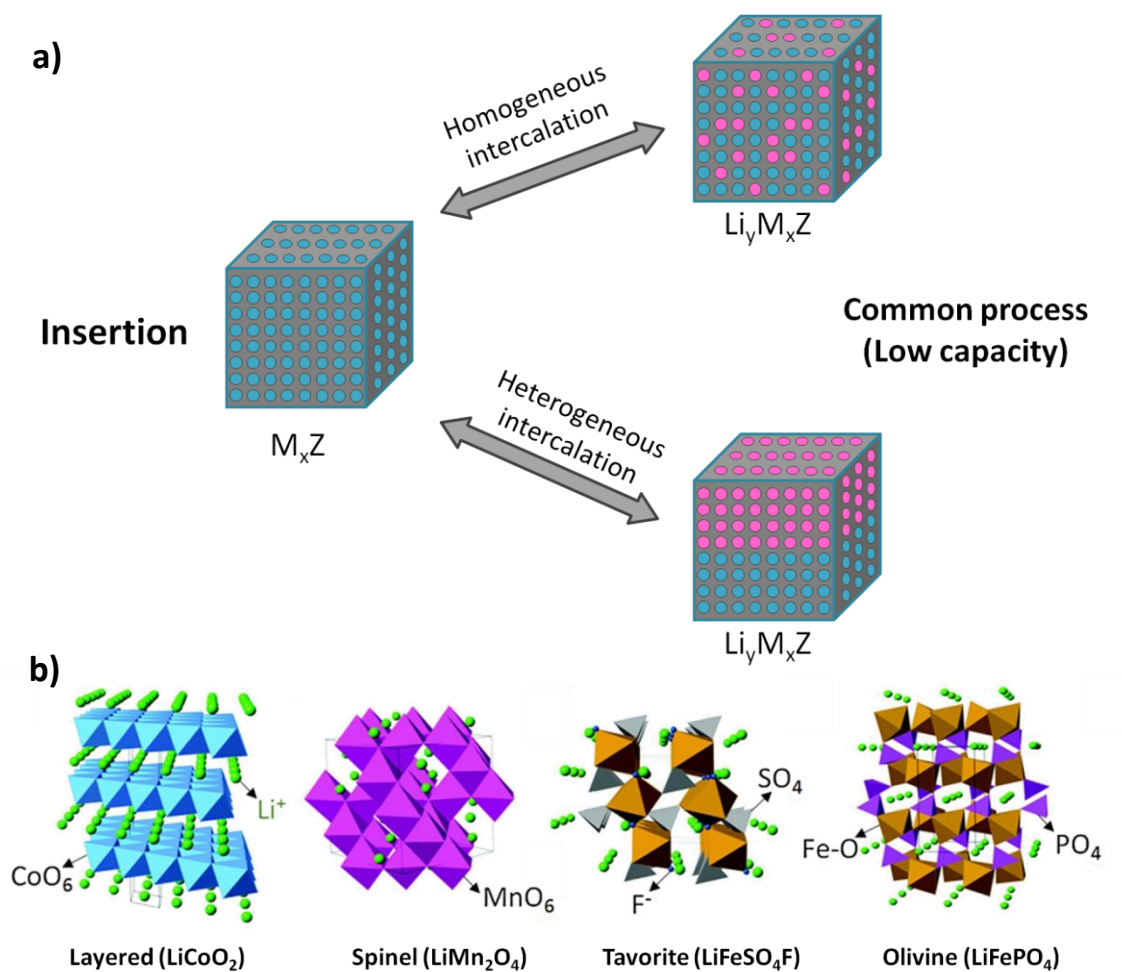


Figure 1.12: a) Diagram showing the principle of insertion; b) structural representation of different classes of insertion cathode material.

Another type of cathode material which attracts more and more attention every day is the conversion cathode.⁹⁴ Instead of having the ions being intercalated within a

material, a chemical reaction occurs with the cathode changing its general composition. The most advance cathode of this class is the sulphur cathode in Li/S batteries. As shown in Figure 1.13, during the discharge the Li ions are inserted within the sulphur element composite to form the new single phase composite Li_2S . Although it is not currently commercially available it exhibits more attractive energy storage properties reaching higher practical capacity value. However it also displays more sluggish insertion/de-insertion kinetics as the chemical reaction is generally slower than ion stripping from a porous material, but one other major issue is the change of volume during the running of the battery, over time reducing the interactions with the different battery components eventually leading to disconnection with the current collector.

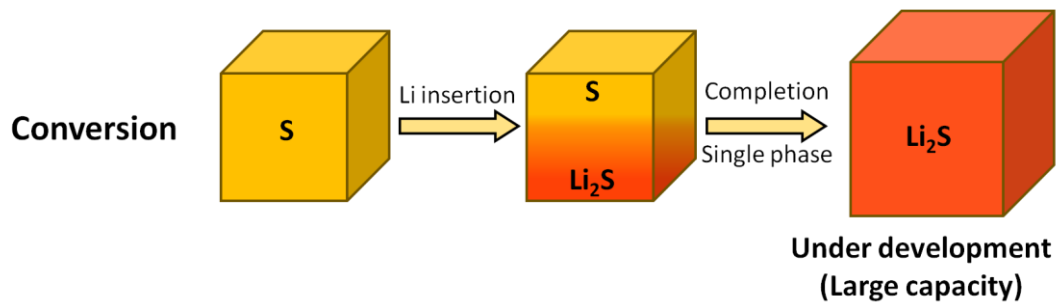


Figure 1.13: Diagram showing the operation of a conversation sulphur cathode in LIB.

1.2.2. Simple rechargeable battery scheme

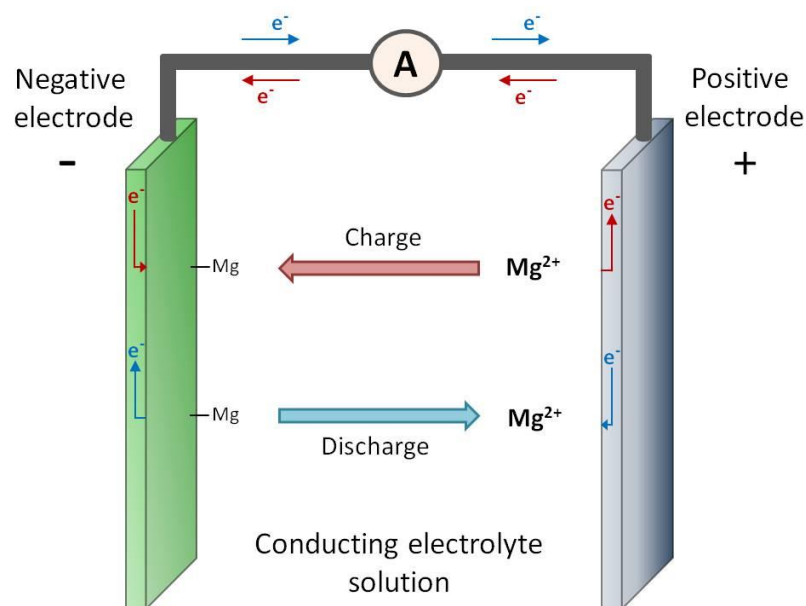


Figure 1.14: Scheme of a rechargeable magnesium battery.

Figure 1.14 shows a general scheme of a rechargeable battery, displaying the electron transfer directions during the charge and the discharge.

1.2.3. Arguments for magnesium batteries

The motives of developing magnesium batteries are based on the theoretical properties of magnesium metal, which promise to provide better storage capacity, more power, sustainability, safety, lower cost and a smaller impact on the environment. In more scientific terms, as a result of the divalency of magnesium its specific volumetric capacity reaches 3832 mAh/cm³, which is nearly twice as much as for lithium (2046 mAh/cm³).⁸ This is a very valuable characteristic in the development of smaller, lighter batteries with a better sustainability. The power is expressed in energy density, which theoretically reaches 4500 Wh/L for magnesium, almost three times the most powerful existing battery (1680 Wh/L for lithium air batteries) and more than a hundred times higher than lead-acid batteries (40 Wh/L).⁹⁵ The sustainability of a battery is defined by the number of charges/discharges the battery can accumulate without losing its capacity, this number being expressed in cycle life. This value is affected by the deposition/dissolution of the metal onto the electrodes which depends on both the electrolyte (conducting substance between electrodes) and the cathode material. The matter of safety also comes into consideration and most current batteries would not fulfil a clean risk assessment. Indeed lead is known to be toxic, but other batteries have flammable compounds, even explosives in particular in lithium batteries. Moreover there is the present dendrite formation in the metallic lithium on the electrodes which can lead to short circuit, a phenomenon not observed with magnesium. As a final argument, the abundance of magnesium in the earth's crust offers significantly more material availability at a lower cost.

Five relatively recent and complete reviews which cover many different aspects of magnesium batteries are recommended for one who wished to acquire more in-depth knowledge in this field.^{2,8,9,96,97} Meanwhile, a concise summary of the area is provided below.

1.2.4. Early studies and first issues

Early studies were focused on the search for a suitable electrolyte possessing high ionic conductivity and inducing reversible deposition. However these studies showed that simple Mg salts such as $\text{Mg}(\text{CF}_3\text{SO}_4)_2$ and $\text{Mg}(\text{ClO}_4)_2$ in standard solvents (*N,N*-dimethylformamide, acetonitrile or propylene carbonate) could not undergo reversible deposition due to the formation of insoluble salts coating the electrode's surface, inhibiting the activity of the electrochemical cell. Addition of water to the system also lead to passivation of the electrode with the formation of magnesium oxides MgO and $\text{Mg}(\text{OH})_2$, retarding the formation of the electro-active species.⁹⁸⁻¹⁰⁰ These early poor results forced the study toward the more reactive organomagnesium and Grignard reagents as potential electrolytes, which showed efficient reversible deposition in ethereal solvents but a too limited oxidative stability to be applicable for batteries.¹⁰¹

The first real breakthrough was introduced by Gregory back in 1990 by investigating the electrochemistry of the reaction of dialkylmagnesium with the strong Lewis acidic organoborons (BBu_3) and aluminium halides (AlCl_3) in ethereal solutions. This coupling showed an increase in the oxidative stability to a more suitable level, which relaunched the interest for magnesium batteries.¹⁰²

1.2.5. Magnesium aluminates as electrolytes

Further to Gregory's concept, Aurbach and co-workers invested a lot of effort in the characterisation and development of magnesium organohaloaluminate compounds as viable electrolytes for a working battery. In their early work they thoroughly studied the electrochemical and the deposition/dissolution properties of magnesium salts $\text{Mg}(\text{AlCl}_{4-n}\text{R}_n)_2$ obtained by mixing commercially available compounds such as Bu_2Mg with AlCl_2R ($\text{R} = \text{Me}, \text{Et}, \text{Bu}$) or AlCl_3 .¹⁰³⁻¹⁰⁶ The study of these electrolytes was conducted in a consistent manner by different groups of researchers using similar material (electrodes) to display an adequate comparison between the electrolytes properties. Most of these materials were based on the first prototype of a magnesium battery built in 2000 which was composed of a Chevrel

phase type cathode containing the Mo_6S_8 cluster and a simple magnesium anode.⁹³ Nevertheless it is important to mention that since then groups of material chemists have made significant progress in developing more efficient Chevrel phase cathodes and magnesium alloy anodes.^{107–109}

Although the improvement of electrochemical properties of the electrolytes is one of the major concerns to forge a practicable battery, it is a necessity to explore more obscure paths in order to achieve a more finalized product but also comprehend its process in more detail. Aurbach moved in this direction by using a variety of analytical methods to have a better understanding of the electrolyte's behaviour in solution, and how the aluminium reagent interacts with the magnesium to lead to the observed enhanced properties.

1.2.5.1. Multinuclear NMR spectroscopy studies of magnesium aluminate solutions

Aurbach and co-workers were not satisfied by preliminary X-ray studies on a single crystal structure obtained from an electrolyte solution, $[\text{AlEtCl}_3]^- [\text{Mg}_2\text{Cl}_3 \cdot 6\text{THF}]^+$, which they believed did not represent the species in solution.¹⁰⁵ They hence decided to use multinuclear NMR spectroscopy, more precisely ^1H , ^{13}C , ^{25}Mg and ^{27}Al , to identify the components resulting from the reaction of Et_2Mg and EtAlCl_2 in THF at different stoichiometric ratios. ^1H and ^{13}C NMR spectroscopy not providing much information in this situation, they mostly turned their interest on ^{27}Al and ^{25}Mg NMR spectroscopy. However it is known that in practice both methods are very sensitive to the geometry of the molecule, and tend to exhibit broad and noisy signals for non-symmetrical species. The ^{27}Al NMR spectroscopy spectrum of three solutions at different stoichiometry lead to three different resonances corresponding to different aluminium species (Figure 1.15a.). When 0.5 equiv. of Et_2Mg was added to EtAlCl_2 , ^1H NMR spectroscopy shows evidence of transmetalation of Et from the magnesium to the aluminium to form a tetracoordinated aluminium species, the ^{27}Al NMR signal shows a broad peak related to a lack of symmetry within the molecule. Given the stoichiometry of the reaction Aurbach proposed $[\text{Et}_2\text{ClAl}-\text{Cl}-\text{AlClEt}_2]^-$ to be the species present in solution. For a 1:1 ratio the main resonance of the ^{27}Al NMR

spectrum shifted, retaining its broad shape meaning the formation of another, non-symmetrical species assigned as $[\text{Et}_3\text{AlCl}]^-$. Finally when 2 equivalents of Et_2Mg was added, a sharp signal was observed, characteristic of a highly symmetrical species, in this case $[\text{AlEt}_4]^-$.¹¹⁰

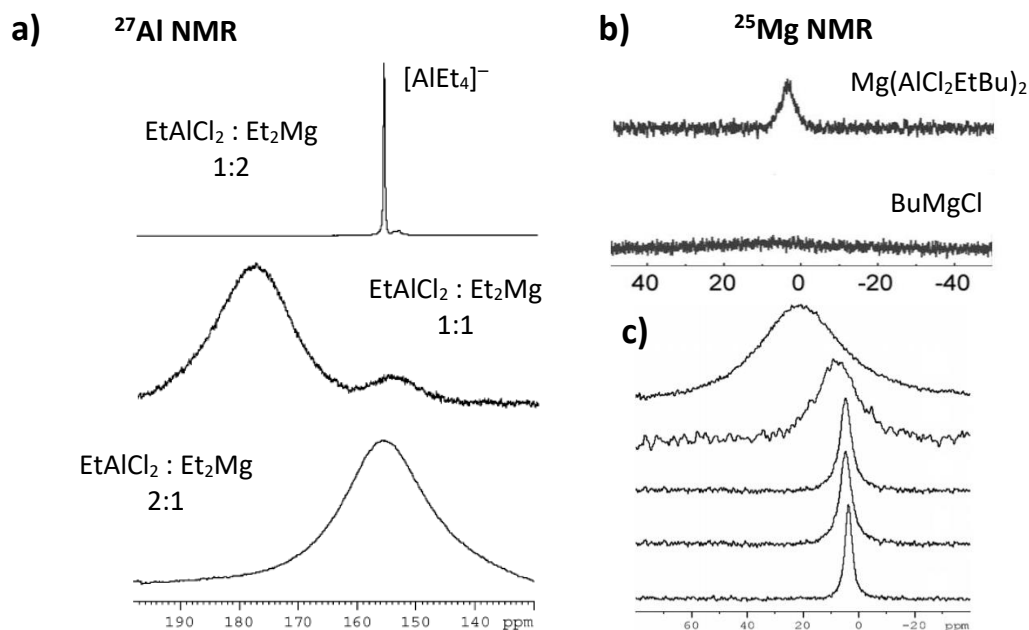


Figure 1.15: **a)** ^{27}Al NMR spectra of the addition of Et_2Mg to EtAlCl_2 at different ratios; **b)** ^{25}Mg NMR spectra of BuMgCl and $\text{Mg}(\text{AlCl}_2\text{EtBu})_2$ in THF; **c)** ^{25}Mg NMR spectra from $\text{Mg}(\text{AlCl}_2\text{R}_2)_2$ with different concentration of TBACl, 0 M, 0.1 M, 0.25 M, 0.5 M, 0.6 M TBACl (bottom to top).

^{25}Mg NMR spectroscopy is not a commonly used method due to its low sensitivity and symmetry dependence but has shown some appealing outcomes, especially in the study of the Schlenk equilibrium in organomagnesium compounds.¹¹¹ A few experiments have been performed on magnesium electrolytes using ^{25}Mg NMR spectroscopy in order to develop a method of characterisation for magnesium electrolytes in solution. Figure 1.15b shows that no resonances are observable for the poorly symmetrical Grignard reagent BuMgCl whereas a solution of $\text{Mg}(\text{AlCl}_2\text{EtBu})_2$ in THF exhibits a noticeable resonance around 5 ppm, a hint of the presence of a more symmetrical species.¹¹² Another study involves the addition of tetrabutylammonium chloride (TBACl) to a $\text{Mg}(\text{AlCl}_2\text{R}_2)_2$ solution in THF ($\text{R} = \text{Et}, \text{Bu}$, Figure 1.15c). The ^{25}Mg NMR spectra shows a change of shift and shape in the electrolyte resonance with the addition of TBACl, where more TBACl was added the higher was the shift and the broader was the resonance. TBA^+ is known to be a stable cation, hence these data

support Aurbach's belief that it either replaces the Mg cation, or it forces the formation of a $[\text{MgCl}_4]^{2-}$ dianion.¹¹³

Both ^{27}Al and ^{25}Mg NMR spectroscopy can be used for characterisation of the electrolytes in solution; however their application is relatively limited as very little information can be gained due to the lack of comparison with similar species but also the weak resolution of the signal when dealing with poorly symmetrical compounds.

1.2.5.2. Raman spectroscopy studies of magnesium aluminate electrolytes

After some unsatisfying results with multinuclear NMR spectroscopy, Aurbach decided to change his focus toward Raman spectroscopy in the hope of observing the Raman active vibrations of the electrolyte resulting in the identification of the species present in solution and in the construction of a comprehensive spectral reference library. This work has been performed in complementarity with single crystal X-Ray diffraction as a support to identify the active vibrations by comparing the results of the electrolyte in the solid-state and in solution. Three major electrolyte systems were studied, $[\text{AlCl}_{4-n}\text{Et}_n]^- [\text{Mg}_2\text{Cl}_3 \cdot 6\text{THF}]^+$ ($n = 1$ or 2), $[\text{AlPh}_4]^- [\text{Mg}_2\text{Cl}_3 \cdot 6\text{THF}]^+$ and $[\text{AlCl}_4]^- [\text{MgCl} \cdot 5\text{THF}]^+$ for which the crystal structures were reported (Figure 1.16).^{41,46,105}

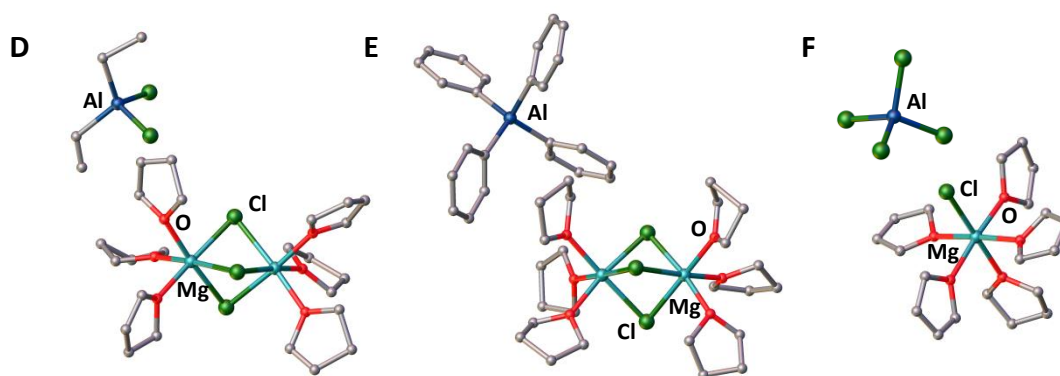


Figure 1.16: Molecular structures of $[\text{AlCl}_2\text{Et}_2]^- [\text{Mg}_2\text{Cl}_3 \cdot 6\text{THF}]^+$, **D**; $[\text{AlPh}_4]^- [\text{Mg}_2\text{Cl}_3 \cdot 6\text{THF}]^+$, **E** and $[\text{AlCl}_4]^- [\text{MgCl} \cdot 5\text{THF}]^+$, **F**.

The crystal structures of the electrolytes studied are all solvent separated ion pairs containing an aluminium anion and a magnesium chloride cation. **D** and **E** both possess the previously introduced cationic dinuclear magnesium species $[\text{Mg}_2\text{Cl}_3 \cdot 6\text{THF}]^+$ when the counter ion is an organohalo- or organo-aluminium anion ($[\text{AlCl}_2\text{Et}_2]^-$ and

[AlPh₄]⁻ respectively). **F** possesses the monomeric magnesium chloride cation [MgCl·5THF]⁺ with a haloaluminium counter anion [AlCl₄]⁻. As mentioned in section 1.1.2 of this chapter, the dinuclear cation seems to be more favoured in a crystal lattice, but the monomeric structure was occasionally observed by X-Ray crystallography giving a clue of a dynamic equilibrium in solution. The electrolytes **D** and **E** were prepared by reacting a Grignard reagent (here EtMgCl and PhMgCl) with an organo- or halo-aluminium species (EtAlCl₂ or AlCl₃) which allows transfer of the ethyl or phenyl groups from the magnesium to the aluminium. These three crystal structures are interesting for studying their Raman spectra for their distinctive aluminium anions and magnesium cations and are thought to give rise to different vibrational bands, more particularly differences between the bridging Mg-Cl-Mg bond and the terminal Mg-Cl bond.

Starting with the aluminium anion [AlCl_{4-n}Et_n]⁻ Aurbach compared the obtained spectrum of the electrolyte in THF with the standard spectra of Et₃Al, Et₂AlCl, EtAlCl₂ (Figure 1.17a). The organohaloaluminium reagents show two signals corresponding to the Al-Cl bonds at lower wavenumbers (250-430 cm⁻¹ region) and to the Al-C bond at higher wavenumbers (450-650 cm⁻¹ region). The intensity of the peaks show dependence with the Et:Cl ratio, as observed by comparing the EtAlCl₂ and Et₂AlCl spectra where the scattering wavenumber corresponding to Al-Cl drops when there is one Cl atom less. The spectrum of supposedly [Et₂AlCl₂]⁻ [Mg₂Cl₃·6THF]⁺ exhibits a new peak around 370 cm⁻¹ assigned to the [Et₂AlCl₂]⁻ anion, the presence of Et₂AlCl and Et₃Al is also noticeable (Figure 1.17a), top spectrum).¹¹⁴

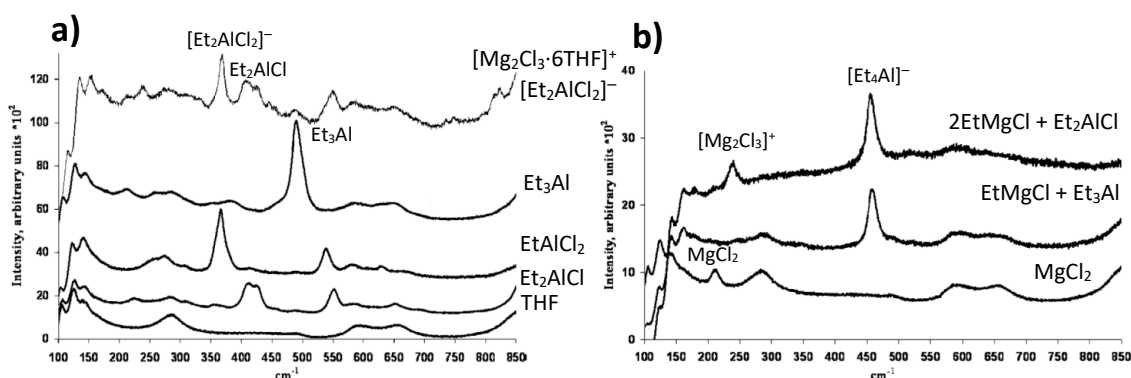


Figure 1.17: **a)** Raman spectra of [Et₂AlCl₂]⁻ [Mg₂Cl₃·6THF]⁺ and Al starting materials in THF; **b)** Raman spectra of two reactions between different ratio of Al and Mg starting material in THF.

The study of the magnesium species vibrational energies is expected to be slightly simpler in theory as only the presence of peaks attributable to Mg-Cl bonds are predicted. Aurbach decided then to measure two samples with different ratios of Mg/Al that would lead to the rational synthesis of $[\text{MgCl}]^+$ (1:1) and $[\text{Mg}_2\text{Cl}_3]^+$ (2:1) using MgCl_2 as a standard (Figure 1.17b). The first system only shows the signal for $[\text{Et}_4\text{Al}]^-$, but the second system exhibits a signal close to MgCl_2 shifted to higher wavelengths which was associated to $[\text{Mg}_2\text{Cl}_3]^+$ by default. This study showed that Raman has a potential application to study the behaviour of these electrolytes in solution, however the $[\text{MgCl}]^+$ cation was not observed likely due to a non Raman active Mg-Cl bond in this specific case. $[\text{Mg}_2\text{Cl}_3]^+$ involving three Mg-Cl four membered rings, a feature known to lead to Raman signal, exhibits a distinguishable signal.

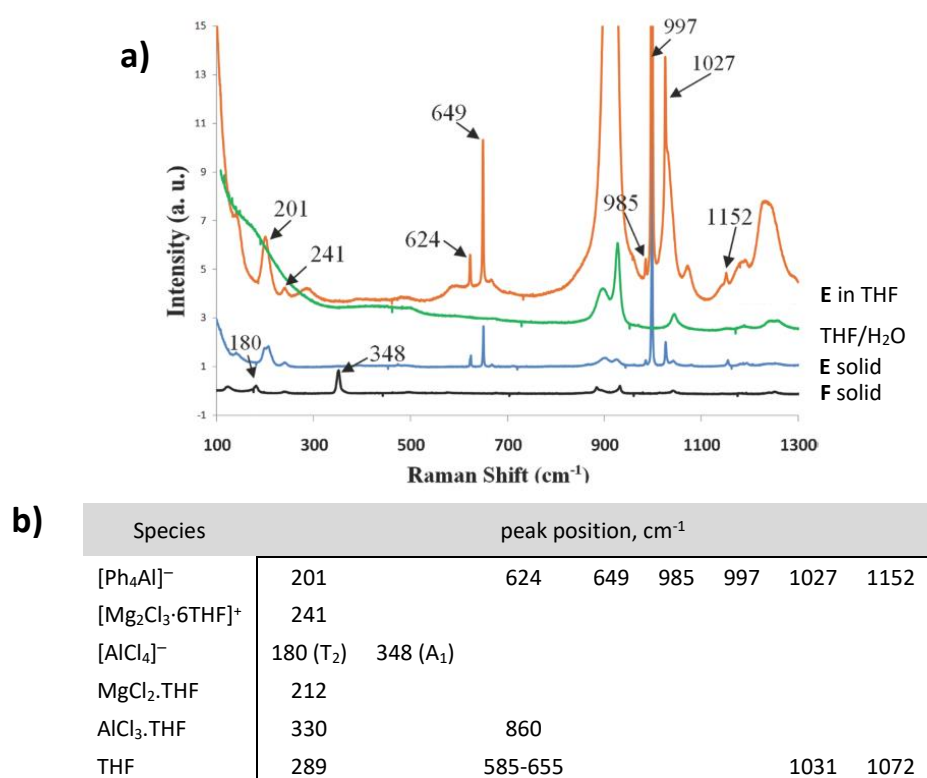


Figure 1.18: a) Raman spectra of E solid, F solid THF/ H_2O solution and F in THF; b) Raman spectral data.

The electrolyte $[\text{AlPh}_4]^- [\text{Mg}_2\text{Cl}_3 \cdot 6\text{THF}]^+$ **E**, entitled all-phenyl complex (APC), was studied both in THF and as a solid powder, however due to very poor solubility in THF $[\text{AlCl}_4]^- [\text{MgCl} \cdot 5\text{THF}]^+$ **F** was only studied as a solid powder. For **E**, the presence of phenyl groups gives rise to a variety of signals past 600 cm^{-1} apart for the usual Al-C

signal around 200 cm^{-1} . Compared to the APC spectrum in solution, the spectrum of the solid exhibits the same signals minus those of THF, displaying an overall tidier spectrum where $[\text{Mg}_2\text{Cl}_3\cdot 6\text{THF}]^+$ can still be observed at 241 cm^{-1} . The spectrum of $[\text{AlCl}_4]^- [\text{MgCl}\cdot 5\text{THF}]^+$ shows the presence of the $[\text{AlCl}_4]^-$ anion however no conclusions can be made on the cation apart from a small “bump” at 241 cm^{-1} that could be the result of some aggregation of the cation to the dinuclear structure (Figure 1.18).⁴¹

1.2.5.3. Crystallographic studies of magnesium battery electrolytes

Since the first release of an electrolyte’s crystal structure, it became popular to reveal the structure of new electrolyte systems whenever possible. Figures 1.19 shows a selection of structures which display similar solvent separated ion pair arrangements, including a magnesium chloride cation and an aluminium, boron or in some cases magnesium centred counter anion. In the presence of the $[\text{Mg}_2\text{Cl}_3\cdot 6\text{THF}]^+$ cation, the aluminium anions demonstrate that a variety of functional groups can be successfully attached to the aluminium atom. Such groups include exclusively chloride atoms (**G**),⁴⁶ aromatic rings (**H**),^{41,79} simple aliphatic groups (**I**),⁴⁶ phenolates (**J**)⁷⁸ and amides (**K**).^{115,116} In terms of application for batteries, all chloro-electrolytes, despite showing high oxidative stability, are very poorly soluble in ethereal solvents; those containing phenyl groups show good electrochemical properties, but have a nucleophilic nature which is not compatible with electrophilic cathode material such as sulphur cathodes; those with aliphatic groups such as ethyl are sulphur compatible, but with an average oxidative stability and electrochemical properties; phenolate improves the oxidative stability while keeping average electrochemical properties and finally amides give a non-nucleophilic electrolyte with enhanced oxidative stability and electrochemical properties, making them arguably the most suitable of those mentioned.

Not only aluminium was used as the Lewis acid stabiliser of Grignard and organomagnesium reagents, boron reagents have also proved to be good candidates to fulfil this task. Despite been studied to a far lesser extent a few crystal structures were obtained using aromatically substituted boron reagents $\text{B}(\text{Ar})_3$ (Ar = aryl group) with PhMgCl to form a magnesium borate containing the usual $[\text{Mg}_2\text{Cl}_3\cdot 6\text{THF}]^+$ cation

(Figure 1.19, L, M).^{117,118} Mohtadi and co-workers aimed to develop a chloride free electrolyte to overcome the corrosive nature of halogens by using borohydride reagents.¹¹⁷ However her attempts to obtain a representative structure of $\text{Mg}(\text{BH}_4)_2$ failed, hence she decided to use carboranes and Grignard reagents to get closer to her goal. This resulted in the formation of the magnesium magnesiate solvent separated ion pair with the anion bearing the two carborane clusters along with a chloride ion (Figure 1.19, N), she however characterised a chloride-free electrolyte earlier this year featuring the DME solvated Mg dication $[\text{Mg}\cdot 3\text{DME}]^{2+}$ with two carborane $[\text{CB}_{11}\text{H}_{12}]^-$ counter anions.^{119–121} Liao and co-workers studied a Lewis acid-free system using phenolate magnesium reagent (DTBP) MgCl (DTBP = 2,6-di-*tert*-butylphenolate) and MgCl_2 mixture at different ratios. The resulting electrolyte structure is another magnesium magnesiate with the $[(\text{DTBP})_3\text{Mg}]^-$ anion (Figure 1.19, O), this system has potential if a strong Lewis acid free electrolyte is required.¹²²

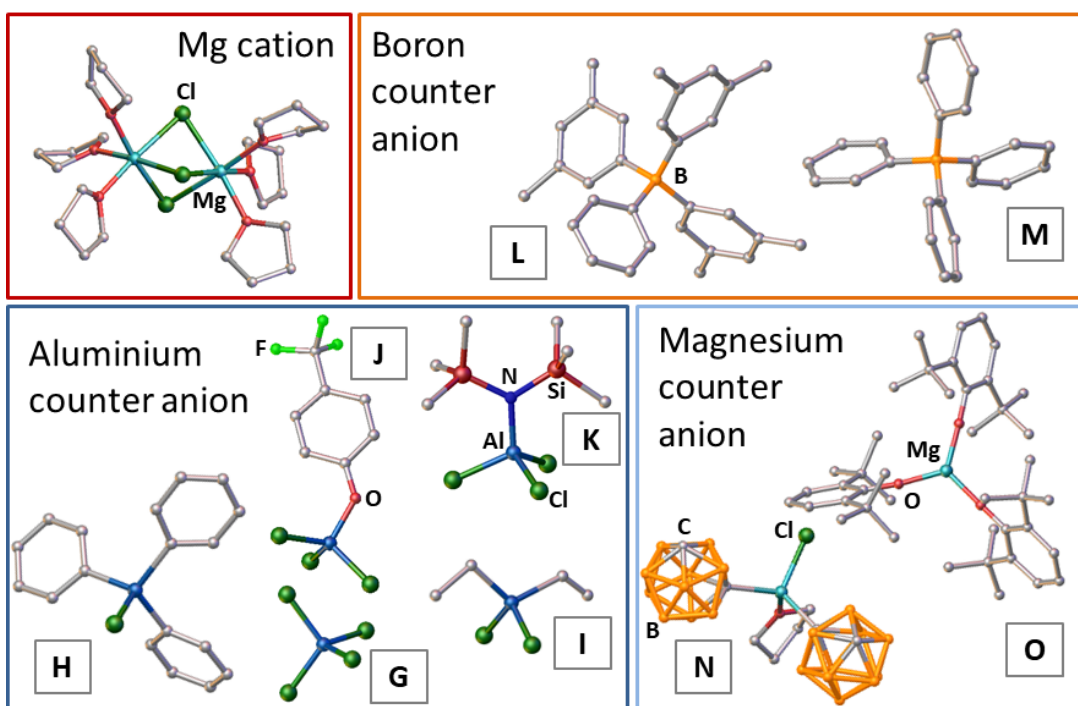


Figure 1.19: Molecular structures of separated ion pair containing the $[\text{Mg}_2\text{Cl}_3\cdot 6\text{THF}]^+$ cation and different aluminium (G-K), boron (L, M) and magnesium (N, O) counter anions.

Li and co-workers studied the behaviour of these electrolytes in DME instead of THF, in addition to their suitable electrochemical results they recently identified the structure which contains the magnesium chloride dication $[\text{Mg}_2\text{Cl}_2\cdot 4\text{DME}]^{2+}$ with two

equivalents of the classical counter anions $[\text{AlCl}_4]^-$ or $[\text{EtAlCl}_3]^-$ (Figure 1.20, **P** and **Q**). This is an example of the effect of the donor solvent on the electrolyte structure and especially on the magnesium chloride cation which has so far been seen essentially in the $[\text{Mg}_2\text{Cl}_3]^+$ form.⁴⁴

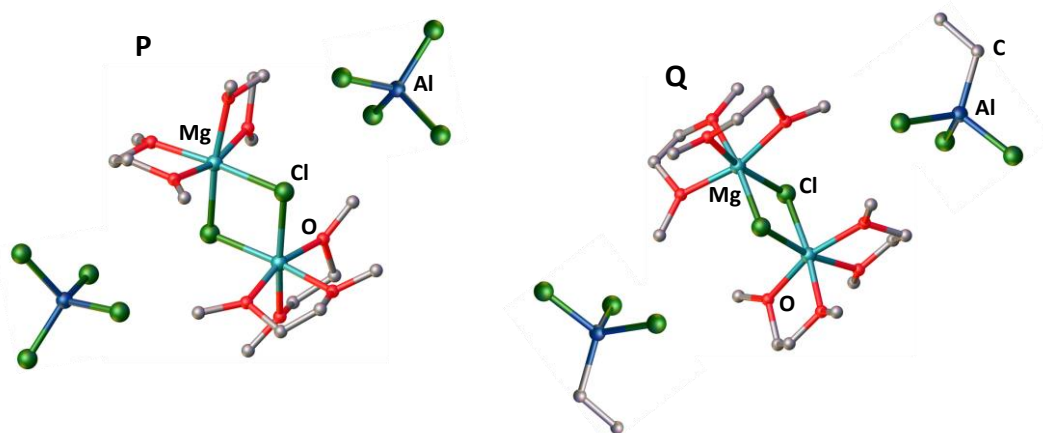


Figure 1.20: Molecular structure of electrolytes containing the $[\text{Mg}_2\text{Cl}_2\cdot 4\text{DME}]^{2+}$ dication and two $[\text{AlCl}_4]^-$, **P** and $[\text{EtAlCl}_3]^-$, **Q** counter anions.

1.2.5.4. Electrochemistry of magnesium aluminate electrolytes

This section summarises the electrochemical behaviour of magnesium aluminate electrolytes. Most experimental studies are performed using two types of cells; a three electrode electrochemical cell or a prototype battery cell. Often the three electrodes of choice in the electrochemical cell are: Mg metal as both the counter and reference electrodes; then either Pt, Al, Ni, Cu, glassy carbon or stainless steel as the working electrode (Figure 1.21a). For the prototype battery cell, it is possible to find it under different forms, a commonly used piece of equipment for the purpose of rechargeable battery research is the Swagelok[®] cell as showed in Figure 1.21b. Another widely used substitute is the coin cell which is constructed the same way as the commercially available button batteries.

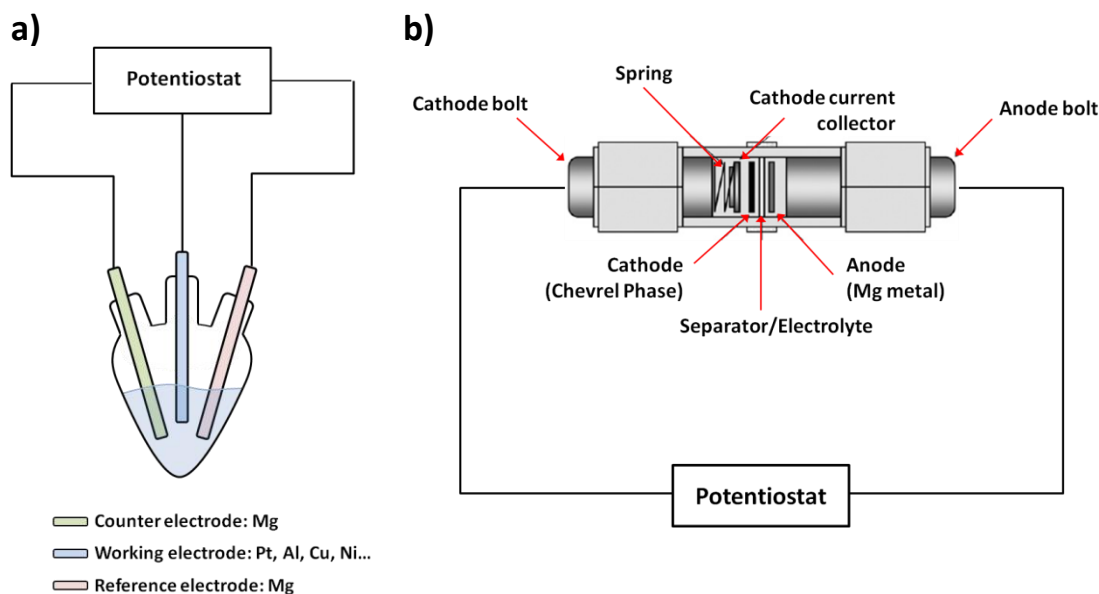


Figure 1.21: Diagrams of **a)** a three electrode electrochemical cell; **b)** a Swagelok battery cell.

Using a three electrode electrochemical cell is interesting for studying the ability of the electrolyte to be reversibly deposited on the electrodes, and also indicates at what voltage the electrolyte starts to decompose. These features can be easily identified by performing a cyclic voltammetric experiment, which measures the current response as a function of applied voltage. The voltage range at which the electrolyte can cycle between without decomposing is known as the electrochemical window. In the example taken from a publication by Aurbach et al., shown in Figure 1.22a, two cyclic voltammograms (CV) corresponding to two different electrolyte solutions are compared.¹²³ The butylethyl complex (BEC) corresponds to an $\text{EtAlCl}_2:\text{MgBu}_2$ mixture in a 1:2 ratio and was used in the first battery prototype. The APC corresponds to a $\text{AlCl}_3:\text{PhMgCl}$ mixture in a 1:2 ratio, for this compound the active species was characterised by X-ray crystallography as $[\text{AlPh}_4]^- [\text{Mg}_2\text{Cl}_3 \cdot 6\text{THF}]^+$ which was previously introduced in section 1.2.5.2. Both CVs show different behaviour depending on the choice of electrolyte, the APC has a smaller polarisation between the reduction peak (negative current) and the oxidation peak (positive current) known as the overpotential. A larger overpotential means that there is a larger excess of energy required by the electrochemical cell to allow the oxidation to take place; in a battery system such surplus of energy will be lost as heat and is hence undesired. After the oxidation peak appeared, the cyclic voltammetry experiment was left running at higher

potential until a new current signal is observed. This new signal is a response from the decomposition of the electrolyte which also creates a current. The APC electrolyte displays higher stability compared to the BEC electrolyte (3.5 V and 2.5 V respectively), this added to the lower overpotential means the APC is obviously a better candidate as an electrolyte for rechargeable Mg batteries and this can easily be determined only by comparing their CVs. The more desirable properties of the APC were attributed to the absence of β -hydrogen present in the alkyl analogue, removing the possibility of a β -hydrogens elimination reaction responsible for the low oxidative stability of the BEC.

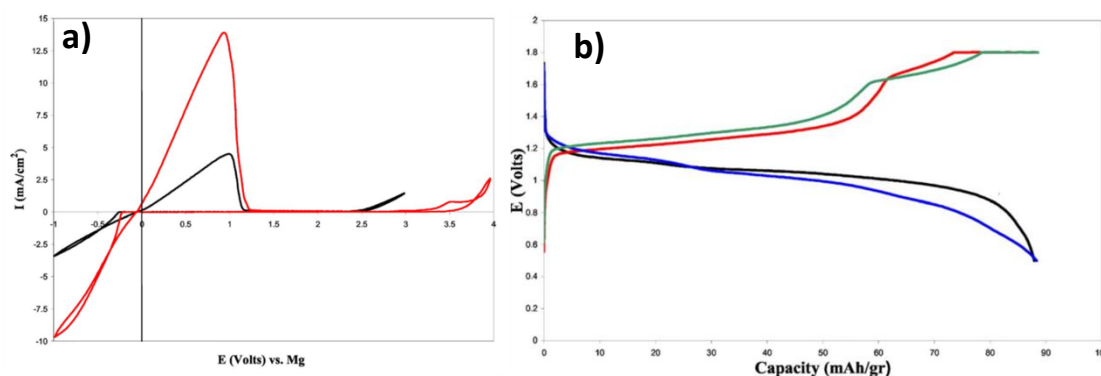


Figure 1.22: **a)** Cyclic voltammograms of a 0.25M BEC solution (black line) and a 0.4M APC solution (red line) measured with Pt electrodes at 25 mV/s; **b)** C/8 charge/discharge profiles of the 3rd (discharge in black, charge in red) and 94th (discharge in blue, charge in green) cycles for a battery with 0.4 M solution of APC in THF, a Mg anode and an Mo₆S₈ cathode.

After determining the ability of an electrolyte to reversibly deposit Mg and in what electrochemical window it can cycle without decomposition, it is necessary to determine if Mg²⁺ ions can be intercalated within an insertion cathode using this electrolyte. Figure 1.22b shows the galvanostatic experiment of a battery using APC as the electrolyte, Mg metal as the anode and the Chevrel phase as the cathode. This experiment allows measurement of the specific capacity this battery system can reach during both the discharge and the charge, also known as the charge/discharge profile of the battery. The rate of charge and discharge is fixed; C/8 means 8h is needed to either charge or discharge the battery, hence the specific capacity is expressed in mA.h per gram of cathode material (mA.h/g). Here the APC electrolyte shows a good compatibility over about 100 cycles with the Chevrel phase, it was also shown to be

compatible with a variety of other cathode materials making it a benchmark electrolyte in the testing of new cathodes.

1.2.5.5. Investigating the operating mechanism of chlorinated magnesium battery electrolyte

One principal aim of studying these electrolytes is to understand their operating mechanisms in the reversible magnesium deposition operation. Like for many chemical systems the attempts to discover its mechanism involves a variety of results covering many different approaches. In this situation a few different groups made efforts to discover the mechanism of these electrolytes, Aurbach observed the correlation between the cyclic efficiency (the ability of the electrolyte to deposit/dissolve) and the morphology of the deposited magnesium onto the electrode.⁹¹ Nakayama proposed a mechanism for magnesium deposition resulting from his studies using different spectroscopic methods, mainly multinuclear NMR spectroscopy (²⁷Al and ²⁵Mg NMR) and X-ray absorption fine structure measurements (Figure 1.23a).^{111,112} Kim investigated the chemical equilibrium, the deposition pathway and the electrolyte oxidation by mean of density functional theory calculations (DFT),¹²⁴ while Liu proposed another mechanism based on mild ionisation mass spectroscopy and ²⁵Mg NMR spectroscopy (Figure 1.23b).¹²⁵

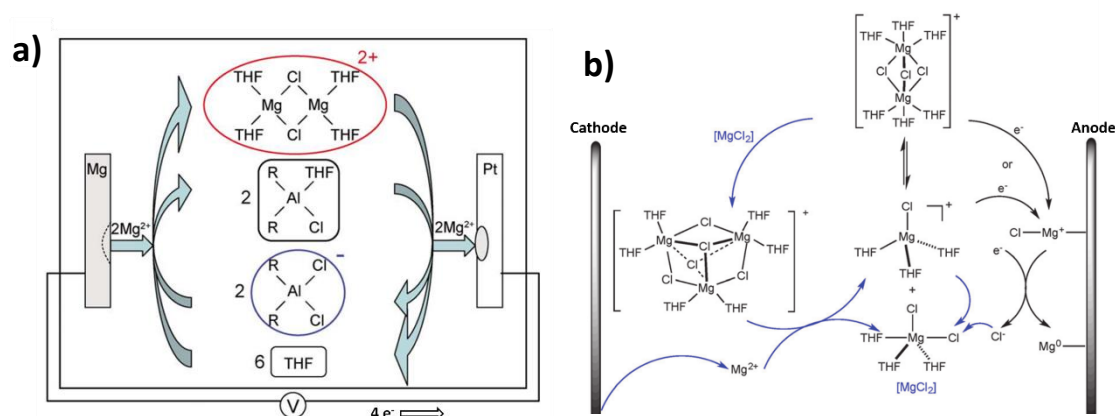


Figure 1.23: a) Proposed mechanism of Mg deposition by Nakamura b) Proposed mechanism of deposition/dissolution of Mg by Liu.

In his proposed mechanism, Nakayama suggested $[\text{Mg}_2\text{Cl}_2 \cdot 4\text{THF}]^{2+}$ as the magnesium intermediate to 2Mg^{2+} cations which then deposits onto the electrode as elemental

magnesium Mg^0 (Figure 1.23a). They claim that the neutral complex $R_2AlCl \cdot THF$ is essential for the reversibility of the reaction. This scheme is however slightly incomplete as it make no reference to the previously studied $[Mg_2Cl_3 \cdot 6THF]^+$ and $[MgCl \cdot 5THF]^+$ cations, which might involve more complicated redistributions. Liu did take into account the different aggregation states of magnesium chloride cations where he believes that the monomeric form $[MgCl]^+$ is the active species leading to magnesium deposition. He proposes that four major species are involved in the process, $[Mg_2Cl_3 \cdot 6THF]^+$, $[Mg_3Cl_5 \cdot 6THF]^+$, $[MgCl \cdot 3 \cdot 5THF]^+$ and $MgCl_2 \cdot nTHF$ ($n=0-4$) all existing in a complicated equilibrium (Figure 1.23b).¹²⁵

1.2.6. Non-corrosive, non-chlorinated magnesium electrolytes

Referencing most of the characterised magnesium electrolytes mentioned above, a recent study suggested that a high content of chloride ions is responsible for the corrosion of battery components made of non-noble metals.⁹⁵ Prospecting for future commercial electrolytes, the preparation of non-corrosive electrolytes is essential in terms of safety and in the making of durable batteries. This issue has raised a lot of effort in the preparation of less or non-corrosive electrolytes by reducing or totally removing the chloride ions from the electrolyte composition.

Preliminary studies by Muldoon et al. propose to make an electrolyte analogous to $[BPh_4]^- [Mg_2Cl_3 \cdot 6THF]^+$ but with a “naked” magnesium dication instead. This could be achieved by reacting $MgPh_2$ with BPh_3 in THF. The resulting solid was poorly soluble in THF, and was recrystallised in acetone to yield $[Mg \cdot 6(acetone)]^{2+} 2[BPh_4]^-$ but displayed no activity as an electrolyte in an Mg battery.⁹⁵ Bartlett et al., instead of completely removing the chloride atoms, studied how reducing the amount of chloride ions affects the corrosion level of the electrolytic mixture (Figure 1.24).¹²⁶ They showed that a mixture of $Al(OPh)_3 \cdot PhMgCl$ displays no obvious corrosion to a stainless steel working electrode after cycling during a cyclic voltammetry experiment. In comparison, using an $AlCl_3 \cdot 2PhMgCl$ mixture as it is, known as the APC, shows a high level of corrosion to stainless steel. It is worth noting that the active electrolytic species from the $Al(OPh)_3 \cdot PhMgCl$ was not characterised by X-Ray crystallography hence the composition of either the anion or the cation is not known.

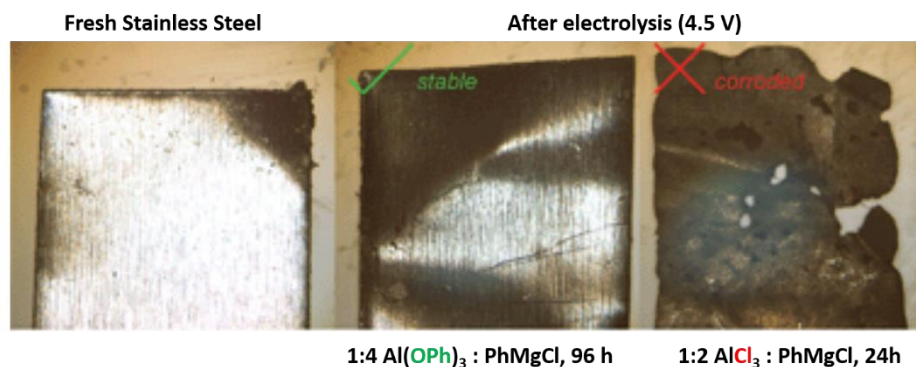


Figure 1.24: Images of stainless steel sheets after electrolysis at 4.5 V using different magnesium aluminate electrolytes.

So far one of the most successful electrolytes possessing no chlorides was developed by Mohtadi et al. This electrolyte was characterised by X-ray crystallography, showing that it possesses a naked magnesium dication $[\text{Mg}\cdot 3\text{DME}]^{2+}$ counterbalanced by two carborane anions $[\text{CB}_{11}\text{H}_{12}]^{-}$, **P**. This electrolyte exhibits good solubility in ethereal solvents of the glyme family and its electrochemical properties are comparable to the APC electrolyte (Figure 1.25).¹²¹

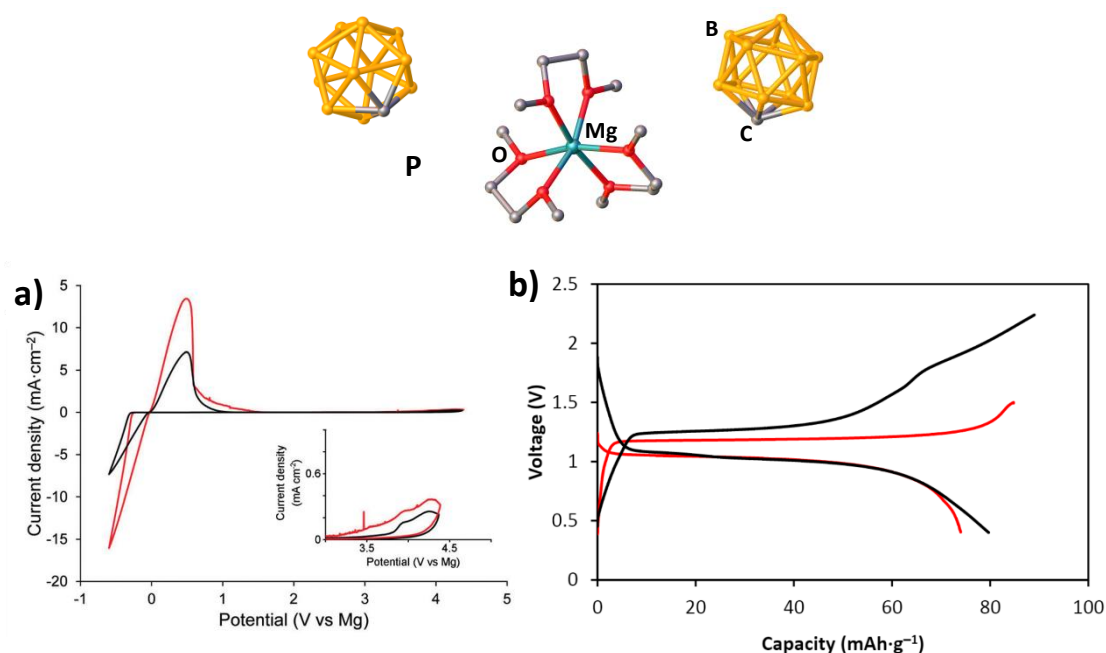


Figure 1.25: Molecular structure of $[\text{Mg}\cdot 3\text{DME}]^{2+} 2[\text{CB}_{11}\text{H}_{12}]^{-}$, **P** (top); **a**) CV of **P** in triglyme (red line) and tetraglyme (black line) using a Pt working electrode at 5 mV/s; **b**) Comparison of the charge/discharge profile between a battery using APC (red curves) and **P** (black curves) as the electrolytes, a Mg anode and the Chevrel phase as the cathode.

Currently, researchers continue investing their efforts in developing new chloro-free compounds displaying good electrolytic properties to propose a variety in choice of non-corrosive electrolyte in Mg batteries. More of such compounds are introduced in this thesis in Section 4.1. of Chapter 4.

- 1 T. Rathman and J. A. Schwindeman, *Org. Process Res. Dev.*, 2014, **18**, 1192–1210.
- 2 H. D. Yoo, I. Shterenberg, Y. Gofer, G. Gershinsky, N. Pour and D. Aurbach, *Energy Environ. Sci.*, 2013, **6**, 2265–2279.
- 3 R. B. Cole, *J. Mass Spectrom.*, 2000, **35**, 763–772.
- 4 A. Banks, *J. Chem. Educ.*, 1991, **68**, 196.
- 5 J. St. Peter, *J. Chem. Educ.*, 1942, **19**, 556–562.
- 6 S. L. Volpe, *Adv. Nutr. An Int. Rev. J.*, 2013, **4**, 378S–383S.
- 7 D. Seyferth, *Organometallics*, 2009, **28**, 1598–1605.
- 8 J. Muldoon, C. B. Bucur and T. Gregory, *Chem. Rev.*, 2014, **114**, 11683–11720.
- 9 P. Saha, M. K. Datta, O. I. Velikokhatnyi, A. Manivannan, D. Alman and P. N. Kumta, *Prog. Mater. Sci.*, 2014, **66**, 1–86.
- 10 P. E. Rakita, *Chlorinated paraffins*, John Wiley & Sons, Inc., Hoboken, NJ, USA, 2005.
- 11 L. Boymond, M. Rottländer, G. Cahiez and P. Knochel, *Angew. Chem. Int. Ed.*, 1998, **37**, 1701–1703.
- 12 P. Knochel, W. Dohle, N. Gommermann, F. F. Kneisel, F. Kopp, T. Korn, I. Sapountzis and V. A. Vu, *Angew. Chem. Int. Ed.*, 2003, **42**, 4302–4320.
- 13 F. M. Piller, P. Appukkuttan, A. Gavryushin, M. Helm and P. Knochel, *Angew. Chem. Int. Ed.*, 2008, **47**, 6802–6806.
- 14 A. Metzger, M. A. Schade and P. Knochel, *Org. Lett.*, 2008, **10**, 1107–1110.
- 15 A. Metzger, F. M. Piller and P. Knochel, *Chem. Commun.*, 2008, 5824–5826.
- 16 A. Krasovskiy, V. Malakhov, A. Gavryushin and P. Knochel, *Angew. Chem. Int. Ed.*, 2006, **45**, 6040–6044.
- 17 N. Boudet, S. Sase, P. Sinha, C. Y. Liu, A. Krasovskiy and P. Knochel, *J. Am. Chem. Soc.*, 2007, **129**, 12358–12359.
- 18 A. Krasovskiy and P. Knochel, *Angew. Chem. Int. Ed.*, 2004, **43**, 3333–3336.
- 19 P. García-Álvarez, D. V. Graham, E. Hevia, A. R. Kennedy, J. Klett, R. E. Mulvey, C. T. O'Hara and S. Weatherstone, *Angew. Chem. Int. Ed.*, 2008, **47**, 8079–8081.
- 20 Y. Kondo, M. Shilai, M. Uchiyama and T. Sakamoto, *J. Am. Chem. Soc.*, 1999, **121**, 3539–3540.

- 21 H. Naka, J. V Morey, J. Haywood, D. J. Eisler, M. McPartlin, F. García, H. Kudo, Y. Kondo, M. Uchiyama and A. E. H. Wheatley, *J. Am. Chem. Soc.*, 2008, **130**, 16193–16200.
- 22 J.-M. L'Helgoual'ch, G. Bentabed-Ababsa, F. Chevallier, M. Yonehara, M. Uchiyama, A. Derdour and F. Mongin, *Chem. Commun.*, 2008, 5375–5377.
- 23 A. Seggio, F. Chevallier, M. Vaultier and F. Mongin, *J. Org. Chem.*, 2007, **72**, 6602–6605.
- 24 E. Hevia, A. R. Kennedy, J. Klett and M. D. McCall, *Chem. Commun.*, 2009, 3240–3242.
- 25 A. Hernán-Gómez, T. D. Bradley, A. R. Kennedy, Z. Livingstone, S. D. Robertson and E. Hevia, *Chem. Commun.*, 2013, **49**, 8659–8661.
- 26 P. C. Andrikopoulos, D. R. Armstrong, H. R. L. Barley, W. Clegg, S. H. Dale, E. Hevia, G. W. Honeyman, A. R. Kennedy and R. E. Mulvey, *J. Am. Chem. Soc.*, 2005, **127**, 6184–6185.
- 27 W. Clegg, S. H. Dale, E. Hevia, G. W. Honeyman and R. E. Mulvey, *Angew. Chem. Int. Ed.*, 2006, **45**, 2370–2374.
- 28 W. Clegg, S. H. Dale, R. W. Harrington, E. Hevia, G. W. Honeyman and R. E. Mulvey, *Angew. Chem. Int. Ed.*, 2006, **45**, 2374–2377.
- 29 R. E. Mulvey, F. Mongin, M. Uchiyama and Y. Kondo, *Angew. Chem. Int. Ed.*, 2007, **46**, 3802–3824.
- 30 V. L. Blair, W. Clegg, B. Conway, E. Hevia, A. Kennedy, J. Klett, R. E. Mulvey and L. Russo, *Chem. Eur. J.*, 2008, **14**, 65–72.
- 31 H. R. L. Barley, W. Clegg, S. H. Dale, E. Hevia, G. W. Honeyman, A. R. Kennedy and R. E. Mulvey, *Angew. Chem. Int. Ed.*, 2005, **44**, 6018–6021.
- 32 S. Sakamoto, T. Imamoto and K. Yamaguchi, *Org. Lett.*, 2001, **3**, 1793–1795.
- 33 Y. Chai, H. Sun, J. Wan, Y. Pan and C. Sun, *Analyst*, 2011, **136**, 4667–4669.
- 34 B. Bogdanovic, N. Janke, C. Krüger, R. Mynott, K. Schlichte and U. Westeppe, *Angew. Chem. Int. Ed.*, 1985, **24**, 960–961.
- 35 J. C. Berthet, P. Thuéry and M. Ephritikhine, *Angew. Chem. Int. Ed.*, 2008, **47**, 5586–5589.
- 36 Y. Wang, B. Quillian, P. Wei, X.-J. Yang and G. H. Robinson, *Chem. Commun.*, 2004, 2224–2225.

- 37 T. D. Blümke, W. Clegg, P. García-Alvarez, A. R. Kennedy, K. Koszinowski, M. D. McCall, L. Russo and E. Hevia, *Chem. Sci.*, 2014, **5**, 3552–3562.
- 38 S. Harder, F. Feil and T. Repo, *Chem. Eur. J.*, 2002, **8**, 1991–1999.
- 39 N. Strelsova, B. Bulychev, V. Belskii and O. Kireeva, *Zh. Obshch. Khim.*, 1991, **61**, 795–802.
- 40 P. Sobota, T. Phzibski, J. Utko and T. Lis, *Inorg. Chem.*, 1989, **28**, 2217–2219.
- 41 N. Pour, Y. Gofer, D. T. Major and D. Aurbach, *J. Am. Chem. Soc.*, 2011, **133**, 6270–6278.
- 42 R. B. Bedford, P. B. Brenner, E. Carter, P. M. Cogswell, M. F. Haddow, J. N. Harvey, D. M. Murphy, J. Nunn and C. H. Woodall, *Angew. Chem. Int. Ed.*, 2014, **53**, 1804–1808.
- 43 H. Eriksson, M. Rtendahl and M. Hå, *Organometallics*, 1996, **15**, 4823–4831.
- 44 Y. Cheng, R. M. Stolley, K. S. Han, Y. Shao, B. W. Arey, N. M. Washton, K. T. Mueller, M. L. Helm, V. L. Sprenkle, J. Liu and G. Li, *Phys. Chem. Chem. Phys.*, 2015, **17**, 13307–13314.
- 45 E. Solari, J. Hesschenbrouck, R. Scopelliti, C. Floriani and N. Re, *Angew. Chem. Int. Ed.*, 2001, **40**, 932–934.
- 46 Z. Zhao-Karger, J. E. Mueller, X. Zhao, O. Fuhr, T. Jacob and M. Fichtner, *RSC Adv.*, 2014, **4**, 26924–26927.
- 47 W. Zhang, J.-P. Hu, X.-F. Ding, Y.-J. Wu and Z.-W. Ye, *Inorg. Chem. Commun.*, 2003, **6**, 1185–1187.
- 48 J. Emsley, *Nature's building blocks: everything you need to know about the elements*, Oxford University Press, 2011.
- 49 J. Boor, *Ziegler-Natta catalysts and polymerizations*, Academic Press, 1979.
- 50 J. K. Groves, *Chem. Soc. Rev.*, 1972, **1**, 73–97.
- 51 L. C. Wieland, H. Deng, M. L. Snapper and A. H. Hoveyda, *J. Am. Chem. Soc.*, 2005, **127**, 15453–15456.
- 52 W. Nagata, M. Yoshioka and S. Hirai, *J. Am. Chem. Soc.*, 1972, **94**, 4635–4643.
- 53 S. Kawamura, K. Ishizuka, H. Takaya and M. Nakamura, *Chem. Commun.*, 2010, **46**, 6054–6056.
- 54 S. Kawamura, T. Kawabata, K. Ishizuka and M. Nakamura, *Chem. Commun.*, 2012, **48**, 9376–9378.

- 55 H. Minami, T. Saito, C. Wang and M. Uchiyama, *Angew. Chem. Int. Ed.*, 2015, **54**, 4665–4668.
- 56 T. Blümke, Y.-H. Chen, Z. Peng and P. Knochel, *Nat. Chem.*, 2010, **2**, 313–318.
- 57 S. Baba and E. I. Negishi, *J. Am. Chem. Soc.*, 1976, **98**, 6729–6731.
- 58 B. Liang, T. Novak, Z. Tan and E. I. Negishi, *J. Am. Chem. Soc.*, 2006, **128**, 2770–2771.
- 59 S. Kawamura, R. Agata and M. Nakamura, *Org. Chem. Front.*, 2015, **2**, 1053–1058.
- 60 S. H. Wunderlich and P. Knochel, *Angew. Chem. Int. Ed.*, 2009, **48**, 1501–1504.
- 61 A. Ecker, E. Weckert and H. Schnöckel, *Nature*, 1997, **387**, 379–381.
- 62 M. Veith, P. König, A. Rammo and V. Huch, *Angew. Chem. Int. Ed.*, 2005, **44**, 5968–5971.
- 63 N. C. Means, C. M. Means, S. G. Bott and J. L. Atwood, *Inorg. Chem.*, 1987, **26**, 1466–1468.
- 64 S. J. Bryan, W. Clegg, R. Snaith, K. Wade and E. H. Wong, *J. Chem. Soc., Chem. Commun.*, 1987, 1223–1224.
- 65 K. C. Williams and T. L. Brown, *J. Am. Chem. Soc.*, 1966, **88**, 5460–5465.
- 66 K. Maruoka, T. Itoh, M. Sakurai, K. Nonoshita and H. Yamamoto, *J. Am. Chem. Soc.*, 1988, **110**, 3588–3597.
- 67 T. Gelbrich, J. Sieler and U. Dümichen, *Zeitschrift für Krist.*, 2000, **215**, 127–130.
- 68 F. Scholz, D. Himmel, H. Scherer and I. Krossing, *Chem. Eur. J.*, 2013, **19**, 109–116.
- 69 I. Krossing, A. Bihlmeier, I. Raabe and N. Trapp, *Angew. Chem. Int. Ed.*, 2003, **42**, 1531–1534.
- 70 F. Scholz, D. Himmel, L. Eisele, W. Unkrig and I. Krossing, *Angew. Chem. Int. Ed.*, 2014, **53**, 1689–1692.
- 71 F. Scholz, D. Himmel, L. Eisele, W. Unkrig, A. Martens, P. Schlüter and I. Krossing, *Chem. Eur. J.*, 2015, **21**, 7489–7502.
- 72 F. Scholz, D. Himmel, F. W. Heinemann, P. v R. Schleyer, K. Meyer and I. Krossing, *Science*, 2013, **341**, 62–64.
- 73 I. Krossing, *Chem. Eur. J.*, 2001, **7**, 490–502.
- 74 I. Krossing and I. Raabe, *Angew. Chem. Int. Ed.*, 2004, **43**, 2066–2090.

- 75 J. F. Kögel, X. Xie, E. Baal, D. Gesevičius, B. Oelkers, B. Kovačević and J. Sundermeyer, *Chem. Eur. J.*, 2014, **20**, 7670–7685.
- 76 C. Temple, A. Jabri, P. Crewdson, S. Gambarotta, I. Korobkov and R. Duchateau, *Angew. Chem. Int. Ed.*, 2006, **45**, 7050–7053.
- 77 C.-C. Chang, M.-D. Li, M. Y. Chiang, S.-M. Peng, Y. Wang and G.-H. Lee, *Inorg. Chem.*, 1997, **36**, 1955–1960.
- 78 E. G. Nelson, J. W. Kampf and B. M. Bartlett, *Chem. Commun.*, 2014, **50**, 5193–5195.
- 79 T. Liu, Y. Shao, G. Li, M. Gu, J. Hu, S. Xu, Z. Nie, X. Chen, C. Wang and J. Liu, *J. Mater. Chem. A*, 2014, **2**, 3430–3438.
- 80 M. Uchiyama, H. Naka, Y. Matsumoto and T. Ohwada, *J. Am. Chem. Soc.*, 2004, **126**, 10526–10527.
- 81 R. E. Mulvey, D. R. Armstrong, B. Conway, E. Crosbie, A. R. Kennedy and S. D. Robertson, *Inorg. Chem.*, 2011, **50**, 12241–12251.
- 82 T. Klatt, K. Groll and P. Knochel, *Chem. Commun.*, 2013, **49**, 6953.
- 83 D. R. Armstrong, E. Crosbie, E. Hevia, R. E. Mulvey, D. L. Ramsay and S. D. Robertson, *Chem. Sci.*, 2014, **5**, 3031–3045.
- 84 M. Armand and J.-M. Tarascon, *Nature*, 2008, **451**, 652–657.
- 85 R. Van Noorden, *Nature*, 2014, **507**, 26–28.
- 86 D. Larcher and J.-M. Tarascon, *Nat. Chem.*, 2015, **7**, 19–29.
- 87 D. Lin, Y. Liu and Y. Cui, *Nat. Nanotechnol.*, 2017, **12**, 194–206.
- 88 X. B. Cheng, R. Zhang, C. Z. Zhao and Q. Zhang, *Chem. Rev.*, 2017, **117**, 10403–10473.
- 89 W. Li, B. Song and A. Manthiram, *Chem. Soc. Rev.*, 2017, **46**, 3006–3059.
- 90 A. Kraytsberg and Y. Ein-Eli, *Adv. Energy Mater.*, 2012, **2**, 922–939.
- 91 N. Nitta, F. Wu, J. T. Lee and G. Yushin, *Mater. Today*, 2015, **18**, 252–264.
- 92 Z. Ma, X. Yuan, L. Li, Z.-F. Ma, D. P. Wilkinson, L. Zhang and J. Zhang, *Energy Environ. Sci.*, 2015, **8**, 2144–2198.
- 93 D. Aurbach, Z. Lu, A. Schechter, Y. Gofer, H. Gizbar, R. Turgeman, Y. Cohen, M. Moshkovich and E. Levi, *Nature*, 2000, **407**, 724–727.
- 94 F. Wu and G. Yushin, *Energy Environ. Sci.*, 2017, **10**, 435–459.
- 95 J. Muldoon, C. B. Bucur, A. G. Oliver, J. Zajicek, G. D. Allred and W. C. Boggess, *Energy Environ. Sci.*, 2013, **6**, 482–487.

- 96 R. Mohtadi and F. Mizuno, *Beilstein J. Nanotechnol.*, 2014, **5**, 1291–1311.
- 97 J. Muldoon, C. B. Bucur and T. Gregory, *Angew. Chem. Int. Ed.*, 2017, **56**, 12064–12084.
- 98 O. R. Brown and R. McIntyre, *Electrochim. Acta*, 1985, **30**, 627–633.
- 99 Z. Lu, A. Schechter, M. Moshkovich and D. Aurbach, *J. Electroanal. Chem.*, 1999, **466**, 203–217.
- 100 E. Peled and H. Straze, *J. Electrochem. Soc.*, 1977, **124**, 1030–1035.
- 101 C. Liebenow, *J. Appl. Electrochem.*, 1997, **27**, 221–225.
- 102 T. D. Gregory, R. J. Hoffman and R. C. Winterton, *J. Electrochem. Soc.*, 1990, **137**, 775–780.
- 103 D. Aurbach, A. Schechter, M. Moshkovich and Y. Cohen, *J. Electrochem. Soc.*, 2001, **148**, A1004–A1014.
- 104 D. Aurbach, R. Turgeman, O. Chusid and Y. Gofer, *Electrochem. Commun.*, 2001, **3**, 252–261.
- 105 D. Aurbach, H. Gizbar, A. Schechter, O. Chusid, H. E. Gottlieb, Y. Gofer and I. Goldberg, *J. Electrochem. Soc.*, 2002, **149**, A115–A121.
- 106 Y. Gofer, R. Turgeman, H. Cohen and D. Aurbach, *Langmuir*, 2003, **19**, 2344–2348.
- 107 Y. NuLi, J. Yang, Y. Li and J. Wang, *Chem. Commun.*, 2010, **46**, 3794–3796.
- 108 R. Zhang, C. Ling and F. Mizuno, *Chem. Commun.*, 2015, **51**, 1487–1490.
- 109 S. Su, Z. Huang, Y. NuLi, F. Tuerxun, J. Yang and J. Wang, *Chem. Commun.*, 2015, **51**, 2641–2644.
- 110 H. Gizbar, Y. Vestfrid, O. Chusid, Y. Gofer, H. E. Gottlieb, V. Marks and D. Aurbach, *Organometallics*, 2004, **23**, 3826–3831.
- 111 R. Benn, H. Lehmkuhl, K. Mehler and A. Ruffńska, *Angew. Chem. Int. Ed.*, 1984, **23**, 534–535.
- 112 Y. Nakayama, Y. Kudo, H. Oki, K. Yamamoto, Y. Kitajima and K. Noda, *J. Electrochem. Soc.*, 2008, **155**, A754–A759.
- 113 Y. Gofer, O. Chusid, H. Gizbar, Y. Vestfrid, H. E. Gottlieb, V. Marks and D. Aurbach, *Electrochem. Solid-State Lett.*, 2006, **9**, A257–A260.
- 114 Y. Vestfried, O. Chusid, Y. Goffer, P. Aped and D. Aurbach, *Organometallics*, 2007, **26**, 3130–3137.

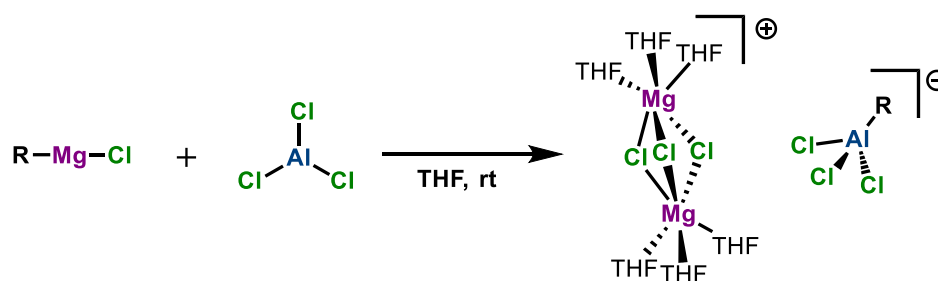
- 115 Z. Zhao-Karger, X. Zhao, O. Fuhr and M. Fichtner, *RSC Adv.*, 2013, **3**, 16330–16335.
- 116 H. S. Kim, T. S. Arthur, G. D. Allred, J. Zajicek, J. G. Newman, A. E. Rodnyansky, A. G. Oliver, W. C. Boggess and J. Muldoon, *Nat. Commun.*, 2011, **2**, 1–6.
- 117 Y.-S. Guo, F. Zhang, J. Yang, F.-F. Wang, Y. NuLi and S.-I. Hirano, *Energy Environ. Sci.*, 2012, **5**, 9100–9106.
- 118 J. Muldoon, C. B. Bucur, A. G. Oliver, T. Sugimoto, M. Matsui, H. S. Kim, G. D. Allred, J. Zajicek and Y. Kotani, *Energy Environ. Sci.*, 2012, **5**, 5941–5950.
- 119 T. J. Carter, R. Mohtadi, T. S. Arthur, F. Mizuno, R. Zhang, S. Shirai and J. W. Kampf, *Angew. Chem. Int. Ed.*, 2014, **53**, 3173–3177.
- 120 O. Tutusaus and R. Mohtadi, *ChemElectroChem*, 2015, **2**, 51–57.
- 121 O. Tutusaus, R. Mohtadi, T. S. Arthur, F. Mizuno, E. G. Nelson and Y. V. Sevryugina, *Angew. Chem. Int. Ed.*, 2015, **54**, 7900–7904.
- 122 B. Pan, J. Zhang, J. Huang, J. T. J. Vaughey, L. Zhang, S.-D. Han, A. K. Burrell, Z. Zhang and C. Liao, *Chem. Commun.*, 2015, **51**, 6214–6217.
- 123 O. Mizrahi, N. Amir, E. Pollak, O. Chusid, V. Marks, H. Gottlieb, L. Larush, E. Zinigrad and D. Aurbach, *J. Electrochem. Soc.*, 2008, **155**, A103–A109.
- 124 D. Y. Kim, Y. Lim, B. Roy, Y.-G. Ryu and S.-S. Lee, *Phys. Chem. Chem. Phys.*, 2014, **16**, 25789–25798.
- 125 T. Liu, J. T. Cox, D. Hu, X. Deng, J. Hu, M. Y. Hu, J. Xiao, Y. Shao, K. Tang and J. Liu, *Chem. Commun.*, 2015, **51**, 2312–2315.
- 126 E. G. Nelson, S. I. Brody, J. W. Kampf and B. M. Bartlett, *J. Mater. Chem. A*, 2014, **2**, 18194–18198.

Chapter 2: Synthesis, Structure and Solution Characterisation of Different Magnesium Cation Aggregates

This chapter presents the results of a synthetic study performed for the development of new magnesium amidohaloaluminate complexes, akin to those described in Chapter 1 and having potential for use in the area of rechargeable battery electrolytes. These results comprise in the first place the elaboration of a new, facile, sturdy method to design customised electrolytes, and then the effect of donor ligands on the aggregation state of the magnesium cation. The characterisation of these species in both solid state and solution was carried out by X-Ray crystallography, electrospray ionisation mass spectrometry, Raman spectroscopy and NMR spectroscopy.

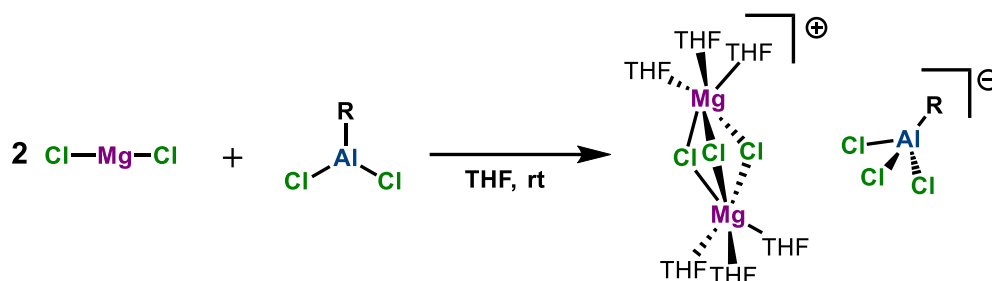
2.1. Introduction

The early preparation of magnesium aluminate electrolytes was based on the Al to Mg reagents stoichiometry giving the best electrochemical properties, usually obtained with a 2:1 ratio.^{1,2} It was only later, when the first relevant crystal structure of a magnesium aluminate species $[\text{EtAlCl}_3]^- [\text{Mg}_2(\mu_2\text{-Cl})_3 \cdot 6\text{THF}]^+$ was published that a better, more rational route was sought. Most methods involve transmetallation of an organic group from the magnesium to the aluminium using Grignard or organomagnesium reagents (RMgCl or R_2Mg) and aluminium trichloride (Scheme 2.1). This method is efficient when using commercially available reagents with a variety of R groups such as phenyl, ethyl, phenolate, amide and chloride. However the reaction's stoichiometry is hard to satisfy due to chloride rearrangements from one reagent to another.³⁻⁵



Scheme 2.1: Unbalanced equation of the preparation of magnesium aluminate electrolytes by transmetallation.

Liu and co-workers developed a cheaper, rational approach reacting MgCl_2 with commercially available aluminium reagents of the type RAlCl_2 or AlR_3 to form $[\text{R}_n\text{AlCl}_{4-n}]^- [\text{Mg}_2(\mu_2\text{-Cl})_3 \cdot 6\text{THF}]^+$ (Scheme 2.2, $\text{R} = \text{Et}, \text{Cl}$). Unfortunately no yields are reported so the efficiency of this route cannot be determined.⁶



Scheme 2.2: Equation of the rational preparation of magnesium aluminate electrolytes developed by Liu.

As mentioned in the previous chapter, the magnesium amidohaloaluminate electrolyte $[(\text{HMDS})\text{AlCl}_3]^- [\text{Mg}_2\text{Cl}_3 \cdot 6\text{THF}]^+$ (Figure 2.1) demonstrated the best properties; non-nucleophilic, high cyclic efficiency, high coulombic efficiency and high oxidative stability.^{7,8} The presence of the Al-N bond is speculated to be the main reason leading to the enhancement of these valuable properties, however it might be worth considering the effect of HMDS, which is known to lead to unusual properties from the presence of the bulky SiMe_3 moiety leading to slightly polarised bonds, increase of lipophilicity and a lack of β -hydrogen atoms increasing the oxidative stability at higher voltages.⁴

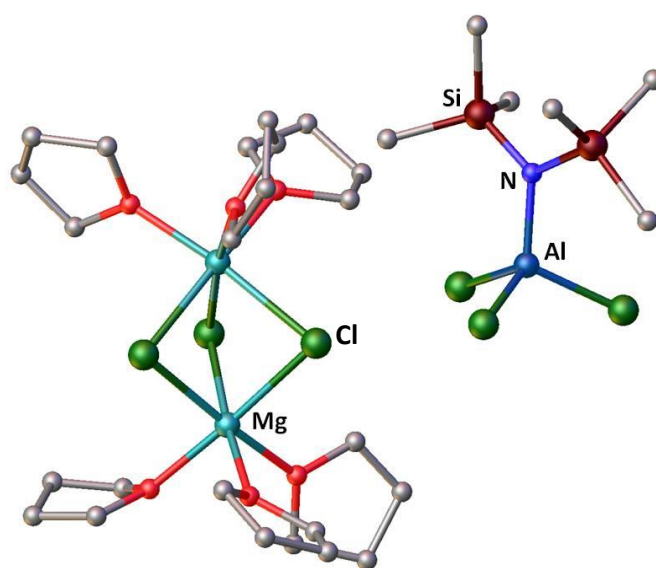


Figure 2.1: Molecular structure of $[(\text{HMDS})\text{AlCl}_3]^- [\text{Mg}_2\text{Cl}_3 \cdot 6\text{THF}]^+$.

As mentioned in Chapter 1 Section 1.2.5 the characterisation of these species in solution is a difficult task due to a lack of diagnostic NMR observable groups in the Mg centred cation. Raman spectroscopy was thought to be a useful technique by Aurbach who attempted to compare their mononuclear all chloro magnesium aluminate compound $[\text{AlCl}_4]^- [\text{MgCl} \cdot 5\text{THF}]^+$ with dinuclear APC $[\text{AlPh}_4]^- [\text{Mg}_2\text{Cl}_3 \cdot 6\text{THF}]^+$ and started to build a library for future reference use.

2.2. A note to the reader

The reader must be aware that this chapter is closely related to Chapter 3 which presents the electrolytic performance of the compounds introduced herein. The original series of compounds whose synthesis is presented encountered obstacles during the battery performance tests. More precisely they were subject to early decomposition during the running of the battery, requiring redesign of these compounds to tackle the decomposition. As a result some cross references with some sections of Chapter 3 will be added in order to help the reader to understand the reason behind certain plans of action.

For ease of discussion, the synthesis supported by molecular structures to confirm identity of target compounds will be presented first, followed by a comparison of their solid state structures and then a comparison of their solution characterisation.

2.3. Synthesis of new magnesium amidohaloaluminates

The initial aim of this project was to reproduce the preparation of the previously reported separated ion pair magnesium amidohaloaluminates $[(\text{R}_2\text{N})\text{AlCl}_3]^- [\text{Mg}_2\text{Cl}_3 \cdot 6\text{THF}]^+$ using a different amide. The amide of choice was the non-commercially available 2,6-diisopropyl-*N*-(trimethylsilyl)aniline (DippNHSiMe₃ Dipp = 2,6-diisopropylphenyl), Figure 2.2. The amine was prepared in the lab according to the literature.⁹ The reason for this choice derives from the presence of a trimethylsilyl arm which hopefully provides the desirable properties introduced earlier

in the HMDS analogue, and combined them with a sterically demanding aryl group, another intensely studied group, onto the aluminium anion.⁴

Preliminary battery tests using magnesium aluminates based with this amine as electrolyte showed their compatibility with a rechargeable magnesium battery cell; however undesired decomposition of these electrolytes was observed. In the necessity to tackle the decomposition the use of other amines was considered instead; 2,6-dimethyl-*N*-(trimethylsilyl)aniline (DmpNHSiMe₃, Dmp = 2,6-dimethylphenyl) and *N*-(trimethylsilyl)aniline (PhNHSiMe₃), two less bulky versions of DippNHSiMe₃ where the two isopropyl groups are replaced by methyl groups or hydrogen atoms, respectively. The bulk of the amide was considered one of the main reason for the decomposition, hence the reason behind using a similar amine with a reduced steric hindrance. The second source of the decomposition was blamed on the presence of an N-SiMe₃ bond which is known to be easily cleavable, therefore another amine without such a bond was sought. In this study the choice was 2,2,6,6-tetramethylpiperidine (TMPH, Figure 2.2), a secondary amine widely employed due to the bulk of four methyl groups protecting the nitrogen atom, lowering its nucleophilicity but increasing its basicity. Originally, all reactions were first performed using DippNHSiMe₃ as the main amine to try and promote this previously designed amine in a new area of chemistry.

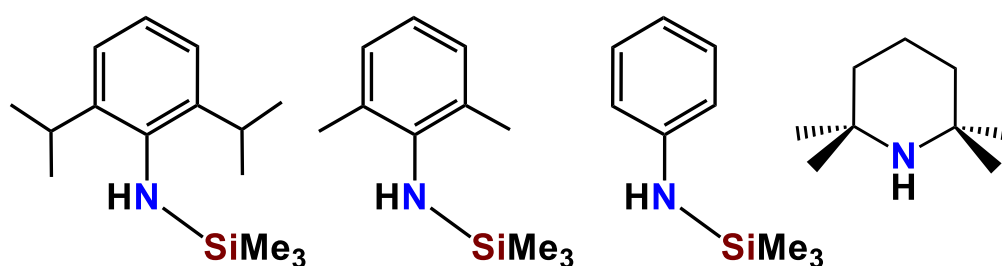
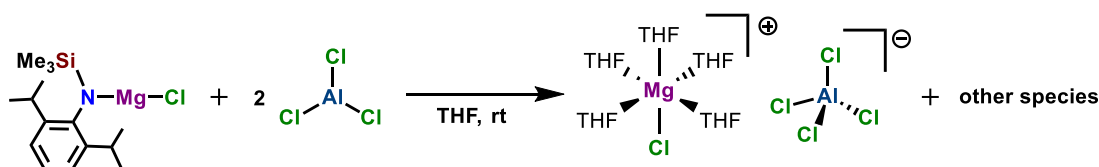


Figure 2.2: Amines used for the magnesium aluminate electrolyte study.

2.3.1. Synthesis of magnesium aluminate compounds possessing a dinuclear cation

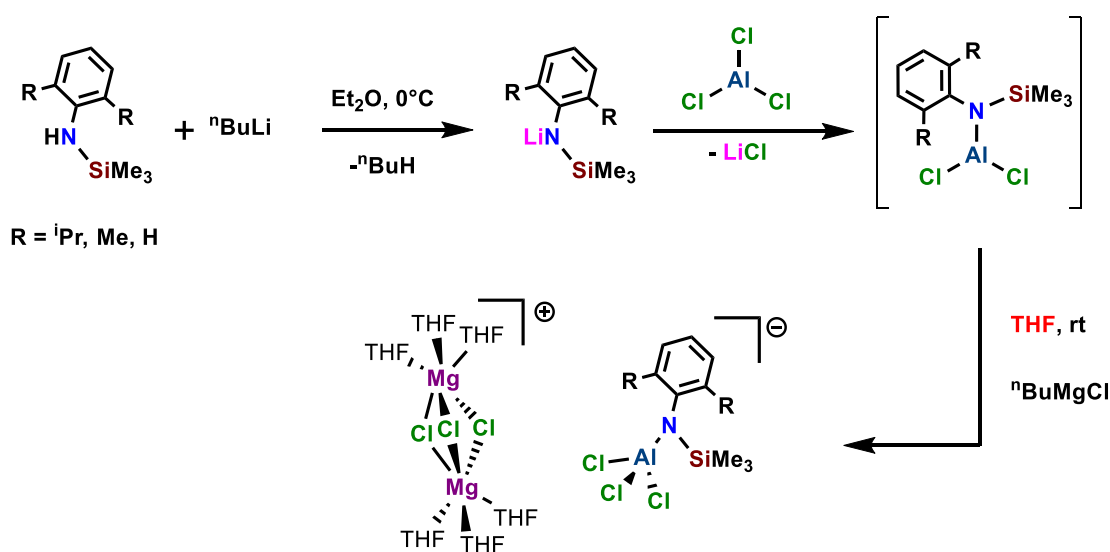
The first step was to reproduce the transmetallation reaction used in the literature to obtain the classical solvent-separated ion pair equivalent to $[(\text{HMDS})\text{AlCl}_3]^- [\text{Mg}_2\text{Cl}_3 \cdot 6\text{THF}]^+$ with DippNHSiMe_3 . Starting by the preparation of the starting materials, the corresponding magnesium bisamide $[(\text{Dipp})(\text{SiMe}_3)\text{N}]_2\text{Mg}$ and Hauser base $[(\text{Dipp})(\text{SiMe}_3)\text{N}]\text{MgCl}$ were prepared by refluxing a mixture of DippNHSiMe_3 with ${}^n\text{Bu}_2\text{Mg}$ (2:1) or ${}^n\text{BuMgCl}$ (1:1) in hexane for 5h. The bisamide magnesium species was previously synthesised and structurally characterised by Ruhlandt-Senge et al.¹⁰ The hexane was replaced by THF and 2 equivalents of AlCl_3 (according to the literature a 1:2 ratio gives better electrochemical properties)⁷ were added to the solution which was stirred for 6h at room temperature. After slow diffusion of hexane a crop of crystals was observed. Unfortunately unit cell measurements revealed the formation of the previously reported “all-chloro complex” by Aurbach, $[\text{AlCl}_4]^- [\text{MgCl} \cdot 5\text{THF}]^+$.⁴ The increased steric bulk of the amine in comparison to the previous literature examples is a potential reason for the unsuccessful transmetallation reaction.



Scheme 2.3: Attempt of the transmetallation reaction for the preparation of magnesium amidohaloaluminate electrolytes.

Inspired by Liu’s approach of reacting commercially available organoaluminium reagents such as EtAlCl_2 or Et_2AlCl with MgCl_2 in THF, $(\text{R}_2\text{N})\text{AlCl}_2$ which is presumably found under its dimeric form $[(\text{Dipp})(\text{SiMe}_3)\text{N}]\text{AlCl}_2$ according to the literature was prepared by reacting the corresponding lithiated amide with one equivalent of AlCl_3 in diethyl ether at 0°C .¹¹ After filtering off the white suspension (LiCl), the ether was replaced by THF and the magnesium reagent, either MgCl_2 , ${}^n\text{BuMgCl}$ or ${}^n\text{Bu}_2\text{Mg}$ was added to the solution at room temperature in a 1:1 ratio

(Scheme 2.4). Using MgCl_2 , a crop of crystals was obtained in THF at -15°C , but using ${}^n\text{BuMgCl}$ or ${}^n\text{Bu}_2\text{Mg}$ required slow diffusion of hexane into the THF solution. The crystals obtained using MgCl_2 were of too poor quality to diffract sufficiently, and the ${}^1\text{H}$ NMR spectrum of the batch displayed resonances corresponding to THF only, suggesting the product is unreacted MgCl_2 . Unlike with MgCl_2 , the X-ray crystallography showed that the crystals obtained using ${}^n\text{BuMgCl}$ or ${}^n\text{Bu}_2\text{Mg}$ corresponded to the targeted product $[(\text{Dipp})(\text{SiMe}_3)\text{NAlCl}_3]^- [\text{Mg}_2\text{Cl}_3 \cdot 6\text{THF}]^+$, **1**, (Figure 2.3). The yield of the reaction is higher when ${}^n\text{BuMgCl}$ is used over ${}^n\text{Bu}_2\text{Mg}$, an observation that can be related to the presence of an extra chloride atom in the reaction which seems to be the limiting element using this pathway. The recovered yield was 44% out of 50% possible due to the Al/Mg 1:1 ratio. Surprisingly, a 1:2 ratio of Al to Mg using similar conditions did not lead to higher yields.



Scheme 2.4: New preparation route for the synthesis of magnesium amidohaloaluminate electrolytes using ArNHSiMe_3 as the amine of choice.

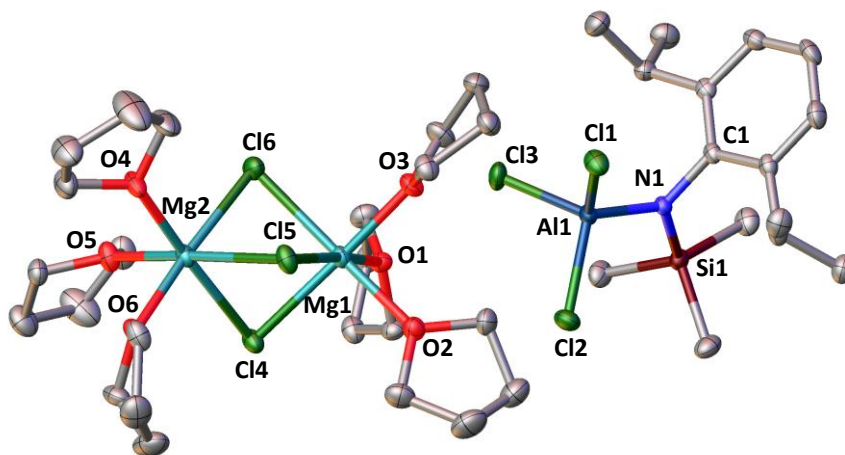


Figure 2.3: Molecular structure of **1** [(Dipp)(SiMe₃)AlCl₃]⁻ [Mg₂Cl₃·6THF]⁺. Hydrogen atoms and disorder present on one of the THF units are omitted for clarity. Thermal ellipsoids are drawn at the 50 % probability level. Selected bond distances (Å) and angles (°): Al1-N1 1.8172(16); Al-Cl 2.1571; N1-C1 1.441(2); N1-Si1 1.7343(16); Mg-Cl 2.5027; Mg1-Mg2 3.1494(9); Mg-O 2.0808; Al1-N1-C1 121.41(12); Al1-N1-Si1 121.98(9); C1-N1-Si1 116.59(12); Mg-Cl-Mg 77.98; Cl-Mg-Cl 84.61; O-Mg-Cl_{trans} 176.91; O-Mg-Cl_{cis} 92.98; O-Mg-O 89.36. Atoms which do not carry a numerical label represent average parameter values.

Following the unsatisfying electrochemical results using compound **1** as a rechargeable magnesium battery electrolyte due to decomposition (see Section 3.2.2), the preparation and X-ray characterisation of [(Dmp)(SiMe₃)AlCl₃]⁻ [Mg₂Cl₃·6THF]⁺, **2** (Figure 2.4), [(Ph)(SiMe₃)AlCl₃]⁻ [Mg₂Cl₃·6THF]⁺, **3** (Figure 2.5), and [(TMP)AlCl₃]⁻ [Mg₂Cl₃·6THF]⁺, **4** (Figure 2.6), was successfully carried out using the same synthetic route, with similar yields to **1** being recovered. The success of this method using different amines proves that this preparation route is general, reproducible and reliable.

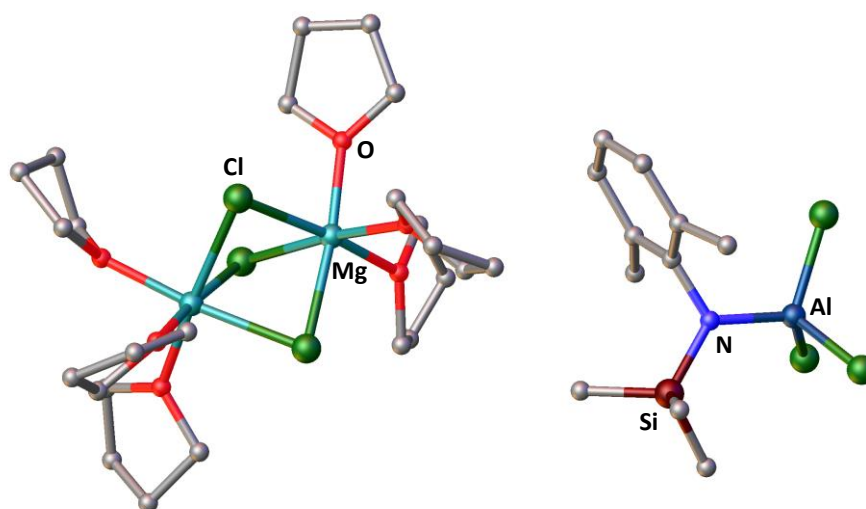


Figure 2.4: Molecular structure of **2** $[(\text{Dmp})(\text{SiMe}_3)\text{AlCl}_3]^- [\text{Mg}_2\text{Cl}_3 \cdot 6\text{THF}]^+$. Hydrogen atoms are omitted for clarity. The structure is represented in a ball and stick style due to the low quality of the data.

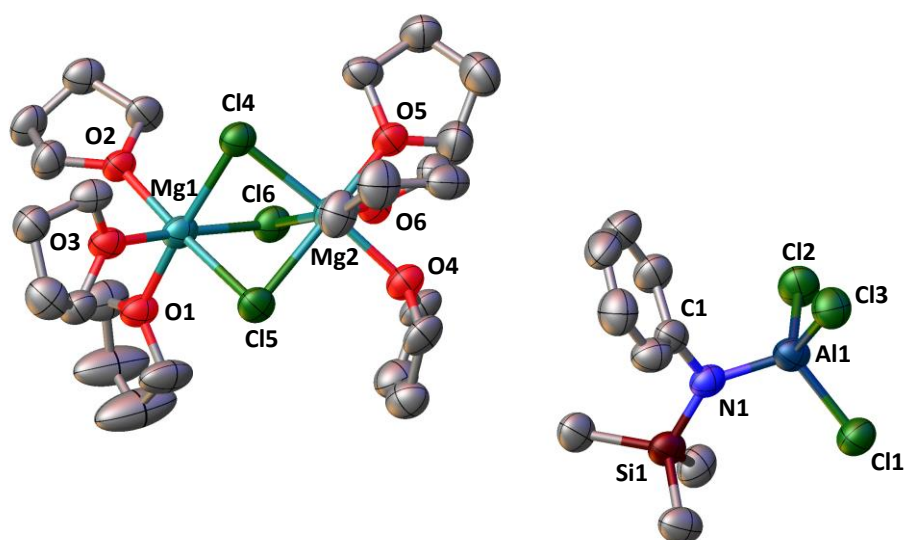


Figure 2.5: Molecular structure of **3** $[(\text{Ph})(\text{SiMe}_3)\text{AlCl}_3]^- [\text{Mg}_2\text{Cl}_3 \cdot 6\text{THF}]^+$. Hydrogen atoms are omitted for clarity. Thermal ellipsoids are drawn at the 50 % probability level. The quality of the data allows to use it for connectivity only hence the bond parameters are not discussed here.

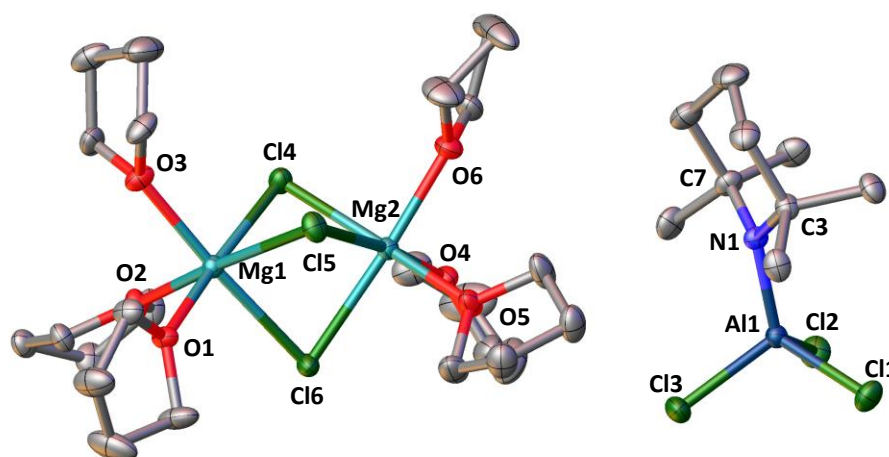


Figure 2.6: Molecular structure of **4** $[(\text{TMP})\text{AlCl}_3]^- [\text{Mg}_2\text{Cl}_3 \cdot 6\text{THF}]^+$. Hydrogen atoms and disorder present on two of the THF units atoms are omitted for clarity. Thermal ellipsoids are drawn at the 50 % probability level. Selected bond distances (Å) and angles ($^\circ$): Al1-N1 1.8340(15); Al-Cl 2.1777; Mg-Cl 2.5096; Mg1-Mg2 3.1405(8); Mg-O 2.0759; Al1-N1-C3 120.39(11); Al1-N1-C7 118.91(11); Mg-Cl-Mg 77.47; Cl-Mg-Cl 85.00; O-Mg-Cl_{trans} 176.38; O-Mg-Cl_{cis} 92.44; O-Mg-O 60.16. Atoms which do not carry a numerical label represent average parameter values.

The structures of **1**, **2**, **3** and **4** differ only by the identity of the amide bound to the aluminium. The literature shows only two crystal structures of a corresponding magnesium amidohaloaluminate, the previously presented $[(\text{HMDS})\text{AlCl}_3]^- [\text{Mg}_2\text{Cl}_3 \cdot 6\text{THF}]^+$ and with the dianionic acenaphthene-1,2-diimine ligand, 1,2-bis[(2,6-diisopropylphenyl)imino]-acenaphthene (dipp-BIAN) to form $[(\text{dipp-BIAN})\text{AlCl}_2]^- [\text{Mg}_2\text{Cl}_3 \cdot 6\text{THF}]^+$ (Figure 2.7).¹²

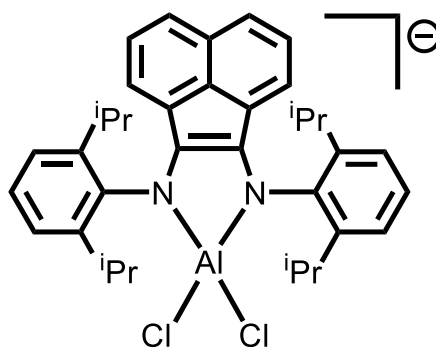


Figure 2.7: Anionic moiety of $[(\text{dipp-BIAN})\text{AlCl}_2]^- [\text{Mg}_2\text{Cl}_3 \cdot 6\text{THF}]^+$

The dinuclear magnesium cation $[\text{Mg}_2\text{Cl}_3 \cdot 6\text{THF}]^+$ in compounds **1**, **2**, **3** and **4**, as seen previously in other relevant magnesium aluminates has a non-crystallographic C_3 axis

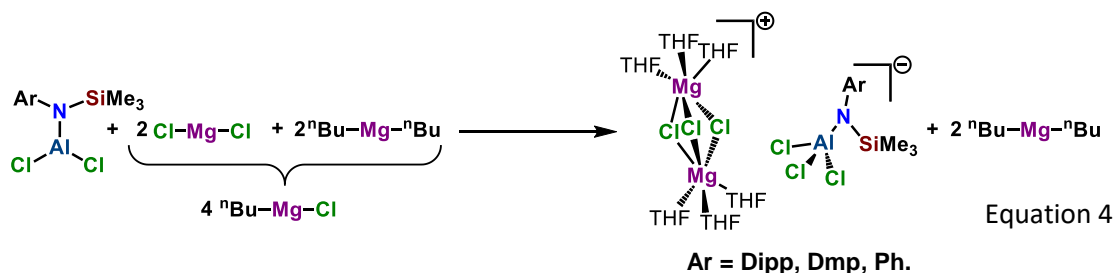
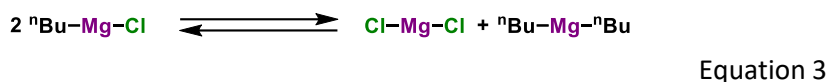
of symmetry passing through the two magnesium atoms, which are in a virtually octahedral environment consisting of three bridging *fac*-chloride anions and three terminal THF molecules. All the different anions adopt distorted tetrahedral geometries, unfortunately due to the too low quality of the X-ray data of compound **2** and **3** their bond length and angles can't be discussed, however their connectivity is definite. The distortion level of a tetrahedral geometry can be represented using the formula proposed by Houser et al. (Equation 2) where α and β corresponds the two largest angles in the four-coordinate species. A τ_4 value closer to 1.0 indicates that a species approaches a perfect tetrahedral geometry; conversely a τ_4 value closer to 0.0 indicates a species adopting a square planar geometry.¹³

$$\tau_4 = \frac{360 - (\alpha + \beta)}{141} \quad \text{Equation 2}$$

At this stage, thanks to the good quality of their X-ray data, only the anions of compounds **1** and **4** can be thoroughly compared. According to the τ_4 values, the anion of **1** possesses a less distorted tetrahedral geometry than the anion of **4** ($\tau_4 = 0.954$ and 0.892 respectively). This could be related to the different steric properties of the amides, TMP has a bulk located directly next to the nitrogen atoms whereas the bulk of DippNSiMe₃ arises from the more distant ⁱPr groups located on the phenyl ring but also the SiMe₃ group more adjacent to the nitrogen atoms. The distortion being bigger in the anion of **4** indicates that the bulk of TMP is more locally pronounced than the bulk of DippNSiMe₃, a statement backed up by the length of the N-Al bond being longer in compound **4** than in compound **1** (1.8341(15) Å and 1.8172(16) Å respectively.)

The overall stoichiometry of the reaction is not efficient as it involves the Schlenk equilibrium (Scheme 2.5; Equation 3) and further Cl rearrangements. Considering that in the case of the new route developed in this study, the Grignard reagent is viewed as a soluble source of MgCl₂ accessible through the Schlenk equilibrium, it would be necessary to use 4 equivalents of ⁿBuMgCl to get a reaction with the right reagent to product ratio (Equation 4). However, the same product is obtained when ⁿBuMgCl is

replaced by ${}^n\text{Bu}_2\text{Mg}$, suggesting the Cl rearrangement involves the “ R_2NAlCl_2 ” intermediate.



Scheme 2.5: Scheme of the Schlenk equilibrium (Equation 3) and synthesis of $[(\text{Ar})(\text{SiMe}_3)\text{NAlCl}_3]^- [\text{Mg}_2\text{Cl}_3 \cdot 6\text{THF}]^+$ in a 1:4 ratio Al/Mg (Equation 4).

2.3.2. Synthesis of magnesium aluminate compounds in MeTHF: Formation of a trinuclear cation

Successful preparation of new magnesium amidohaloaluminates possessing different amides was achieved. Yet, apart from changing the anion and proposing a new synthetic pathway the contribution to magnesium electrolyte chemistry is meagre. Following this the true interest was to conserve the same anion but alter the magnesium cation composition in order to study how the cation affects the electrochemical properties of an electrolyte. This is believed to be especially important in understanding the mechanistic process the electrolyte undergo during the reversible deposition of magnesium ions in the battery. A few studies postulate on the involvement of different magnesium chloride cationic species which adopts different aggregation states.^{14–18} Developing electrolytes with different cations could be a step forward toward understanding what structural/aggregation features enhance the performance of an electrolyte. By searching the crystallographic database we discovered chloromagnesium cations with a different aggregation level at the cation when Et_2O was solvating the metal instead of THF. The chloromagnesium cation in Et_2O forms the trinuclear aggregate $[\text{Mg}_3\text{Cl}_5 \cdot 6\text{Et}_2\text{O}]^+$, in the database only three structures possess such a cation plus two others with two or three chloride atoms

replaced by bromide atoms.^{19–23}

None of these are paired with an aluminium anion but most anions contain heavier group 13 atoms Ga or In. Examining the structure, it is obvious that the extra lateral bulk on the Et₂O ligand prevents the coordination of three donors per metal as observed with THF in [Mg₂Cl₃·6THF]⁺. Only having two ligands, even if Et₂O is singularly more encumbering than THF, there is vacant space for a smaller unit to coordinate the magnesium site. With the absence of another donor ligand there is space for an extra molecule of MgCl₂·2Et₂O to co-complex to the cation through the chloride atoms, maintaining a six coordinate octahedral magnesium centre. Thinking ahead and considering a battery system we decided that Et₂O was not a good choice of solvent due to its very low boiling point and volatility.

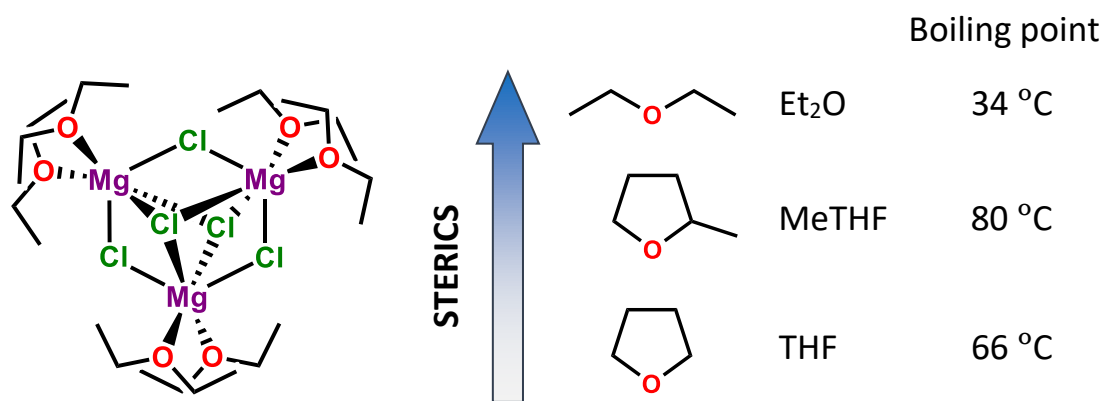


Figure 2.8: Structural representation of [Mg₃Cl₅·6Et₂O]⁺ (left) and visual comparison of the steric hindrance and boiling point between Et₂O, MeTHF and THF (right).

Aiming to find another donor solvent providing a similar bulk to Et₂O but displaying more attractive properties required for a rechargeable magnesium battery system our choice moved towards 2-methyltetrahydrofuran (MeTHF). Visually its bulk seems situated between Et₂O and THF where the additional lateral methyl group mimics one arm of the Et₂O molecule; moreover its boiling point is higher than THF, meeting the properties stipulated for an electrolytic solvent in battery systems (Figure 2.8). Furthermore MeTHF is praised for its environmentally friendly assets, awarding it the green solvent title which arises from the natural origin of its precursor (furfural from corncob and bagasse), its poor miscibility with water and its lower volatility which make its purification/isolation more environmentally friendly.²⁴

Using the same synthetic route as previously, the DippNSiMe₃ amide was first attached to the aluminium atom via the lithium amide intermediate, then 1 equivalent of ⁿBuMgCl (pre-prepared as a 0.5M solution by reacting ⁿBuCl with Mg metal in MeTHF so as to avoid the presence of THF) or ⁿBu₂Mg was added. X-ray quality colourless crystals were obtained by slow diffusion of hexane to yield the magnesium aluminate compound [(Dipp)(SiMe₃)NAlCl₃]⁻ [Mg₃Cl₅·6MeTHF]⁺, **5**. The aluminium anion is unchanged compared to **1** but the cation successfully adopts the sought-after higher aggregation state of a trinuclear species (Figure 2.9). The yield of the reaction is rather low with 31% but according to the Mg to Al ratio used in the reaction a maximum yield of only 33% is possible.

The cation of **5** contains a six membered (MgCl)₃ ring capped on either side by a μ³ bridging chloride anion. In each case, the magnesium centres are in a distorted octahedral environment made up of two mutually cis- O Lewis donor atoms from the MeTHF, two trans-Cl(μ₂) and two cis-Cl(μ₃). Compared to [Mg₃Cl₅·6Et₂O]⁺ the presence of MeTHF over Et₂O satisfyingly did not change the geometry of the trinuclear structure. Most bond lengths and angles remain within the same range, even the parameters most likely to be affected such as the Mg-O average bond distances (2.035 and 2.056 Å for compound **5** and [Mg₃Cl₅·6Et₂O]⁺ respectively) and the O-Mg-O angle (90.67 and 91.2 Å respectively). Even if these values suggest that MeTHF is slightly less bulky than Et₂O the difference is clearly minor.

Repeating this reaction with slightly less bulky amide DmpNSiMe₃ produced crystalline material (named compound **6**) but no matter how big or good looking they are the diffraction was too weak to provide a solvable data set. Lacking the X-ray characterised structure identifying the cation aggregation, efforts were invested using electrospray ionisation mass spectrometry (ESI-MS) instead, which confirms the presence of the trinuclear aggregation in MeTHF solution; the results are discussed later within this chapter in Section 2.7. Using PhNSiMe₃, TMP and even HMDS a poorly soluble microcrystalline solid is produced at the end of the reaction in MeTHF only. Attempts to characterise these solids by X-ray crystallography failed and ¹H NMR spectroscopy in d₈-THF of the solid did not display resonances corresponding to the amide. Analysing an aliquot from the mother liquor shows resonances of the

free amines, the reason for the non-formation of the product is not clear but after a few failed repeats further attempts were aborted.

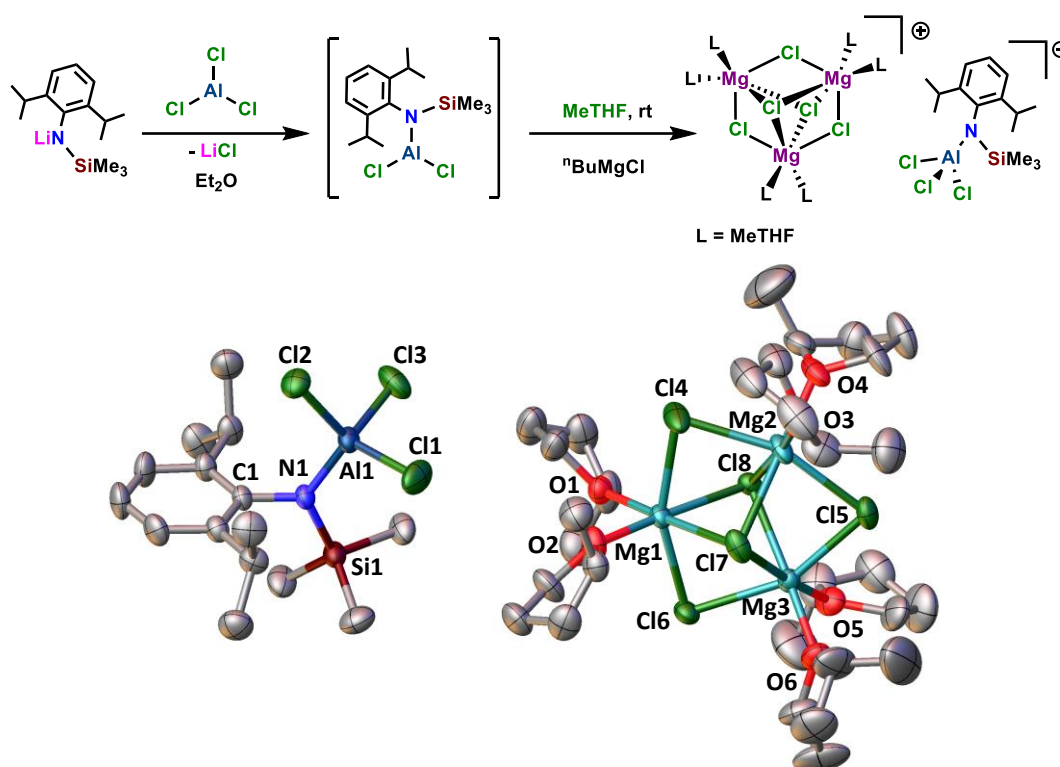


Figure 2.9: Molecular structure of **5** [(Dipp)(SiMe₃)NAlCl₃]⁻ [Mg₃Cl₅·6MeTHF]⁺. Hydrogen atoms and disorder present on five of the MeTHF units are omitted for clarity. Thermal ellipsoids are drawn at the 50 % probability level. Selected bond distances (Å) and angles (°): Al1-N1 1.819(3); N1-C1 1.443(4); N1-Si1 1.735(3); Mg-Mg 3.2936; Mg-Cl(μ₂) 2.4929; Mg-Cl(μ₃) 2.5555; O-Mg 2.034; Al1-N1-C1 119.58(19); Al1-N1-Si1 121.98(9); C1-N1-Si1 116.54(19); Cl(μ₂)-Mg-Cl(μ₂) 157.25; Cl(μ₃)-Mg-Cl(μ₃) 83.84; Cl(μ₂)-Mg-Cl(μ₃) 81.58; 157.25 Mg-Cl(μ₂)-Mg 82.68; Mg-Cl(μ₃)-Mg 80.24; O-Mg-Cl(μ₂)_{cis} 98.11; O-Mg-Cl(μ₃)_{trans} 176.52; O-Mg-Cl(μ₃)_{cis} 93.95; O-Mg-O 88.28. Atoms which do not carry a numerical label represent average parameter values.

2.3.3. Use of multidentate Lewis donor ligands

The previous section clearly shows how changing the donor ligand coordinated to the Mg atoms affects the aggregation state of the cation. The major criteria responsible for this modification being the sterics of the donor ligand use, it was tempting to consider the different Lewis donors often encountered in organometallic synthesis and observe how the cation aggregation reorganises itself. Here the study focuses on N-polydentate ligands; namely the bidentate ligand *N,N,N',N'*-tetramethylethylenediamine (TMEDA), the tridentate ligand *N,N,N',N'',N''*-pentamethyldiethylenetriamine (PMDETA) and the tetradentate ligand tris[2-(dimethylamino)ethyl]amine (Me₆TREN) (Figure 2.10).

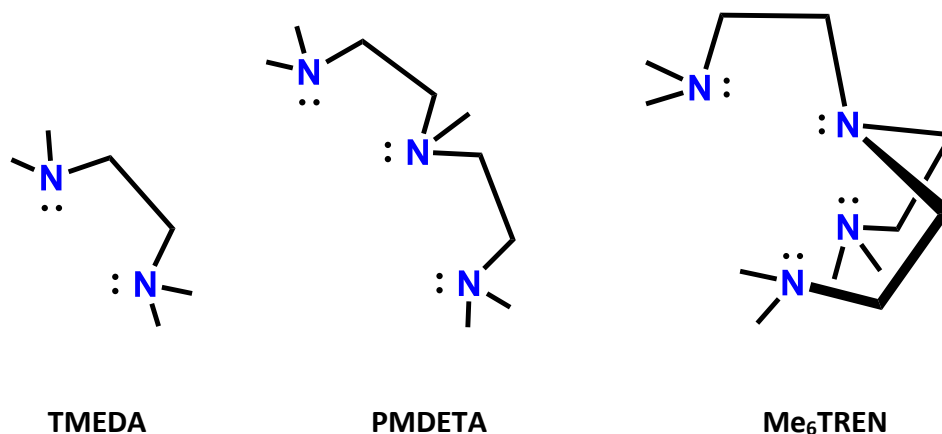


Figure 2.10: Multidentate ligand donors used in the pursuit of magnesium amidohaloaluminates in an attempt to control the cation aggregation state.

2.3.4. Use of TMEDA: Formation of a trinuclear cation

Utilizing the previously discussed protocol in THF, TMEDA was then introduced to a solution of “(Dipp)(SiMe₃)AlCl₂”, before adding ⁿBuMgCl, unfortunately no crystals were formed by slow diffusion of hexane. Alternatively, an excess of TMEDA was added to a solution of previously isolated crystals of complex **1** in THF. X-ray quality crystals were obtained from a toluene/THF solution representing the magnesium aluminate [(Dipp)(SiMe₃)AlCl₃]⁻ [Mg₃Cl₅·3TMEDA]⁺, **7**, in a 21 % yield (Figure 2.11). The anion of **6** is unchanged compared to **1**, however for its cation the TMEDA ligands replaces the THF units, engendering a change in aggregation from dinuclear to trinuclear. The structure of the new product, being richer in Mg, suggests that some sort of disproportionation occurred after the addition of TMEDA to a solution of compound **1**, explaining the low yield of the reaction. Consequently some neutral aluminium species should be formed as a by-product unless the magnesium cation is able to adopt smaller aggregation states in solution. Regardless, this reaction proves that the dinuclear magnesium cation [Mg₂Cl₃·6THF]⁺ can easily change its aggregation state in bulk THF upon the addition of the slightly stronger coordinating bidentate ligand. This observation is a slim hint that the change in the cation’s aggregation state from dinuclear to trinuclear does not require a large input of energy, hence both dinuclear and trinuclear species could be present in solution before addition of TMEDA as predicted by Liu et al.¹⁸

Crystals of compound **7** were found to be twinned. The raw data was processed as originating from two crystals related by the matrix 1.0017 -0.0014 0.7028 -0.0009 -1.0026 0.0008 0.0002 -0.0005 -1.0013 and the reflection data was presented as a hklf 5 formatted file. Refinement against this file gave a model that was far superior in terms of R factors, displacement ellipsoid shapes and residual electron density peaks than a model refined against a dataset with no twin treatment. The BASF parameter was refined to 0.3918(6). Structurally the trinuclear core of the cation of **7** is identical to the cation of **5**, and is unaffected by the ligand change. From the bidentate nature of the TMEDA and particularly the presence of a CH₂-CH₂ backbone, the N-Mg-N angle is more restricted than the O-Mg-O angle (84.12 and 88.28° respectively) where the terminal MeTHF molecules are free to adopt more favoured positions with wider angles. In the crystallographic database the [Mg₃Cl₅·3TMEDA]⁺ cation was previously observed with iron counter anions [Fe(Bn)₃]⁻ and [Fe(Bn)₄]⁻ (Bn = benzyl) while studying iron-catalysed Kumada cross-coupling reaction systems.²⁵

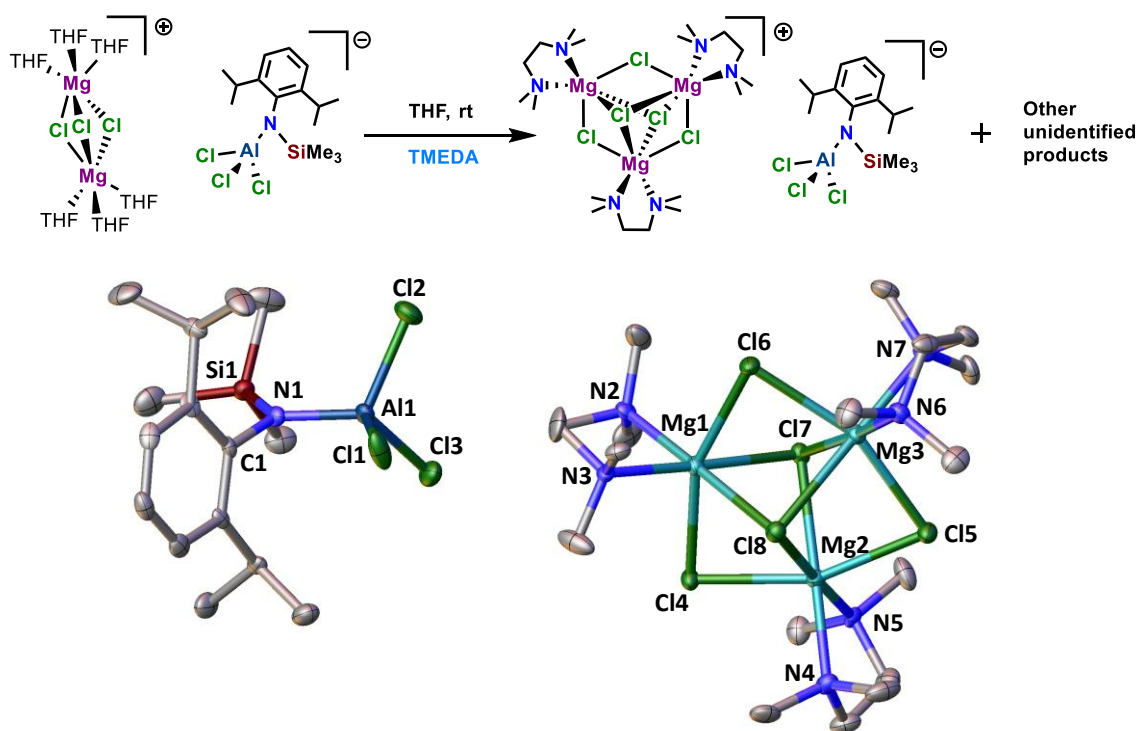


Figure 2.11: Molecular structure of **7** [(Dipp)(SiMe₃)AlCl₃]⁻ [Mg₃Cl₅·3TMEDA]⁺. Hydrogen atoms are omitted for clarity. Thermal ellipsoids are drawn at the 50 % probability level. Selected bond distances (Å) and angles (°): Al1-N1 1.819(3); N1-C1 1.443(4); N1-Si1 1.735(3); Mg-Mg 3.287; Mg-Cl(μ₂) 2.489; Mg-Cl(μ₃) 2.573; N-Mg 2.190; Al1-N1-C1 116.3(3); Al1-N1-Si1 125.4(2); C1-N1-Si1 118.2(3); Cl(μ₂)-Mg-Cl(μ₂) 157.31; Cl(μ₃)-Mg-Cl(μ₃) 84.92; Cl(μ₂)-Mg-Cl(μ₃) 81.67; Mg-Cl(μ₂)-Mg 82.65; Mg-Cl(μ₃)-Mg 79.42; N-Mg-Cl(μ₂)_{cis} 98.38; N-Mg-Cl(μ₃)_{trans} 178.32; N-Mg-Cl(μ₃)_{cis} 95.48; N-Mg-N 84.12. Atoms which do not carry a numerical label represent average parameter values.

Due to the poor solubility and hence inapplicability of **7** as an electrolyte the study of TMEDA solvates was not pursued further.

2.3.5. Use of PMDETA

Following the success of reacting compound **1** with bidentate N-donor TMEDA, the same protocol was repeated using tridentate PMDETA, expecting that it could act as an isodentate surrogate for three molecules of THF, yielding a dinuclear N-solvated cation similar to **1**. Using the same procedure employed to prepare compound **7**, but replacing TMEDA by PMDETA, a solid precipitated within 5 minutes after the addition of the tridentate ligand. Upon heating a solution was obtained and X-Ray quality crystals grew upon slow cooling. Despite our expectations, PMDETA did not replace the THF molecules to keep the dinuclear cation aggregation but instead generated a neutral magnesium dichloride complex $\text{MgCl}_2\cdot\text{PMDETA}$, **8**, (Figure 2.12). In a previous study by Zhao-Karger et al., the presence of the related tridentate O-donor bis(2-methoxyethyl)ether (diglyme) in a similar system also results in a neutral magnesium complex over the formation of a magnesium aluminate compound.²⁶ This suggests that acyclic tridentate donors do not possess the correct spatial conformation of their donor atoms to adequately protect one end of a $[\text{Mg}_2\text{Cl}_3]^+$ fragment as they are aligned for *mer* rather than *fac* coordination to an octahedral metal centre, while they do not have the requisite number of donor atoms to protect a mononuclear or trinuclear cation.

Complex **8** is a five-coordinate magnesium monomer, where the three nitrogen atoms of PMDETA and two chlorides atoms place the Mg atom in a geometry lying between square pyramid and trigonal bipyramidal. The τ_5 equation (Equation 5) developed by Addison et al. allows the determination of a 5 coordinate element adopts a square pyramidal or trigonal bipyramidal geometry. In this equation α and β are the two largest angles, and $\alpha \leq \beta \leq 180^\circ$. When $\tau_5 = 1$ the structure adopts a trigonal bipyramidal geometry and when $\tau_5 = 0$ the structure adopts a square pyramid geometry. In the case of Mg in the structure of compound **8** the τ_5 value is equal to 0.34, meaning that its geometry is situated in between both geometries but with a greater affinity for the square pyramidal geometry.

$$\tau_5 = \frac{\beta - \alpha}{60}$$

Equation 5

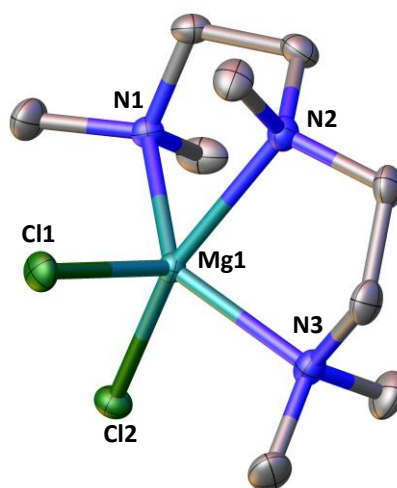


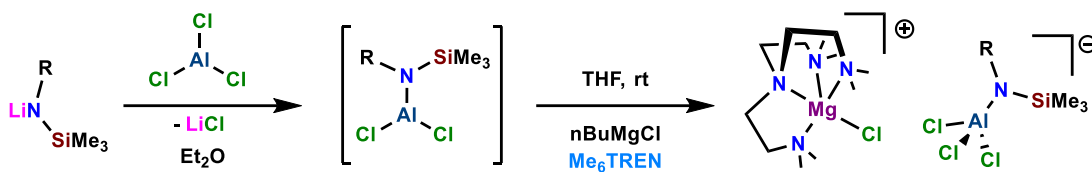
Figure 2.12: Molecular structure of one of the independent molecules of complex **8** [$\text{MgCl}_2 \cdot \text{PMDETA}$]. Hydrogen atoms are omitted for clarity. Thermal ellipsoids are drawn at the 50 % probability level. Selected bond distances (Å) and angles (°): Mg1–Cl1 2.3913(7) [2.3770(6)]; Mg1–Cl2 2.3108(7) [2.3371(6)]; Mg1–N1 2.1932(15) [2.1886(13)]; Mg1–N2 2.3230(13) [2.2959(13)]; Mg1–N3 2.2142(15) [2.2226(13)]; Cl1–Mg1–Cl2 106.26(3) [105.26(3)]; Cl1–Mg1–N1 93.44(4) [93.19(4)]; Cl2–Mg1–N1 109.78(4) [106.25(4)]; Cl1–Mg1–N2 96.84(4) [98.09(4)]; Cl2–Mg1–N2 156.89(4) [156.78(4)]; Cl1–Mg1–N3 93.20(4) [92.27(4)]; Cl2–Mg1–N3 109.25(4) [113.79(4)]; N1–Mg1–N2 78.91(5) [79.78(5)]; N1–Mg1–N3 136.63(5) [136.49(5)]; N2–Mg1–N3 78.42(5) [78.48(5)]. Bond parameters of second independent molecule are in parentheses. Atoms which do not carry a numerical label represent average parameter values.

The monomeric motif of compound **8** is commonly observed in the literature with dialkyl-, dialkoxide- and dihalide-magnesium compounds using PMDETA.^{27,28} When using the analogous ethereal ligand diglyme, the absence of one terminal methyl groups on the outer O-donor atoms leave enough space for the molecule to dimerise via chloride bridges, leaving the Mg atom in a distorted octahedral geometry.²⁶ As mentioned in the previous paragraph it is the more favoured *mer* alignment of the donor atoms of the ligand which is the most probable reason why they don't replace the THF units in $[\text{Mg}_2\text{Cl}_3 \cdot 6\text{THF}]^+$ which adopts a *fac* arrangement. It is however not impossible for a PMDETA ligand to rearrange itself so the donor atoms are not aligned, and was observed in two cases where the molecule adopts a distorted tetrahedral geometry, allowing the formation of the mononuclear Mg cation $[\text{MgCp} \cdot \text{PMDETA}]^+$ (Cp = cyclopentadienyl, C_5H_5^-).^{29,30} There is however a major

steric and electronic difference between a Cp group and a halogen atom, which seems to be key to stabilise such a conformation.

2.3.6. Use of Me₆TREN: Formation of a mononuclear cation

The largest multidentate N-donor ligand of the series, Me₆TREN, is known to easily cap one hemisphere of reasonably small metal atoms and is often exploited to trap sensitive mononuclear organometallic species.^{31–33} By repeating the procedure to synthesise compound **1** in THF, but introducing the tripodal ligand before the addition of ⁿBuMgCl, X-ray quality single crystals were obtained from an Et₂O/THF mixture. As anticipated the tetradentate ligand occupies one hemisphere of the metal to yield [(Dipp)(SiMe₃)NAlCl₃]⁻ [MgCl·Me₆TREN]⁺, **9**, in a yield of 65 % (Figure 2.13). This result unequivocally confirmed our view that a mononuclear MgCl cation could be prepared on demand by fully occupying one hemisphere of the metal to prevent oligomerisation and represents the first example of [MgCl·Me₆TREN]⁺ to be synthesised and crystallography characterised. Moreover, this represents potentially a key breakthrough for the solution study of mononuclear magnesium aluminate battery electrolyte complexes since the previously synthesised monomeric THF solvate displays poor solubility even in polar THF.⁴ The synthesis and characterisation of other mononuclear magnesium aluminates using the less sterically hindered amines, DmpNHSiMe₃, PhNHSiMe₃ and HMDS(H) was also successful yielding [(Dmp)(SiMe₃)NAlCl₃]⁻ [MgCl·Me₆TREN]⁺, **10**, yield: 63 % (Figure 2.14); [(Ph)(SiMe₃)NAlCl₃]⁻ [MgCl·Me₆TREN]⁺, **11**, yield: 69 % (Figure 2.15) and [(HMDS)AlCl₃]⁻ [MgCl·Me₆TREN]⁺, **12** (Figure 2.16).



R = Dipp, Dmp, Ph, SiMe₃

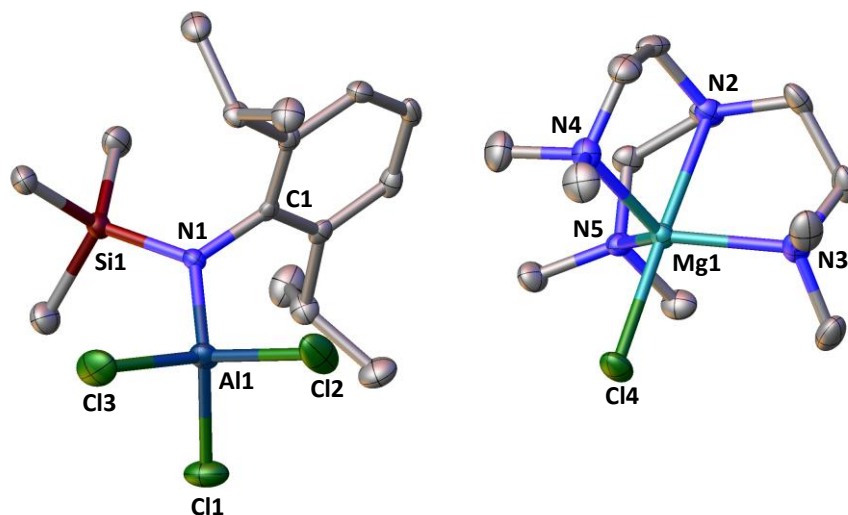


Figure 2.13: Molecular structure of **9** [(Dipp)(SiMe₃)AlCl₃]⁻ [MgCl·Me₆TREN]⁺. Hydrogen atoms are omitted for clarity. Thermal ellipsoids are drawn at the 50 % probability level. Selected bond distances (Å) and angles (°): Al1–N1 1.817(3); N1–C1 1.438(4); N1–Si1 1.735(3); Mg1–Cl4 2.3229(2); Mg1–N2 2.219; Mg–N_{eq} 2.182; Al1–N1–C1 116.3(3); Al1–N1–Si1 122.75(14); C1–N1–Si1 117.54(19); N2–Mg1–Cl4 178.28(6); N_{eq}–Mg1–Cl4 98.98; N2–Mg1–N_{eq} 81.06; N_{eq}–Mg1–N_{eq} 117.61. Atoms which do not carry a numerical label represent average parameter values.

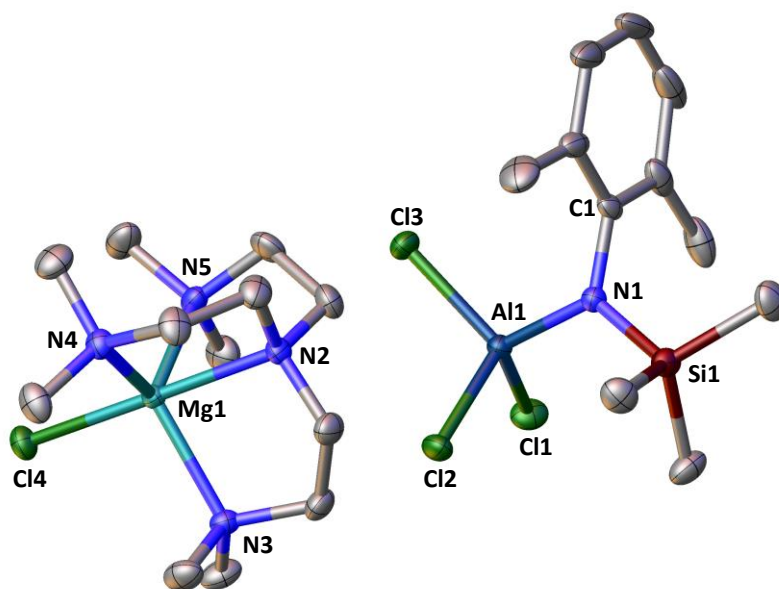


Figure 2.14: Molecular structure of **10** [(Dmp)(SiMe₃)AlCl₃]⁻ [MgCl·Me₆TREN]⁺. Hydrogen atoms are omitted for clarity. Thermal ellipsoids are drawn at the 50 % probability level. Selected bond distances (Å) and angles (°): Al1–N1 1.811(2); N1–C1 1.431(4); N1–Si1 1.734(2); Mg1–Cl4 2.3195(11); Mg1–N2 2.214(3); Mg–N_{eq} 2.184; Al1–N1–C1 117.22(18); Al1–N1–Si1 122.49(14); C1–N1–Si1 120.23(19); N2–Mg1–Cl4 178.34(8); N_{eq}–Mg1–Cl4 99.18; N2–Mg1–N_{eq} 80.81; N_{eq}–Mg1–N_{eq} 117.50. Atoms which do not carry a numerical label represent average parameter values.

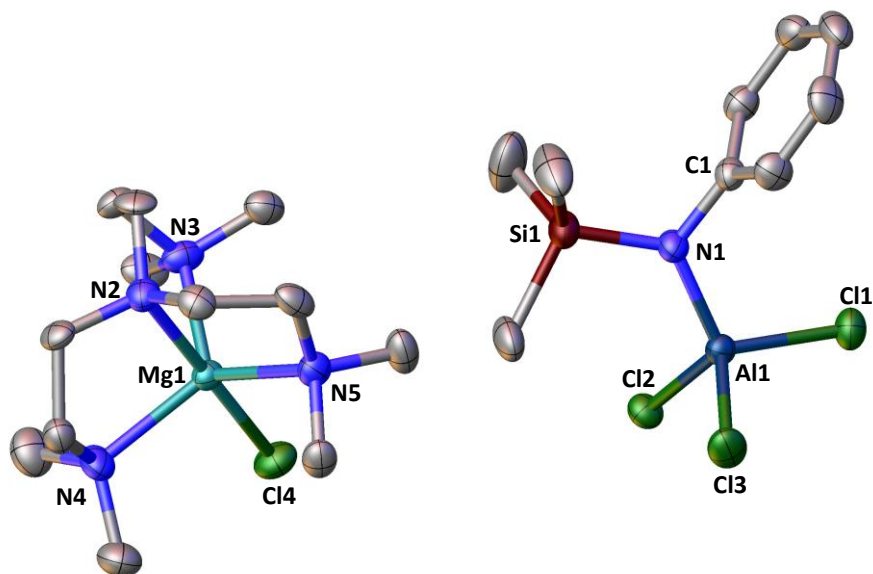


Figure 2.15: Molecular structure of **11** [(Ph)(SiMe₃)NAlCl₃]⁻ [MgCl·Me₆TREN]⁺. Hydrogen atoms and disorder present on each arm of the Me₆TREN unit are omitted for clarity. Thermal ellipsoids are drawn at the 50 % probability level. Selected bond distances (Å) and angles (°): Al1-N1 1.811(4); N1-C1 1.430(6); N1-Si1 1.735(4); Mg1-Cl4 2.3155(16); Mg1-N2 2.211(4); Mg-N_{eq} 2.188; Al1-N1-C1 118.8(3); Al1-N1-Si1 125.4(2); C1-N1-Si1 115.3(3); N2-Mg1-Cl4 179.47(13); N_{eq}-Mg1-Cl4 98.98; N2-Mg1-N_{eq} 81.02; N_{eq}-Mg1-N_{eq} 117.71. Atoms which do not carry a numerical label represent average parameter values.

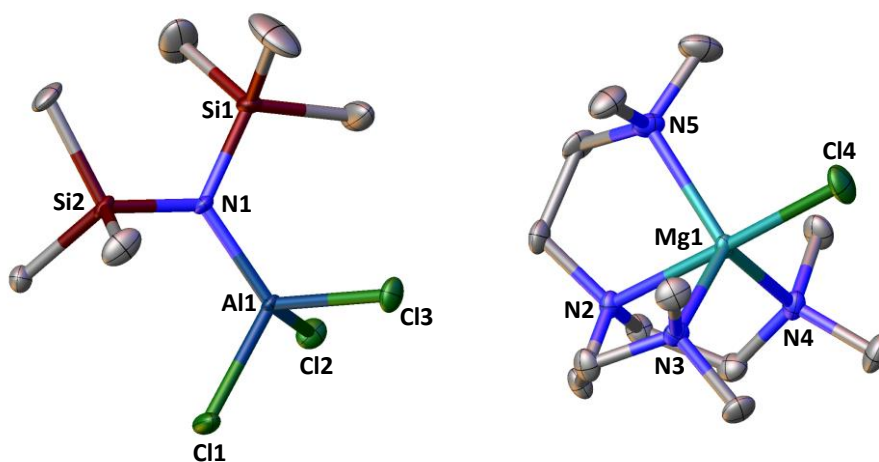


Figure 2.16: Molecular structure of **12** [(HMDS)AlCl₃]⁻ [MgCl·Me₆TREN]⁺. Hydrogen atoms are omitted for clarity. Thermal ellipsoids are drawn at the 50 % probability level. Selected bond distances (Å) and angles (°): Al1-N1 1.8227(17); N1-Si 1.7374; Mg1-Cl4 2.3083(8); Mg1-N2 2.2262(17); Mg-N_{eq} 2.1901; Al-N-Si 119.44; N2-Mg1-Cl4 178.38(5); N_{eq}-Mg1-Cl4 99.22; N2-Mg1-N_{eq} 80.77; N_{eq}-Mg1-N_{eq} 117.47. Atoms which do not carry a numerical label represent average parameter values.

The mononuclear cation $[\text{MgCl}\cdot\text{Me}_6\text{TREN}]^+$ of compounds **9**, **10**, **11** and **12** are all identical with only irrelevant variations. Structurally the Mg centre lies in a trigonal bipyramidal environment with the central nitrogen and chloride occupying axial positions with the three pendant arm N-donor atoms occupying equatorial sites. The Me_6TREN ligand is versatile and in certain cases it can adapt to the coordination sphere of a metal by acting as a tridentate ligand, with one arm left uncoordinated (e.g. $\text{LiHMDS}\cdot\text{Me}_6\text{TREN}$, $2\text{-}^t\text{BuC}_5\text{H}_5\text{NLi}\cdot\text{Me}_6\text{TREN}$).^{34,35} Because of this ability, the representation of these compounds in solid state is not necessarily the same as in the solution state. The characterisation of Mg reagents with Me_6TREN was only studied in one previous publication by Hazari et al. where the $[\text{MgBr}\cdot\text{Me}_6\text{TREN}]^+$ cation was observed, as well as the neutral $\text{Me}_2\text{Mg}\cdot\text{Me}_6\text{TREN}$ where Me_6TREN acts as a tridentate ligand.

2.4. X-ray crystallographic comparison of magnesium aluminate complexes

This synthetic study has shown how the use of different donor ligands controls the aggregation state (mono-, di- and trinuclear) of the cation in previously introduced magnesium amidohaloaluminate compounds. This discussion will review the pertinent bond lengths and angles of the obtained structures to show the effect of the different amides on the aluminium anion (focussing specifically on **1**, **10**, **11**, **12** and **4**), the effect of the different cation aggregations on the anion and in more detail the difference between the aggregation state of the cations of **1** (dinuclear) **5**, **7** (trinuclear), and **9** (mononuclear).

2.4.1. Crystallographic study of the aluminium anion

In the literature there are only a few examples of a magnesium aluminate solvent-separated ion pair with a magnesium chloride cation which is not $[\text{Mg}_2\text{Cl}_3\cdot 6\text{THF}]^+$; specifically $[\text{MgCl}\cdot 5\text{THF}]^+$ with an “all-chloro” counter aluminium anion $[\text{AlCl}_4]^-$, $[\text{Mg}_2\text{Cl}_2\cdot 4\text{DME}]^{2+}$ with two $[\text{AlCl}_4]^-$ or $[\text{EtAlCl}_3]^-$ counter anions and

finally the naked magnesium dication $[\text{Mg}\cdot 6\text{THF}]^{2+}$ with two counter anions, $[\text{AlMe}_4]^-$ or $[\text{AlCl}_4]^-$ counter anions.^{4,26,36,37} The first part of the anion study will discuss the effect the different cation aggregations have on a common aluminium anion. The following discussion will then discuss the bond lengths and angles of anions containing different amides, a study related to the electrochemistry of these compounds presented in Chapter 3. The relationship between the amide and the electrochemistry was linked due to the early decomposition of compounds possessing the DippNSiMe₃ amide, requiring the use of less bulky substituents on the phenyl ring. Studying the changes occurring in the anion structure using different amides can give an insight if the extra sterics from the ⁱPr groups of the Dipp is influential in the solid state.

2.4.1.1. Effect of the magnesium cation on the aluminium anion

Table 2.1: Selected bond lengths and angles for the $[(\text{Dipp})(\text{SiMe}_3)\text{NAlCl}_3]^-$ anion of **1**, **5**, **7** and **9**.

	1	5	7	9
Cation aggregation state	dinuclear	trinuclear	trinuclear	mononuclear
Donor ligand	THF	MeTHF	TMEDA	Me ₆ TREN
<i>Selected bond lengths (Å)</i>				
N1-Al1	1.8172(16)	1.819(3)	1.815(4)	1.809(6)
Al1-Cl1	2.1483(7)	2.1396(13)	2.152(2)	2.143(3)
Al1-Cl2	2.1648(7)	2.1646(14)	2.168(2)	2.166(3)
Al1-Cl3	2.1582(7)	2.1524(14)	2.155(2)	2.152(3)
Al1-Cl mean	2.1571	2.1522	2.158	2.154
<i>Selected bond angles (°)</i>				
N1-Al1-Cl1	113.00(6)	111.41(9)	112.13(15)	110.3(2)
N1-Al1-Cl2	111.32(6)	114.80(10)	113.16(16)	116.7(2)
N1-Al1-Cl3	112.50(6)	111.25(10)	113.37(16)	109.3(2)
N1-Al1-Cl mean	112.27	112.49	112.89	112.10
Cl1-Al1-Cl2	107.19(3)	105.65(6)	107.24(9)	105.90(12)
Cl1-Al1-Cl3	106.74(3)	108.54(6)	106.32(9)	109.97(13)
Cl2-Al1-Cl3	105.65(3)	104.75(6)	103.99(8)	104.34(12)
Cl-Al1-Cl mean	106.53	106.31	105.85	106.74

Table 2.1 shows that the anions of **1**, **5**, **7** and **9** are nearly identical, thus insinuating that the presence of different coordinating ligands and the different aggregation states adopted by the magnesium chloride cations do not alter or interact with the aluminium anion. The slight differences in the N-Al and Al-Cl bond lengths are too insignificant and can potentially be attributed to a difference of packing in the crystal lattice. The same observations can be made with the N-Al-Cl and Cl-Al-Cl bond angles. This result is not a surprise and is to be expected in a solvent-separated ion pair structure.

2.4.1.2. Effect of the amide on the aluminium anion

Table 2.2: Selected bond lengths and angles for the anions of **1**, **10**, **11**, **12** and **4**. * N1-Si2 bond length; † Si1-N1-Si2 bond angle; ‡ Al1-N1-Si2 bond angle.

	1	10	11	12	4
<i>Selected bond lengths (Å)</i>					
Amide	DippN(SiMe ₃)	DmpN(SiMe ₃)	PhN(SiMe ₃)	HMDS	TMP
N1-Al1	1.8172(16)	1.8114(17)	1.811(4)	1.8227(17)	1.8341(15)
Cl1-N1	1.441(2)	1.431(4)	1.430(6)	1.7410(17)*	--
N1-Si1	1.7343(16)	1.734(2)	1.735(4)	1.7339(17)	--
Al1-Cl1	2.1483(7)	2.1675(8)	2.1551(15)	2.1624(7)	2.1787(7)
Al1-Cl2	2.1648(7)	2.1682(8)	2.1751(15)	2.1727(7)	2.1774(7)
Al1-Cl3	2.1582(7)	2.1422(7)	2.1641(15)	2.1679(7)	2.1772(7)
Al1-Cl mean	2.1571	2.1593	2.1648	2.1677	2.1777
<i>Selected bond angles (°)</i>					
Al1-N1-Si1	121.98(3)	122.48(10)	125.4(2)	118.26(9)	--
Cl1-N1-Si1	116.59(12)	120.24(13)	115.3(3)	120.00(9) [†]	--
Cl1-N1-Al1	121.42(12)	117.22(18)	118.8(3)	120.63(10) [‡]	--
N1-Al1-Cl1	113.00(6)	115.74(6)	110.76(13)	114.06(6)	118.31(5)
N1-Al1-Cl2	111.32(6)	110.52(6)	112.27(13)	113.92(6)	115.89(5)
N1-Al1-Cl3	112.50(6)	109.93(6)	112.90(13)	112.01(6)	111.61(5)
N1-Al1-Cl mean	112.27	112.06	111.98	113.33	115.27
Cl1-Al1-Cl2	107.19(3)	103.70(3)	106.72(6)	105.26(3)	98.09(3)
Cl1-Al1-Cl3	106.74(3)	107.36(3)	108.48(7)	105.19(3)	105.08(3)
Cl2-Al1-Cl3	105.65(3)	109.29(3)	105.37(6)	105.59(3)	106.30(3)
Cl-Al1-Cl mean	106.53	106.78	106.86	105.35	103.15

Due to the low X-ray data quality of compounds **2** and **3**, direct comparisons with compounds containing the dinuclear cation exclusively is not possible. But after

establishing that the magnesium cation, whatever its aggregation level, doesn't interfere with the aluminium anion it allows us to compare the anions possessing different amide groups even if the counter cation is different.

Table 2.2 displays selected bond lengths and angles of the anions of compounds **1**, **10**, **11**, **12** and **4**. Overall there is no major impact on the anions when the nature of the amide is changed. A slight difference is perhaps observed when TMP is used, where the N-Al bond length seems to increase, while the Cl-Al-Cl bond angle slightly decreases with the bulkiness of the amide. To extend this point a similar observation can be made with [(Dipp)(SiMe₃)NAlCl₃]⁻ compared to [(Dmp)(SiMe₃)NAlCl₃]⁻ and [(Ph)(SiMe₃)NAlCl₃]⁻ (longer N-Al bond and smaller Cl-Al-Cl angle with DippN(SiMe₃)), but these differences are not significant enough to make any firm conclusions. Another minimal trend can be noticed when comparing the Al-N-Si angle, which unsurprisingly decreases with the bulk of the substituents on the aryl ring.

In electrochemical testing, Al-bound amides were shown to improve the magnesium aluminates attributes as electrolytes.^{7,8} This study showed that by changing the amide the general structure of the magnesium aluminate is conserved and the bond lengths and angles do not give conclusive information on the stability of the aluminate. From these observations, and relating them to the low oxidative stability of both the [(Dipp)(SiMe₃)NAlCl₃]⁻ and [(Dmp)(SiMe₃)NAlCl₃]⁻ anions over the [(Ph)(SiMe₃)NAlCl₃]⁻ demonstrated in Chapter 3, the reason for the destabilisation is more likely to be an electronic effect arising from the substituents instead of a steric effect. The impact of the TMP on the anion is more pronounced, suggesting the anion will be less stable due to the longer N-Al bonds and smaller Cl-Al-Cl angle. Moreover a theoretical study calculated the HOMO-LUMO energy gap involved in different aluminate anions [R_nAlCl_{4-n}]⁻ (n = 1, 2, 3 and R = Cl, Et, Mes, TMP, Ph, HMDS, OPh), which is believed to be a good indication of the oxidative stability of the corresponding electrolyte. Among the different ligands used the anion containing TMP possesses the lowest energy gap, hence possessing the lowest oxidative stability of those studied.

2.4.2. Crystallographic study of the magnesium chloride cation

The structures **1**, **5**, **7** and **9** possess this time the same anion $[(\text{Dipp})(\text{SiMe}_3)\text{NAlCl}_3]^-$ but by using a different donor solvent (THF, MeTHF) or introducing selected multidentate donor ligands (Me_6TREN , TMEDA) the aggregation state of the cation was altered, leading to the formation of the commonly observed dinuclear cation $[\text{Mg}_2\text{Cl}_3 \cdot 6\text{THF}]^+$ **1**, two trinuclear cations with the novel cation $[\text{Mg}_3\text{Cl}_5 \cdot 6\text{MeTHF}]^+$ **5** and $[\text{Mg}_3\text{Cl}_5 \cdot 3\text{TMEDA}]^+$ **7** (previously observed by Bedford with an iron-centred counter anion),²⁵ and finally the novel monomeric cation $[\text{MgCl} \cdot \text{Me}_6\text{TREN}]^+$ **9**. As mentioned earlier, magnesium aluminate electrolyte literature displays only two different aggregation states of magnesium chloride cations (excluding $[\text{Mg}_2\text{Cl}_3 \cdot 6\text{THF}]^+$), the monomer $[\text{MgCl} \cdot 5\text{THF}]^+$ and the recently published dicationic dimer $[\text{Mg}_2\text{Cl}_2 \cdot 4\text{DME}]^{2+}$ (DME: 1,2-dimethoxyethane, also called glyme).^{4,26} In this section a comparative discussion between the bond lengths and angles of the different cation structures of **1**, **5**, **7** and **9** will be presented.

Table 2.3: Selected average bond lengths and angles for the cations of **1**, **5**, **7** and **9**.

	1	5	7	9
Cation aggregation state	dinuclear	trinuclear	trinuclear	mononuclear
Donor ligand	THF	MeTHF	TMEDA	Me_6TREN
<i>Selected average bond lengths (Å)</i>				
Mg-Cl(μ^2)	2.5027	2.4929	2.489	--
Mg-Cl(μ^3)	--	2.5555	2.573	--
Mg-Cl _{term}	--	--	--	2.3229(13)
Mg-N _{ax}	--	--	--	2.219(3)
Mg-N _{eq}	--	--	--	2.182
Mg-N	--	--	2.189	--
Mg-O	2.0808	2.034	--	--
Mg-Mg	3.1494(9)	3.2905	3.297	--
<i>Selected average bond angles (°)</i>				
Cl(μ^2)-Mg- Cl(μ^2)	84.61	157.25	157.32	--
Cl(μ^3)-Mg- Cl(μ^3)	--	83.84	84.92	--
Cl(μ^2)-Mg- Cl(μ^3)	--	81.58	81.02	--
Mg-Cl(μ^2)-Mg	77.98	82.69	82.65	--
Mg-Cl(μ^3)-Mg	--	80.24	79.42	--

N-Mg-Cl(μ^2) _{cis}	--	--	98.38	--
N-Mg-Cl(μ^3) _{cis}	--	--	96.00	--
N-Mg-Cl(μ^3) _{trans}	--	--	178.36	--
N _{ax} -Mg-Cl	--	--	--	178.28
N _{eq} -Mg-Cl	--	--	--	98.98
O-Mg-Cl(μ^2) _{cis}	92.98	98.11	--	--
O-Mg-Cl(μ^2) _{trans}	176.91	--	--	--
O-Mg-Cl(μ^3) _{cis}	--	93.95	--	--
O-Mg-Cl(μ^3) _{trans}	--	176.52	--	--
N _{ax} -Mg-N _{eq}	--	--	--	81.06
N _{eq} -Mg-N _{eq}	--	--	--	117.61

Table **2.3** shows that the terminal Mg-Cl_{term} bond length from **9** is unsurprisingly the shortest at 2.3229(13) Å against an average of 2.5027 for an Mg-Cl(μ^2) bond in the dinuclear cation of **1**, and average of 2.573 for an Mg-Cl(μ^3) bond in the trinuclear cation of **7**; a shorter bond is often associated with a stronger one. Compared to the terminal bond from the crystal structure of the THF solvated neutral magnesium chloride MgCl₂·4THF from the CCDC,³⁸ the Mg-Cl_{term} bond from **9** is also shorter (Mg-Cl 2.443 Å average bond length for MgCl₂·4THF), which is to be expected since the Mg²⁺ centre is only sharing its charge with a single Cl⁻. Compared to the neutral structure of MgCl₂·PMDETA in compound **8** (selected bond length and angles in Section 2.3.5), the difference of the Mg-Cl_{term} bond lengths is less pronounced with a bond only 0.036 Å shorter for **9** (Mg-Cl 2.351 Å average bond length for **8**). A similar observation with MgBr bonds supports this theory, where a [MgBr·Me₆TREN]⁺ cation has a shorter metal halide bond length than MgBr₂·4THF.^{39,40} However the effect of the nature of the donor ligand (N or O) or the number of donor atoms on the terminal Mg-Cl bond cannot be excluded as in comparison to the previously demonstrated penta-THF solvated monomer [MgCl·5THF]⁺ by Aurbach, the Mg-Cl bond is slightly longer (2.391 Å) than its Me₆TREN analogue. For the bridging chlorides, the Mg-Cl(μ_3) bond is slightly longer than the Mg-Cl(μ_2) bond, and therefore expected to be more easily replaced. This statement can be strengthened by a “rogue” crystal structure obtained in the same batch of **5**, where a *n*-butoxide group (presumably obtained by hydrolysis from the ⁿBuMgCl solution) replaced a capping Cl atom to give [Mg₃Cl₄(OⁿBu)·6MeTHF]⁺ **13** (Figure **2.17**). A similar structure with a [MgCl₃·THF]⁻

counteranion was reported in a magnesium battery paper where the two capping Cl atoms are replaced by two *n*-butoxides in $[\text{Mg}_3\text{Cl}_3(\text{O}^n\text{Bu})_2 \cdot 6\text{THF}]^+$.⁴¹

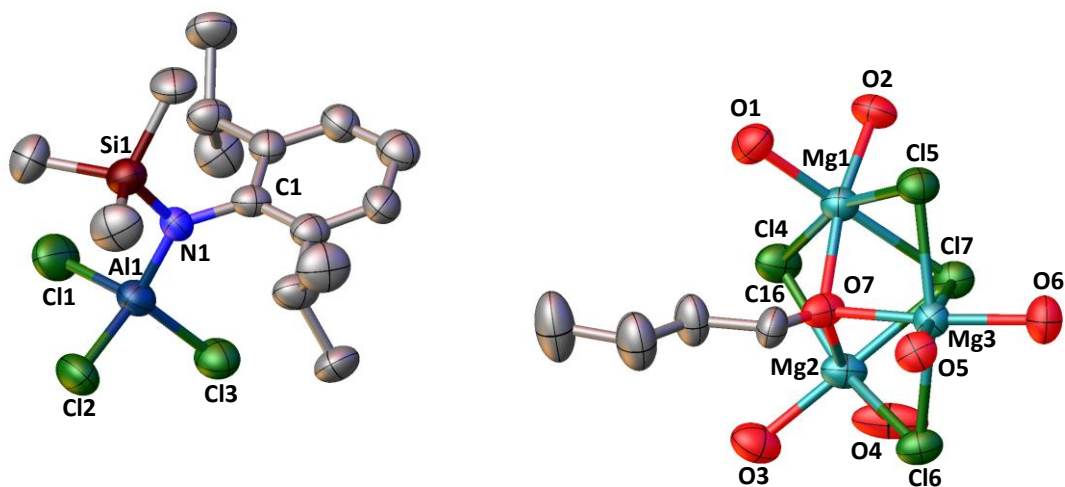


Figure 2.17: Molecular structure of **13** $[(\text{Dipp})(\text{SiMe}_3)\text{NAlCl}_3]^- [\text{Mg}_3\text{Cl}_4(\text{O}^n\text{Bu}) \cdot 6\text{MeTHF}]^+$. Hydrogen atoms and the carbon atoms of the MeTHF molecules are omitted for clarity. Thermal ellipsoids are drawn at the 50 % probability level. The quality of this structure is hindered by the high disorder involved in the MeTHF units, this structure is only the result of impurities present in the sample hence the bond parameters are not discussed.

The table also shows that the Mg-Cl(μ_2)-Mg bond angles of **1** have an average acute angle of 77.98° , for **5** and **7** the angle opens more giving 82.69° and 82.65° respectively, while the Mg-Cl(μ_3)-Mg angles are also in the same range (80.24° , **5**; 79.42° , **7**). These values reflect their participation in both four-membered and six-membered rings within the trinuclear species. As expected, for the trinuclear species (**5** and **7**) the Cl(μ_2)-Mg-Cl(μ_2) angles are wider to be able to form the (MgCl)₃ trimeric ring (157.25° , **5**; 157.32° , **7**) whereas the Cl(μ_3)-Mg-Cl(μ_3) angles (83.84° , **5**; 84.92° , **7**) are similar to the Cl(μ_2)-Mg-Cl(μ_2) angles of the dinuclear cation **1** (84.61°). These observations allow the proposal of an alternative view to the trinuclear cation which could be seen as a dinuclear $[\text{Mg}_2\text{Cl}_3]^+$ cation being coordinated by one molecule of MgCl_2 (Figure 2.18). The N-Mg-Cl(μ_3)_{cis} and O-Mg-Cl(μ_3)_{cis} angles are also slightly different where TMEDA leads to a more open angle by just over 2° , the same observation is made with the angles N-Mg-Cl(μ_3)_{trans} and O-Mg-Cl(μ_3)_{trans}. For the monomer **9**, the N_{ax}-Mg-Cl angle is nearly linear at a 178.36° angle and the N_{eq}-Mg-Cl angle is more open than a right angle at 98.98° showing the equatorial N atoms are slightly out of a perfect equatorial plane. These data show that Me₆TREN is capping one hemisphere of the magnesium atom.

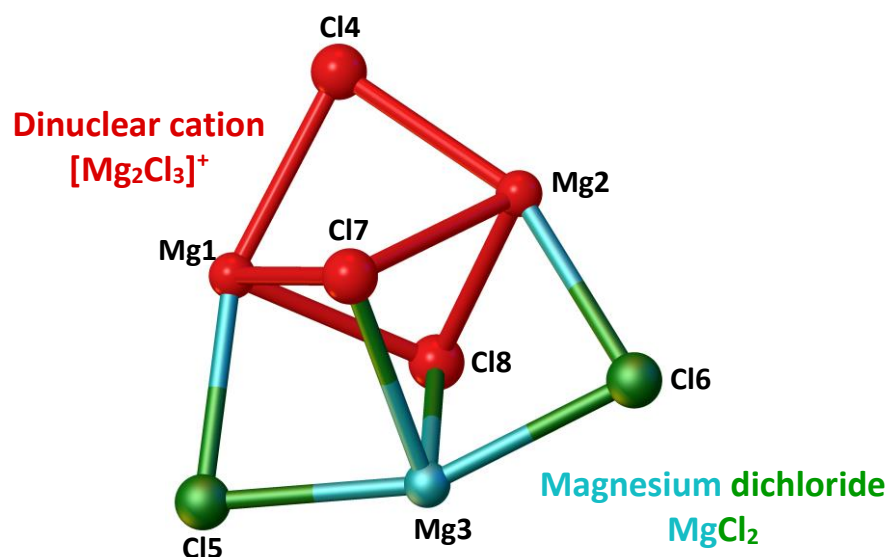
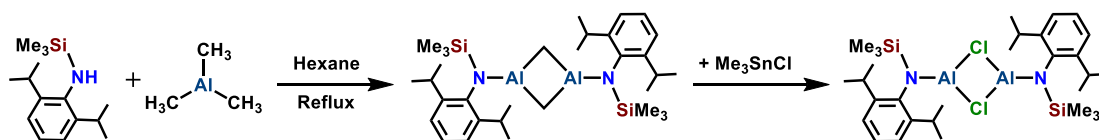


Figure 2.18: Alternative view of the molecular structure of the $[Mg_3Cl_5]^+$ core, the donor ligands were removed for more clarity.

2.4.3. Further crystallographic studies

In addition to the structures obtained for the product of each reaction, it is important to investigate the crystal structure of the starting material as well. Hence the structure of “(Dipp)(SiMe₃)AlCl₂” was sought to see if there is a match with the dimer [(Dipp)(SiMe₃)AlCl₂]₂ introduced by Roesky and co-workers, who obtained it by an alternative method, namely treating [(Dipp)(SiMe₃)AlMe₂]₂ with trimethyltin chloride (Scheme 2.6).^{11,42}



Scheme 2.6: Roesky's synthetic pathway to prepare [(Dipp)(SiMe₃)AlCl₂]₂.

Crystals were obtained from a solution in THF at -70°C after the addition of one equivalent of (Dipp)(SiMe₃)NLi to AlCl₃ in Et₂O, followed by filtration of the resulting LiCl. The structure obtained upon cooling at -70°C was the solvent separated

lithium aluminate $[(\text{Dipp})(\text{SiMe}_3)\text{AlCl}_3]^- [\text{Li}\cdot 4\text{THF}]^+$ **14**, in a yield of 55 % (Figure 2.19). It was surprising at first thought as the LiCl precipitate was fully filtered to obtain a clear solution, but the product must have resulted from the slight solubility of LiCl in Et₂O, it is however evidence that this other side product should be considered in the reaction. This observation may somehow turn to our advantage as the $[(\text{Dipp})(\text{SiMe}_3)\text{AlCl}_3]^-$ anion is already formed, hence boosting the yield in further reaction to give magnesium complexes, which is limited by the Cl ratio.

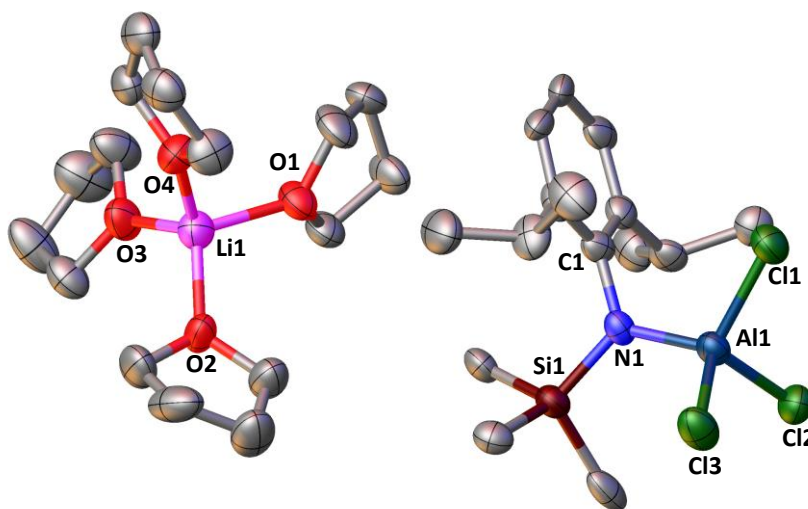


Figure 2.19: Molecular structure of **14** $[(\text{Dipp})(\text{SiMe}_3)\text{AlCl}_3]^- [\text{Li}\cdot 4\text{THF}]^+$. Hydrogen atoms are omitted for clarity. Thermal ellipsoids are drawn at the 50 % probability level.

A related structure was obtained when the same synthesis used to prepare compound **1** was performed in DME instead of THF, in an attempt to obtain two $[(\text{Dipp})(\text{SiMe}_3)\text{AlCl}_3]^-$ anions with the previously demonstrated $[\text{Mg}_2\text{Cl}_2\cdot 4\text{DME}]^{2+}$ dication.⁴³ However the crystals obtained after addition of ⁿBuMgCl to “(Dipp)(SiMe₃)AlCl₂” and slow diffusion of hexane, gave another solvent separated lithium aluminate $[(\text{Dipp})(\text{SiMe}_3)\text{AlCl}_3]^- [\text{Li}\cdot 3\text{DME}]^+$ **15**, yield: 60 % (Figure 2.20).

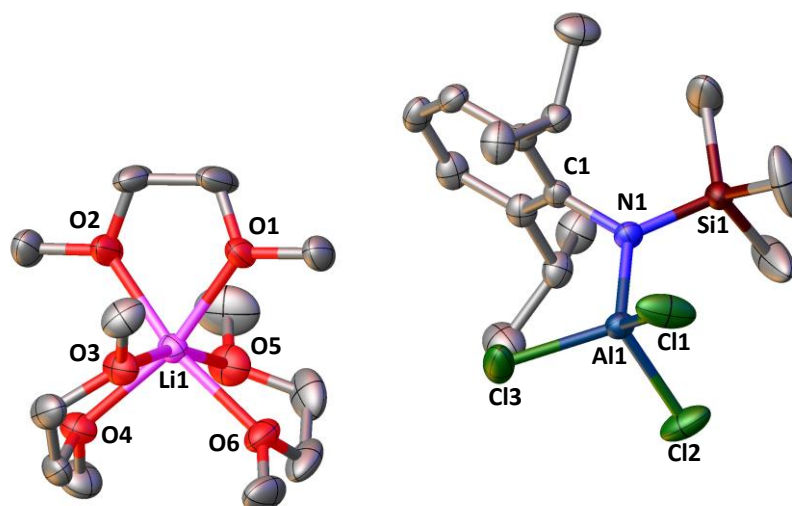


Figure 2.20: Molecular structure of **15** [(Dipp)(SiMe₃)AlCl₃]⁻ [Li·3DME]⁺. Hydrogen atoms are omitted for clarity. Thermal ellipsoids are drawn at the 50 % probability level. Selected bond distances (Å) d angles (°): Li-O 2.113; Al1-N1 1.820(2); Al-Cl 2.1581; N1-C1 1.439(3); N1-Si1 1.740(2); Al1-N1-C1 118.82(18); Al1-N1-Si1 118.05(18); C1-N1-Si1 123.13(13); O-Li-O 77.81*; O1-Li1-O3 93.2(2); O1-Li1-O4 165.0(3); O1-Li1-O5 98.3(2); O1-Li1-O6 94.2(2), O2-Li1-O3 101.1(2); O2-Li1-O4 91.2(2); O2-Li1-O5 93.2(2); O2-Li1-O6 166.6(3); O3-Li1-O4 163.2(3); O3-Li1-O6 90.2(2); O4-Li1-O6 98.2(2). Atoms which do not carry a numerical label represent average parameter values. * Bite angle of DME.

2.5. Introduction: characterisation techniques for the solution studies of magnesium aluminates

2.5.1. Raman spectroscopy

Raman spectroscopy is a close relative to Infra-Red (IR) spectroscopy as both provide information about the vibrational and rotational state of the molecule studied (Figure 2.21b). Their differences arise from the collection of the information; IR spectroscopy recognises changes in the dipole moment of a molecule, whereas Raman spectroscopy detects polarization variations of this molecule by measuring the scattering light. In more detail, a molecule is irradiated by a monochromatic light, often a laser beam, which disrupts the electron cloud causing changes in the polarisation. The molecule gains energy and is excited to a so called “virtual state” which lies lower than the real excited state of the molecule. From this phenomenon, three types of lights

are scattered and measured: namely Stokes, anti-Stokes and Rayleigh scattering (Figure 2.21a).

Raman spectroscopy is widely used in a number of areas requiring microscopic, non-damaging chemical analysis and imaging measurements. It is quick, sensitive, easy to use and the analyte can be solid, gaseous or liquid but also gel, slurry or a powder. The fields using Raman spectroscopy generally consist of pharmaceuticals and cosmetic companies, geologists and mineralogists, material developments (carbon material and semiconductors) and finally life science.⁴⁴⁻⁴⁹

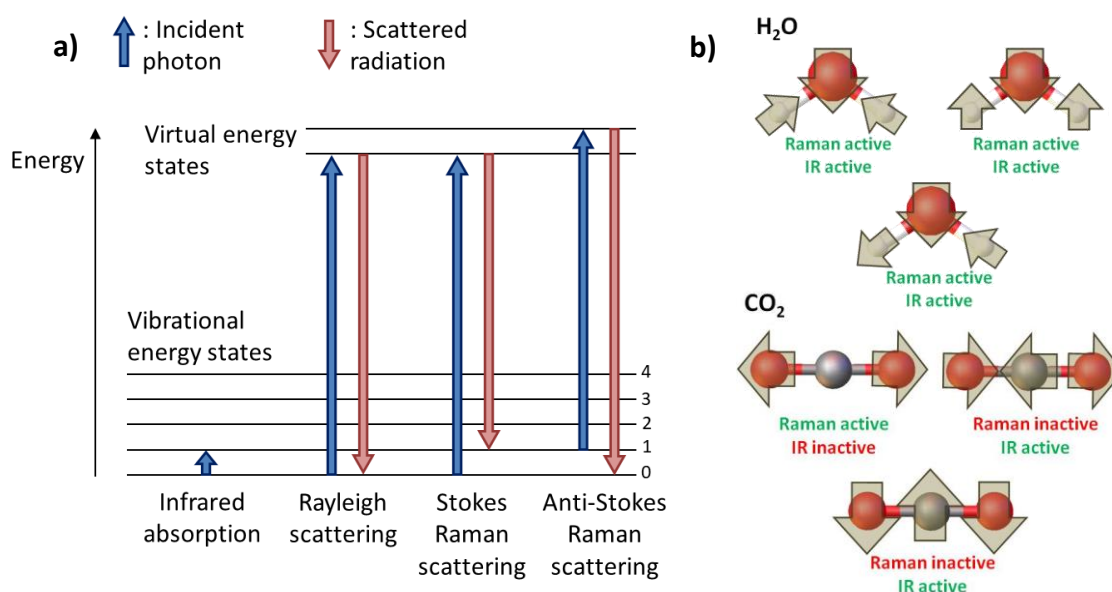


Figure 2.21: a) diagram showing the three types of light scattered in Raman spectroscopy; b) Different vibrational states observed in Raman and IR spectroscopy.

Because of certain Raman inactive vibrations, there is a certain limitation in the recognition of a few types of compounds. Therefore, in most cases Raman spectroscopy is chosen for molecules containing features leading to strong Raman spectral bands; these features can be summarised as symmetrical stretching, multiple bonds, rings and heavier atoms.

Raman spectroscopy was previously used in a few studies of magnesium aluminate electrolytes, both in solution and solid state. Section 1.2.5.2 of Chapter 1 covers these studies in more details.

2.5.2. Electrospray ionisation mass spectrometry

In an ESI-MS, the metal capillary from which the solution of the sample arises is subjected to a high voltage. An electric field is created and the emerging sample solution undergoes electrophoretic movement in response to this electric field. The positive ion mode forces the anions to migrate toward the metal capillary by inducing a positive potential (oxidation), whereas the cations will be repulsed from the metal capillary and be attracted by the counter-electrode situated a short distance from the end of the capillary (Figure 2.22). The pull of the cations at the edge of the capillary creates a surface tension to form a cone called the Taylor cone, where its tip is its least stable part, creating a fine strand which breaks to form a mist of charged microdroplets progressively decreasing in size to nanodroplets. In the negative mode the process is simply reversed where the reduction occurs at the capillary and the oxidation at the counter-electrode.^{50–56} ESI-MS gradually made its way to a very useful method for the characterisation of organometallic reagents. Its strength emanates from its ability to specifically deduce the stoichiometry of a studied compound but also its aggregation state in solution and the solvation on a metal centre. Its capability to exclusively detect the charged species present in solution gives the chance to observe ionic behaviour in solution often involved in organometallic reactions originating from the electronic differences between the metal and the organic moieties.^{57–60}

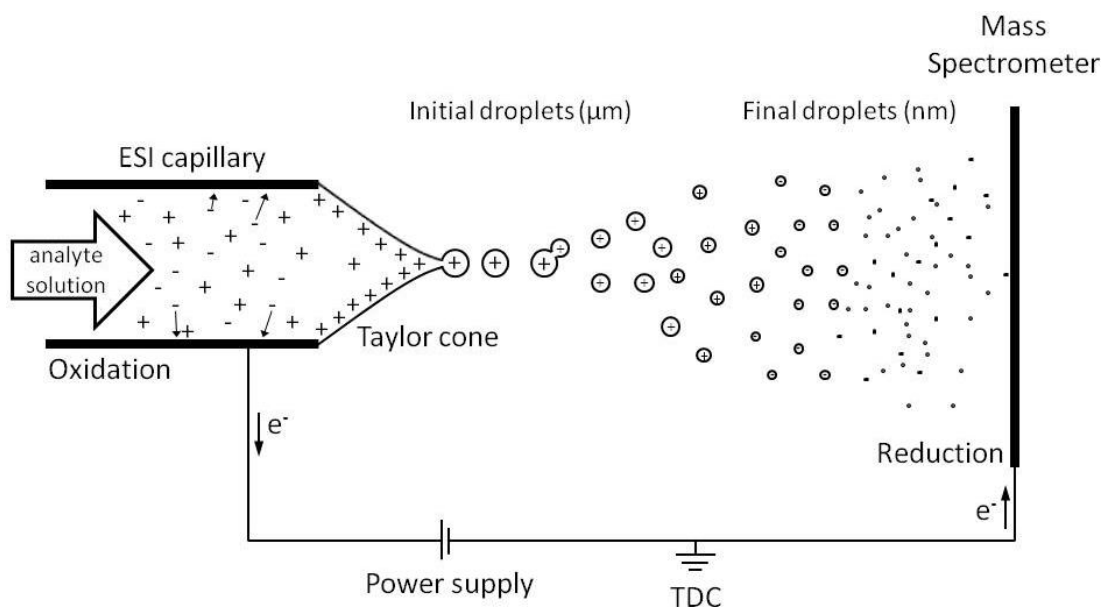


Figure 2.22: Schematic illustration of ESI-MS process in the positive ion mode.

Subambient pressure ionisation with nanoelectrospray mass spectrometry, a mild variant of ESI-MS, was used by Liu and co-workers where they observed the presence of the mononuclear magnesium chloride cation $[\text{MgCl}\cdot 3\text{THF}]^+$ in a THF solution of $[\text{Ph}_3\text{AlCl}]^- [\text{Mg}_2\text{Cl}_3\cdot 6\text{THF}]^+$.¹⁸

2.6. Raman spectroscopy results

This section presents preliminary results performed on Raman spectroscopy, in collaboration with Professor Duncan Graham within the University of Strathclyde, for dinuclear **1**, trinuclear **5** and mononuclear **9**. As a reminder, Raman spectroscopy was used by Aurbach on his magnesium aluminate electrolytes where his aim was to observe different vibrational bands corresponding to both the aluminium anion and the magnesium cation leading to characterisation of these electrolytes in solution. Here we want to investigate this technique with the compounds presented in Section 2.3 possessing the common anion $[(\text{Dipp})(\text{SiMe}_3)\text{NAlCl}_3]^-$ but different cations $[\text{Mg}_2\text{Cl}_3\cdot 6\text{THF}]^+$, $[\text{Mg}_3\text{Cl}_5\cdot 6\text{MeTHF}]^+$ and $[\text{MgCl}\cdot \text{Me}_6\text{TREN}]^+$. First their study in solid state using pure isolated compounds was carried out to identify the “fingerprint” signals specific to the different aggregation states and more precisely the different energies between the different Mg-Cl bonds $[\text{Mg}-\text{Cl}_{\text{term}}$, $\text{Mg}-(\mu_2-\text{Cl})$ and $\text{Mg}-(\mu_3-\text{Cl})]$. This work was then extended to the study of these compounds in solution in the hope of observing any presence of a dynamic equilibrium between the different aggregates, a proposition made by Liu et al. who believe that they are key components involved in the reversible deposition mechanism of a Mg battery using electrolytes possessing the $[\text{Mg}_2\text{Cl}_3\cdot 6\text{THF}]^+$ cation.¹⁸

2.6.1. Raman spectroscopy studies in the solid state

All samples were crushed using a mortar and pestle in the glove box and flame sealed in small melting point capillaries as done for the solution samples. The measurements were performed with a lower energy laser (785 nm) to avoid any possible degradation of the sample, but also to limit the background noise frequently observed for solid samples. The measurements focused on the AlCl_3 and MgCl_2 region ($150 - 550 \text{ cm}^{-1}$) for more clarity. Each sample displays vibrational bands for

$[(\text{Dipp})(\text{SiMe}_3)\text{NAlCl}_3]^-$ identified by comparison with the spectra of DippNHSiMe_3 and AlCl_3 (Figure 2.24). The strong vibrational band of the samples corresponding to the Al-Cl bond shifted from 356 to 328 cm^{-1} , it is however harder to say how much the signals for the amine changed due to weaker signal intensity. Moreover these weak but numerous amine signals seem to overlap with the vibrational bands of Mg-Cl bonds, especially for the major one at 240 cm^{-1} . A few differences between the samples can however be spotted, especially with the two signals at 242 and 272 cm^{-1} ; for **5** (Figure 2.23, black spectrum) the intensity is stronger for the signal at 242 cm^{-1} , for **1** (pink spectrum) the two signals are more even and finally **9** (green spectrum) displays only a signal at 272 cm^{-1} . It is however not clear if these changes are influenced by differences in Mg-Cl bonds or if they come from the amine itself.

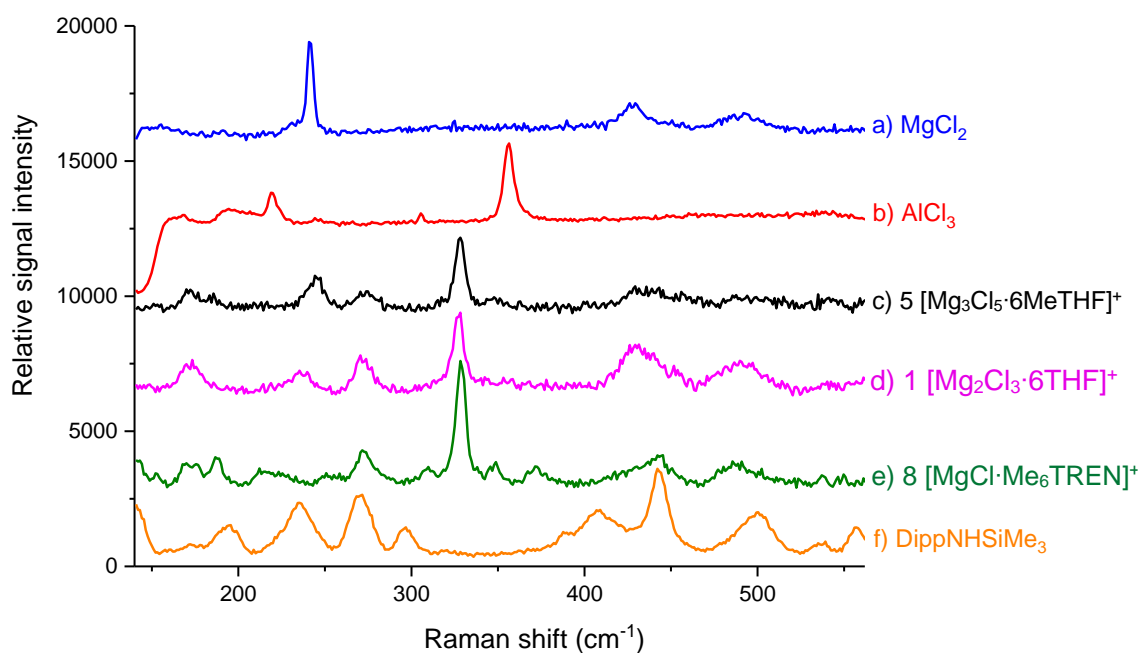


Figure 2.23: Raman spectra of a powder sample of a) MgCl_2 b) AlCl_3 c) **5** d) **1** e) **9** f) DippNHSiMe_3 (liquid).

2.6.2. Raman spectroscopy studies in solution

Although no conclusive results were obtained from the study of the compounds in solid state, the solution analysis was still carried out, hoping to observe

complementary information. Three samples were prepared in the glove box, where 0.1 M solutions were prepared in THF for compounds **1** and **9**, and in MeTHF for compound **5** to preclude Lewis donor exchange and then aggregation state change. These solutions were then transferred in small melting point glass capillaries prior to flame sealing using a Bunsen burner. The 633 nm monochromatic laser was manually focused on the capillary, but unfortunately the signal displayed peaks almost exclusively corresponding to THF for compounds **1** and **9** (Figure 3.24), and MeTHF for compound **5** (Figure 2.23). The solutions of MgCl₂ and AlCl₃ in THF show characteristic signals at 207 and 321 cm⁻¹ respectively. The spectra of **1** and **9** display small vibrational bands at 321 cm⁻¹ showing presence of an aluminium species if not AlCl₃ itself. A signal from MeTHF appeared at a similar wavelength but the related signal for **5** is stronger than the MeTHF standard showing evidence of an aluminium species as well. However no spectra from the magnesium aluminates display vibrational bands near the MgCl₂ or even signals for DippN(SiMe₃). This seems an odd result as the literature shows successful acquisition of strong emission of vibrational bands with [EtAlCl₃]⁻ [Mg₂Cl₃·6THF]⁺, which is in theory less Raman active than **1** due to the absence of an aromatic group.

These results are only preliminary and further experiments using different parameters could supply more characteristic spectra. Such changes could involve the use of less powerful laser source (785 nm) which could attenuate the strong vibrational bands from the THF and MeTHF, but also the use of more concentrated solution, and the use of a larger sample container. The very narrow capillary tubes and the manual focus of the laser do not combine to give accuracy in the measurement, using sealed vials instead would allow the use of auto-focusing apparatus newly acquired.

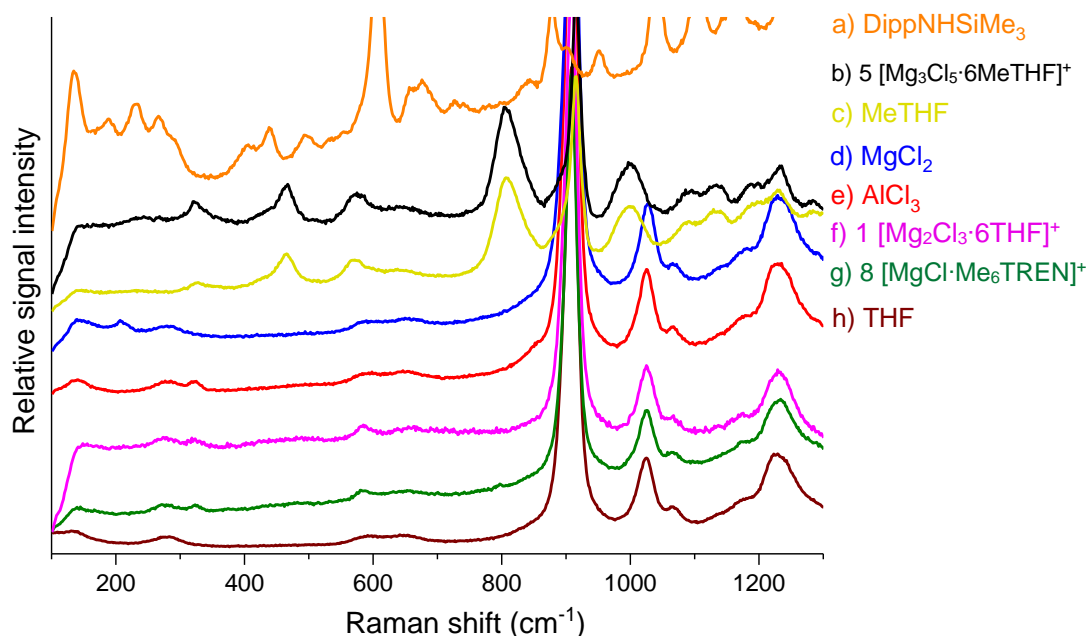


Figure 2.24: Raman spectra of **a)** pure DippNHSiMe₃ **b)** 0.1 M solution of **5** in MeTHF **c)** MeTHF **d)** MgCl₂ solution 0.1M in THF; **e)** AlCl₃ solution 0.1 M in THF; **f)** 0.1 M solution of **1** in THF; **g)** 0.1 M solution of **9** in THF; **h)** THF.

2.6.3. Raman spectroscopy summary

Both solution and solid studies of compounds **1**, **5** and **9** using Raman spectroscopy shows no apparent pattern identifying the presence of different aggregation level in their cations. The spectra of the solid state study display only subtle differences which, due to the lack of existing library of similar compounds, did not give conclusive information. Even without the characteristic features in the Raman spectra corresponding to the different cation aggregation hoped for from the solid state study, the study with the compounds in solution went ahead. The spectra in solution exhibit almost exclusively overpowering bands corresponding to THF or MeTHF, whereas the signals of interest at lower shifts seemed to be too low in intensity to be accurately observed. According to these results Raman spectroscopy doesn't appear to be a powerful method to study and analyse the different aggregations in both solid state and solution. It was therefore decided to focus on a different technique to achieve a successful study, namely Electrospray-Ionisation Mass Spectrometry.

2.7. Electrospray ionisation mass spectrometry studies

This section presents the results of the ESI-MS measurements performed at Georg-August Universität in Göttingen thanks to a close collaboration with Professor Konrad Koszinowski. These measurements were carried out on solutions of pure isolated crystals of **1**, **2**, **4**, **6**, **8** and **9** in THF and **5** in MeTHF. Supplementary experiments were made by running **1** in MeTHF, hoping to see the behaviour of the THF solvated cation of **1** $[\text{Mg}_2\text{Cl}_3 \cdot 6\text{THF}]^+$ in bulk MeTHF and vice-versa with the MeTHF solvated cation of **5** $[\text{Mg}_3\text{Cl}_5 \cdot 6\text{MeTHF}]^+$ in bulk THF. Finally a study of the effect of the sample concentration on the aggregation state of the cation of **1** was carried out.

2.7.1. ESI-MS of the aluminium anions

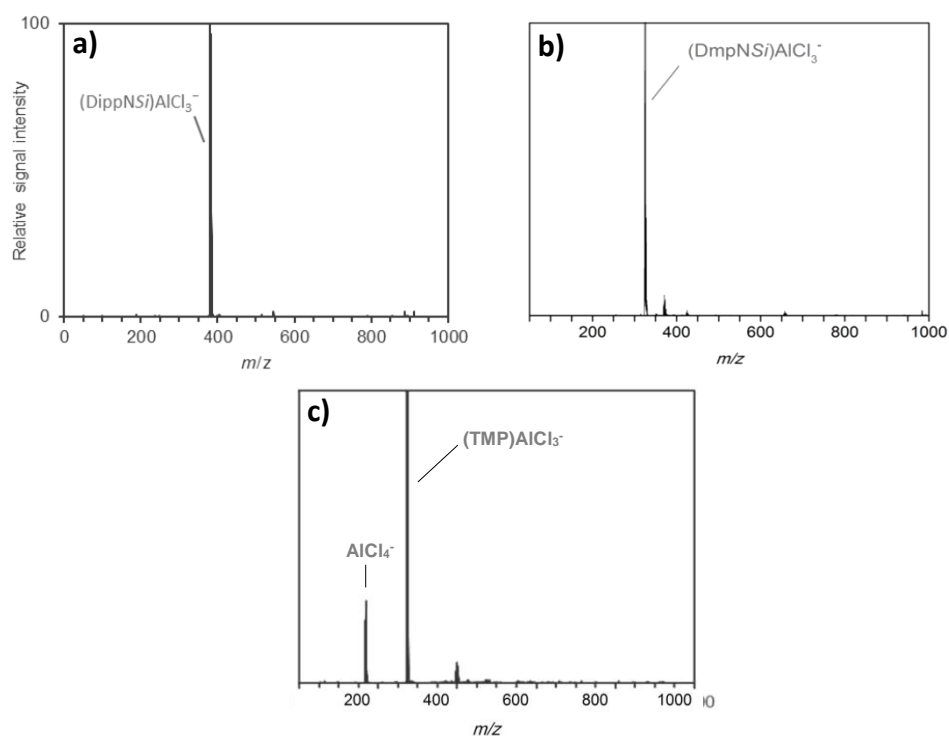


Figure 2.25: a) Negative-ion mode ESI-mass spectrum of a 20 mM solution of $[(\text{Dipp})(\text{SiMe}_3)\text{AlCl}_3]^- [\text{Mg}_2\text{Cl}_3 \cdot 6\text{THF}]^+$, **1** in THF; b) Negative-ion mode ESI mass spectrum of a 20 mM solution of $[(\text{Dmp})(\text{SiMe}_3)\text{AlCl}_3]^- [\text{Mg}_2\text{Cl}_3 \cdot 6\text{THF}]^+$, **2**, in THF; c) Negative-ion mode ESI-mass spectrum of a 20 mM solution of $[(\text{TMP})\text{AlCl}_3]^- [\text{Mg}_2\text{Cl}_3 \cdot 6\text{THF}]^+$, **4**, in THF.

Negative-ion mode ESI-MS of a THF solution of **1** $[(\text{Dipp})(\text{SiMe}_3)\text{NAlCl}_3]^-$ $[\text{Mg}_2\text{Cl}_3 \cdot 6\text{THF}]^+$ and **2** $[(\text{Dmp})(\text{SiMe}_3)\text{NAlCl}_3]^-$ $[\text{Mg}_2\text{Cl}_3 \cdot 6\text{THF}]^+$ led to exclusive detection of the anionic compound of this salt (Figure 2.25 a and b). For all other salts investigated which contained these two amines (**5**, **7** and **9** with $\text{DippN}(\text{SiMe}_3)$, **2** with $\text{DmpN}(\text{SiMe}_3)$), virtually the same result was obtained. These findings strongly suggest that solutions of these salts all contain the crystallographically characterised free $[(\text{Dipp})(\text{SiMe}_3)\text{NAlCl}_3]^-$ and $[(\text{Dmp})(\text{SiMe}_3)\text{NAlCl}_3]^-$ to a significant extent. Some signals corresponding to $[(\text{Dipp})(\text{OSiMe}_3)\text{NAlCl}_3]^-$ and $[(\text{Dmp})(\text{OSiMe}_3)\text{NAlCl}_3]^-$ which can come from the preparation step of the amine itself, or from oxygen insertion into the desired product during the ESI measurement, are observed in small proportions at higher masses. For $[(\text{TMP})\text{AlCl}_3]^-$ $[\text{Mg}_2\text{Cl}_3 \cdot 6\text{THF}]^+$ the presence of $[\text{AlCl}_4]^-$ is also observed, which can be related to the X-Ray study which showed that the comparison of the bond lengths and angles of the TMP containing anion hinted to a less stable structure (longer N-Al bonds) compared to anions possessing $\text{DippN}(\text{SiMe}_3)$ or $\text{DmpN}(\text{SiMe}_3)$. The observed isotope patterns of $[(\text{Dipp})(\text{SiMe}_3)\text{NAlCl}_3]^-$ and $[(\text{Dmp})(\text{SiMe}_3)\text{NAlCl}_3]^-$ shown in Figure 2.26 are also consistent with the simulated ones where the typical patterns for chlorides and carbons are present.

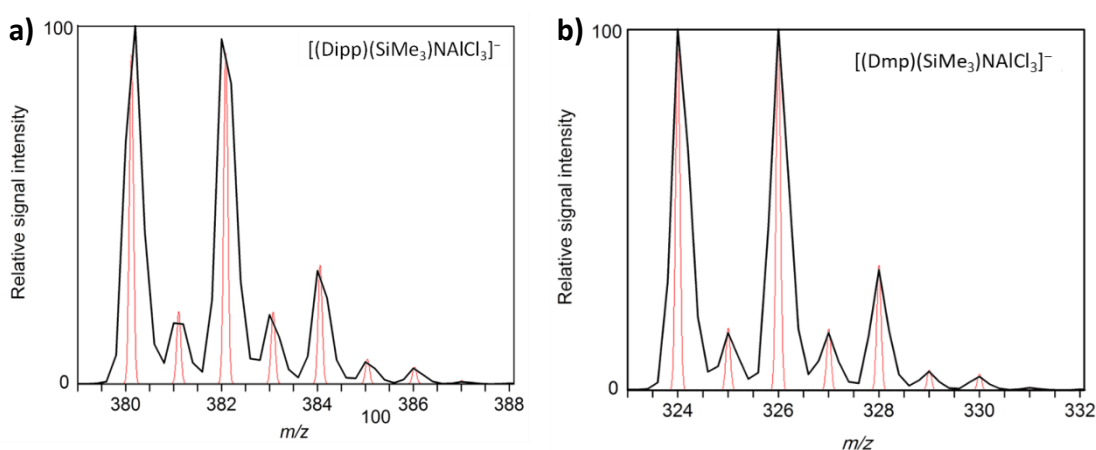


Figure 2.26: a) Comparison of observed (black) and simulated (red) isotope pattern of $[(\text{Dipp})(\text{SiMe}_3)\text{NAlCl}_3]^-$; b) Comparison of observed (black) and simulated (red) isotope pattern of $[(\text{Dmp})(\text{SiMe}_3)\text{NAlCl}_3]^-$.

2.7.2. ESI-MS of the different magnesium cations

In positive-ion mode, the THF solvated dinuclear magnesium cations $[\text{Mg}_2\text{Cl}_3 \cdot 6\text{THF}]^+$ of **1**, **2** and **4** display virtually identical spectra in THF (see Figure 2.27a for the spectrum of **1**) where the trinuclear complex $[\text{Mg}_3\text{Cl}_5 \cdot n\text{THF}]^+$ ($n = 5$ and 6) is predominantly observed, but also to a slightly lesser extent the dinuclear complex $[\text{Mg}_2\text{Cl}_3 \cdot n\text{THF}]^+$ ($n = 3, 4$ and 5). Finally the mononuclear species $[\text{MgCl} \cdot 3\text{THF}]^+$ is also detected in small quantities. It is not clear whether all these different aggregates of the magnesium cation were already present in the original sample solution or whether they formed during the ESI process. The ESI process produces charged nanodroplets, which permanently lose solvent molecules due to evaporation. The increased effective concentration in these nanodroplets can lead to shifts of aggregation equilibria and thus, to formation of the observed trinuclear ions.^{61,62} The concentration dependent measurements of **1** at 5, 15, 30 and 50 mM in THF, displayed in Figure 2.27b, show that the relative abundance of the mononuclear ion decreases as a function of concentration, as expected through on the basis of the law of mass action. The fraction of the dinuclear ions slightly increases with higher concentrations, whereas that of their trinuclear counterparts decreases slightly, the reason for this decrease not being obvious.

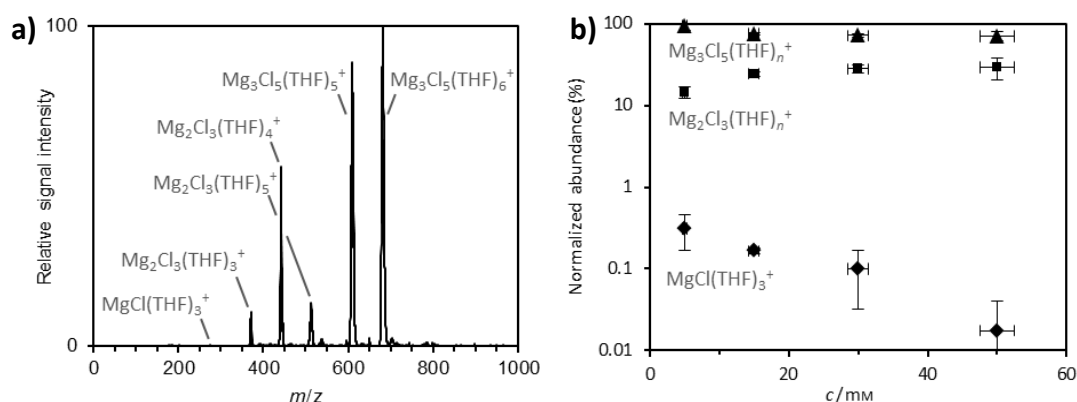


Figure 2.27: a) positive-ion mode ESI mass spectrum of a 20 mM solution of $[(\text{Dipp})(\text{SiMe}_3)\text{AlCl}_3]^- [\text{Mg}_2\text{Cl}_3 \cdot 6\text{THF}]^+$, **1**, in THF; b) concentration dependence of the normalized abundances of mono-, di- and trinuclear cations observed upon positive-mode ESI of solutions of **1** at 5, 15, 30 and 50 mM in THF.

Further information was obtained from the gas-phase fragmentation experiments shown in Figure 2.28. The Mg complexes binding THF exclusively dissociate by

losing one or two solvent molecules. The larger and more fully solvated ions lose one THF molecule so easily that it occurred without a touch of excitation energy, as the poorer mass resolution of the observed isotope patterns for these species indicates (Figure 2.28a). For the smaller, less solvated molecules the loss of one THF requires more excitation energy inducing the concomitant addition of one water molecule to counter the decrease in the coordination number (the ion trap mass spectrometer inevitably contains a low partial pressure of background water) (Figure 2.28b).

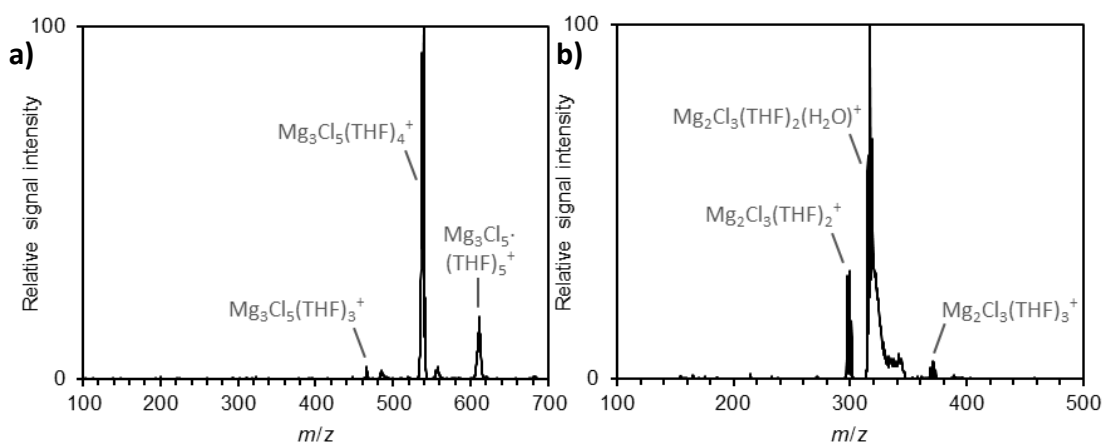


Figure 2.28: a) Mass spectrum of mass-selected $[\text{Mg}_3\text{Cl}_5 \cdot 5\text{THF}]^+$ ($m/z = 610$) and its fragment ions produced upon collision induced dissociation ($V_{\text{exc}} = 0.45$ V) b) Mass spectrum of mass-selected $[\text{Mg}_2\text{Cl}_3 \cdot 3\text{THF}]^+$ ($m/z = 371$) and its fragment ions produced upon collision induced dissociation ($V_{\text{exc}} = 0.40$ V).

As mentioned in the previous paragraph, higher solvation of the cation leads to poor resolution of the isotope pattern where broad signals give rise to a few peaks only which seems to be in accordance with the simulated isotope pattern. Less solvated cations led however to cleaner, well resolved isotope patterns which match the simulated ones.

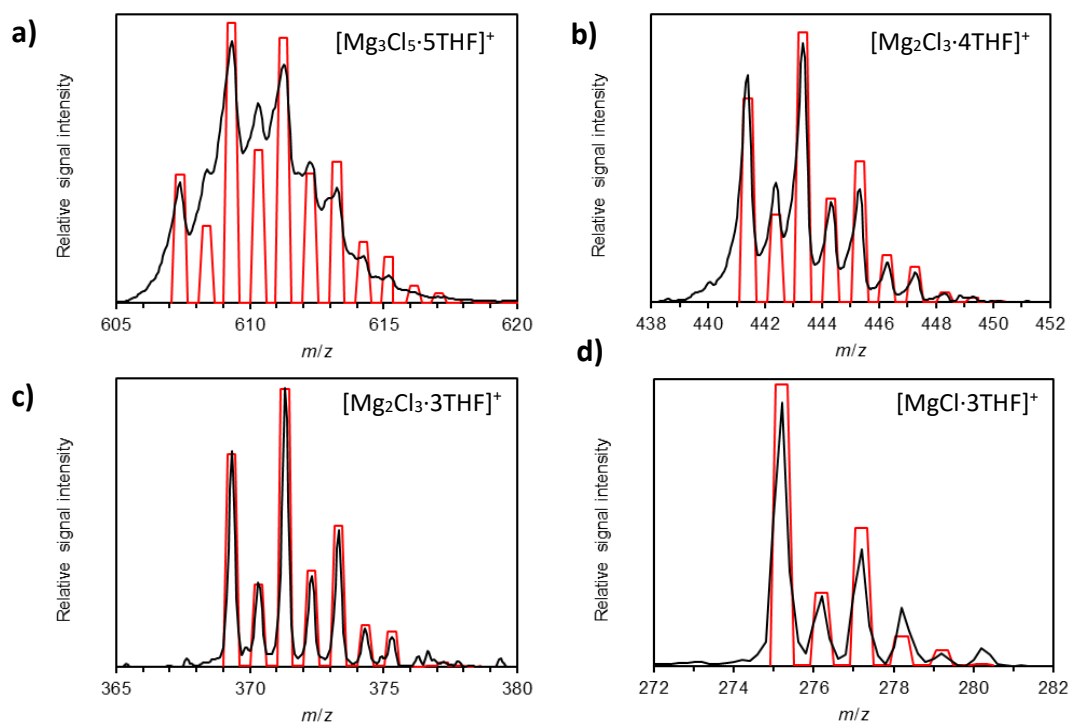


Figure 2.29: Compound **1**: **a)** Comparison of observed (black) and simulated (red) isotope pattern of $[\text{Mg}_3\text{Cl}_5\cdot 5\text{THF}]^+$; **b)** Comparison of observed (black) and simulated (red) isotope pattern of $[\text{Mg}_2\text{Cl}_3\cdot 4\text{THF}]^+$; **c)** Comparison of observed (black) and simulated (red) isotope pattern of $[\text{Mg}_2\text{Cl}_3\cdot 3\text{THF}]^+$; **d)** Comparison of observed (black) and simulated (red) isotope pattern of $[\text{MgCl}\cdot 3\text{THF}]^+$.

The positive-ion mode of a solution of **5** $[(\text{Dipp})(\text{SiMe}_3)\text{NAlCl}_3]^- [\text{Mg}_3\text{Cl}_5\cdot 6\text{MeTHF}]^+$ results in the detection of the trinuclear ions $[\text{Mg}_3\text{Cl}_5\cdot n\text{MeTHF}]^+$ ($n = 4$ and 5). In comparison with the previous spectra with **1** in THF, the nuclearity of the present complexes is significantly shifted toward the higher aggregation state, in accordance with the behaviour in the solid state (Figure 2.30a). As previously observed with the THF solvated cations, the higher MeTHF solvate easily loses one solvent molecule upon collision induced dissociation but the less solvated species require more energy, which often results in coordination of water molecules present in the ion trap so the Mg atom conserves a suitable coordination number (Figure 2.30b). Again, the MeTHF richer cation displays a poorly resolved isotope pattern due to the easy association/dissociation of a fifth MeTHF (Figure 2.30 c and d).

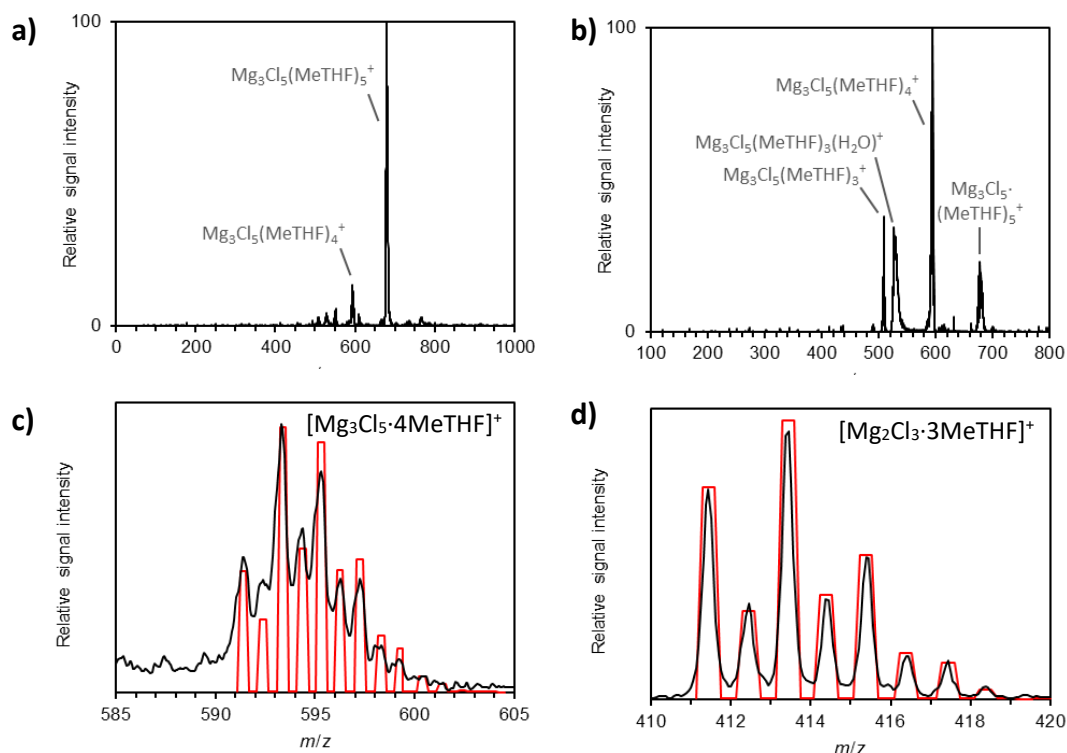


Figure 2.30: **a)** Positive-ion mode ESI mass spectrum of a 20 mM solution of [(Dipp)(SiMe₃)AlCl₃]⁻ [Mg₃Cl₅·6MeTHF]⁺, **5**, in MeTHF; **b)** Mass spectrum of mass-selected [Mg₃Cl₅·6MeTHF]⁺ (*m/z* 679) and its fragment ions produced upon collision induced dissociation (*V*_{exc} = 0.40 V); **c)** Comparison of observed (black) and simulated (red) isotope pattern of [Mg₃Cl₅·4MeTHF]⁺; **d)** Comparison of observed (black) and simulated (red) isotope pattern of [Mg₂Cl₃·3MeTHF]⁺

Another study was made by measuring the ESI-MS spectrum of a solution of the MeTHF solvated compound **5** [(Dipp)(SiMe₃)AlCl₃]⁻ [Mg₃Cl₅·6MeTHF]⁺ in THF. The recorded spectrum shows that all the MeTHF molecules were replaced by THF present in large excess (Figure 2.31a). The control reverse experiment, where the THF solvated compound **1** [(Dipp)(SiMe₃)AlCl₃]⁻ [Mg₂Cl₃·6THF]⁺, was dissolved in MeTHF, was performed. This results in the replacement of most THF molecules by MeTHF, but a couple of complexes retain a single THF molecule as well (e.g. [Mg₃Cl₅·THF·4MeTHF]⁺, Figure 2.31b). This incomplete exchange indicates that the coordinating power of THF with the Mg atom is stronger than that of MeTHF, as expected on the basis of the steric bulk of the ligand.

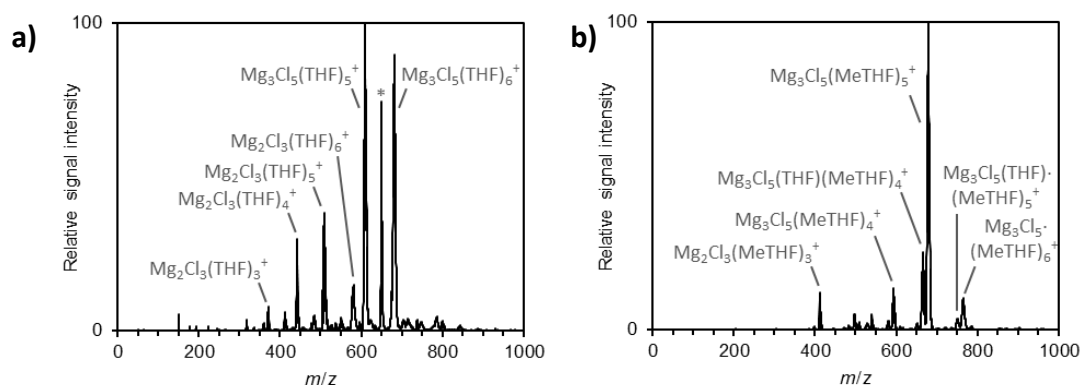


Figure 2.31: **a)** Positive-ion mode ESI mass spectrum of a 20 mM solution of **5** [(Dipp)(SiMe₃)AlCl₃]⁻ [Mg₃Cl₅·6MeTHF]⁺ in THF; **b)** positive-ion mode ESI mass spectrum of a 20-Mm solution of **1** [(Dipp)(SiMe₃)AlCl₃]⁻ [Mg₂Cl₃·6THF]⁺ in MeTHF.

Moving to the N-chelating ligand containing compound, **7** [(Dipp)(SiMe₃)AlCl₃]⁻ [Mg₃Cl₅·3TMEDA]⁺, the sample was run at lower concentration due to its poor solubility in THF. The ions observed belong exclusively to the homologous series [Mg_nCl_{2n-1}·nTMEDA]⁺, where n = 1, 2 and 3 (Figure 2.32a), which all exhibit a 1:1 stoichiometry of magnesium and TMEDA. Likewise, the absence of any THF adducts points to the lack of empty coordination sites at the magnesium centre. Upon collision induced dissociation, the ions exchanged a TMEDA ligand for water only to a minor extent, and due to the presence of the stronger coordinating TMEDA ligand, mainly decomposed by the expulsion of a neutral MgCl₂·TMEDA fragment (Figure 2.32 c and d). This result supports previous observations that [Mg₃Cl₅]⁺ could be viewed as [Mg₂Cl₃]⁺ coordinated by a neutral molecule of MgCl₂, and in the same way, [Mg₂Cl₃]⁺ viewed as [MgCl]⁺ coordinated by MgCl₂ (Section 2.4.3; Figure 2.18). Because of the absence of association/dissociation of TMEDA, the corresponding isotope pattern of the homologous series is well resolved (Figure 2.32 b and Chapter 6 Section 6.2.7 Figure 6.5).

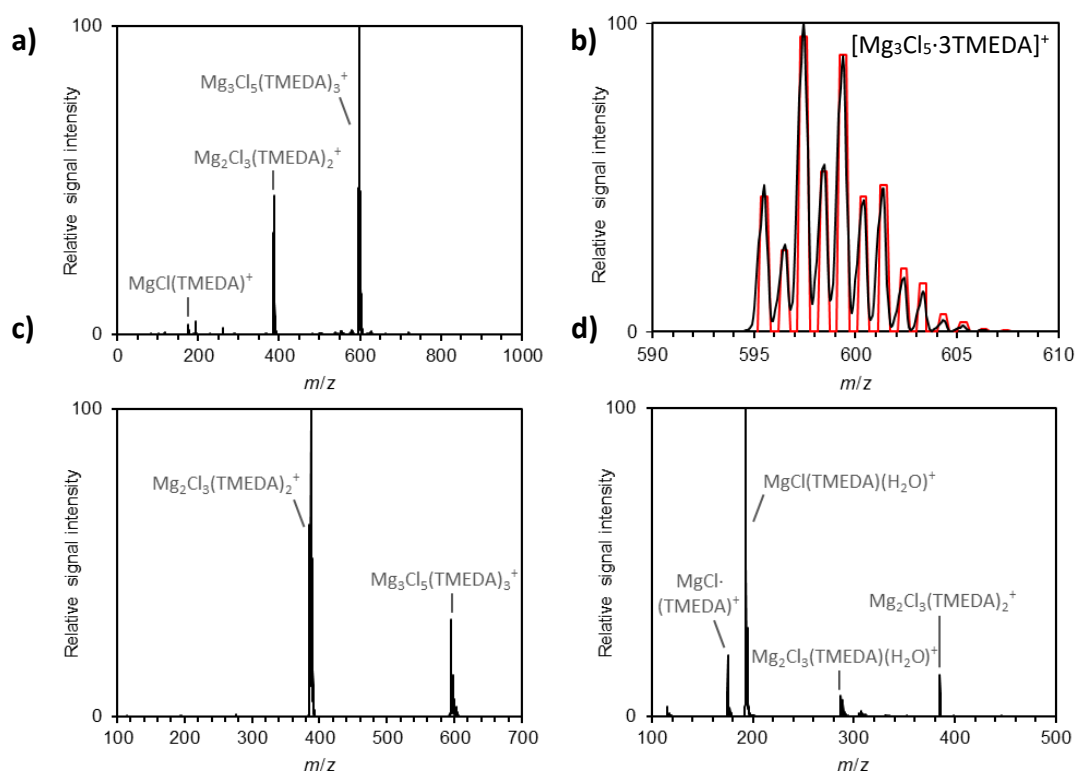


Figure 2.32: **a)** Positive-ion mode ESI mass spectrum of a saturated solution of **7** [(Dipp)(SiMe₃)AlCl₃]⁻ [Mg₃Cl₅·3TMEDA]⁺ in THF; **b)** Comparison of observed (black) and simulated (red) isotope pattern of [Mg₃Cl₅·3TMEDA]⁺; **c)** Mass spectrum of mass-selected [Mg₃Cl₅·3TMEDA]⁺ (*m/z* 599) and its fragment ions produced upon collision induced dissociation (*V*_{exc} = 0.60 V); **d)** Mass spectrum of mass-selected [Mg₂Cl₃·2TMEDA]⁺ (*m/z* 387) and its fragment ions produced upon collision induced dissociation (*V*_{exc} = 1.20 V).

For the Me₆TREN coordinated cations of **9**, [MgCl·Me₆TREN]⁺, the X-Ray characterised mononuclear cations [MgCl·Me₆TREN]⁺ and its dinuclear homologue [Mg₂Cl₃·2Me₆TREN]⁺ were observed (Figure 2.33a). Like in the case with TMEDA, these chelated ions display a 1:1 Mg:ligand stoichiometry and do not bind to THF. In addition, ions containing the protonated ligand were detected. Because of its high Brønsted basicity, the ligand can easily react with traces of protic contaminants remaining in the glassware used or the ESI source. During collision induced dissociation of the dinuclear ion, the loss of neutral MgCl₂·Me₆TREN was observed whereas its mononuclear counterpart undergoes partial decomposition of the ligand (Figure 2.33 c and d). As observed for TMEDA, due to the strong coordinating

properties of Me₆TREN and hence its weak dissociation, the isotope pattern of the two species are generally well resolved (Figure 2.33 b and Chapter 6.2.7. Figure 6.6).

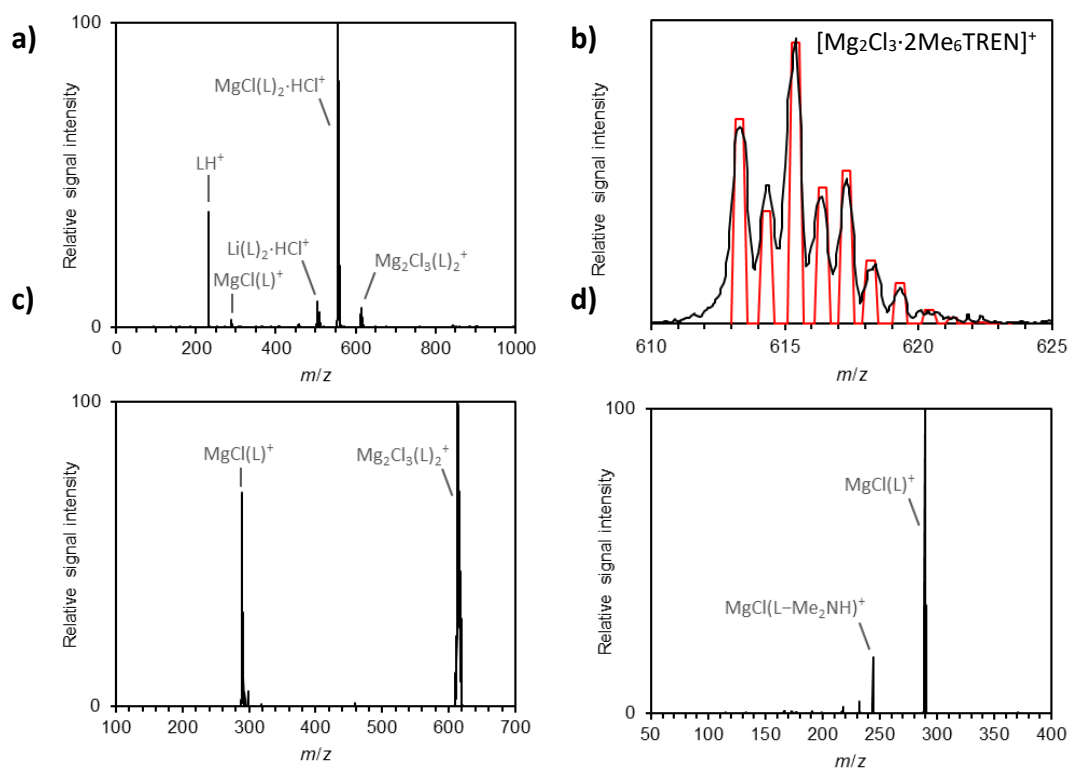


Figure 2.33: **a)** Positive-ion mode ESI mass spectrum of a 20 mM solution of **9** [(Dipp)(SiMe₃)AlCl₃]⁻ [MgCl·Me₆TREN]⁺ in THF; **b)** Comparison of observed (black) and simulated (red) isotope pattern of [Mg₂Cl₃·2Me₆TREN]⁺; **c)** Mass spectrum of mass-selected [Mg₂Cl₃·2Me₆TREN]⁺ (*m/z* 615) and its fragment ions produced upon collision induced dissociation (*V*_{exc} = 0.30 V); **d)** Mass spectrum of mass-selected [MgCl·Me₆TREN]⁺ (*m/z* 289) and its fragment ions produced upon collision induced dissociation (*V*_{exc} = 0.45 V). (L = Me₆TREN).

2.7.3. ESI-MS study of compound 6 in MeTHF

This section shows an ESI-MS study on a crystalline product whose X-ray data was too weak to be solvable, compound **6**. The product was obtained after following the same procedure used to prepare compound **5** but using DmpNHSiMe₃ over DippNHSiMe₃ as the amine of choice, hoping to make [(Dmp)(SiMe₃)AlCl₃]⁻ [Mg₂Cl₃·6MeTHF]⁺, **6**. The other interest of this study is to show that without a successful characterisation of the solid state structure of these types of magnesium aluminate compounds, both the anion and the cation can still be successfully identified in solution using ESI-MS.

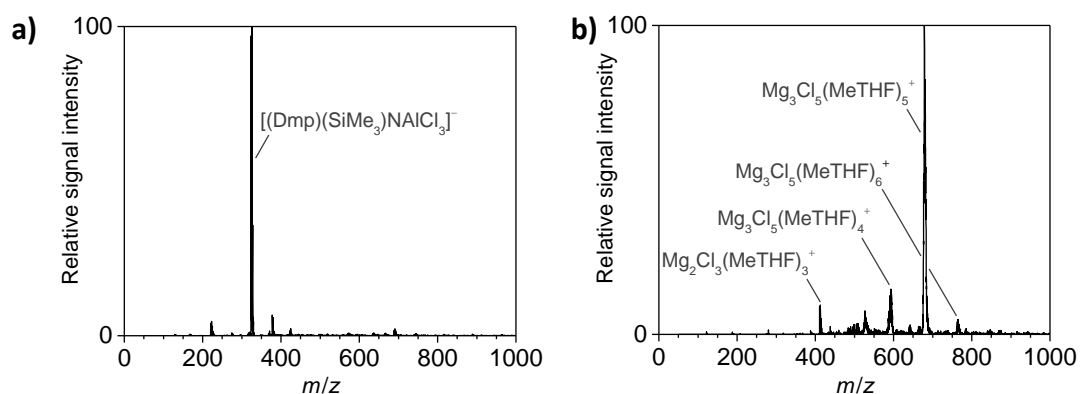


Figure 2.34: a) Negative-ion mode ESI-mass spectrum of a 20 mM solution of compound **6** in MeTHF; b) Positive-ion mode ESI mass spectrum of a 20 mM solution of compound **6** in MeTHF.

Figure 2.34 shows the ESI-MS spectra of compound **6**, presumed to be $[(\text{Dmp})(\text{SiMe}_3)\text{AlCl}_3]^- [\text{Mg}_3\text{Cl}_5 \cdot 6\text{MeTHF}]^+$. The negative-ion mode spectrum shown in Figure 2.34a indisputably shows the presence of the expected anion $[(\text{Dmp})(\text{SiMe}_3)\text{AlCl}_3]^-$. The positive-ion mode spectrum displayed in Figure 2.34b exhibits three different signals for trinuclear species possessing a divergent number of coordinated MeTHF units. This trinuclear species is the same as the ones observed in compound **5**. Other than the signals for trinuclear aggregates, a minor peak representing a dinuclear species is also observed. This species does not appear in the spectrum of compound **5**, but looking more closely at the spectrum the peak is present as well, but in much lower quantities. The spectrum of positive-ion mode of compound **6** is most related to the spectrum of **5** (Figure 2.30a) over the spectrum of **1** (Figure 2.27a), hence the cation was attributed as the trinuclear species $[\text{Mg}_3\text{Cl}_5 \cdot 6\text{MeTHF}]^+$. This result shows that ESI-MS can be a fast technique to characterize the structure of a compound in solution without knowing its solid state structure. This technique can be very useful to study a solution of an electrolyte generated in-situ without prior purification and characterisation through crystallisation and X-ray diffraction study, allowing a direct identification of the species involved, but also giving information on the purity of the mixture when compared with a purified electrolyte in solution.

2.8. NMR studies

Previous multinuclear NMR studies from the literature on these magnesium aluminate complexes (^{27}Al , ^{25}Mg , ^1H and ^{13}C NMR spectroscopy) were not conclusive especially due to the lack of symmetry within the molecule for ^{27}Al and ^{25}Mg , and also the lack of ^1H and ^{13}C active groups on the magnesium cation. This section shows the ^1H and ^{13}C NMR spectroscopic studies of the magnesium amidohaloaluminate compounds **1**, **5**, **7** and **9** (i.e. all containing the same $[(\text{Dipp})(\text{SiMe}_3)\text{NAlCl}_3]^-$ anion paired with a different cation). Even knowing that it might be difficult to study the behaviour of these compounds in solution by this method, it is still a common technique extensively used in organometallic chemistry and worthy of some attention.

The ^1H spectra of all purified isolated crystals shown in Figure 2.35 were collected in d_6 -benzene (C_6D_6). The solubility of these compounds in C_6D_6 is fairly low but apart for compound **7**, all samples displayed suitable spectra for ^1H ; unfortunately the concentration was too low to observe the resonance corresponding to quaternary carbons in the ^{13}C NMR spectra. Figure 3.35 shows that surprisingly the resonances of the amides are remarkably different between the three different compounds. The resonances for the aromatic protons are relatively similar for DippNHSiMe_3 , **1** and **5** where all three protons are displayed as a multiplet formed from signal overlapping. For **9** the multiplet is resolved into a doublet more downfield (equivalent *meta*-CH protons at 7.24 ppm) and a triplet (*ortho*-CH at 7.10 ppm). The protons from the CH of the isopropyl groups are deshielded when the amine was bound to the aluminium; however the deshielding effect observed for **9** seemed to be more pronounced (4.45 ppm) than for **1** and **5** (3.90 and 3.88 ppm respectively). The resonance of the methyl groups of the isopropyl group shows similar results where the resonance of **9** is again more deshielded with a larger split of the two doublets corresponding to two inequivalent CH_3 groups (1.64 and 1.53 ppm). **1** also exhibits two doublets but they are very close leading to overlap (1.33 and 1.31 ppm). For **5** the resonance possesses the same shift as **1** but due to the presence of a MeTHF resonance at a similar shift, it is hard to clarify the splitting pattern. Again, for SiMe_3 the resonance of **9** (0.64 ppm) is more deshielded than those of **1** and **5** (both 0.35 ppm). The reasons for these differences, and especially the differences for the shifts of **9** compared to **1** and **5**, are

not obvious as the $[(\text{Dipp})(\text{SiMe}_3)\text{AlCl}_3]^-$ anion is expected to be the same for all the different compounds as observed in the crystallographic study and with the ESI-MS study, hence this suggests an influence of the cation. The ^{13}C NMR spectra did not give more information as some of the resonances are generally too weak to be resolved.

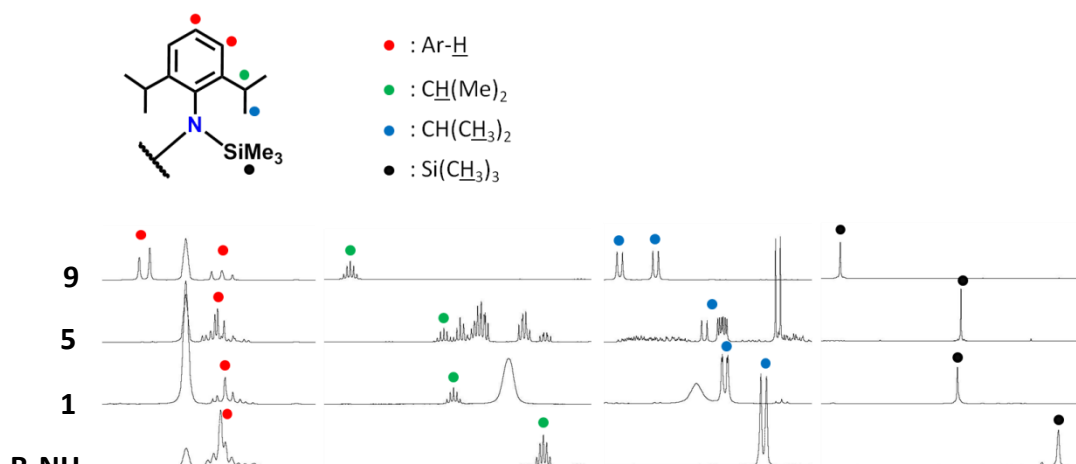


Figure 2.35: ^1H NMR spectra of (bottom to top) **R₂NH** (DippNHSiMe₃), **1** ($[(\text{Dipp})(\text{SiMe}_3)\text{AlCl}_3]^- [\text{Mg}_2\text{Cl}_3 \cdot 6\text{THF}]^+$), **5** ($[(\text{Dipp})(\text{SiMe}_3)\text{AlCl}_3]^- [\text{Mg}_3\text{Cl}_5 \cdot 6\text{MeTHF}]^+$), **9** ($[(\text{Dipp})(\text{SiMe}_3)\text{AlCl}_3]^- [\text{MgCl} \cdot \text{Me}_6\text{TREN}]^+$).

The NMR study was repeated using d_8 -THF instead of C_6D_6 , which leads to stronger signal intensity due to higher solubility. Unlike with C_6D_6 , the proton resonances corresponding to $[(\text{Dipp})(\text{SiMe}_3)\text{AlCl}_3]^-$ (**1**, **5**, **7** and **9**) all possessed the same chemical shifts (Table 2.4). Comparing the shifts of the free donor ligands with these results showed that all but MeTHF were still coordinated to Mg, confirming the similar observations made with the ESI-MS where THF did not replace TMEDA or Me₆TREN (see Table 2.5). Thanks to the greater solubility of the magnesium aluminate compounds in d_8 -THF, a resonance in the ^{27}Al NMR spectrum was observed in the form of a broad peak at 100 ppm. These results could imply that benzene is somehow responsible for the ^1H NMR spectroscopy resonance shifts observed earlier with compound **9**. By simple comparisons and observations, the speculation would be that the benzene affects the cation as it is the only variable factor with **5** and **1** which subsequently affect the anion giving rise to different resonances.

Table 2.4: ^1H (top) and ^{13}C (bottom) NMR spectroscopic data for the anionic moieties of complexes **1**, **5**, **7**, **9** and DippNHSiMe₃ in d_8 -THF.

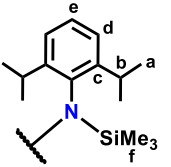
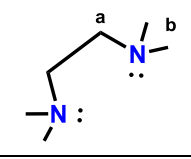
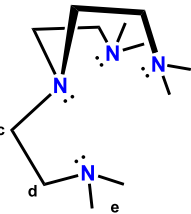
	1	5	7	9	DippNHSiMe ₃
Cation nuclearity	dinuclear	trinuclear	trinuclear	mononuclear	
a	1.13 26.1/25.2	1.13 26.1/25.2	1.14 26.2	1.15 26.3/25.2	1.17 24.1
b	3.88 27.8	3.89 27.8	3.88 27.9	3.88 27.9	3.51 28.9
c	- 147.4	- 147.4	- 147.6	- 147.4	- 145.5
d	6.83 123.0	6.84 123.0	6.85 123.0	6.88 123.0	6.98 123.4
e	6.74 122.2	6.74 122.2	6.75 122.3	6.78 122.3	6.93 124.3
f	0.04 3.1	0.05 3.1	0.04 3.1	0.05 2.9	0.12 1.0

Table 2.5: Comparison of the resonances between free TMEDA and Me₆TREN with the corresponding ligands coordinated to Mg in compounds **7** and **9** by ^1H NMR spectroscopy in d_8 -THF.

	Resonance	7	9	Free ligand
	δ_a	2.38		2.30
	δ_b	2.25		2.14
	δ_c		2.92	2.54
	δ_d		2.79	2.30
	δ_e		2.49	2.15

2.9. Conclusion of the solution-state characterisation

In summary, ESI-MS appears a suitable method to observe the equilibrium between the mono-, di- and trinuclear chloro-magnesium cations in THF solutions. It also shows the influence of the concentrations on this equilibrium where the minor presence of the mononuclear cation $[\text{MgCl}\cdot 3\text{THF}]^+$ decreases at higher concentration. Presence of the stronger coordinative ligands TMEDA and Me_6TREN leads to dissociation of the neutral $\text{MgCl}_2\cdot\text{L}$ ($\text{L} = \text{TMEDA}$ or Me_6TREN) instead of the dissociation of the ligand itself, as observed with THF and MeTHF. Preliminary results using Raman spectroscopy were not as successful as the study of magnesium aluminate compounds in THF solution leading to almost exclusively vibrational bands for the THF. Solid samples however gave hope in observing a difference in the vibrational energies arising from different Mg-Cl bonding modes (Mg-(μ_2 -Cl) in **1** and **5**, Mg-(μ_3 -Cl) in **5** and Mg-Cl_{term} in **9**). NMR spectroscopy continues to be a limited tool for these compounds, where even if some differences are observed in C_6D_6 , the measurements in d_8 -THF display identical chemical shifts which do not give information on the aggregation state of the magnesium cation.

2.10. Conclusion of the solid-state characterisation

This section presented a sturdy synthetic route to synthesise magnesium amidohaloaluminate compounds in THF adopting the generally observed solvent-separated ion pair structure $[(\text{R}_2\text{N})\text{AlCl}_3]^- [\text{Mg}_2\text{Cl}_3\cdot 6\text{THF}]^+$ using the different amines DippNHSiMe₃, DmpNHSiMe₃, PhNHSiMe₃ and TMPH. This was necessary as following previously discussed transmetallation protocols failed to provide access to such species.³⁻⁵ The isolated yields are moderate with 30-44 % for a non-rational reaction which is affected by an inefficient stoichiometry according to the final product.

Following the setup of this new synthetic route to prepare amidohaloaluminate anions easily, our interest was the modification of the magnesium cation aggregation. This was simply achieved by using a variety of Lewis donors, coordinating to the

magnesium atoms in different fashions and by altering its bulk the aggregation of the cation was readily altered to give a mononuclear $[\text{MgCl}\cdot\text{Me}_6\text{TREN}]^+$, a dinuclear species $[\text{Mg}_2\text{Cl}_3\cdot 6\text{THF}]^+$ and two trinuclear species $[\text{Mg}_3\text{Cl}_5\cdot 6\text{MeTHF}]^+$ and $[\text{Mg}_3\text{Cl}_5\cdot 3\text{TMEDA}]^+$. The easy control of new aggregation states in magnesium aluminate compounds is a major advance as it strongly supports a mechanism for electrolyte deposition suggested by Liu and co-workers who believe this involves a mixture of the dinuclear species $[\text{Mg}_2\text{Cl}_3\cdot 6\text{THF}]^+$, the trinuclear species $[\text{Mg}_3\text{Cl}_5\cdot 6\text{THF}]^+$ and the mononuclear $[\text{MgCl}\cdot 5\text{THF}]^+$ aggregates, all found in an equilibrium in solution (Figure 2.36). Although the monomer was observed in solution using the mild conditions of a sub-ambient pressure ionisation with nanoelectrospray mass spectrometry, the trinuclear species was not.¹⁸ The crystal structure of a magnesium amidohaloaluminate in its mononuclear and trinuclear form was, to the best of our knowledge, never observed. The electrochemistry measurements of these potential electrolytes is presented in the next chapter, hence it is not possible to observe the influence of the cation's aggregation, but at this stage of the study it was interesting to know the difference between a magnesium deficient electrolyte (mononuclear cation) and a magnesium rich electrolyte (trinuclear cation).

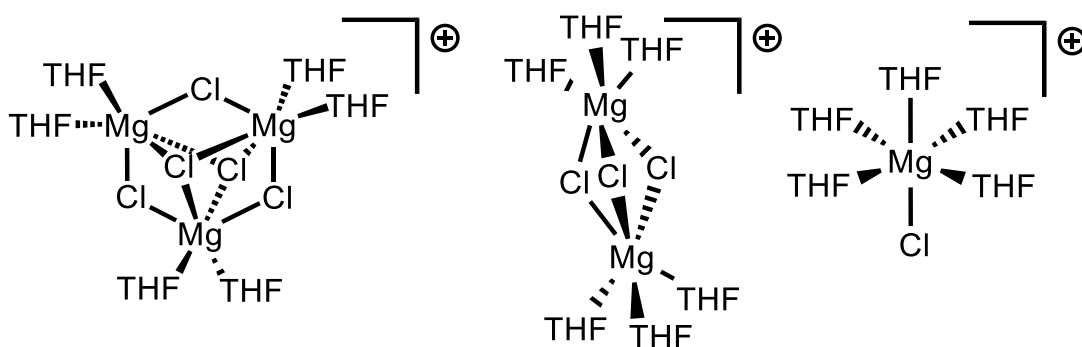


Figure 2.36: Magnesium chloride cations implicated in magnesium aluminate solution chemistry.

This study supports the existence of the different aggregation in a solution of magnesium aluminate electrolyte, however solid-state structures often do not reflect what is really happening in solution. A few techniques were mentioned in previous papers which are proven to have potential for the identification of species in solution, such as Raman spectroscopy, electrospray ionization mass spectrometry and to a lesser

extent NMR spectroscopy. Complementarily to the solid state studies with X-Ray crystallography, these techniques were used to investigate the behaviour of these magnesium amidohaloaluminates compounds in solution and form the cornerstone of the second part of this chapter.

- 1 D. Aurbach, Z. Lu, A. Schechter, Y. Gofer, H. Gizbar, R. Turgeman, Y. Cohen, M. Moshkovich and E. Levi, *Nature*, 2000, **407**, 724–727.
- 2 H. D. Yoo, I. Shterenberg, Y. Gofer, G. Gershinsky, N. Pour and D. Aurbach, *Energy Environ. Sci.*, 2013, **6**, 2265–2279.
- 3 D. Aurbach, H. Gizbar, A. Schechter, O. Chusid, H. E. Gottlieb, Y. Gofer and I. Goldberg, *J. Electrochem. Soc.*, 2002, **149**, A115–A121.
- 4 N. Pour, Y. Gofer, D. T. Major and D. Aurbach, *J. Am. Chem. Soc.*, 2011, **133**, 6270–6278.
- 5 E. G. Nelson, J. W. Kampf and B. M. Bartlett, *Chem. Commun.*, 2014, **50**, 5193–5195.
- 6 T. Liu, Y. Shao, G. Li, M. Gu, J. Hu, S. Xu, Z. Nie, X. Chen, C. Wang and J. Liu, *J. Mater. Chem. A*, 2014, **2**, 3430–3438.
- 7 Z. Zhao-Karger, X. Zhao, O. Fuhr and M. Fichtner, *RSC Adv.*, 2013, **3**, 16330–16335.
- 8 H. S. Kim, T. S. Arthur, G. D. Allred, J. Zajicek, J. G. Newman, A. E. Rodnyansky, A. G. Oliver, W. C. Boggess and J. Muldoon, *Nat. Commun.*, 2011, **2**, 1–6.
- 9 Y. W. Chao, P. A. Wexler and D. E. Wigley, *Inorg. Chem.*, 1989, **28**, 3860–3868.
- 10 W. Vargas, U. Englich and K. Ruhlandt-Senge, *Inorg. Chem.*, 2002, **41**, 5602–5608.
- 11 M. Schiefer, H. Hatop, H. W. Roesky, H. G. Schmidt and M. Noltemeyer, *Organometallics*, 2002, **21**, 1300–1303.
- 12 A. N. Lukoyanov, I. L. Fedushkin, M. Hummert and H. Schumann, *Russ. Chem. Bull.*, 2006, **55**, 422–428.
- 13 L. Yang, D. R. Powell and R. P. Houser, *Dalton Trans.*, 2007, 955–964.
- 14 C. J. Barile, E. C. Barile, K. R. Zavadil, R. G. Nuzzo and A. A. Gewirth, *J. Phys. Chem. C*, 2014, **118**, 27623–27630.
- 15 C. J. Barile, R. G. Nuzzo and A. A. Gewirth, *J. Phys. Chem. C*, 2015, **119**, 13524–13534.
- 16 P. Canepa, S. Jayaraman, L. Cheng, N. N. Rajput, W. D. Richards, G. S. Gautam, L. A. Curtiss, K. A. Persson and G. Ceder, *Energy Environ. Sci.*, 2015, **8**, 3718–3730.

- 17 L. F. Wan and D. Prendergast, *J. Am. Chem. Soc.*, 2014, **136**, 14456–14464.
- 18 T. Liu, J. T. Cox, D. Hu, X. Deng, J. Hu, M. Y. Hu, J. Xiao, Y. Shao, K. Tang and J. Liu, *Chem. Commun.*, 2015, **51**, 2312–2315.
- 19 B. Werner, T. Kräter and B. Neumüller, *Zeitschrift für Anorg. und Allg. Chemie*, 1995, **621**, 346–358.
- 20 D. Loos, K. Eichkorn, J. Magull, R. Ahlrichs and H. Schnöckel, *Zeitschrift für Anorg. und Allg. Chemie*, 1995, **621**, 1582–1588.
- 21 W. Zhang, J.-P. Hu, X.-F. Ding, Y.-J. Wu and Z.-W. Ye, *Inorg. Chem. Commun.*, 2003, **6**, 1185–1187.
- 22 J. K. Vohs, L. E. Downs, M. E. Barfield, K. Latibeaudiere and G. H. Robinson, *J. Organomet. Chem.*, 2003, **666**, 7–13.
- 23 P. C. Andrews, P. C. Junk, I. Nuzhnaya, L. Spiccia and N. Vanderhoek, *J. Organomet. Chem.*, 2006, **691**, 3426–3433.
- 24 V. Pace, P. Hoyos, M. Fernández, J. V Sinisterra and A. R. Alcántara, *Green Chem.*, 2010, **12**, 1380–1382.
- 25 R. B. Bedford, P. B. Brenner, E. Carter, P. M. Cogswell, M. F. Haddow, J. N. Harvey, D. M. Murphy, J. Nunn and C. H. Woodall, *Angew. Chem. Int. Ed.*, 2014, **53**, 1804–1808.
- 26 Z. Zhao-Karger, J. E. Mueller, X. Zhao, O. Fuhr, T. Jacob and M. Fichtner, *RSC Adv.*, 2014, **4**, 26924–26927.
- 27 W. Teng, M. Guino-o, J. Hitzbleck, U. Englich and K. Ruhlandt-Senge, *Inorg. Chem.*, 2006, **45**, 9531–9539.
- 28 R. I. Yousef, B. Walfort, T. Ruffer, C. Wagner, H. Schmidt, R. Herzog and D. Steinborn, *J. Organomet. Chem.*, 2005, **690**, 1178–1191.
- 29 D. R. Armstrong, R. Herbst-Irmer, A. Kuhn, D. Moncrieff, M. A. Paver, C. A. Russell, D. Stalke, A. Steiner and D. S. Wright, *Angew. Chem. Int. Ed.*, 1993, **32**, 1774–1776.
- 30 A. Jaenschke and U. Behrens, *Z. Naturforsch. B*, 2008, **634**, 461–469.
- 31 D. Mukherjee, H. Osseili, T. P. Spaniol and J. Okuda, *J. Am. Chem. Soc.*, 2016, **138**, 10790–10793.
- 32 D. R. Armstrong, M. G. Davidson, D. Garcia-Vivo, A. R. Kennedy, R. E. Mulvey and S. D. Robertson, *Inorg. Chem.*, 2013, **52**, 12023–12032.

- 33 M. G. Davidson, D. Garcia-Vivo, A. R. Kennedy, R. E. Mulvey and S. D. Robertson, *Chem. Eur. J.*, 2011, **17**, 3364–3369.
- 34 D. M. Cousins, M. G. Davidson, C. J. Frankis, D. García-Vivó and M. F. Mahon, *Dalton Trans.*, 2010, **39**, 8278–8280.
- 35 S. D. Robertson, A. R. Kennedy, J. J. Liggat and R. E. Mulvey, *Chem. Commun.*, 2015, **51**, 5452–5455.
- 36 O. Michel, C. Meermann, K. W. Törnroos and R. Anwander, *Organometallics*, 2009, **28**, 4783–4790.
- 37 W. Li, S. Cheng, J. Wang, Y. Qiu, Z. Zheng, H. Lin, S. Nanda, Q. Ma, Y. Xu, F. Ye, M. Liu, L. Zhou and Y. Zhang, *Angew. Chem. Int. Ed.*, 2016, **55**, 6516–6520.
- 38 S. Parsons, S. Pace, N. Bushmann, P. Bailey and P. A. Wood, *CCDC 247832 CSD Commun.*, 2004, DOI: 10.5517/cc89wl0.
- 39 L. M. Guard and N. Hazari, *Organometallics*, 2013, **32**, 2787–2794.
- 40 J. W. Clary, T. J. Rettenmaier, R. Snelling, W. Bryks, J. Banwell, W. T. Wipke and B. Singaram, *J. Org. Chem.*, 2011, **76**, 9602–9610.
- 41 C. Liao, B. Guo, D. D.-E. Jiang, R. Custelcean, S. M. Mahurin, X.-G. Sun and S. Dai, *J. Mater. Chem. A*, 2014, **2**, 581–584.
- 42 S. D. Waezsada, F.-Q. Liu, E. F. Murphy, H. W. Roesky, M. Teichert, I. Usón, H.-G. Schmidt, T. Albers, E. Parisini and M. Noltemeyer, *Organometallics*, 1996, **16**, 1260–1264.
- 43 Y. Cheng, R. M. Stolley, K. S. Han, Y. Shao, B. W. Arey, N. M. Washton, K. T. Mueller, M. L. Helm, V. L. Sprenkle, J. Liu and G. Li, *Phys. Chem. Chem. Phys.*, 2015, **17**, 13307–13314.
- 44 T. Vankeirsbilck, A. Vercauteren, W. Baeyens, G. Van der Weken, F. Verpoort, G. Vergote and J. P. Remon, *TrAC - Trends Anal. Chem.*, 2002, **21**, 869–877.
- 45 L. V. Harris, I. B. Hutchinson, R. Ingle, C. P. Marshall, A. Olcott Marshall and H. G. M. Edwards, *Astrobiology*, 2015, **15**, 420–429.
- 46 Y. Zhu, S. Murali, W. Cai, X. Li, J. W. Suk, J. R. Potts and R. S. Ruoff, *Adv. Mater.*, 2010, **22**, 3906–3924.
- 47 R. Jiang, B. Li, C. Fang and J. Wang, *Adv. Mater.*, 2014, **26**, 5274–5309.
- 48 D. Graham, *Angew. Chem. Int. Ed.*, 2010, **49**, 9325–9327.

- 49 H. N. Xie, R. Stevenson, N. Stone, A. Hernandez-Santana, K. Faulds and D. Graham, *Angew. Chem. Int. Ed.*, 2012, **51**, 8509–8511.
- 50 J. V Iribarne and B. A. Thomson, *J. Chem. Phys.*, 1976, **64**, 2287–2240.
- 51 B. A. Thomson and J. V Iribarne, *J. Chem. Phys.*, 1979, **71**, 4451–2287.
- 52 J. B. F. M. Yamashita, *J. Phys. Chem.*, 1984, **88**, 4451–4459.
- 53 P. Kebarle, *J. Mass Spectrom.*, 2000, **35**, 804–817.
- 54 R. B. Cole, *J. Mass Spectrom.*, 2000, **35**, 763–772.
- 55 P. Kebarle and U. H. Verkcerk, *Mass Spectrom. Rev.*, 2009, **28**, 898–917.
- 56 L. Konermann, E. Ahadi, A. D. Rodriguez and S. Vahidi, *Anal. Chem.*, 2013, **85**, 2–9.
- 57 P. Chen, *Angew. Chem. Int. Ed.*, 2003, **42**, 2832–2847.
- 58 K. Koszinowski, *J. Am. Chem. Soc.*, 2010, **132**, 6032–6040.
- 59 J. E. Fleckenstein and K. Koszinowski, *Organometallics*, 2011, **30**, 5018–5026.
- 60 D. Schröder, L. Ducháčková, J. Tarábek, M. Karwowska, K. J. Fijalkowski, M. Ončák and P. Slavíček, *J. Am. Chem. Soc.*, 2011, **133**, 2444–2451.
- 61 V. B. Di Marco and G. G. Bombi, *Mass Spectrom. Rev.*, 2006, **25**, 347–379.
- 62 N. G. Tsierkezos, J. Roithová, D. Schröder, M. Ončák and P. Slavíček, *Inorg. Chem.*, 2009, **48**, 6287–6296.

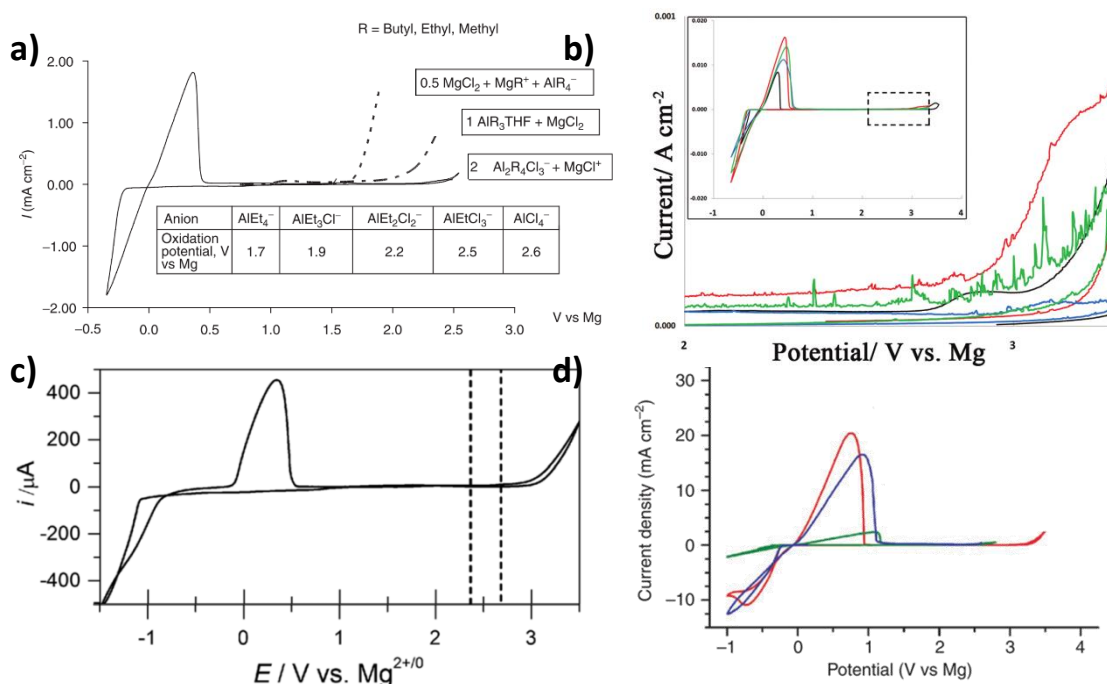
Chapter 3: The Influence of Cation Aggregation State on Battery Performance on Magnesium Amidohaloaluminate Electrolytes

This chapter presents the battery performance employing magnesium amidohaloaluminates possessing different cation aggregations as electrolytes. First the behaviour of the fully characterised series containing the DippN(SiMe₃) amido ligand is presented. The battery tests of this series are hindered by their low oxidative stability, dramatically affecting the electrochemical window. The link between low oxidative stability and the organometallic fragment of the electrolyte was previously proposed in the literature.¹ The provenance of the oxidative stability in our system was studied and reassessed. Synthesis and characterisation of another full series using less bulky amines was sought but not reached, hampered by troubles to produce another electrolyte possessing the trinuclear cation. The electrochemical experimental results using these partially characterised series are presented as well.

3.1. Introduction

A multitude of different research groups generate their electrolytic solutions by adding a group 13 Lewis acid to a THF solution of organomagnesium reagent. When a highly active electrolytic mixture allowing reversible Mg deposition is discovered, the X-ray characterised “active” species often possesses the widely observed dinuclear magnesium cation $[\text{Mg}_2\text{Cl}_3 \cdot 6\text{THF}]^+$ in THF. The electrolytes often only vary by the nature or composition of the counter anion, and from these studies it is manifest that the anion is closely related to the electrochemical window size.²⁻⁶ When the anionic moiety contains alkyl groups, the observed oxidative stability of the electrolyte varies from 1.7 to 2.5 V (Graph **3.1a**).⁷ These values are among the lowest observed in the literature and were proven to be induced by the Al-C bond cleavage via a β -hydride elimination mechanism.⁸⁻¹¹ Changing from an alkyl group to a phenyl group, which doesn't possess β -hydrogens, the oxidative stability is improved to 2.7 V (Graph **3.1b**).¹⁰ Moving away from anions possessing an Al-C bond, alternative electrolytes were developed using alkoxide groups which enable the formation of a stronger Al-O bond. Bartlett et al. used the fluorinated phenoxide 4-(trifluoromethyl)-

phenolate (FMP) enhancing the electrochemical window up to 2.9 V (Graph 3.1c).⁴ To date the highest observed oxidation stability using a magnesium organhaloaluminate electrolyte was observed using the amido group HMDS, containing an Al-N bond. This electrolyte is stable up to 3.3 V and owing to the non-nucleophilic nature of the Al-N bond, its compatibility with a sulphur cathode was also demonstrated (Graph 3.1d).^{3,12}



Graph 3.1: Cyclic voltammogram of **a)** THF solutions of $[\text{AlCl}_{4-n}\text{Et}_n]^- [\text{Mg}_2\text{Cl}_3 \cdot 6\text{THF}]^+$; **b)** THF solutions of the APC electrolyte (black: APC 1:1; red: 0.4 M APC; blue: 0.4 M APC + 0.8 M LiCl; green: 0.25 M APC) ; **c)** 0.5 M THF solution of $[(\text{FMP})\text{AlCl}_3]^- [\text{Mg}_2\text{Cl}_3 \cdot 6\text{THF}]^+$; and **d)** THF solution of $[(\text{HMDS})\text{AlCl}_3]^- [\text{Mg}_2\text{Cl}_3 \cdot 6\text{THF}]^+$ (0.2 M, red) $(\text{HMDS})\text{MgCl}$ (0.4M, green) and 3:1 mixture of $(\text{HMDS})\text{MgCl}:\text{AlCl}_3$ (0.4 M according to Mg, blue). The CVs were run in a 3 electrode cell using Mg as the counter and reference electrodes, an Au working electrode for a) and a Pt working electrode for b), c) and d).

These publications agree with each other that $[\text{Mg}_2\text{Cl}_3 \cdot 6\text{THF}]^+$ is the electrochemically active species in MIBs. In other words, it is a good carrier for Mg^{2+} ions from one electrode to another, additionally allowing reversible Mg insertion and deposition at the electrolyte/electrode interfaces. The aluminium anion is not directly linked to the reversible deposition of Mg, although in certain electrolytic systems Al deposition was detected. Such behaviour is observed during the conditioning of the fully inorganic electrolyte $[\text{AlCl}_4]^- [\text{Mg}_2\text{Cl}_3 \cdot 6\text{THF}]^+$ (magnesium aluminium chloride complex or

MACC). The conditioning of an electrolyte refers to the need for repeated cycling in an electrochemical cell, generating an equilibrium favouring the more active species present in the electrolytic solution. Irreversible Al or even Mg deposition occurs at the electrodes until an ideal Mg to Al ratio is achieved, displaying a high Coulombic efficiency.¹³

Apart from extensive studies on electrolytes containing different anions, developing electrolytes possessing a different cation than $[\text{Mg}_2\text{Cl}_3 \cdot 6\text{THF}]^+$ is more of a challenge. Aurbach et al. synthesised the fully inorganic magnesium aluminate compound $[\text{AlCl}_4]^- [\text{MgCl} \cdot 5\text{THF}]^+$ which possesses the mononuclear analogue of $[\text{Mg}_2\text{Cl}_3 \cdot 6\text{THF}]^+$. Unfortunately, no electrochemical studies were recorded due to the low solubility of the salt in commonly used solvents.¹⁰ Li et al. studied the electrochemical performances of the MgCl_2 - AlCl_3 mixture in DME, a mixture which promotes the formation of the MACC electrolyte in THF. The change of solvent from the monodentate to the chelating ligand affected the cationic structure to form the magnesium chloride dinuclear dication $[\text{Mg}_2\text{Cl}_2 \cdot 4\text{DME}]^{2+}$. A high electrochemical activity was observed for this electrolyte using a standard three electrodes cell, but no further discussions were provided regarding the differences induced by the presence of a new cationic species over the usually observed $[\text{Mg}_2\text{Cl}_3 \cdot 6\text{THF}]^+$ cation.¹⁴ Dai et al. characterised a magnesium magnesiate $[\text{MgCl}_3 \cdot \text{THF}]^- [\text{Mg}_3\text{Cl}_3(\text{OBu})_2 \cdot 6\text{THF}]^+$ from a 1:1 mixture of $(\text{BuO})\text{MgCl}:\text{AlCl}_3$ in THF.¹⁵ This structure is reminiscent of the formation of a magnesium magnesiate separated ion pair motif $[\text{BuMgCl}_2 \cdot \text{THF}]^- [\text{Mg}_2\text{Cl}_3 \cdot 6\text{THF}]^+$ isolated from Grignard solution by Yamaguchi et al.¹⁶ In this case the ^tBu group is replaced by ^nBuO which prefers to stay on the cation over the anion, forming a trinuclear species. This potentially implies that $[\text{MgCl}_3 \cdot \text{THF}]^- [\text{Mg}_3\text{Cl}_3(\text{OBu})_2 \cdot 6\text{THF}]^+$ is in fact a representation of the starting material $(\text{O}^n\text{Bu})\text{MgCl}$ altered by the Schlenk equilibrium and that some other Al containing species also exist in the solution. No comments were made whether the anion $[\text{MgCl}_3 \cdot \text{THF}]^-$, possessing a Mg atom, is involved in the redox process, or if the cation $[\text{Mg}_3\text{Cl}_3(\text{O}^n\text{Bu})_2 \cdot 6\text{THF}]^+$ displays an electrochemical response different than that seen for $[\text{Mg}_2\text{Cl}_3 \cdot 6\text{THF}]^+$, especially in terms of intercalation or deposition at the electrodes interface.

To summarise, a couple of chloromagnesium cations were discovered and characterised, yet no association between the electrochemical performance of an

electrolyte and its cation structure was proposed. In this chapter, a series of potential electrolytes containing a common anion but different cations were studied in order to identify what cation aggregation is most beneficial in an MIB system.

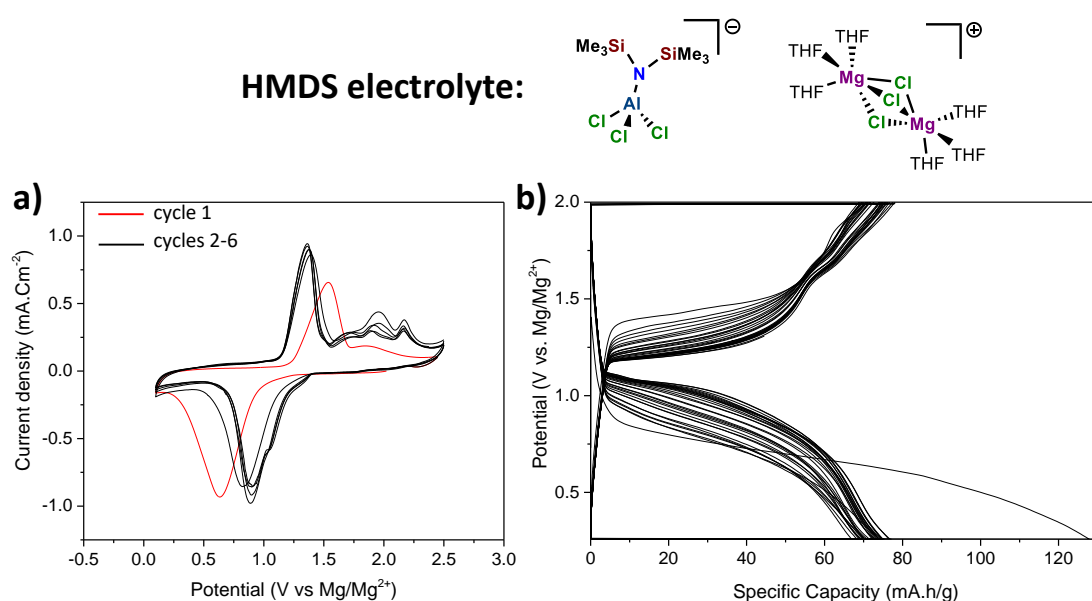
3.2. Experimental results

In this study three different aggregations of magnesium cation are studied in the electrolytic solution of an MIB cell. The type of cell employed in this study was a Swagelok cell, using polished Mg metal as the anode, the Chevrel phase Mo_6S_8 as the cathode material and two current collectors made of Inconel 625. The first of the three cations aggregation studied was the dinuclear cation $[\text{Mg}_2\text{Cl}_3 \cdot 6\text{THF}]^+$, used as the standard reference electrolyte of the series due to its already known electrolytic activity. Then moving to the trinuclear cation $[\text{Mg}_3\text{Cl}_5 \cdot 6\text{MeTHF}]^+$ whose behaviour in a battery is unknown, it would be interesting to see if the 3:1 Mg to Al ratio makes this electrolyte more economically attractive or if the size of the aggregate alters the electrolyte/electrode interface interplay. Finally by testing the mononuclear cation $[\text{MgCl} \cdot \text{Me}_6\text{TREN}]^+$, it would be compelling to see if the presence of a tetradentate ligand coordinated to the Mg atom still allows the release of the Mg^{2+} ions to be intercalated within the Chevrel phase. The use of $[\text{Mg}_3\text{Cl}_5 \cdot 3\text{TMEDA}]^+$ was not attempted in this study due to its lower solubility in THF.

In the literature, most electrochemical tests done by cyclic voltammetry (CV) were measured using a three electrodes cell with a noble metal working electrode. In this study we prefer to focus on the properties of these electrolytes within a full battery prototype instead, containing an insertion cathode so the effect that the cation aggregation has on the MIBs is more representative.

3.2.1. Battery test: [(HMDS)AlCl₃]⁻ [Mg₂Cl₃·6THF]⁺ electrolyte

The known electrolyte [(HMDS)AlCl₃]⁻ [Mg₂Cl₃·6THF]⁺ (referred to as the HMDS electrolyte in this thesis) was first studied. This experiment is not a repeat from the literature because no CVs were recorded using a battery cell with an insertion cathode such as the Chevrel phase. Additionally, it is necessary to have a reference for a dinuclear species already known to be active so a comparison with the unstudied compound [(Dipp)(SiMe₃)NAlCl₃]⁻ [Mg₂Cl₃·6THF]⁺ (**1**) can be made.



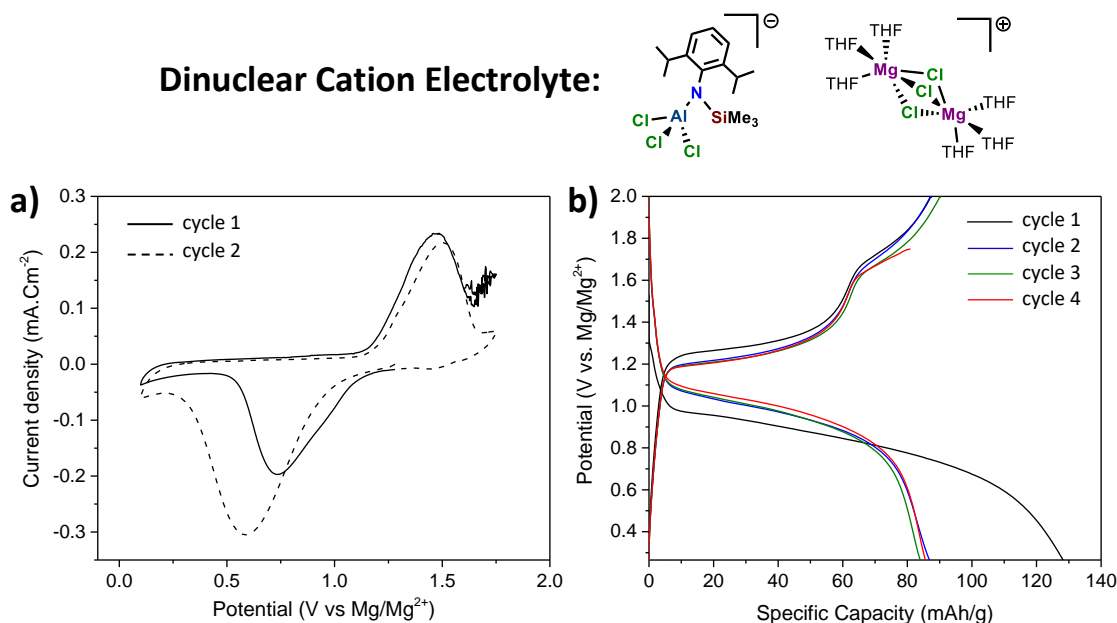
Graph 3.2: **a)** CV cycles (six cycles, the first cycle displayed in red), 0.1 mV/s, and **b)** C/10 charge/discharge profiles (30 cycles) for a rechargeable battery with 0.175 M solution of [(HMDS)AlCl₃]⁻ [Mg₂Cl₃·6THF]⁺ in THF, a Mg anode and an Mo₆S₈ cathode.

The CV displayed in Graph 3.2a shows the redox peaks exhibited by the HMDS electrolyte confirming reversibility of this battery. The reduction peak corresponds to the discharge of the battery, which occurs at 0.90 V after the first cycle. The oxidation peak corresponds to the charge of the battery and occurs at 1.36 V after the first cycle. The first cycle is different than the following ones, where the redox peaks are further apart leading to a higher overpotential. A high overpotential means that the battery cell needs more energy to charge the battery, this surplus of energy is lost thermodynamically, reducing the efficiency of the battery. Visually a good assumption

can be made regarding the quality of the intercalation kinetics of the electrolyte within the Mo_6S_8 structure. The broadness of a redox peak is directly related to the intercalation, the broader the peak the slower the intercalation. For this battery the kinetics are rather sluggish compared with what is observed in Li batteries.¹⁷ This is thought to be caused by strong interactions involving the divalent Mg^{2+} ions and the electrodes, requiring higher potential to achieve continuous intercalation.¹⁸ Some electrochemical responses are observed at higher potential than the main oxidation peak, indicating the presence of different known sites within the Chevrel phase. The response appearing at higher potential means that there is a requirement for higher energy to strip the Mg atom out of the active material.¹⁹ In a less obvious way, a shoulder can be observed in the reduction peak also corresponding to the intercalation of Mg^{2+} ions in those different sites.²⁰

Graph **3.2b** represents the galvanostatic experiment using the same battery system. The first cycle is significantly different from the following ones as it reaches the maximum theoretical specific capacity of the Chevrel phase (128 mAh/g). All the subsequent charge/discharge cycles have a lower specific capacity with a retention varying from 66 to 78 mAh/g. The difference between the first cycles and the following ones is a feature linked to the partial charge trapping phenomenon occurring in the Chevrel phase, where some Mg atoms cannot be released from the structure.²¹ Eventually, running the battery at higher temperature is known to increase the kinetics and the deintercalation of the Mg^{2+} .^{22,23} The overpotential of the first cycle (0.72 V) is more important than the following cycles, which themselves see their overpotential improve cycle after cycle, only displaying 0.12 V at cycle 30. Overall in our system this battery exhibits an electrochemical window and specific capacity similar to the literature.

3.2.2. Battery test: [(Dipp)(SiMe₃)AlCl₃]⁻ electrolyte series

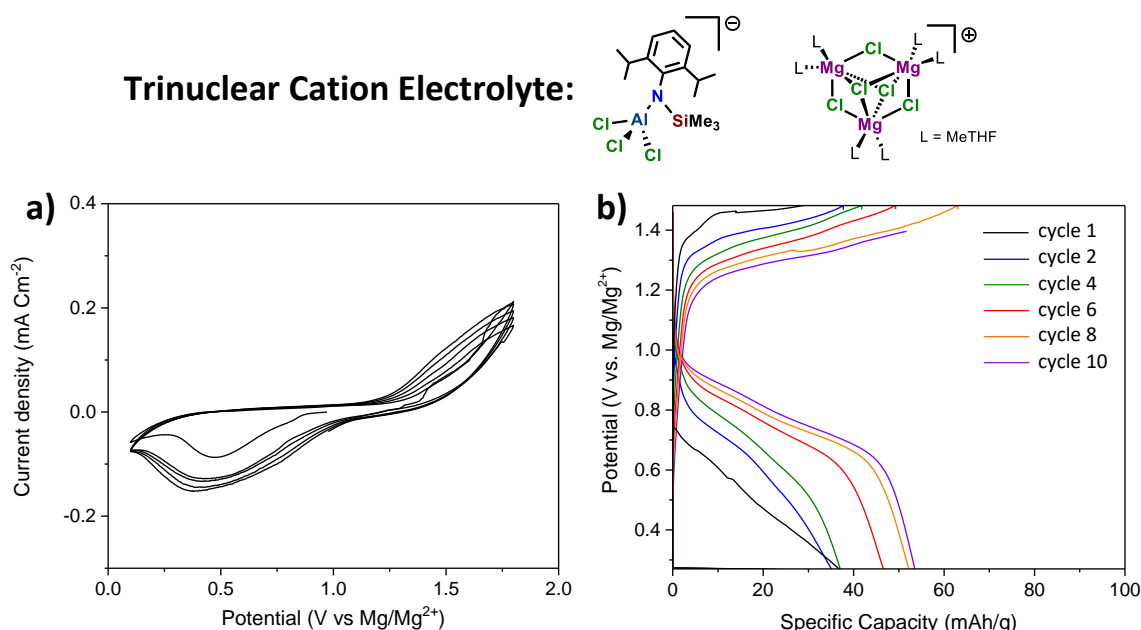


Graph 3.3: a) CV cycles, 0.1 mV/s, and b) C/10 charge/discharge profiles for a rechargeable battery with 0.175 M solution of [(Dipp)(SiMe₃)AlCl₃]⁻ [Mg₂Cl₃·6THF]⁺ (**1**) in THF, a Mg anode and an Mo₆S₈ cathode.

Graph 3.3 shows the electrochemical behaviour of compound **1** in an Mg²⁺/Mo₆S₈ battery cell. The CV in Graph 3.3a displays reversible Mg deposition in this system, meaning that compound **1** is compatible with the Chevrel phase. As observed for the HMDS electrolyte the reduction peak of the first cycle at 0.58 V is shifted toward lower potential compared to the reduction peak of the second cycle, appearing at 0.74 V. The oxidation peaks of the two cycles appear at more similar voltages (1.47 V and 1.51 V in cycle 1 and 2 respectively). The intercalation/deintercalation kinetics with compound **1** are even more sluggish than for the HMDS electrolyte, which could be affected by the presence of the DippN(SiMe₃) amido unit on the anion. DippN(SiMe₃), due to the presence of the Dipp group, is larger than the simpler HMDS group, and as a result the ion transport velocity of the electrolyte in the electrolytic solution while the battery is running is reduced. A small shoulder in the broad reduction peak of the second cycle is also observed, corresponding to the intercalation of Mg²⁺ ions in the different sites of Chevrel phase as observed for the HMDS electrolyte. The most obvious and unwanted feature is the early decomposition of the electrolyte, which

takes place after only two cycles between 0.1 – 1.75 V. As mentioned earlier the oxidative stability is very dependent on what organic group is located on the aluminium anion. In this case the DippN(SiMe₃) amide could be considered similar to HMDS as one of the N-SiMe₃ arm is present. But the aforementioned bulk from the 2,6-diisopropylphenyl group could be responsible for the destabilisation of the anion, either by affecting the Al-N bond or inducing cleavage of the silazane bond. The reason for the low observed oxidative stability is further discussed in Section 3.2.3.

For similar reasons the charge/discharge profile displayed in Graph 3.3b of the battery could run only for four cycles before the electrolyte started to decompose. The first four cycles of this battery are very similar to the battery using the HMDS electrolyte. The first cycle reaches the theoretical specific capacity (128 mA.h/g) while the following cycles attain 85 mA.h/g, a higher value than with the HMDS electrolyte. The overpotential is higher during the first the first cycle (0.3 V) than for the following ones (0.17 V at cycle 4) overall behaving slightly better than the HMDS electrolyte in an MIB during the early cycles but failing to sustain this enhanced performance.

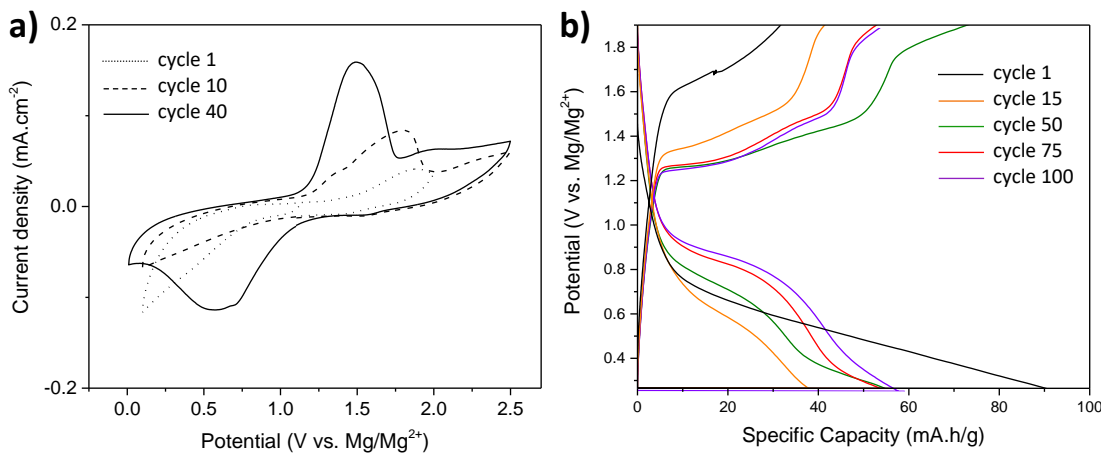
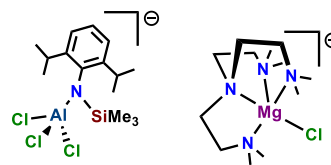


Graph 3.4: a) CV cycles, 0.1 mV/s, cycles 9-13 and b) C/10 charge/discharge profiles for a rechargeable battery with 0.117 M solution of [(Dipp)(SiMe₃)AlCl₂]⁻ [Mg₃Cl₅·6MeTHF]⁺ (**5**) in MeTHF, a Mg anode and an Mo₆S₈ cathode.

Graph **3.4** shows the electrochemical behaviour of compound **5** in an $\text{Mg}^{2+}/\text{Mo}_6\text{S}_8$ battery cell. The CV in Graph **3.4a** displays reversible Mg deposition occurring in this system, meaning that compound **5** is compatible with the Chevrel phase. The first few cycles between 0.1-2.0 V showed very small redox response and decomposition at voltage higher than 1.9 V. Reducing the maximum voltage down to 1.8 V showed no sign of decomposition but an oxidation peak only partially appearing, suggesting that the deintercalation process happens at a voltage neighbouring 1.8 V and higher. This voltage is significantly higher than for compound **1**, implying that the trinuclear cation aggregation requires a higher charge voltage, hence more energy, than the dinuclear cation aggregation. During the discharge the reduction peak at 0.39 V is very broad, reflecting more sluggish insertion kinetics than for compound **1**.

The galvanostatic experiment showed in Graph **3.4b** was run between 0.1 - 1.5 V as previous attempts at 2 V shows decomposition of the electrolyte during the first cycle. The charge/discharge profile of this battery tells a similar story to the CV, where the first cycle which usually approaches the theoretical specific capacity of the Chevrel phase barely reaches 35 mA.h/g, related to the near absence of Mg^{2+} intercalation during the conditioning period of the electrolyte. The specific capacity slowly recovers during the following cycles reaching 54 mA.h/g in the 10th cycle, but displaying an overall high overpotential for all the cycles (0.6 V).

Mononuclear Cation Electrolyte:



Graph 3.5: a) CV cycles, 0.1 mV/s, and b) C/10 charge/discharge profiles for a rechargeable battery with 0.35 M solution of $[(\text{Dipp})(\text{SiMe}_3)\text{AlCl}_3]^- [\text{MgCl}\cdot\text{Me}_6\text{TREN}]^+$ (**9**) in THF, a Mg anode and an Mo_6S_8 cathode.

Graph 3.5 shows the electrochemical behaviour of compound **9** in an $\text{Mg}^{2+}/\text{Mo}_6\text{S}_8$ battery cell. The CV in Graph 3.5a displays reversible Mg deposition occurring in this system, meaning that compound **9** is compatible with the Chevrel phase. Trying to avoid the early decomposition observed with compounds **1** and **4**, the CV was first run up to 2 V. In the first few cycles there were no obvious sign of reversible cycling apart for a “bump” appearing just under 2 V. The electrochemical window was expanded to 2.5 V in the following cycles revealing a more pronounced anodic peak which increases in current intensity with the number of cycles. Not only the current density was improved but the peak also shifted to lower voltage decreasing the overpotential of the battery. The most defined oxidation response forms a peak at 1.53 V. The reduction peak itself is not observed in the early cycles but gains rapidly in intensity after 20 cycles to form a broad peak at 0.6 V. This electrolyte seems to be subject to a severe need for conditioning before being electrochemically active. In contrast with the two previous electrolytes, the mononuclear cation displays a very high oxidative stability. Compound **9** can cycle between 0.1 – 2.5 V without sign of decomposition, and still behaves well when increasing the voltage up to 3 V (8 cycles at this voltage with only minor decomposition).

The charge/discharge profile of this battery displayed in Graph **3.5b** shows a slow start, which was to be expected from the CV. The first cycle doesn't approach the theoretical specific capacity of the Chevrel phase but only exhibits a modest 90 mA.h/g. The first charge only loads back to 36 mA.h/g. but from there the specific capacity recovers and kept increasing in every following cycle to reach 59 mA.h/g in the 100th cycle. The overpotential also improves during the experiment, starting from 0.95 V in the early cycles to 0.4 V in the late cycles. Being very stable and displaying a large electrochemical window compared to compounds **1** and **5**, this electrolyte becomes highly interesting despite the rather modest specific capacity and capacity retention.

This study gives a small insight into how these different cation aggregations affect the battery performance, but the early decomposition of electrolytes **1** and **5** at a voltage neighbouring 2 V prevent a thorough comparison, which we were hoping to achieve over 100 cycles. Further comments discussing the difference in behaviour of these electrolytes is treated more in depth in the Results and Discussion section (Section 3.3). The next section discusses the possible reasons causing the low oxidative stability of these electrolytes.

3.2.3. Investigating the low oxidative stability of the [(Dipp)(SiMe₃)NAlCl₃]⁻ series

First a literature search with organometallic compounds containing the DippN(SiMe₃) amido group was undertaken. Ruhlandt-Senge et al. studied the structure of magnesium reagents with secondary amines possessing one aryl and one trimethylsilane group. In this study they observed how the different bulk of these amines affects the structure of the corresponding magnesium amide reagents, while in association with the already sterically demanding ligand HMPA (hexamethylphosphoramide, O=P(NMe₂)₃). Their discovery is summarised in Figure **3.1**, where by comparing the difference in bond lengths they were able to classify the amines by bulk. PhN(SiMe₃) appears to be the least bulky of their series, followed by HMDS, MesN(SiMe₃) and finally DippN(SiMe₃). DippN(SiMe₃) was found to be so bulky that it induces ion dissociation to form a separated ion pair with [(N(SiMe₃)]⁻ as

the anion and [(Dipp)(SiMe₃)NMg·3HMPA]⁺ as the cation (IV). This indicates that in our series we chose a very bulky amine, which is more likely to decrease the stability of the aluminium-centred anion during the running of the MIB.

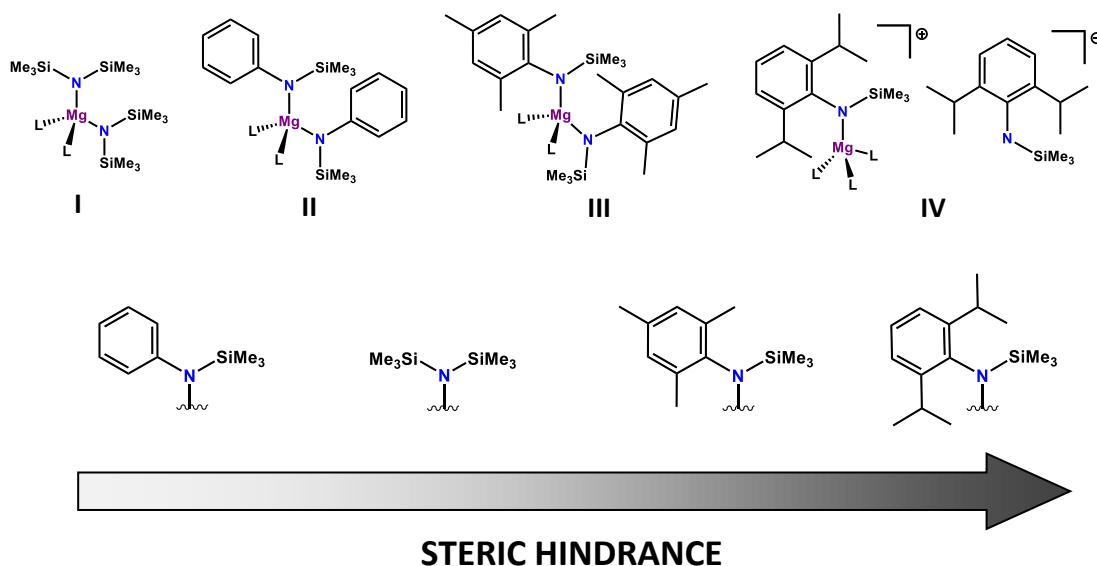


Figure 3.1: Effect of the steric properties of secondary amines possessing a SiMe₃ group on magnesium amide compounds.

In two different studies, the energy of the HOMO-LUMO gap arising from the chemical bond between the aluminium atom and the ligand was calculated by DFT calculations.^{6,10} This allows an estimation regarding the oxidative stability of the anion, where the larger the energy gap the greater the stability toward oxidation. Zhao-Karger et al. published a list of aluminium anions [R_nAlCl_{4-n}]⁻ (n = 1, 2, 3 and R = Cl, Et, Me, TMP, Ph, HMDS, OPh) where the energy levels from both the HOMO and the LUMO were calculated in different ether solvents; namely THF, diglyme and tetraglyme. The theoretical study was repeated with our systems and the HOMO-LUMO gaps from anions [(Dipp)(SiMe₃)NAlCl₃]⁻, [(Dmp)(SiMe₃)NAlCl₃]⁻ and [(Ph)(SiMe₃)NAlCl₃]⁻ were determined. The calculations were carried out using the Gaussian 09 program with the DFT-B3LYP functionals and the 6-311++G(d,p) basis set, and for the solvation calculations the method in G09 used was IEFPCM with its built in parameters for THF. The outcome of our calculations shows contradictory results with what was concluded from the study from Ruhlandt-Senge et al. where the amido ligand PhNSiMe₃, being less bulky was thought to be a

good candidate to enhance the stability of the corresponding aluminium anion. **Figure 3.2** shows that the HOMO-LUMO gaps from $[(\text{Dipp})(\text{SiMe}_3)\text{NAlCl}_3]^-$ and $[(\text{Dmp})(\text{SiMe}_3)\text{NAlCl}_3]^-$ are relatively close (5.73 and 5.80 eV respectively) as the energy level of their LUMOs adopts the same value (-0.02 eV) and their HOMOs vary only slightly (5.75 and 5.82 eV respectively). In contrast to the LUMOs of $[(\text{Dipp})(\text{SiMe}_3)\text{NAlCl}_3]^-$ and $[(\text{Dmp})(\text{SiMe}_3)\text{NAlCl}_3]^-$ which are delocalised around the anion, the LUMO of $[(\text{Ph})(\text{SiMe}_3)\text{NAlCl}_3]^-$ is located at the π -system of the phenyl ring, dramatically lowering its energy level to -0.12 eV. This can be attributed to the absence of substituents on the phenyl ring, increasing the electron withdrawing nature of this ligand. Similar observations can be made for the HOMO, which adopts a more aromatic nature, increasing the energy level to -5.66 eV giving the smallest HOMO-LUMO gap of the series ($\Delta E = 5.54$ eV). These results suggest that using PhNSiMe_3 as the amido ligand increases the nucleophilicity of the Al-N bond hence lowering the oxidative stability.

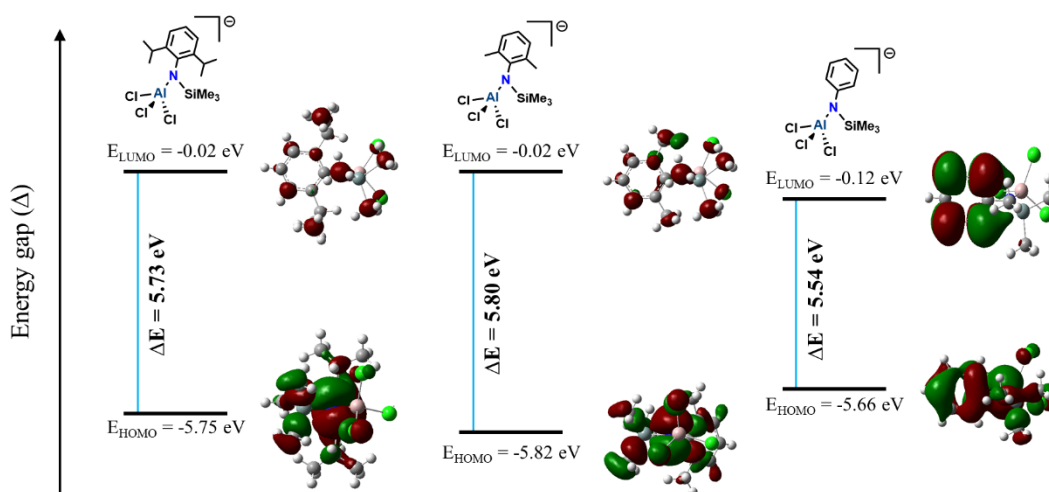
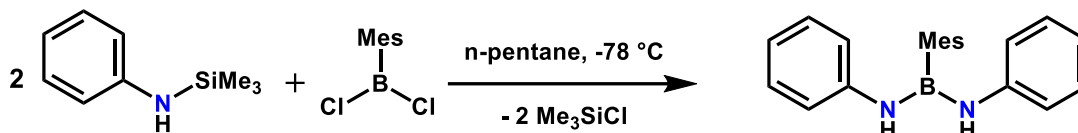


Figure 3.2: Calculations of HOMO and LUMO energy levels for anions $[(\text{Dipp})(\text{SiMe}_3)\text{NAlCl}_3]^-$, $[(\text{Dmp})(\text{SiMe}_3)\text{NAlCl}_3]^-$ and $[(\text{Ph})(\text{SiMe}_3)\text{NAlCl}_3]^-$.

Another discovery potentially responsible for decomposition of the electrolyte, through side product formation, is the use of amines like $\text{PhNH}(\text{SiMe}_3)$ with a Lewis acid such as dichloro(mesityl)borane (MesBCl_2) to induce cleavage of the N-SiMe₃ bond and form a new B-N bond (Scheme 3.1).²⁴ Our electrolytes possess an AlCl_3 type Lewis acid moiety which could potentially react with the $\text{DippN}(\text{SiMe}_3)$ groups,

cleaving away the silazane group under electrochemical conditions. Even if the Al-N bond might still be intact the side products can continue reacting, decomposing the electrolyte further. There are many other examples of Me_3SiCl elimination occurring in different organometallic/inorganic systems.²⁵⁻²⁷



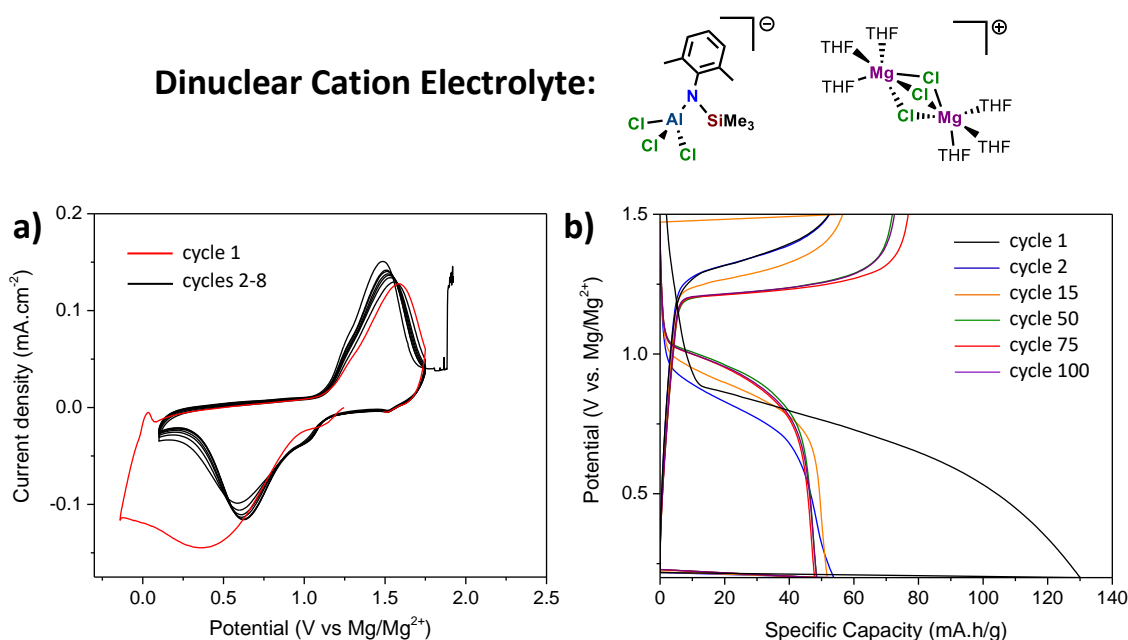
Scheme 3.1: Silazane cleavage of PhNH(SiMe₃) induced by a Lewis acidic borane.

As presented in Chapter 2, different series of electrolytes with different cation aggregation but with a reduced bulk on the amide were sought. Difficulties in obtaining a new series were encountered, especially regarding the structural characterisation of an electrolyte possessing the trinuclear species $[\text{Mg}_3\text{Cl}_5 \cdot 6\text{MeTHF}]^+$. Using either DmpNSiMe₃ or PhNSiMe₃, the magnesium aluminate compound possessing the dinuclear and mononuclear cation were synthesised and characterised by X-Ray (See compounds **2**, **3**, **10** and **11** in Chapter 2 Section 2.4 for full details). For DmpNSiMe₃ good looking crystals were obtained in MeTHF but did not diffract strongly enough, so instead we turned to ESI-MS to characterise the ionic species present in solution. The spectrum matched the one obtained for compound **5** in the positive mode, where the higher aggregates are favoured suggesting the formation of $[(\text{Dmp})(\text{SiMe}_3)\text{NAlCl}_3]^- [\text{Mg}_3\text{Cl}_5 \cdot 6\text{MeTHF}]^+$. For PhNSiMe₃ the reaction in MeTHF yields a poorly soluble microcrystalline solid, which couldn't be identified. Finally, a series was also sought using HMDS, where the mononuclear version was obtained and characterised by X-Ray. However similar results were obtained with PhNSiMe₃ regarding the trinuclear species.

In order to identify if the presence of an N-SiMe₃ bond is a source of early decomposition through silazane cleavage, a series was sought with another secondary bulky amine such as TMP. The bulk of TMP, compared to DippN(SiMe₃), arises from the methyl groups adjacent to the nitrogen which affects the Al-N bond directly. Using DFT calculation studies, the HOMO-LUMO energy gap in the $[(\text{TMP})\text{AlCl}_3]^-$ anion

was determined at 5.05 eV, an energy gap lower than for $[(\text{Ph})(\text{SiMe}_3)\text{NAlCl}_3]^-$ hence very low oxidative stability is anticipated.⁶

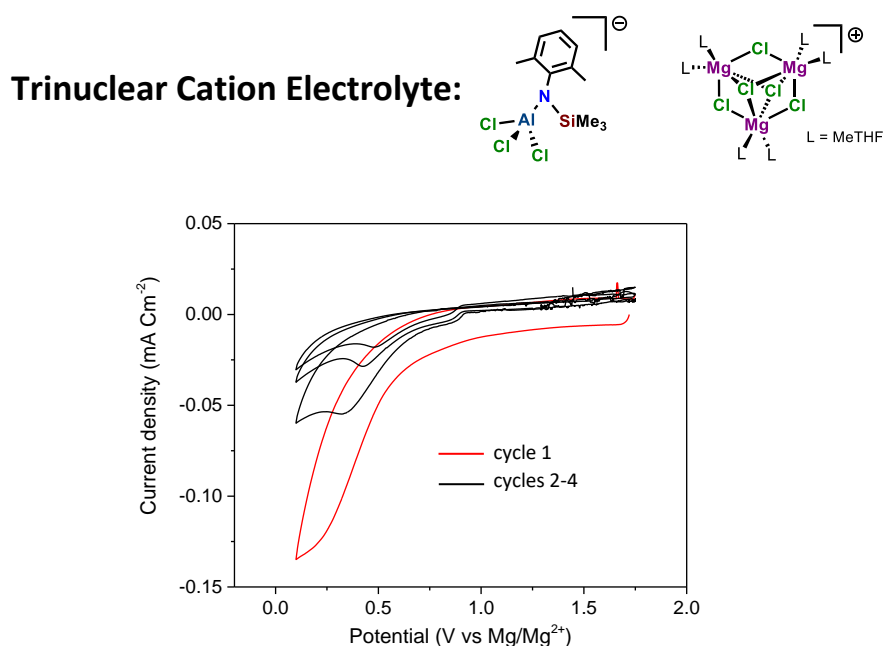
3.2.4. Battery test: $[(\text{Dmp})(\text{SiMe}_3)\text{NAlCl}_3]^-$ electrolyte series



Graph 3.6: **a)** CV cycles, 0.1 mV/s, and **b)** C/10 charge/discharge profiles for a rechargeable battery with 0.175 M solution of $[(\text{Dmp})(\text{SiMe}_3)\text{NAlCl}_3]^- [\text{Mg}_2\text{Cl}_3 \cdot 6\text{THF}]^+$ (**2**) in THF, a Mg anode and an Mo_6S_8 cathode.

Graph 3.6 shows the electrochemical behaviour of compound **2** in an $\text{Mg}^{2+}/\text{Mo}_6\text{S}_8$ battery cell. The CV displayed in Graph 3.6a confirms the reversible Mg deposition ability of this system, meaning that compound **2** is compatible with the Chevrel phase. This battery manages to cycle for at least 8 cycles between 0.1 – 1.75 V without obvious signs of decomposition, but increasing the maximum voltage to 2V induces decomposition around 1.9 V. These observations agree with the idea that changing the amido group $\text{DippN}(\text{SiMe}_3)$ for the less bulky $\text{DmpN}(\text{SiMe}_3)$ improved the oxidative stability. The reduction peak appears at 0.6 V and the oxidation peak at 1.5 V, both peaks are relatively well defined. The shape of the redox peaks is relatively broad, matching what was observed with compound **1**, implying similar sluggish insertion kinetics.

The charge/discharge profile of the battery was cycled between 0.2 – 1.5 V, choosing a lower voltage from what the CV suggested the electrolyte would be stable at (1.75 V) in order to avoid as much decomposition as possible and run the battery for at least 100 cycles. As a result of this small electrochemical window, the battery is not able to charge to its maximum capacity, lowering the overall specific capacity. The first cycle reaches the theoretical capacity of the Chevrel phase; the battery then displays a discharge specific capacity varying between 47 and 55 mA.h/g. During the first 30 cycles the battery charges at the same capacity, which changes in the next cycles where the battery appears to charge to higher capacity than it discharges. Simultaneously the overpotential improves slightly (from 0.37 V to 0.2 V). These odd observations appeared when the battery was transferred from one potentiostat to another due to a failure of the first machine.



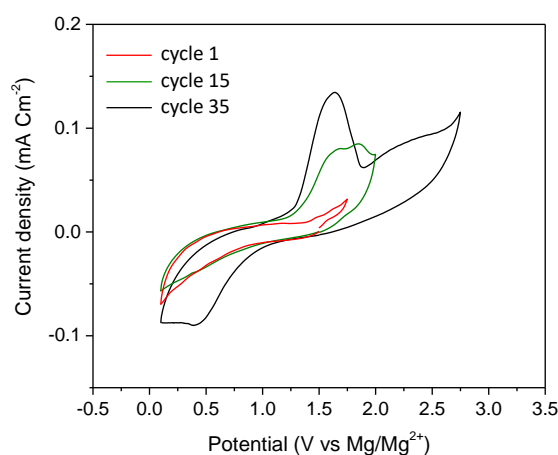
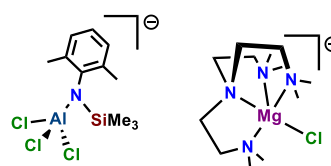
Graph 3.7: CV cycles, 0.1 mV/s, of a rechargeable battery with 0.117 M solution compound **7** dissolved in MeTHF, using a Mg anode and an Mo₆S₈ cathode.

The CV of the crystals of compound **7** believed to correspond to [(Dmp)(SiMe₃)NAlCl₃]⁻ [Mg₃Cl₅·6MeTHF]⁺ show the presence of a reduction peak around 0.2 V, but no oxidation peak was observed. The previously studied CV obtained for compound **6** showed that the trinuclear cation needs conditioning for the oxidation peak to appear after at least 4 cycles. In this case the compound decomposes

just after the 4th cycle preventing us from knowing if the conditioning would eventually allow reversible Mg deposition. The low oxidative stability of this compound was not expected due to the improved electrochemical window obtained with compound **2** over compound **1**.

The charge/discharge profile of this system was not run due to a combination of long experiment time (1.5 months for 100 cycles at C/10) and limited access to multiple channels of the potentiostat. This experiment would be however informative if any Mg²⁺ ions are interacting with the Chevrel phase.

Mononuclear Cation Electrolyte:



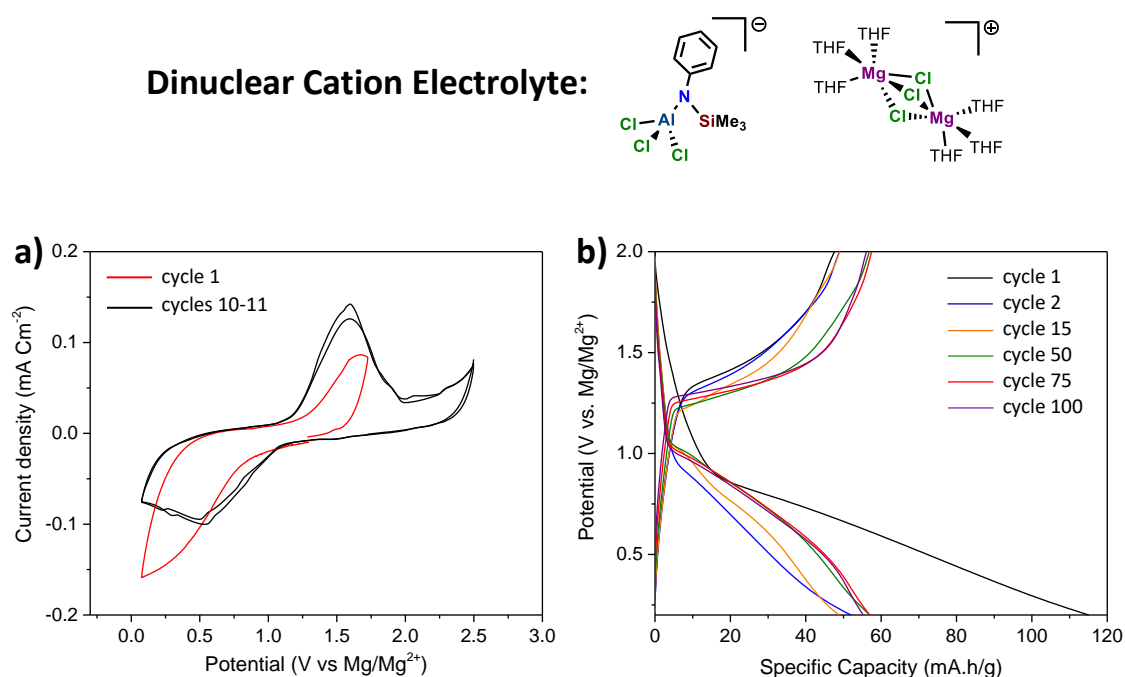
Graph 3.8: CV cycles, 0.1 mV/s, for a rechargeable battery with 0.35 M solution of [(Dmp)(SiMe₃)AlCl₃]⁻ [MgCl·Me₆TREN]⁺ (**10**) in THF, a Mg anode and an Mo₆S₈ cathode.

Graph **3.8** represents the CV of a battery using compound **10** in THF as the electrolyte. The CV displays reversible Mg deposition, meaning that compound **10** is also compatible with the Chevrel phase. After conditioning of the electrolyte for 30 cycles the CV displays a well-defined oxidation peak at 1.6 V, and a reduction peak at 0.42 V. This CV possesses the same peculiarities observed with compound **9** (Graph 3.5a), such as the serious need for conditioning and the greatly improved oxidative stability compared to the dinuclear and trinuclear analogue species. The similarities with

compound **9** are not unexpected as both electrolytes possess the same $[\text{MgCl}\cdot\text{Me}_6\text{TREN}]^+$ cation but these matching results start to expose a general trend in the electrochemical properties of electrolytes possessing this common cation. Whether it is the aggregation level, the presence of the Me_6TREN or both which is responsible for these properties was not recognised but is discussed further in Section 3.3.

The galvanostatic experiment showing charge/discharge profile of the battery was not run for this electrolyte, but will be in due time adding more to the postulate that the mononuclear cation $[\text{MgCl}\cdot\text{Me}_6\text{TREN}]^+$ has an electrochemical behaviour specific to itself.

3.2.5. Battery test: $[(\text{Ph})(\text{SiMe}_3)\text{NAlCl}_3]^-$ electrolyte series



Graph 3.9: a) CV cycles, 0.1 mV/s, and b) C/10 charge/discharge profiles for a rechargeable battery with 0.175 M solution of $[(\text{Ph})(\text{SiMe}_3)\text{NAlCl}_3]^- [\text{Mg}_2\text{Cl}_3\cdot 6\text{THF}]^+$ (**3**) in THF, a Mg anode and an Mo_6S_8 cathode.

Graph **3.9** shows the electrochemical behaviour of compound **3** in an $\text{Mg}^{2+}/\text{Mo}_6\text{S}_8$ battery cell. The CV in Graph **3.9a** displays reversible Mg deposition in this system,

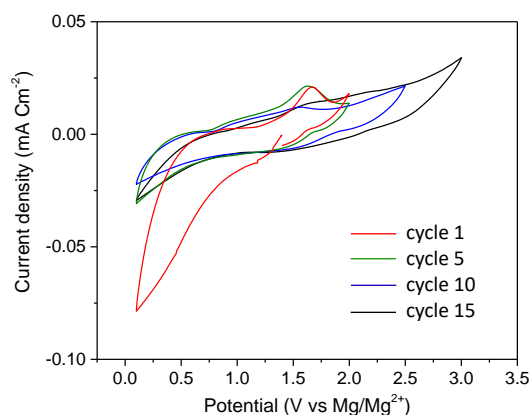
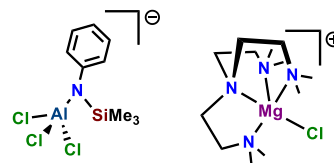
meaning that compound **3** is compatible with the Chevrel phase. The first cycles were run with the smaller electrochemical window 0.1 – 1.75 V, not allowing the oxidation peak at 1.67 V to appear completely. After a few cycles the electrolyte showed no decomposition and the electrochemical window was extended to 2.5 V. Using this window the CV shows well defined redox peaks, the reduction peak operating at 0.5 V and the oxidation peak operating at 1.6 V. Both peaks are rather broad, corresponding to sluggish insertion kinetics as observed for the previous electrolytes. The electrolyte decomposes at 2.5 V after the 12 cycles, exhibiting an oxidative stability lower than the corresponding HMDS electrolyte but much higher than the DippN(SiMe₃) and DmpN(SiMe₃) electrolytes.

The charge/discharge profile of this battery displayed in Graph **3.9b** was run between 0.2 – 2 V and shows no sign of decomposition for 100 cycles. The first cycle doesn't reach the theoretical specific capacity of the Chevrel phase as observed for the other electrolytes possessing the dinuclear cation (Graph 3.2 b; 3.3 b; 3.6 b) and instead only displays a capacity of 115 mA.h/g. The capacity retention of the subsequent cycles is good, starting from 48 mA.h/g and increases with the cycles to 58 mA.h/g. The overall capacity of this battery is lower than other electrolytes possessing the dinuclear cation which showed capacities no lower than 66 mA.h/g when ran between the same electrochemical window. There is still the possibility of an error during the weighing of the Chevrel phase, either manual or instrumental but this is unlikely. The shape of charge/discharge curves in this battery is notably different, they look more like straight lines especially during the discharge whereas in the other experiments the curves are more curvilinear. Because of these shapes an accurate reading of the overpotential is more difficult, but according to the CV it can be measured as 0.55 V ($V_{ox} - V_{red}/2$).

These experiments show that the least bulky amide of the series PhN(SiMe₃) has improved oxidative stability over the bulkier amides DippN(SiMe₃) and DmpN(SiMe₃). However the HMDS electrolyte still displays a much higher oxidative stability although it was assessed as being only slightly more sterically hindered than PhN(SiMe₃). We believe that the difference of stability between PhNSiMe₃ and HMDS is related to the N-SiMe₃ bond; where possessing two SiMe₃ groups generate an evenly distributed polarisation around the N atom. Replacing one SiMe₃ group for an aryl group will unbalance the polarisation leading to easier cleavage of the N-SiMe₃

bond. Attempts to synthesise an amine similar but without the N-SiMe₃ such as PhNH(^tBu) using a method developed by Knochel et al. was attempted but aborted due to low yields.²⁸

Mononuclear Cation Electrolyte:

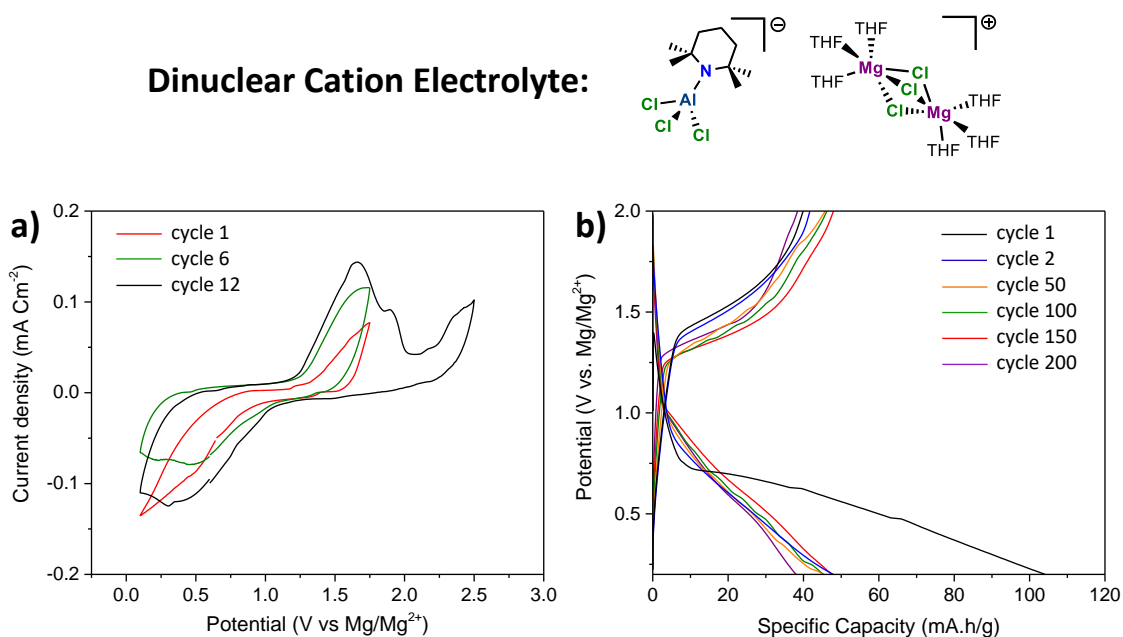


Graph 3.10: CV cycles, 0.1 mV/s, for a rechargeable battery with a saturated solution of [(Ph)(SiMe₃)AlCl₃]⁻ [MgCl·Me₆TREN]⁺ (**11**) in THF, a Mg anode and an Mo₆S₈ cathode.

Graph 3.10 shows the CV of a battery using compound **11** in THF as the electrolyte. The first 6 cycles show a redox activity with low current intensity when cycling between 0.1 – 2.0 V. After increasing the electrochemical window to 2.5 V the redox peaks diminished before eventually disappearing, increasing the window further to 3.0 V did not show signs of improvement. This result was unexpected according to the previous batteries run with electrolytes possessing the mononuclear cation [MgCl·Me₆TREN]⁺, which usually exhibits a neat redox activity after conditioning of the electrolyte. There are however uncertainties regarding the purity of this compound as the isolated product in the reaction mixture was a mixture of crystalline material and amorphous solid. After isolation the solubility of the product was affected and a clear solution was not achieved at a concentration of 0.35 M. The presence of a solid within the battery cell could be an obstacle to the electrolyte/interface interplay, affecting the electrode as a passivating layer would. According to ¹H NMR spectroscopy the product is clean with a 1:1 ratio PhN(SiMe₃) : Me₆TREN and no other resonance signals such as THF which could indicate presence of a fully inorganic

salt. A repeat of the experiment using a new fresh sample needs to be made to confirm this result before any further conclusions are drawn.

3.2.6. Battery test: $[(\text{TMP})\text{AlCl}_3]^- [\text{Mg}_2\text{Cl}_3 \cdot 6\text{THF}]^+$ electrolyte



Graph 3.11: a) CV cycles, 0.1 mV/s, and b) C/10 charge/discharge profiles for a rechargeable battery with 0.175 M solution of $[(\text{TMP})\text{AlCl}_3]^- [\text{Mg}_2\text{Cl}_3 \cdot 6\text{THF}]^+$ (**4**) in THF, a Mg anode and an Mo_6S_8 cathode.

Graph **3.11** shows the electrochemical behaviour of compound **4** in an $\text{Mg}^{2+}/\text{Mo}_6\text{S}_8$ battery cell. The CV in Graph **3.11a** displays reversible Mg deposition in this system, meaning that compound **4** is compatible with the Chevrel phase. According to the DFT calculation of the HOMO-LUMO gap of the $[(\text{TMP})\text{AlCl}_3]^-$ anion, the oxidative stability of this electrolyte was expected to be low. Hence a smaller electrochemical window of 0.1 – 1.75 V was first used. Within this window a redox activity is observed but only half formed oxidation peaks are observed. Increasing the maximum potential to 2.5 V displays a more defined CV with a broad reduction peak around 0.45 V and a main oxidation peak at 1.66 V as well as a shoulder at 1.86 V. The increase in current intensity observed after 2.25 V is more likely linked to decomposition of the electrolyte. At this electrochemical window setup, the battery was able to run for 7 cycles before the electrolyte completely decomposed. In contrast to the DFT

calculation results, this experiment shows an improvement of the oxidative stability over compounds **1** and **2**, a stability more comparable to compound **3**.

The charge/discharge profile of this battery displayed in Graph **3.11b** was run between 0.2 – 2 V and shows no obvious sign of decomposition for 200 cycles. As observed for compound **3** the first cycle doesn't reach the theoretical specific capacity of the Chevrel phase but only displays a capacity of 105 mA.h/g. The specific capacity is stable along the experiment ranging between 45 and 51 mA.h/g, but starts to diminish after 150 cycles possibly due to slow decomposition of the electrolyte over time. The shape of the curves is similar to the ones observed using compound **3**, with a less curvilinear nature during the discharge. Because of the straightness of these curves, the overpotential couldn't be determined by the galvanostatic cycling experiment, using the CV it was determined at 0.6 V.

As noted for compound **3**, the high oxidative stability of this system doesn't agree with the DFT calculations of the low HOMO-LUMO energy gap present in the anion. Having the smallest energy gap $[(\text{TMP})\text{AlCl}_3]^-$ was thought to possess a lower oxidative stability in comparison to all the other anions. This emphasises the idea that the N-SiMe₃ bond is the weak feature in these amines, and that the sterics and electronic effects resulting from the aryl group induce a more facile cleavage of the bond. In order to evaluate the ability of an amide to undergo silazane cleavage, some adjustments in the method of DFT calculations could be attempted.

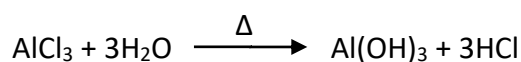
3.3. Discussion

Overall none of the series studied did successfully show a straightforward trend mostly due to the low stability of the trinuclear compounds precluding a charge discharge/profile with more than 11 cycles. At this stage the experimental results classify the electrolytes possessing the lowest aggregation state in their cation as the best performing electrolytes.

The dinuclear species displays good specific capacities, higher than 80 mA.h/g for compound **1** and 50 mA.h/g for compound **2**, but knowing that the maximum voltage has been lowered to 1.5 V these were expected to be higher. Apart from the low

oxidative stability these electrolytes suffer, they behave very similarly to what can be found in the literature for electrolytes possessing the dinuclear cation $[\text{Mg}_2\text{Cl}_3 \cdot 6\text{THF}]^+$.

The mononuclear species has a much higher oxidative stability compared to the higher aggregations, but suffers from conditioning, large overpotential and moderately low specific capacity considering the large electrochemical window (up to 2 V). As mentioned in Section 3.1 the reason for low oxidative stability was related to the anion and more specifically the nature of the organoaluminium bond. But in these series all three electrolytes possess the same aluminium anions, challenging this original statement. One of the reasons for the improved oxidative stability of the mononuclear species is the presence of the tetradentate ligand Me_6TREN coordinated to Mg which could somehow interact with the aluminium anion, increasing its stability. The crystal structure of compound **9** did not give any hints of secondary interactions between the anion and the ligand, however in solution and under the influence of an applied voltage the structure observed in solid state can conceivably adopt a different composition. Considering the ESI-MS data with compound **9**, we can observe that the basic nature of the ligand allows interactions with traces of acidic species to form hydrochloride salts such as $[\text{MgCl} \cdot 2\text{Me}_6\text{TREN} \cdot \text{HCl}]^+$ (see Figure 2.33 in Section 2.7.2). The traces of acid in the ESI-MS were attributed to the presence of acetic acid used to clean the ion trap prior to starting the experiment. Here, during the electrochemical experiment the battery runs in a tight but not 100% reliable air and moisture free environment, moreover with the presence of an AlCl_3 related species known to react with water to form HCl (Scheme 3.2) can lead to traces of acid which will then interact with the electrolyte.



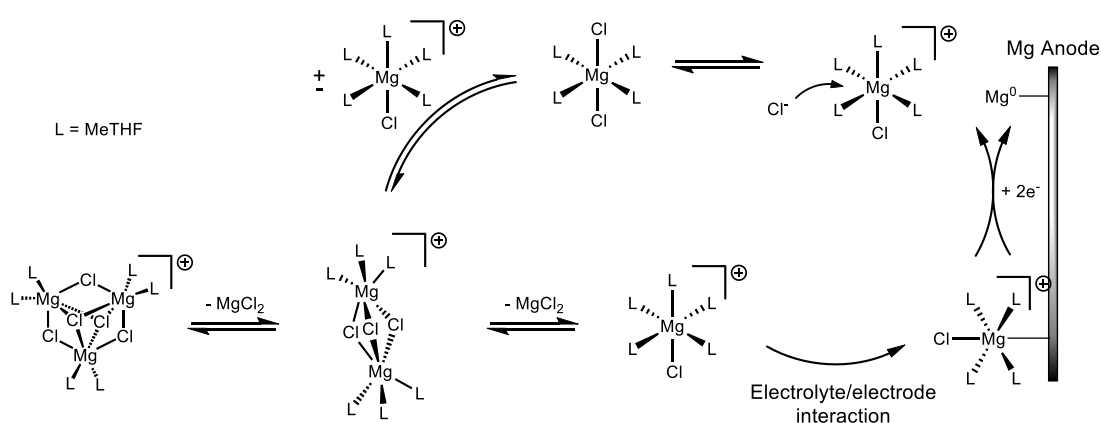
Scheme 3.2: Reaction of AlCl_3 with water.

According to the ESI-MS experiments of compounds **1** and **6** no species containing HCl are formed due to the absence of basic amido groups such as those presented in Me_6TREN . While not observed, it is possible that the presence of the HCl unit within the cation also interacts with the counter anion and affects its electrochemical stability.

It would be interesting to undertake an NMR spectroscopic study of the post-cycled electrolyte to observe what species are present, and identify how the electrolyte structurally changes to form the more sturdy active species.

However attractive the higher oxidative stability of **9** is, the Me₆TREN ligand is also linked to undesirable properties. Although it was a welcome surprise to observe that the Mg atom is still available for intercalation/deposition despite being tightly held by the tetradentate ligand, the battery displays a large overpotential and a relatively low capacity. The specific capacity seems to recover after every cycle, a behaviour comparable to the need for conditioning of the MACC electrolyte.^{13,29} Cycling the electrolyte creates an equilibrium involving different species. This equilibrium favours the formation of more active compounds which are capable of intercalating or depositing at the electrodes with the requirement of a smaller amount of energy. The conditioning of the mononuclear electrolyte eventually overcomes this hindrance caused by the Me₆TREN, forming species where the Mg atom is more readily available; this could include species with an Me₆TREN unit not fully coordinated to the Mg atom, decreasing the energy requirements to release it for intercalation/deposition. A not fully coordinated Me₆TREN ligand around a metal centre is not unusual and was previously observed and characterised.^{30,31}

The electrolyte possessing the trinuclear cation exhibits low specific capacity in the range 35 - 54 mA.h/g, as well as a large overpotential of 0.60 V. Only 11 cycles of the charge/discharge profile were recorded, but the specific capacity seems to recover after every cycle. Like for the mononuclear species, this feature is more likely to be linked to a need for conditioning of the electrolyte. There we can speculate that the higher aggregation of the cation [Mg₃Cl₅·6MeTHF]⁺ requires time and energy to break down to the dinuclear and further to mononuclear species before the Mg²⁺ ions can finally be available for the intercalation or deposition. In Scheme 3.3 a mechanism is proposed for the deposition of Mg involving the possible different aggregations present in MeTHF, the scheme is very similar to a mechanism proposed by Liu et al.³²



Scheme 3.3: Proposed mechanism including the different cation aggregations involved in the deposition of Mg in MeTHF.

Theoretical calculations performed by Ceder et al. showed that the mononuclear cation $[\text{MgCl}\cdot 3\text{THF}]^+$ is more favoured in bulk THF solutions, and that its conversion to the trinuclear cation $[\text{Mg}_3\text{Cl}_5]^+$ requires almost 1 eV to occur (Figure 3.3).³³ Assuming the inverse conversion in MeTHF, where the higher aggregates are promoted over the mononuclear species, there will also be a requirement of free energy to achieve disaggregation of the more favoured trinuclear species. The energy needed for this conversion, even if not being as high as 1 eV, would hence be a significant hindrance to efficient insertion kinetics and result in poor overall capacity instead.

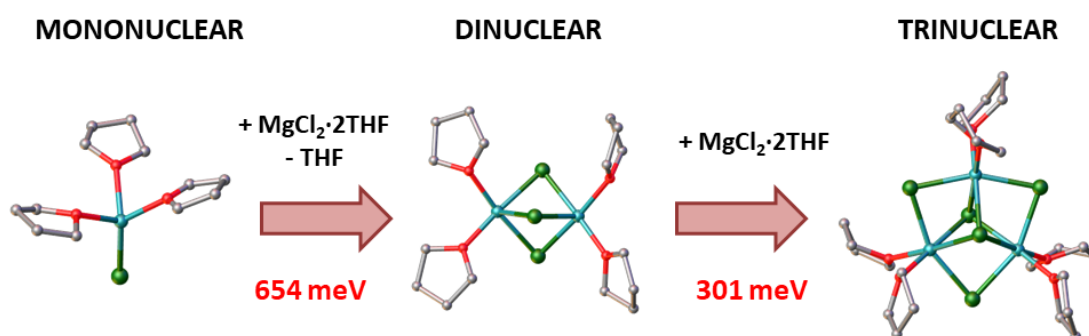
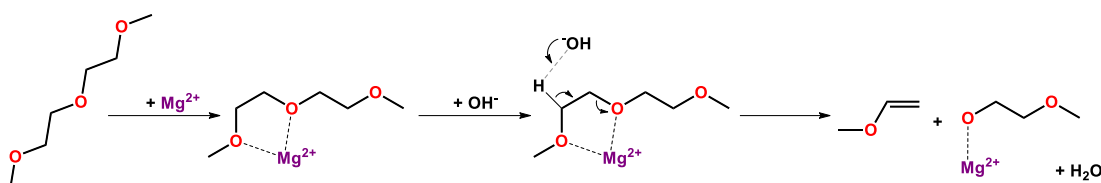


Figure 3.3: Relative free energy required for the conversion of lower to higher chloromagnesium cation aggregates.

Aside from the actual intercalation/deposition ability of the trinuclear species, whether using a less bulky amine or not the electrolytes display very early degradation, even at a voltage as low as 1.5 V. For this reason the role of the cation in the oxidative stability

limitations was reassessed and it is believed that in the case of the trinuclear species, the cation is prone to a more facile decomposition than the anion. If this is the case it makes it hard to justify the presence of such species in the mechanism of a rechargeable battery in THF. An equilibrium between different species tends to favour the formation of more thermodynamically stable compounds. In a pure THF solution with no presence of other Lewis donor ligands, the aggregation of the cation is already at equilibrium with different aggregations, as observed by ESI-MS. By DFT calculations the mononuclear aggregation $[\text{MgCl}\cdot 3\text{THF}]^+$ was determined to be the most favoured hence we would be inclined to accept that in THF, the battery mechanism would settle the equilibrium toward the cations with a lower aggregation level. In MeTHF, the ESI-MS data shows that the higher aggregations are favoured; the equilibrium is therefore expected to disfavour the formation of lower aggregations. To occur, the disaggregation would require a larger amount of energy, which would itself be lost as heat in the battery, lowering considerably its efficiency. It would be interesting to investigate the battery performance of an electrolyte in a mixture of THF:MeTHF at different ratios, and see if there is an improvement in oxidative stability as the THF installs a new equilibrium richer in small aggregates. Finally, it is worth considering the stability of MeTHF itself at higher voltage, while THF is known to be robust, the electrochemical window of MeTHF was not assessed and could be a determinant factor in the decomposition of the electrolyte.³⁴ A new study by Prendergast et al. using a combination of in situ X-ray photoelectron spectroscopy and first-principle calculations identified the plausible decomposition causes at the electrode/electrolyte interface. The electrolyte used in their study, $\text{Mg}(\text{TFSI})_2$ (TFSI = bis(trifluoromethane)sulfonimide) in diglyme, is different than the chloro-containing magnesium aluminates presented in this chapter but important insights can be gained by their studies. Diglyme is known to be stable up to a voltage exceeding what an MIB can achieve; however, it was shown that in the presence of nucleophilic OH^- ions which can be generated by either presence of moisture or $\text{Mg}(\text{OH})_2$ impurities from the Mg anode, a diglyme ligand coordinated to an Mg^{2+} dication can be deprotonated (Scheme 3.4).³⁵ This would result in the cleavage of the ether molecule which can produce a variety of magnesium oxides, themselves known to be poorly soluble in many solvents hence creating a passivating layer. It is not known if the deprotonation

of MeTHF is favoured over THF, but it could be investigated in order to find out if the solvent itself reduces the oxidative stability of the electrolytic solution in our case.



Scheme 3.4: Proposed mechanism for the decomposition of diglyme induced by the chelation of Mg^{2+} in the presence of OH^- .

The comparison of compound **3** and **4** with the other electrolytes were discussed within their own sections and are not discussed further here.

3.4. Conclusion and future work

Following the preparation and characterisation of a series of electrolytes possessing the anion $[(Dipp)(SiMe_3)AlCl_3]^-$ and counter cations with different aggregation levels the study of these electrolytes in a rechargeable battery was undertaken. What could have been a relatively straightforward study ended up hampered by the low oxidative stability of these compounds. Attempts to create a new series with less bulky amines to prevent early decomposition of the electrolyte was not entirely successful, as the characterisation of a compound with the trinuclear species $[Mg_3Cl_5 \cdot 6MeTHF]^+$ was not achieved. Using the observations gathered from all the battery experiments performed on the different electrolytes, the low oxidative stability was associated with a variety of different reasons. The bulk of the amide used for the anion has a role as the oxidative stability improves when it is lowered. Whether it affects the stability of the N-Al bond or the ability of the N-SiMe₃ to be cleaved was not established. Determining by DFT calculation the HOMO-LUMO energy gap of the anion tells us that amides with a substituent on the aryl group should give electrolytes with higher oxidative stability. Contrarily the experimental results show the inversed behaviour where compound **3** has a higher oxidative stability than compounds **1** and **2**. Moreover within a series there is a difference in oxidative stability depending on the cation aggregation.


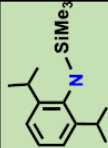
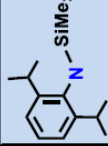
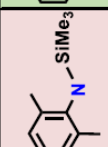
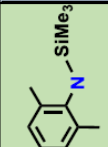
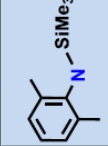
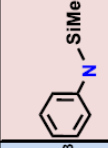
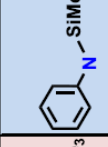
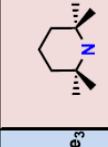

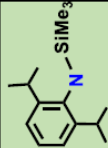
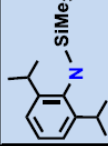
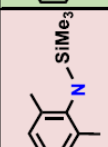
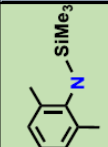
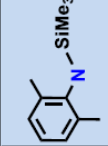
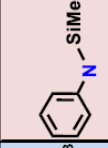
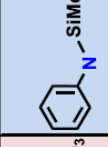
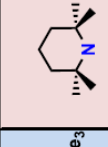
In the literature the highest oxidative stability of a magnesium battery electrolyte was obtained with a dinuclear cation, ruling out its involvement in the decomposition of electrolytes **1**, **2** and **3**. However when the mononuclear cation $[\text{MgCl}\cdot\text{Me}_6\text{TREN}]^+$ is present the electrolyte displays much higher oxidative stability. This property is associated to the presence of the Me_6TREN and arises from properties such as its basic nature, which can produce new active side products from species formed by the decomposition of the electrolyte (HCl from the reaction of AlCl_3 related species with water), ending up boosting the oxidative stability. The use of such ligands as additives could be of interest when confronted with an electrolyte exhibiting decomposition problems. Regarding the electrolytes possessing the trinuclear cation, their electrochemical properties were not fully evaluated due to their severe decomposition even at a voltage as low as 1.5 V. A debate whether this low oxidative stability was caused by the cation aggregation or the use of MeTHF over THF was lead, whereas the low specific capacity and high overpotential were linked to the energy requirement to break down the aggregation and free an Mg^{2+} ion for intercalation/deposition.

A summary of the battery performance of the electrolytes is shown in Table 3.1

In order to observe and identify the influence of the different cation aggregates on a rechargeable battery prototype the galvanostatic cycling experiment can be repeated for compounds **1**, **5** and **9**, but with a reduced maximum voltage. As observed with compound **2** which also decomposes between 0.1-2.0 V, reducing the maximum voltage to 1.5 V allowed us to obtain a charge/discharge profile of at least 100 cycle. Therefore, performing the same experiment with the same parameters, and especially the same electrochemical window, for compounds **1**, **5** and **9** in such a way that no decomposition interfere would allow a direct comparison of their behaviour.

It would be also interesting to figure out if these early decompositions are influenced by the steric or electronic, or both properties of the amine. Therefore, a larger screening using a variety of similar amines possessing different properties would give an insight regarding which of these properties are desired and which ones induce decomposition. For such a study of a certainly large number of electrolytes, including their synthesis, characterisation and purification, it would only be required to run cyclic voltammetry experiments which would quickly identify the oxidative stability of the electrolyte.

Table 3.1: Battery performance summary of the chapter.

Amido ligand									
HMDS									
Reduction peak (V)	0.9	0.73	0.39	0.60	0.64	0.34	0.42	0.50	below 0.1
Oxidation peak (V)	1.36	1.47	above 1.8	1.53	1.48	--	1.60	1.60	1.63
Charge/discharge cycles number (electrochemical window)	30 (0.1 – 2 V)	4 (0.1 – 2 V)	11 (0.1 – 1.5 V)	100 (0.1 – 2 V)	100 (0.1 – 1.5 V)	--	--	100 (0.1 – 2 V)	--
Specific capacity 1 st cycle (mA.h/g)	128	128	35	90	128	--	--	115	--
Specific capacity range (mA.h/g)	66 - 78	84 - 87	35 - 54	36 - 59	46 - 55	--	--	48 - 58	--
Overpotential (V)	0.12	0.14	0.6	0.95 – 0.4	0.2	--	0.6	0.55	--
									200 (0.1 – 2 V)
									105
									41 - 51
									0.6

 Dinuclear cation  Trinuclear cation  Mononuclear cation

- 1 J. Zhu, Y. Guo, J. Yang, Y. Nuli, F. Zhang, J. Wang and S. I. Hirano, *J. Power Sources*, 2014, **248**, 690–694.
- 2 J. Muldoon, C. B. Bucur, A. G. Oliver, T. Sugimoto, M. Matsui, H. S. Kim, G. D. Allred, J. Zajicek and Y. Kotani, *Energy Environ. Sci.*, 2012, **5**, 5941–5950.
- 3 Z. Zhao-Karger, X. Zhao, O. Fuhr and M. Fichtner, *RSC Adv.*, 2013, **3**, 16330–16335.
- 4 E. G. Nelson, J. W. Kampf and B. M. Bartlett, *Chem. Commun.*, 2014, **50**, 5193–5195.
- 5 T. Liu, Y. Shao, G. Li, M. Gu, J. Hu, S. Xu, Z. Nie, X. Chen, C. Wang and J. Liu, *J. Mater. Chem. A*, 2014, **2**, 3430–3438.
- 6 Z. Zhao-Karger, J. E. Mueller, X. Zhao, O. Fuhr, T. Jacob and M. Fichtner, *RSC Adv.*, 2014, **4**, 26924–26927.
- 7 H. Gizbar, Y. Vestfrid, O. Chusid, Y. Gofer, H. E. Gottlieb, V. Marks and D. Aurbach, *Organometallics*, 2004, **23**, 3826–3831.
- 8 D. Aurbach, H. Gizbar, A. Schechter, O. Chusid, H. E. Gottlieb, Y. Gofer and I. Goldberg, *J. Electrochem. Soc.*, 2002, **149**, A115–A121.
- 9 Y. Gofer, O. Chusid, H. Gizbar, Y. Vestfrid, H. E. Gottlieb, V. Marks and D. Aurbach, *Electrochem. Solid-State Lett.*, 2006, **9**, A257–A260.
- 10 N. Pour, Y. Gofer, D. T. Major and D. Aurbach, *J. Am. Chem. Soc.*, 2011, **133**, 6270–6278.
- 11 Y. Gofer, O. Chusid and D. Aurbach, in *Encyclopedia of Electrochemical Power Sources*, 2009, pp. 285–301.
- 12 H. S. Kim, T. S. Arthur, G. D. Allred, J. Zajicek, J. G. Newman, A. E. Rodnyansky, A. G. Oliver, W. C. Boggess and J. Muldoon, *Nat. Commun.*, 2011, **2**, 1–6.
- 13 C. J. Barile, E. C. Barile, K. R. Zavadil, R. G. Nuzzo and A. A. Gewirth, *J. Phys. Chem. C*, 2014, **118**, 27623–27630.
- 14 Y. Cheng, R. M. Stolley, K. S. Han, Y. Shao, B. W. Arey, N. M. Washton, K. T. Mueller, M. L. Helm, V. L. Sprenkle, J. Liu and G. Li, *Phys. Chem. Chem. Phys.*, 2015, **17**, 13307–13314.
- 15 C. Liao, B. Guo, D. D.-E. Jiang, R. Custelcean, S. M. Mahurin, X.-G. Sun and S. Dai, *J. Mater. Chem. A*, 2014, **2**, 581–584.
- 16 S. Sakamoto, T. Imamoto and K. Yamaguchi, *Org. Lett.*, 2001, **3**, 1793–1795.

- 17 H. Li, T. Ichitsubo, S. Yagi and E. Matsubara, *J. Mater. Chem. A*, 2017, **5**, 3534–3540.
- 18 M. D. Levi and D. Aurbach, *J. Power Sources*, 2005, **146**, 349–354.
- 19 T. Ichitsubo, S. Yagi, R. Nakamura, Y. Ichikawa, S. Okamoto, K. Sugimura, T. Kawaguchi, A. Kitada, M. Oishi, T. Doi and E. Matsubara, *J. Mater. Chem. A*, 2014, **2**, 14858–14866.
- 20 D. Aurbach, Z. Lu, A. Schechter, Y. Gofer, H. Gizbar, R. Turgeman, Y. Cohen, M. Moshkovich and E. Levi, *Nature*, 2000, **407**, 724–727.
- 21 O. Mizrahi, N. Amir, E. Pollak, O. Chusid, V. Marks, H. Gottlieb, L. Larush, E. Zinigrad and D. Aurbach, *J. Electrochem. Soc.*, 2008, **155**, A103–A109.
- 22 M. D. Levi, H. Gizbar, E. Lancry, Y. Gofer, E. Levi and D. Aurbach, *J. Electroanal. Chem.*, 2004, **569**, 211–223.
- 23 E. Lancry, E. Levi, Y. Gofer, M. Levi, G. Salitra and D. Aurbach, *Chem. Mater.*, 2004, **16**, 2832–2838.
- 24 T. Lorenz, A. Lik, F. A. Plamper and H. Helten, *Angew. Chem. Int. Ed.*, 2016, **55**, 7236–7241.
- 25 A. Schulz, A. Villinger and A. Westenkirchner, *Inorg. Chem.*, 2013, **52**, 11457–11468.
- 26 M. Gómez, C. Hernández-Prieto, A. Martín, M. Mena and C. Santamaría, *Inorg. Chem.*, 2016, **55**, 3815–3821.
- 27 C. Hering-Junghans, A. Schulz, M. Thomas, A. Villinger, D. G. Truhlar, A. D. Phillips, A. L. Rheingold, L. Stark and D. Walsh, *Dalton Trans.*, 2016, **45**, 6053–6059.
- 28 V. Dhayalan, C. Samann and P. Knochel, *Chem Commun*, 2015, **51**, 3239–3242.
- 29 K. A. See, K. W. Chapman, L. Zhu, K. M. Wiaderek, O. J. Borkiewicz, C. J. Barile, P. J. Chupas and A. A. Gewirth, *J. Am. Chem. Soc.*, 2016, **138**, 328–337.
- 30 D. M. Cousins, M. G. Davidson, C. J. Frankis, D. García-Vivó and M. F. Mahon, *Dalton Trans.*, 2010, **39**, 8278–8280.
- 31 S. D. Robertson, A. R. Kennedy, J. J. Liggat and R. E. Mulvey, *Chem. Commun.*, 2015, **51**, 5452–5455.
- 32 T. Liu, J. T. Cox, D. Hu, X. Deng, J. Hu, M. Y. Hu, J. Xiao, Y. Shao, K. Tang and J. Liu, *Chem. Commun.*, 2015, **51**, 2312–2315.

- 33 P. Canepa, S. Jayaraman, L. Cheng, N. N. Rajput, W. D. Richards, G. S. Gautam, L. A. Curtiss, K. A. Persson and G. Ceder, *Energy Environ. Sci.*, 2015, **8**, 3718–3730.
- 34 N. Kumar and D. J. Siegel, *J. Phys. Chem. Lett.*, 2016, **7**, 874–881.
- 35 Y. Yu, A. Baskin, C. Valero-Vidal, N. T. Hahn, Q. Liu, K. R. Zavadil, B. W. Eichhorn, D. Prendergast and E. J. Crumlin, *Chem. Mater.*, 2017, **29**, 8504–8512.

Chapter 4: Synthetic Design of Novel Chloro-Free Electrolytes

This chapter discusses the organometallic synthetic design approach to chloro-free magnesium electrolytes. Our angle of approach was inspired by “sought after” magnesium compounds mentioned in the literature by electrochemists with rudimentary synthetic knowledge.¹ First an easy synthetic pathway to prepare and characterise magnesium aluminates with a “naked” Mg^{2+} cation is proposed. Unanticipated physical properties make these desired compounds insoluble, necessitating alternative solutions. A solution to this problem was achieved by reducing the ionic charges involved in the separated ion pair structure these compounds adopt, instead targeting complexes which have only a 1+ and a 1- moiety. Finally preliminary results of the electrochemical performance of these compounds in MIB are introduced.

4.1. Introduction

Steady progress in Mg-ion battery electrolyte development is slowly settling and some electrolytes reach anodic stability values approaching Li electrolytes for Li-ion batteries. The fully inorganic electrolyte $[\text{AlCl}_4]^- [\text{Mg}_2\text{Cl}_3 \cdot 6\text{THF}]^+$ (MACC) is stable up to 3.4 V, a feat made possible by the absence of organometallic bonds linked to low oxidative stability.²⁻⁵ This value, versus the 4 - 4.5 V oxidative stability for alkyl carbonate/ LiPF_6 lithium electrolytes looks relatively low, however any value in the 3-3.5 V range for an MIB is already an achievement outmatching many top commercially available rechargeable batteries.⁶ With such recent progress it is time to take a step further for the achievement of a commercially viable battery and start tackling current undesired roadblocks encumbering the prototypes on their way to the production plant. Many of these roadblocks involve the electrolyte where the most notorious properties are the low voltage stability, air sensitivity and corrosion.⁷ It is also worth mentioning another major obstacle more related to the materials aspect of the battery system, namely the cathode material. Current state of the art cathodes give limited options in high voltage candidates, dramatically affecting the expansion of powerful MIBs, no matter how efficient the electrolyte is.^{8,9}

This chapter focuses on the development of a novel class of electrolyte by getting rid of the halogen atoms, more precisely the chloride atoms. Halogens are believed to be

responsible for the corrosion of the battery cell and current collectors, which are commonly made of non-noble metals for cost reasons. A lot of effort has been invested in studying such electrolytes by using a few different approaches. To only cite a few examples; Remhof et al. developed solid-state electrolytes using modified $\text{Mg}(\text{BH}_4)_2$ reagents,¹⁰ Mohtadi et al. used carborane chemistry as weakly coordinating counter anions to a naked magnesium dication to form $2[\text{CB}_{11}\text{H}_{12}]^- [\text{Mg}\cdot 3\text{DME}]^{2+}$,^{11,12} Wright, Grey et al. synthesised and characterised the magnesium analogue to the widely used lithium electrolyte LiPF_6 in acetonitrile to formulate $2[\text{PF}_6]^- [\text{Mg}\cdot 6\text{CH}_3\text{CN}]^{2+}$,¹³ or finally the use of magnesocene (MgCp_2) by Wachtler et al. (Figure 4.1).¹⁴ If these new chloro-free electrolytes possess their own flaws such as low battery performances for solid-state $\text{Mg}(\text{BH}_4)_2$, high cost of carborane starting material for $2[\text{CB}_{11}\text{H}_{12}]^- [\text{Mg}\cdot 3\text{DME}]^{2+}$, passivation of electrode material for $2[\text{PF}_6]^- [\text{Mg}\cdot 6\text{CH}_3\text{CN}]^{2+}$ or the low oxidative stability of magnesocene, they are nevertheless of extreme importance for the progress leading to future breakthroughs in this field.

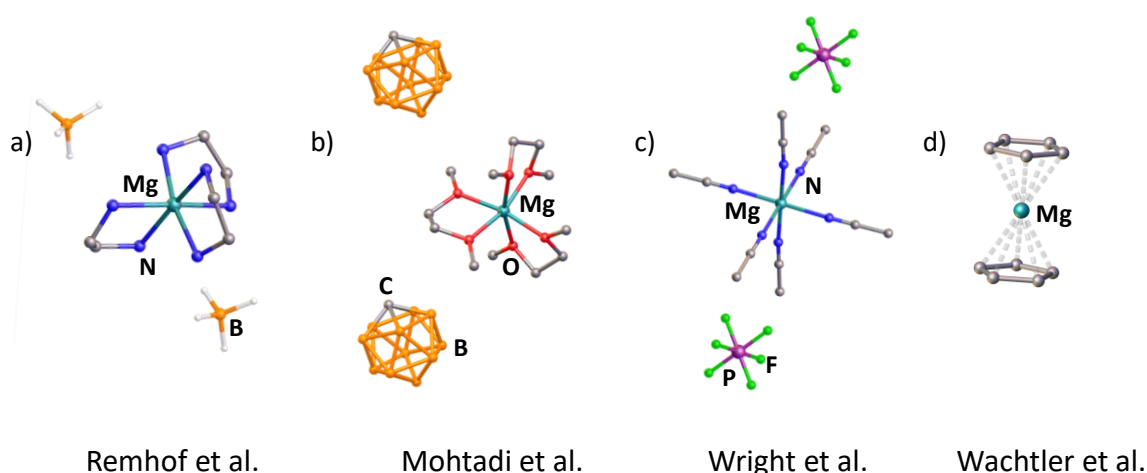
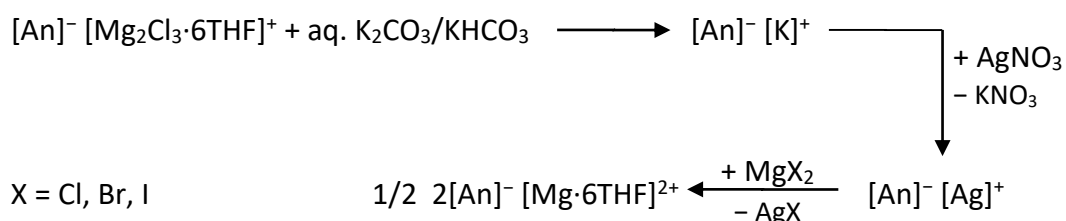


Figure 4.1: Structure of chloro-free magnesium compounds used as electrolytes for MIB; **a)** $2[\text{BH}_4]^- [\text{Mg}\cdot 3\text{en}]^{2+}$, **b)** $2[\text{CB}_{11}\text{H}_{12}]^- [\text{Mg}\cdot 3\text{DME}]^{2+}$, **c)** $2[\text{PF}_6]^- [\text{Mg}\cdot 6\text{CH}_3\text{CN}]^{2+}$, **d)** MgCp_2 .

4.2. Synthesis of novel chloro-free magnesium aluminates

In a perspective article Muldoon et al. discuss the urgent need for new advances in chloro-free electrolytes and mention that it would be the “holy grail of electrolyte development to have a universal synthetic method to readily convert the magnesium

dimer $(\text{Mg}_2\text{Cl}_3 \cdot 6\text{TTHF})^+$ into the corresponding naked magnesium analogue". To achieve such a challenge they propose a series of salt metathesis reactions to promote ion exchange of the magnesium dinuclear cation $[\text{Mg}_2\text{Cl}_3 \cdot 6\text{TTHF}]^+$ to make the potassium analogue using aq. $\text{K}_2\text{CO}_3/\text{KHCO}_3$. This first step allows subsequent ion exchange to the silver salt using AgNO_3 to finally get the naked $[\text{Mg} \cdot 6\text{TTHF}]^{2+}$ cation in a third and final ion exchange using magnesium halide salts (Scheme 4.1).



Scheme 4.1: Methodology proposed by Muldoon et al. to synthesise a magnesium electrolyte possessing the naked magnesium dication $[\text{Mg} \cdot 6\text{TTHF}]^{2+}$ from the dinuclear cation $[\text{Mg}_2\text{Cl}_3 \cdot 6\text{TTHF}]^+$.

In addition to the undesired multistep reaction using two alternative metals including expensive AgNO_3 , the requirement for a water stable anion is indispensable to survive an aqueous work up. This greatly limits the choice of the counter anions often responsible for the air and moisture sensitivity of magnesium electrolytes.¹⁵ In this example they report examples with crystal structures using the boron centred anion $[(\text{C}_6\text{F}_5)_3\text{B}(\text{C}_6\text{H}_5)]^-$ (Figure 4.2) and extend the method in a patent document with other boron anions exclusively. It is believed that this route is not applicable to aluminium chemistry due to the more moisture sensitive nature of organoaluminium compounds. No detailed procedure of the reaction is thoroughly described and the physical and electrochemical properties of the final compound are not included giving no insight of yield, solubility or electrochemical performance on these compounds.¹⁶

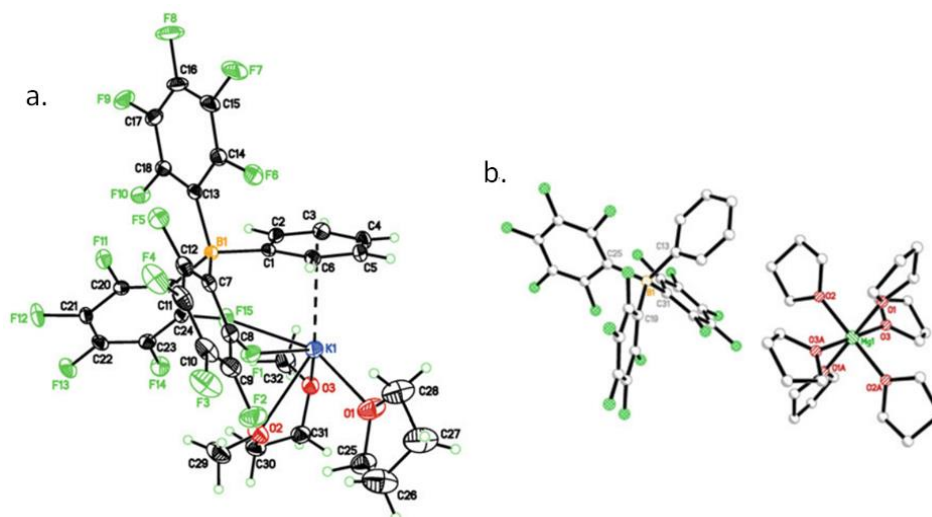


Figure 4.2: Crystal structure of **a**) $[(\text{C}_6\text{F}_5)_3\text{B}(\text{C}_6\text{H}_5)]^- [\text{K}\cdot\text{DME}\cdot\text{THF}]^+$ potassium salt analogue of $[(\text{C}_6\text{F}_5)_3\text{B}(\text{C}_6\text{H}_5)]^- [\text{Mg}_2\text{Cl}_3\cdot 6\text{THF}]^+$; **b**) $2[(\text{C}_6\text{F}_5)_3\text{B}(\text{C}_6\text{H}_5)]^- [\text{Mg}\cdot 6\text{THF}]^{2+}$ naked magnesium salt analogue of $[(\text{C}_6\text{F}_5)_3\text{B}(\text{C}_6\text{H}_5)]^- [\text{Mg}_2\text{Cl}_3\cdot 6\text{THF}]^+$. Pictures screenshotted from Rechargeable Batteries; Zhang, Z., Zhang, S. S., Eds.; Green Energy and Technology; Springer International Publishing: New York, 2015; pp 611–635 due to the absence of the corresponding data in the CSD database.

Developing a magnesium chloro-free electrolyte possessing the naked magnesium dication $[\text{Mg}\cdot 6\text{THF}]^{2+}$ with aluminium counter anions over its boron counterpart is more attractive financially and sustainably due to the much higher abundance of Al over B (Al is estimated to be 2000 times more abundant). Given the demanding route to convert $[\text{Mg}_2\text{Cl}_3\cdot 6\text{THF}]^+$ to $[\text{Mg}\cdot 6\text{THF}]^{2+}$ and especially using aqueous conditions, for example the conspicuous synthetic approach is more likely to be rational, whereby $2[\text{AlR}_4]^- [\text{Mg}\cdot 6\text{THF}]^{2+}$ (where R is not a halogen) is made directly by using non halogenated starting materials and involving no multiple ion exchange steps. The literature issued some synthetic examples of related compounds by simple transmetallation reaction from a magnesium reagent MgR_2 to two molar equivalents of another organometallic reagent MR_n successfully forming $2[\text{MR}_{n+1}]^- [\text{Mg}\cdot 6\text{THF}]^{2+}$ ($\text{M} = \text{Mn}$,¹⁷ La and Nd,¹⁸ Sn and Pb,¹⁹ Zn²⁰).

In this study a few possible pathways have been investigated to establish the most cost and time efficient method. The first methodology was to employ metal aluminium hydride chemistry where preliminary tests showed that LiAlH_4 reacts readily with 4 equivalents of pyrrole to form $[\text{Al}(\text{pyrrolyl})_4]^- [\text{Li}\cdot 4\text{THF}]^+$. Then using $[\text{Al}(\text{pyrrolyl})_4]^- [\text{Li}\cdot 4\text{THF}]^+$, the Mg derivative was prepared by a single metal ion exchange process

similar to what Muldoon et al. proposed. The second methodology was to use a more rational way by following the transmetallation method from the literature mentioned in the previous paragraph, and synthesise the targeted product, $2[\text{AlR}_4]^- [\text{Mg}\cdot 6\text{THF}]^{2+}$ (where R = Ph or pyrrole) (more details in the following sections). To reach these objectives, the choice of the R group is important and must be of moderate size for the aluminium centre to accommodate four of them while maintaining adequate chemical and electrochemical stability of the anion.

4.2.1. Attempted preparation of chloro-free magnesium aluminates using aluminium hydride starting materials

The aluminium hydride bonds from LiAlH_4 are known to react readily with protons of an acidic nature, often including N-H and O-H bonds, enabling the formation of related Al-NR₂ or Al-OR bonds and releasing H₂ as a by-product.^{21,22} This makes an attractive approach to prepare desired amido or alkoxo $[\text{AlR}_4]^-$ anions (R = amide or alkoxide) when using alanate compounds such as LiAlH_4 or NaAlH_4 as starting material. Then, through a single metathesis reaction using magnesium halide salts, the alkali metal can be exchanged for an Mg atom.

Treatment of LiAlH_4 with 4 equivalents of pyrrole in THF at room temperature results in immediate release of hydrogen gas. After the end of the effervescence a small volume of toluene was added and the mixture was placed in a freezer. A crop of crystals was obtained overnight and the compound was characterised by X-ray diffraction as $[\text{Al}(\text{pyrrolyl})_4]^- [\text{Li}\cdot 4\text{THF}]^+$, **16**, in a 60% yield (Figure 4.3).

The structure of compound **16** represents a solvent separated ion pair lithium aluminate with a “naked Li” cation coordinated by four THF molecules in a tetrahedral geometry. The counter anion is a tetra-pyrrolylaluminate moiety also adopting a tetrahedral geometry. The moderately low quality of the data only allow this crystal structure to be used for connectivity and no further comments can be made on its bond lengths and angles. ¹H, ¹³C, ⁷Li and ²⁷Al NMR spectroscopy of **16** in C₆D₆ is consistent with the solid state crystal structure where a considerable downfield shift of the resonance corresponding to the α-position compared to pyrrole is observed (7.25 and 6.37 ppm respectively). A 1:2 hydrogen ratio between the free pyrrole and THF resonances in

^1H NMR also matches the solid state structure. Finally ^{27}Al NMR also confirms nicely the presence of the $[\text{Al}(\text{pyrrolyl})_4]^-$ anion by displaying a well-defined sharp resonance peak at 98.15 ppm. The presence of such a well-defined peak is characteristic of an Al atom in a highly symmetrical environment and possessing exclusively the same ligands.

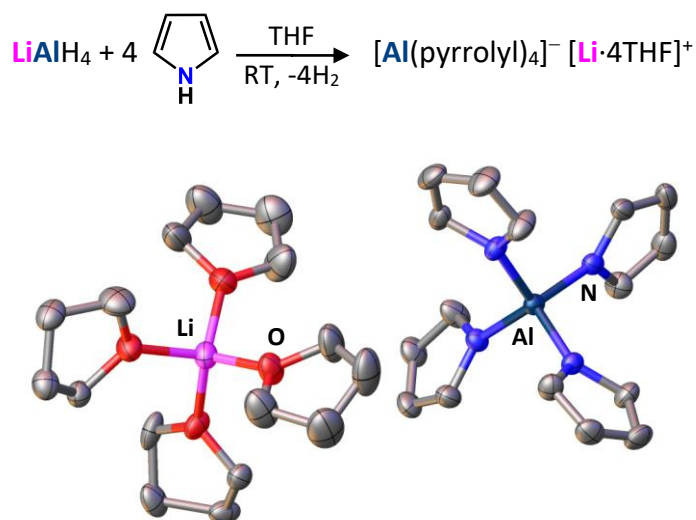
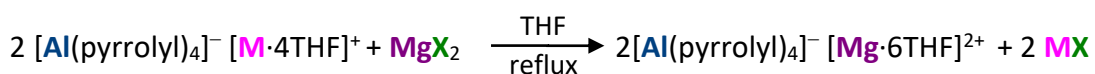


Figure 4.3: Scheme of the preparation (top) and molecular structure (bottom) of **16** $[\text{Al}(\text{pyrrolyl})_4]^- [\text{Li}\cdot 4\text{THF}]^+$. Hydrogen atoms and positioning disorder of all the THF units are omitted for clarity. Thermal ellipsoids are drawn at the 30 % probability level.

This successful preliminary result shows the ease of formation of a chloro-free aluminium anion using pyrrole groups. The reason for the choice of pyrrole over another amine includes its aromaticity, which makes it the amino equivalent of the widely used APC electrolyte and its small size. Being smaller than a phenyl group, from which the $[\text{Al}(\text{Ph})_4]^-$ anion is known in the literature, it was expected that four pyrrolyl groups would easily be accommodated around the Al atom.²³ From there the next logical step is to use this compound and exchange the Li atom for an Mg atom through salt metathesis reactions using MgX_2 ($\text{X} = \text{Cl}, \text{Br}$ or I).

Starting with the simple magnesium salt MgCl_2 , the metathesis reaction was attempted by stirring the reaction mixture in THF under reflux. At the end of the reaction a solid was observed, it is not clear if this solid is a result of the reaction or undissolved MgCl_2 , the solid was isolated, washed with THF and dried under vacuum. Tentative attempts at recrystallisation in a variety of dry solvents possessing different polarities failed due

to the extreme insolubility of the precipitate. For the same reasons NMR spectroscopy of the solid shows no resonances and NMR spectroscopy of the filtrate showed resonances corresponding to **16** exclusively. A screening of this reaction procedure was performed by varying the alkali-metal from Li to Na and the halogens of the magnesium salts changed for Br, I or isoelectronic -O^tBu groups (Scheme 4.2). The idea behind this screening is to seek a better match between the alkali-metal and the halogen atom sizes and polarisation properties, favouring the formation of the desired product $2[\text{Al}(\text{pyrrolyl})_4]^- [\text{Mg}\cdot 6\text{THF}]^{2+}$. For example by-product NaCl has a less polarized ionic bond compared to LiCl. $\text{Mg}(\text{O}^t\text{Bu})_2$ was also attractive to use in this situation as the alkali-metal alkoxide by-product is highly soluble in THF, hence limiting the formation of poorly soluble compounds in the final mixture. Disappointingly $\text{Mg}(\text{O}^t\text{Bu})_2$ itself was insoluble in THF, a problem often related to formation of large magnesium alkoxide oligomers²⁴, no apparent reactivity was observed. Overall this screening was unsuccessful in ameliorating the outcome of the metathesis reaction and the presence of an insoluble product persisted.

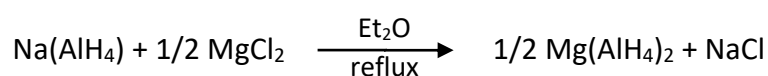


M = Li, Na

X = Cl, Br, I, O^tBu

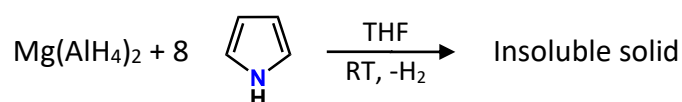
Scheme 4.2: Reaction of alkali-metal tetrapyrrolyl aluminates $[\text{Al}(\text{pyrrolyl})_4]^- [\text{M}\cdot 4\text{THF}]^+$ with different magnesium simple salts.

Trying to get around the problem of these reactions, the alternative way using metal hydride chemistry to make the desired product $2[\text{Al}(\text{pyrrolyl})_4]^- [\text{Mg}\cdot 6\text{THF}]^{2+}$ is to directly use $\text{Mg}(\text{AlH}_4)_2$ instead of LiAlH_4 as the starting material. According to the literature itself the preparation of $\text{Mg}(\text{AlH}_4)_2$ uses the same salt metathesis procedure showed in Scheme 4.1 using NaAlH_4 and MgCl_2 under reflux, followed by a Soxhlet extraction in Et_2O (Scheme 4.3).^{25–27}



Scheme 4.3: Preparation of $\text{Mg}(\text{AlH}_4)_2$ according to the literature.

Following this procedure, a cloudy mixture was obtained, however efforts to grow a crystal crop were unsuccessful, providing no X-ray confirmation for the identity of the product as $\text{Mg}(\text{AlH}_4)_2$. The solvent was removed to yield a white solid which was used as $\text{Mg}(\text{AlH}_4)_2$, keeping in mind that according to the literature a residual amount of NaCl is usually still present in about 2 to 6 wt. % in the final product.²⁷ Addition of 8 equivalents of pyrrole to a highly dilute solution of $\text{Mg}(\text{AlH}_4)_2$ lead to the formation of H_2 gas and an insoluble solid giving similar results with the metathesis reaction with compound **16**.

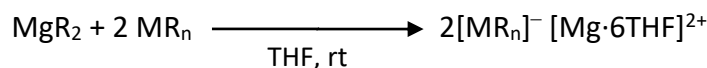


Scheme 4.4: Reaction of $\text{Mg}(\text{AlH}_4)_2$ with pyrrole.

Using alanate chemistry for the preparation of chloro-free magnesium organoaluminate reagents seems an attractive and easy route in theory, yet the outcome of such a strategy led to formation of a product which couldn't be successfully identified by common available techniques due to its insolubility. At this stage it was not ruled out that the actual desired product was in fact insoluble, hence unusable as a battery electrolyte. Without any means of characterisation, the possibility to form an undesired product such as mixed amide/hydride aluminate or contacted magnesium aluminate compounds was still contemplated. Efforts to access the targeted $2[\text{Al}(\text{pyrrolyl})_4]^- [\text{Mg}\cdot 6\text{THF}]^{2+}$, the transmetallation procedure from the literature previously mentioned is presented hereinafter.

4.2.2. Synthesis and characterisation of $2[\text{Al}(\text{pyrrolyl})_4]^- [\text{Mg}\cdot 6\text{THF}]^{2+}$ by transmetallation reaction

In order to synthesise $2[\text{Al}(\text{pyrrolyl})_4]^- [\text{Mg}\cdot 6\text{THF}]^{2+}$ according to the transmetallation method proposed in the literature mentioned in Section 4.2 (Scheme 4.5), the synthesis of previously unreported starting materials $\text{Al}(\text{pyrrolyl})_3$ and $\text{Mg}(\text{pyrrolyl})_2$ was first undertaken.



M = Al, Mn, Zn, Sn, La, Nd, Pb.

Scheme 4.5: Literature method for the preparation of naked magnesium cation with a variety of counter metal anions by transmetallation reaction.

The synthetic preparation of $\text{Al}(\text{pyrrolyl})_3$ was adapted from the synthesis of $\text{AlPh}_3 \cdot \text{OEt}_2$ reported by Westerhausen.²⁸ A solution of pyrrolyllithium was first prepared by adding an equimolar amount of $n\text{BuLi}$ to pyrrole in Et_2O . This solution was then added to a freshly made solution of AlCl_3 in a 3:1 ratio. A non-miscible brown oil was formed alongside a white solid (LiCl), the solvent system was changed to toluene which solubilised the oil and the solid by-product was filtered. From the resulting brown solution crystals were grown at $-35\text{ }^\circ\text{C}$ from a toluene/hexane mixture and were characterised by X-ray crystallography as $\text{Al}(\text{pyrrolyl})_3 \cdot \text{OEt}_2$, **17** in a yield of 65 % (Figure 4.4).

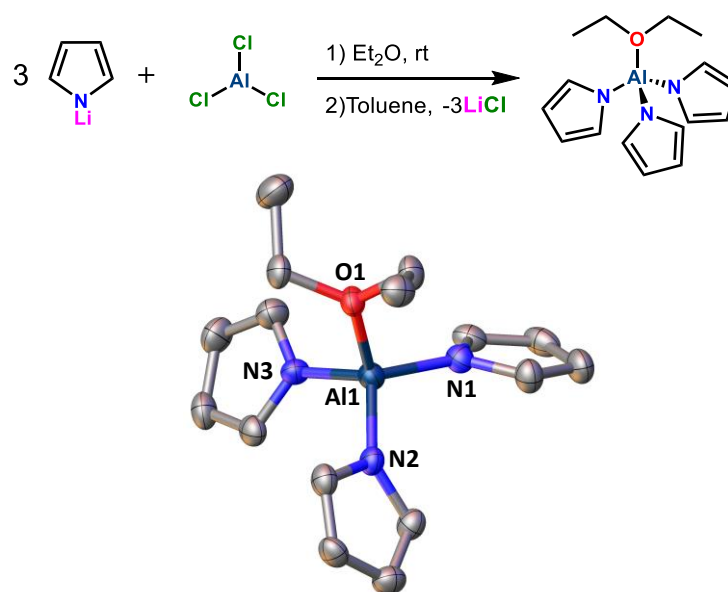


Figure 4.4: Scheme of the preparation (top) and molecular structure (bottom) of **17** $\text{Al}(\text{pyrrolyl})_3 \cdot \text{OEt}_2$. Hydrogen atoms are omitted for clarity. Thermal ellipsoids are drawn at the 50 % probability level. Selected bond distances (Å) and angles ($^\circ$): Al-N 1.8335; Al1-O1 1.8477(17); N-Al-N 112.17; O-Al-N 106.62. Atoms which do not carry a numerical label represent average parameter values.

Compound **17** is a four coordinated aluminium tris(amide) monomeric compound in a tetrahedral geometry. In the literature there are 10 entries for $\text{AlR}_3\cdot\text{OEt}_2$ compounds where R is an aryl, benzyl, siloxide, silyl, thiolate or halide group, however **17** is the first amido analogue.^{29–34} Comparing the known compounds to **17**, the small size of the pyrrole groups allows **17** to have a lower steric hindrance level and adopt a less distorted tetrahedral geometry with an average N-Al-N angle of 112.17° , N-Al-O of 106.61° and a τ_4 value of 0.955.³⁵ ^1H NMR spectroscopy of **17** in C_6D_6 is, to an extent, different from compound **16** where the downfield shift of the α -position is not as strongly observed. The ^{27}Al NMR spectrum shows a very broad signal at 97.68 ppm, typical for an aluminium reagent possessing different groups, here the amide and Et_2O .

The preparation of $\text{Mg}(\text{pyrrolyl})_2$ was straightforward due to the high acidity of the proton on pyrrole (pKa: 23.0) which eases its deprotonation using $n\text{Bu}_2\text{Mg}$ in THF, without the need for heat. Crystals were grown from a hexane/THF mixture and were characterised by X-ray crystallography as $\text{Mg}(\text{pyrrolyl})_2\cdot 4\text{THF}$, **18**; in a 60% yield (Figure 4.5).

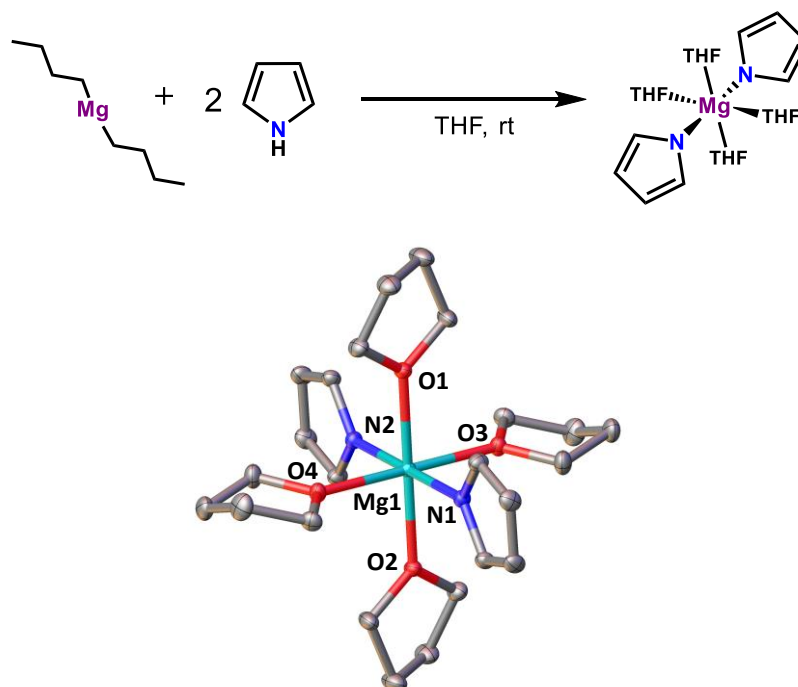


Figure 4.5: Scheme of the preparation (top) and molecular structure (bottom) of **18** $\text{Mg}(\text{pyrrolyl})_2\cdot 4\text{THF}$. Hydrogen atoms and disorder present on one of the THF units are omitted for clarity. Thermal ellipsoids are drawn at the 30 % probability level. Selected bond distances (Å) and angles ($^\circ$): Mg-N 2.1049; Mg-O 2.1534; O1-Mg1-O3 90.50(5); O1-Mg1-O4 89.50; O1-Mg1-O2 180.00; O-Mg-O 180.00; O-Mg-N 90.00, N-Mg-N 180.00. Atoms which do not carry a numerical label represent average parameter values.

Compound **18** is a six coordinate homoleptic amidomagnesium monomeric compound in an octahedral geometry where the two pyrrolyl groups are trans to each other. It is the first diamidomagnesium compound with 4 THF molecules coordinated to the magnesium, other diamidomagnesium compounds typically only have space for 2 THF molecules around the magnesium due to the greater steric effect of the amines used.^{36–39} This emphasises the choice to pursue a small amine such as pyrrole as the bulk of most amines, even of moderate size, seems to affect the coordination sphere of Al or Mg very easily.

Adding a THF solution of **18** to a THF solution of **17** under stirring causes the formation of an insoluble precipitate, reminiscent of the results presented in section 4.2.1. Controlling the reaction rate by layering solutions of the two reagents so they diffuse slowly overnight produced a crop of large crystals. X-ray diffraction showed the successful acquisition of the target molecule $2[\text{Al}(\text{pyrrolyl})_4]^- [\text{Mg}\cdot 6\text{THF}]^{2+}$, **19** in an excellent yield of 95 % (Figure 4.6).

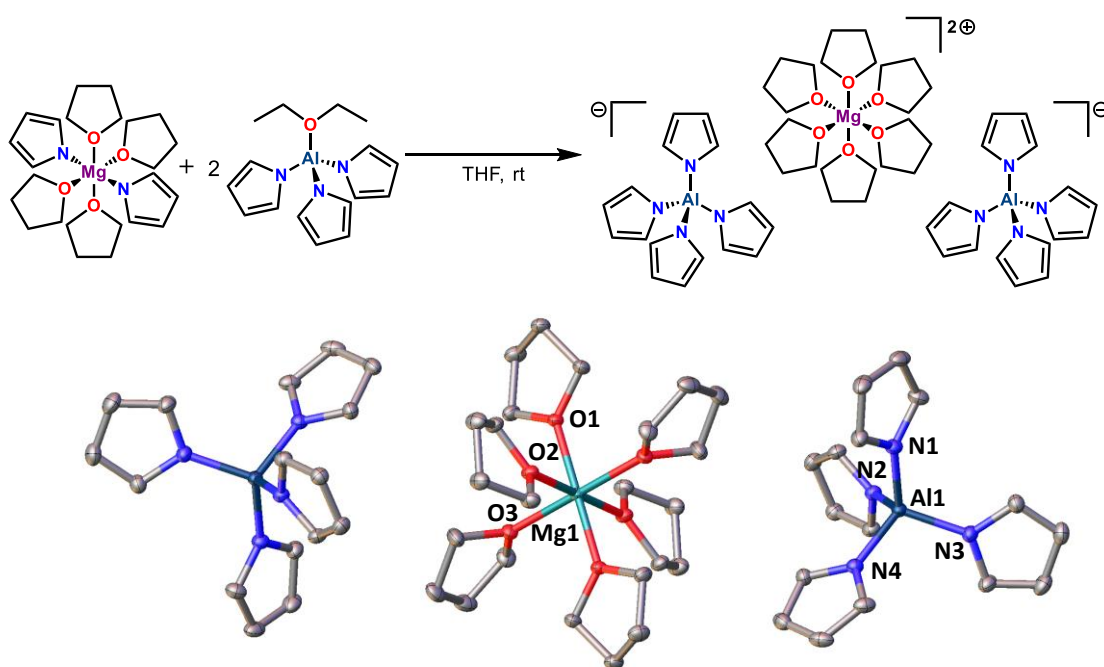


Figure 4.6: Scheme of the preparation (top) and molecular structure (bottom) of **19** $2[\text{Al}(\text{pyrrolyl})_4]^- [\text{Mg}\cdot 6\text{THF}]^{2+}$. Hydrogen atoms and disorder present on one of the THF units are omitted for clarity. Thermal ellipsoids are drawn at the 30 % probability level. Selected bond distances (Å) and angles (°): Al-N 1.8531; Mg-O 2.1035; N-Al-N 109.47; O1-Mg1-O2 90.54(4); O1-Mg1-O3 90.35(4); O2-Mg1-O3 90.69(4). Atoms which do not carry a numerical label represent average parameter values.

Compound **19** displays a separated ion pair structure where the dication $[\text{Mg}\cdot 6\text{THF}]^{2+}$ is a 6 coordinated “naked Mg” cation with an octahedral MgO_6 core geometry. The geometry of the $[\text{Al}(\text{pyrrolyl})_4]^-$ counter anions is the same as observed in compound **16**, a 4 coordinate Al in a distorted tetrahedral geometry ($\tau_4 = 0.943$). Higher quality data allows us to discuss bond distances and angles, overall showing a low distortion level of the anion with no strain within the structure, sometime seen as a small indication of a stabilised molecule. As a preliminary safety test a small amount of crystalline material was carefully added to a container filled with water, where the solid floated with an absence of apparent reactivity, showing the non-pyrophoric/flammable nature of the compound. Attempts to dissolve the isolated crystals of **19** in THF were proven unsuccessful. Further trials with other ethereal solvents such as DME, diglyme or tetraglyme and non-polar solvents were also futile. The insolubility is such that no NMR resonance signals of **19** were observed in d_8 -THF, even after subsequent heating or sonication of the sample. Successful ^1H , ^{13}C and ^{27}Al NMR spectroscopy was obtained when changing the solvent to more polar d_6 -DMSO. The presence of the anion $[\text{Al}(\text{pyrrolyl})_4]^-$ was identified in ^1H NMR with the α -position of the pyrrolyl shifting upfield, opposed to the downfield shift observed in C_6D_6 , and a 8:6 pyrrolyl to THF ratio. The resonances corresponding to the THF units appeared as free THF molecules, suggesting that DMSO replaced them at the Mg centre. The ^{27}Al NMR spectrum, as observed for **16**, displays a sharp well defined resonance at 97.45 ppm distinctive to a symmetrical aluminium compound.

Previously studied electrolytes with naked magnesium cations were shown not to be very soluble in bulk THF either, but instead mixtures of solvents were used to increase the solubility of these compounds. For example the Cl containing THF solvated magnesium aluminate $2[\text{AlCl}_4]^- [\text{Mg}\cdot 6\text{THF}]^{2+}$ is first prepared in ionic liquid PYR14-TFSI (1-Butyl-1-methylpyrrolidinium bis(trifluoromethane-sulfonyl)imide) before adding THF (1:1) to obtain the active electrolytic solution used in a Mg/S battery.⁴⁰ In another example, the CH_3CN solvated electrolyte $2[\text{PF}_6]^- [\text{Mg}\cdot 6\text{CH}_3\text{CN}]^{2+}$ is only soluble up to 0.17 M in acetonitrile, but this can be increased up to 0.71 M in a 1:1 mixture of THF/ CH_3CN , it is however not mentioned if the compound is soluble in bulk THF.¹³ The final example is with carborane based electrolyte $2[\text{CB}_{11}\text{H}_{12}]^- [\text{Mg}\cdot 3\text{DME}]^{2+}$ which is, according to the literature, insoluble in THF but soluble in

linear polyethers such as DME, diglyme and tetraglyme. However, this electrolyte possesses rather odd properties as it is soluble at low temperature (-15°C) but insoluble at higher temperature (room temperature and above) in these donor solvents.¹² Some of these examples possess different counter anions which could be a potential candidate leading to higher solubility. Yet we can also observe an importance in the solvation shell around the Mg cation, a notion backed-up in the present study by the fact that compound **19** is soluble in DMSO which replaces the THF molecules without affecting the aluminium anion. In a rechargeable battery, DMSO is not an ideal solvent due to its high melting point (19°C) and its very strong coordination ability with metals. For battery tests of compound **19** conducted in DMSO please refer to Section 4.3.1.

4.2.3. Changing the solvation shell of the Mg²⁺ dication in 2[Al(pyrrolyl)₄]⁻ [Mg·6THF]²⁺

Aiming to overcome the solubility issue of 2[Al(pyrrolyl)₄]⁻ [Mg·6THF]²⁺ compromising the use of such a compound as a chloro-free electrolyte in Mg-ion batteries and inspired by previously studied successful electrolytes, the solvation shell around the Mg²⁺ cation was altered. This work was carried out by adding the heptadentate ligand tris[2-(2-methoxyethoxy)ethyl]amine (TMEA, ligand L₁) during the preparation of Mg(pyrrolyl)₂, before following the same procedure used for the preparation of **19** to form 2[Al(pyrrolyl)₄]⁻ [Mg·L₁]²⁺, **20**; Yield : 90 % (Figure 4.7).

Compound **20** has a very similar separated ion pair motif to compound **19** but where L₁ replaces the 6 THF units to form a 7 coordinated Mg²⁺ dication. The geometry around the Mg atom could be best described as midway between capped octahedral and end-capped trigonal prismatic. The overall data quality for this structure was lowered by the fact that ligand L₁ is distributed over at least three different positions causing difficulties to refine the data efficiently. L₁ surrounds the Mg atom almost completely more like a cryptand rather than a Me₆TREN ligand would do. ¹H, ¹³C and ²⁷Al NMR spectra in d₆-DMSO are consistent with what was previously observed for compound **19** and shows the presence of the anion [Al(pyrrolyl)₄]⁻, unaffected by the

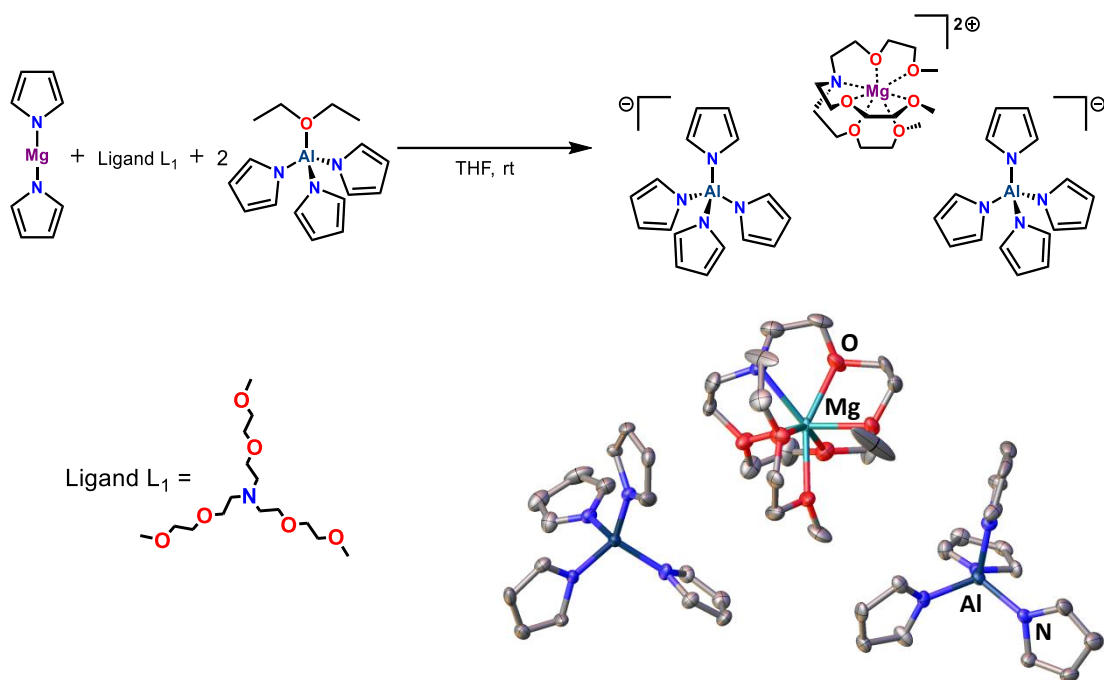


Figure 4.7: Scheme of the preparation (top) and molecular structure (bottom) of **20** $2[\text{Al}(\text{pyrryl})_4]^- [\text{Mg} \cdot \text{L}_1]^{2+}$. Hydrogen atoms are omitted for clarity. Thermal ellipsoids are drawn at the 30 % probability level. Due to complications with the disorder located on the ligand around the Mg atom the bond parameters will not be discussed.

presence of DMSO and on the Mg atom the TMEA ligand is now free and is replaced by DMSO (according to the ^1H NMR spectrum).

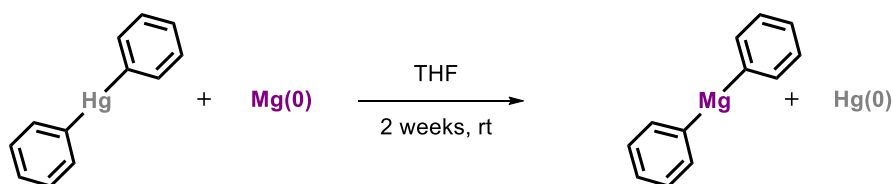
Unfortunately the change of solvation of the magnesium cation from THF to multidentate ligand TMEA did not improve the solubility of the complex. In the search for another reason why $2[\text{Al}(\text{pyrryl})_4]^- [\text{Mg}]^{2+}$ is not soluble, the question on whether the choice of pyrrole might be affecting the solubility was raised. The blame on the pyrrolyl groups was mainly considered because the solubility of $\text{Mg}(\text{pyrryl})_2 \cdot 4\text{THF}$ is itself low as it crystallises at room temperature from a fairly dilute THF solution. The idea was then to find another group to replace pyrrolyl, still small enough for four of them being tolerated around the Al atom. On account of a limited choice for small amines, other organic groups were also considered.

4.2.4. Changing the organic group around the Al anion in $[\text{Mg}]^{2+} 2[\text{AlR}_4]^-$ compounds

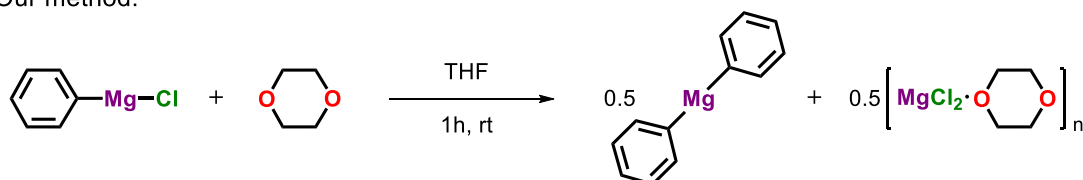
The first chosen alternative group to pyrrolyl was phenyl, a practical option as the $[\text{Al}(\text{Ph})_4]^-$ anion was already characterised structurally by Westerhausen et al. but first and foremost it is present in the widely used benchmark electrolyte $[\text{Al}(\text{Ph})_4]^- [\text{Mg}_2\text{Cl}_3 \cdot 6\text{THF}]^+$ known as the “All-phenyl complex” (APC).^{23,28} The change from an amido group to a phenyl group is not ideal due to the nucleophilic nature of the Al-C bond increasing the chance of side reactions, notably in Mg/S MIB. Yet the making of a chloro-free APC electrolyte is still attractive and would allow a direct comparison between the two electrolytes performances.^{41,42}

The synthesis of $2[\text{Al}(\text{Ph})_4]^- [\text{Mg} \cdot 6\text{THF}]^{2+}$ was made following the same procedure employed for compound **19**. Starting materials AlPh_3 and MgPh_2 are already known in the literature and were both characterised by X-ray. $\text{AlPh}_3 \cdot \text{OEt}_2$ was prepared according to the literature,²⁸ but MgPh_2 was prepared by using the 1,4-dioxane precipitation method to alter the Schlenk equilibrium toward the formation of the homoleptic organomagnesium reagent, over the use of organomercury compounds (Scheme 4.6).⁴³ Reacting MgPh_2 with AlPh_3 by slow diffusion in THF yielded colourless X-ray quality crystals of the desired $2[\text{Al}(\text{Ph})_4]^- [\text{Mg} \cdot 6\text{THF}]^{2+}$, **21**; Yield : 96 % (Figure 4.8).

Previously reported method:



Our method:



Scheme 4.6: Preparation of MgPh_2 by (top) the previous method proposed using HgPh_2 ; (bottom) precipitation of MgCl_2 using dioxane.

Compound **21** adopts the same separated ion pair as compounds **19** and **20**. According to the CCDC the $[\text{Al}(\text{Ph})_4]^-$ anion was only observed four times, and all of them paired with a Group 2 centred metal cation (Mg, Ca or Sr).^{23,28,41,42} Apart for the change from pyrrolyl to phenyl groups, hence giving Al-C bonds longer than the Al-N bonds, the bond angles are virtually identical. The change from pyrrolyl to phenyl was unsuccessful in improving the solubility of the chloro-free magnesium organoaluminates possessing a naked Mg cation. Pyrrolyl and phenyl groups are both aromatic species which are known to interact between each other through their π systems. None of these π interactions are observed in the crystallographic data for both structures, however it might be interesting to synthesise an analogous compound with non-aromatic groups, hence limiting potential π interactions and increasing the agostic interactions instead. Going back to amines, the choice of the ligand balanced toward cyclic amine piperidine ($\text{C}_5\text{H}_{10}\text{NH}$) for its relatively small size, limiting the steric hindrance around the aluminium anion.

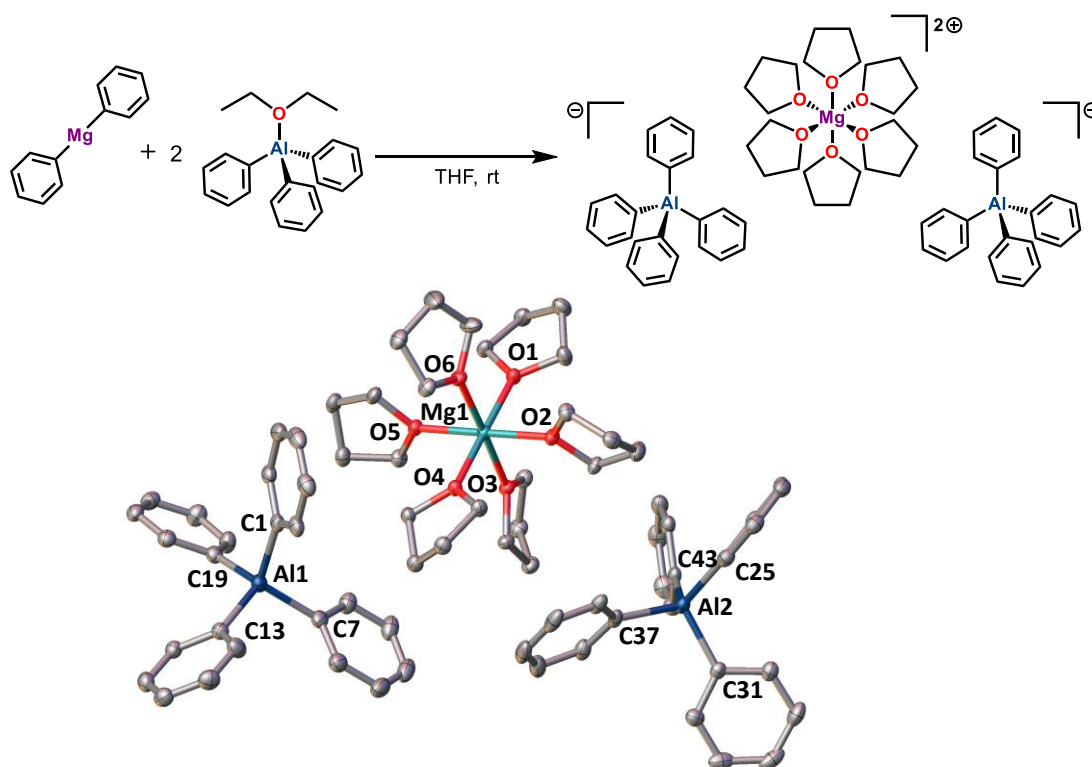


Figure 4.8: Scheme of the preparation (top) and molecular structure (bottom) of **21** $2[\text{Al}(\text{Ph})_4]^- [\text{Mg}\cdot 6\text{THF}]^{2+}$. Hydrogen atoms and disorder present on one of the THF units are omitted for clarity. Thermal ellipsoids are drawn at the 30 % probability level. Selected bond distances (\AA) and angles ($^\circ$): Al-C 2.013; Mg-O 2.0969; C-Al-C 109.44; O-Mg-O_{cis} 90.00; O-Mg-O_{trans} 179.79; C-Al-C 109.44. Atoms which do not carry a numerical label represent average parameter values.

Limited literature was found on either of the necessary starting materials $\text{Al}(\text{C}_5\text{H}_{10}\text{N})_3$ or $\text{Mg}(\text{C}_5\text{H}_{10}\text{N})_2$. The preparation of $\text{Al}(\text{C}_5\text{H}_{10}\text{N})_3$ was attempted by Smith et al. using AlH_3 with three equivalents of $\text{C}_5\text{H}_{10}\text{NH}$ however no crystallographic characterisation was made.⁴⁴ In this work the so far effective metathesis method used to prepare $\text{Al}(\text{pyrrolyl})_3$ and AlPh_3 was adopted instead (Figure 4.9). $\text{Mg}(\text{C}_5\text{H}_{10}\text{N})_2$ was prepared by adding two equivalents of $\text{C}_5\text{H}_{10}\text{NH}$ to a solution of ${}^n\text{Bu}_2\text{Mg}$ in THF and heating under reflux for 3h.⁴⁵ All were prepared in-situ then the two solutions in THF were slowly diffused into each other, after a weekend some small X-ray quality crystals were formed. Unfortunately, the desired compound $2[\text{Al}(\text{C}_5\text{H}_{10}\text{N})_4]^- [\text{Mg}\cdot 6\text{THF}]^{2+}$ was not formed, but only the starting material $\text{Al}(\text{C}_5\text{H}_{10}\text{N})_3$, **22** crystallised (Figure 4.9).

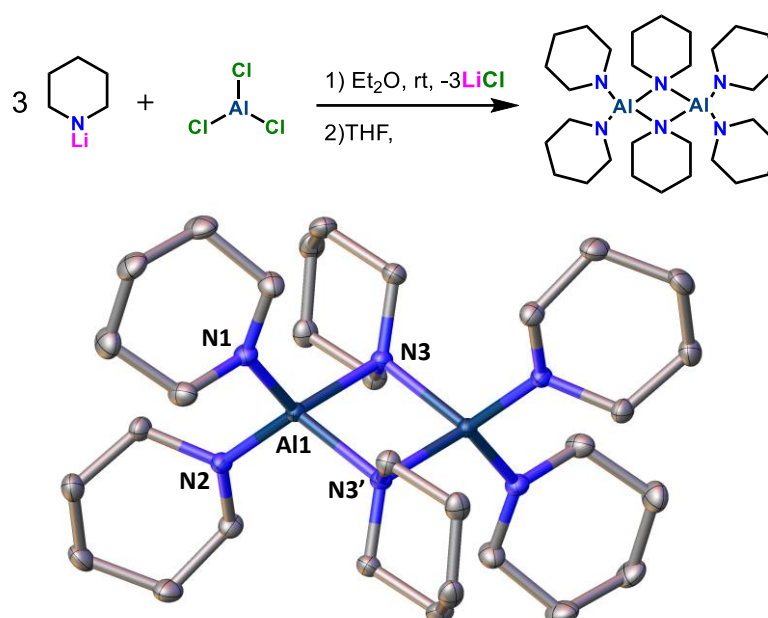


Figure 4.9: Scheme of the preparation of (top) and molecular structure (bottom) **22** $\text{Al}(\text{C}_5\text{H}_{10}\text{N})_3$. Hydrogen atoms are omitted for clarity. Thermal ellipsoids are drawn at the 50 % probability level. Selected bond distances (Å) and angles (°): Al1-N1 1.8108(12); Al1-N2 1.8117(12); Al1-N3 1.9674(13); Al1-N3' 1.9846(12); N1-Al1-N2 110.60(6); N1-Al1-N3 114.28(6); N1-Al1-N3' 114.36(6); N2-Al1-N3 116.84(6); N2-Al1-N3' 111.18(6).

Compound **22** possesses a dimeric structure with the typical 3-centre 2-electron bonds of electron deficient bridging Al-N-Al bonds. The Al_2N_2 4-membered ring is planar with cyclic Al-N bond lengths longer than for the Al-N bond length of the terminal amido groups (1.976 Å and 1.811 Å respectively), and all piperidine rings are in the chair configuration. In general this structure is very similar to the characterised dimeric

structure of the pyrrolidine equivalent. The reason why $\text{Al}(\text{C}_5\text{H}_{10}\text{N})_3$ dimerises instead of coordinating with a donor molecule to form a monomer is ambiguous. The dative bond with the nitrogen seems preferred in this case, in contrast to compound **17** where the Al atom coordinates to an Et_2O molecule instead of another pyrrolyl unit. Could this aggregation be a reason why the transmetallation from Mg to Al is not occurring, as breaking the dimer needs more energy?

This section shows that changing the ligands around the Al atom for different small groups was not successful to increase the solubility of the targeted chloro-free magnesium aluminate compounds. After doing some enquiries in text books and other academic support, the insolubility of these types of ionic compounds manifestly emanates from the high attraction forces of the negative anions towards positively charged cations. The stronger the attractive force between the opposite charged ions, the more tightly the ions are held together and the more the ions are kept in the solid state as no dissociation is likely to occur. The strength of this attraction is greatly influenced by the charges the ions hold. Basically compounds with small charges such as a singularly charged anion paired with a singularly charged cation will have a better solubility than compounds with larger charges involved which is the case in this work with a doubly charged cation balanced by two singularly charged anions (Figure 4.10).

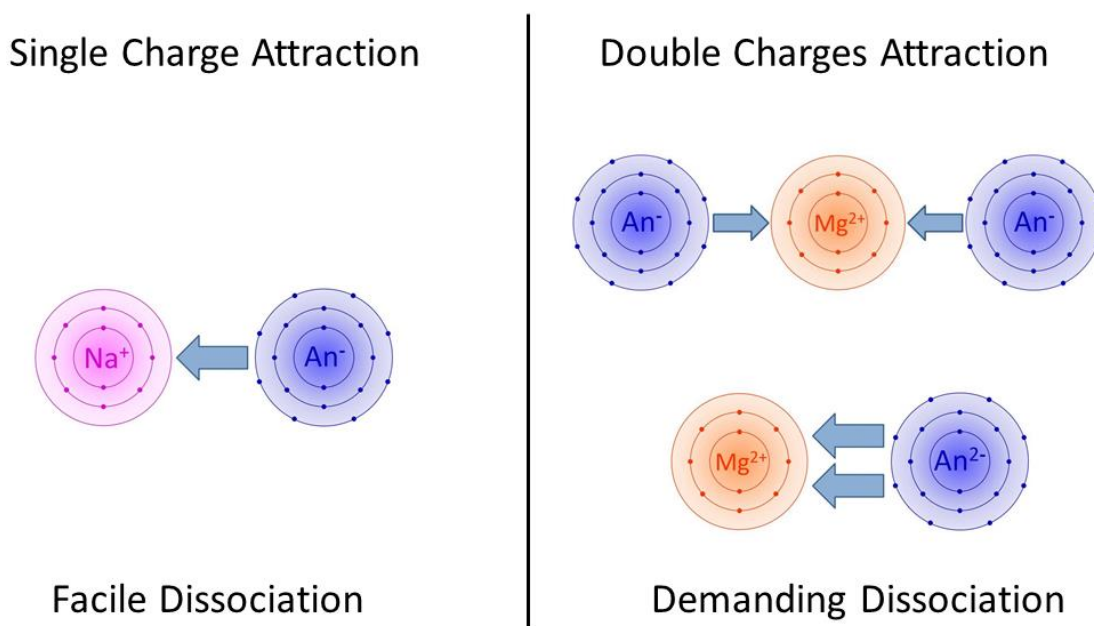


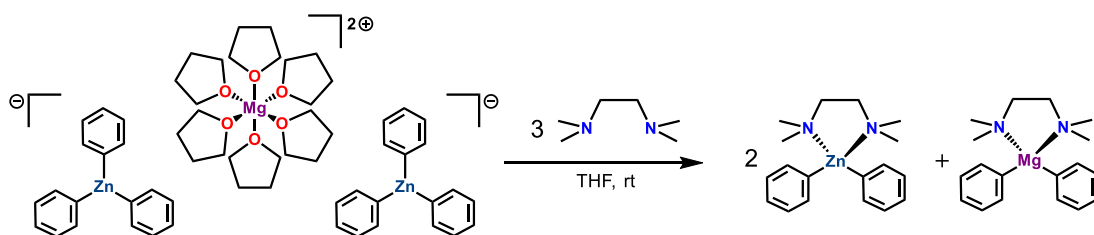
Figure 4.10: Relationship between ionic charge attraction and dissociation in ionic complexes.

Aiming to reduce the forces involved between these charges, two options were considered. Firstly changing the metal of choice of the counter anion to alter the electronegativity and the size of the species, hence possibly affecting the forces of these attractions. Secondly, finding a way to prepare a 1+/1- chloro-free ion pair.

4.2.5. Changing the metal of the anionic group

When looking for a new element to replace Al in the counter anion, a cheap, abundant and environmentally benign replacement was sought in order to keep as many attractive features displayed by magnesium aluminate electrolytes. First zinc was considered a good match as previous characterisation of magnesium zincates $2[\text{Zn}(\text{benzyl})_3]^- [\text{Mg}\cdot 6\text{THF}]^{2+}$ and $2[\text{Zn}(\text{o-C}_6\text{H}_4\text{OMe})_3]^- [\text{Mg}\cdot 6\text{THF}]^{2+}$ was achieved.^{20,46} The presence of only three groups around the Zn metal centre allows a more flexible choice of ligands with different sizes.

In this work ZnPh_2 was used and mixed with 0.5 equivalents of a MgPh_2 solution in THF, after stirring the solution for 5 minutes a precipitate is formed. The precipitate dissolves when gently heating the mixture to yield a crystalline solid upon cooling. Unfortunately no matter how slow the crystallisation process is, the crystals formed are too small to be characterised by X-ray. ^1H NMR spectroscopy did not give enough information to determine the compound constitution apart from the presence of Ph groups and free THF molecules. Trying to change the way the compound packs in the crystal structure, two equivalents of TMEDA (according to Mg) was added to the reaction mixture to form a clear solution. By means of ^1H NMR spectroscopy, the spectrum showed that the products of the reaction were identified as a 1:2 mixture of $\text{MgPh}_2\cdot\text{TMEDA}$ and $\text{ZnPh}_2\cdot\text{TMEDA}$, where the resonances corresponding to $\text{MgPh}_2\cdot\text{TMEDA}$ (7.64 and 6.94 ppm) were observed as well as the resonances corresponding to $\text{ZnPh}_2\cdot\text{TMEDA}$ (7.85 and 7.35 ppm). The addition of TMEDA induced disproportionation into more stable homometallic compounds $\text{ZnPh}_2\cdot\text{TMEDA}$ and $\text{MgPh}_2\cdot\text{TMEDA}$ as previously observed in the literature (Scheme 4.7).²⁰



Scheme 4.7: Disproportionation reaction of magnesium zincate reagents to more stable homoleptic monometallic reagents influenced by the addition of TMEDA in ideal stoichiometric conditions.

A similar reaction was repeated with iron, and more particularly using $\text{Fe}(\text{HMDS})_2$ which is known to form a sodium ferrate with anionic $[\text{Fe}(\text{HMDS})_3]^-$ species.⁴⁷ Addition of 2 equivalents of $\text{Fe}(\text{HMDS})_2$ to 1 equivalent of $\text{Mg}(\text{HMDS})_2$ in THF formed a dark orange solution, either removing all the solvent or trying to crystallise anything from hexane gave a sticky oily compound which could not be characterised.

The last element attempted was the heavier group 13 element gallium which behaves very similarly to Al but whose size is different. Gallium (Ga^{3+}) has a smaller atomic radius (122.1 vs. 142.2 pm) yet a larger ionic radius (47 – 62 vs. 39 – 54 pm; first number for a 4 coordinated species, second number for a 6 coordinated species), and different electronic properties (electronegativity: 1.8 vs. 1.5). The low cost and abundance making Zn or Fe attractive compounds to study is lost with gallium, being only the 35th most abundant element in the earth's crust just below lithium and niobium. It is however more abundant than the already widely used element boron, whose abundance in the earth's crust lies down in 41st place.

In the attempt to make $2[\text{Ga}(\text{Ph})_4]^- [\text{Mg}\cdot 6\text{THF}]^{2+}$, the starting material GaPh_3 was synthesised by the same synthetic method used to prepare AlPh_3 , a different procedure than what is proposed in the literature.⁴⁸ The presence of donor ligand Et_2O gave the new solvated crystal structure $\text{GaPh}_3\cdot\text{OEt}_2$, **23**, characterised by X-ray crystallography; Yield : 71 % (Figure 4.11).

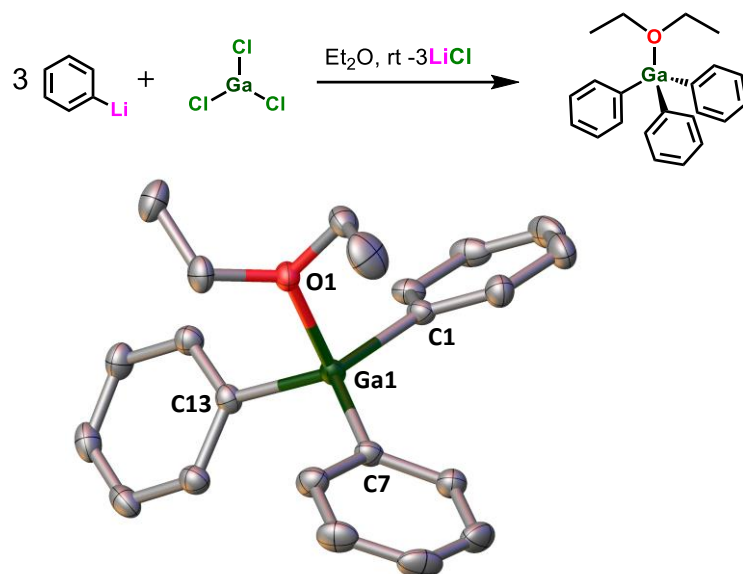


Figure 4.11: Scheme of the preparation (top) and molecular structure (bottom) of **23** GaPh₃·OEt₂. Hydrogen atoms are omitted for clarity. Thermal ellipsoids are drawn at the 50 % probability level. Selected bond distances (Å) and angles (°): Ga1-O1 2.0918(11); Ga-C 1.9765; C-Ga-C 116.86; O-Ga-C 100.32. Atoms which do not carry a numerical label represent average parameter values.

Compound **23** is a 4 coordinated mononuclear species which possesses the same tetrahedral geometry as AlPh₃·OEt₂; where Ga-C distances are almost identical to Al-C distances and the O-Ga bond length is only slightly longer than O-Al (2.0918(11) and 1.922 Å respectively). O-Ga-C angles are smaller (100.32 vs. 103.61 ° for O-Al-C) and C-Ga-C larger (116.85 vs. 114.64° for C-Al-C) which put GaPh₃·OEt₂ in a slightly more distorted tetrahedral geometry than AlPh₃·OEt₂. ($\tau_4 = 0.889$ and 0.919 respectively).

Adding a solution of 2 equivalents of GaPh₃·OEt₂ in THF to a solution of MgPh₂·4THF by slow diffusion reaction yielded X-ray quality crystals of chloro-free magnesium gallate 2[Ga(Ph)₄]⁻ [Mg·6THF]²⁺, **24** in a 84 % yield (Figure 4.12). The structure represents a separated ion pair identical to 2[Al(Ph)₄]⁻ [Mg·6THF]²⁺ with only small variation in bond length between Ga-C and Al-C (average of 2.012 and 2.023 Å respectively). Unfortunately changing from Al to Ga did not improve the solubility of the compound.

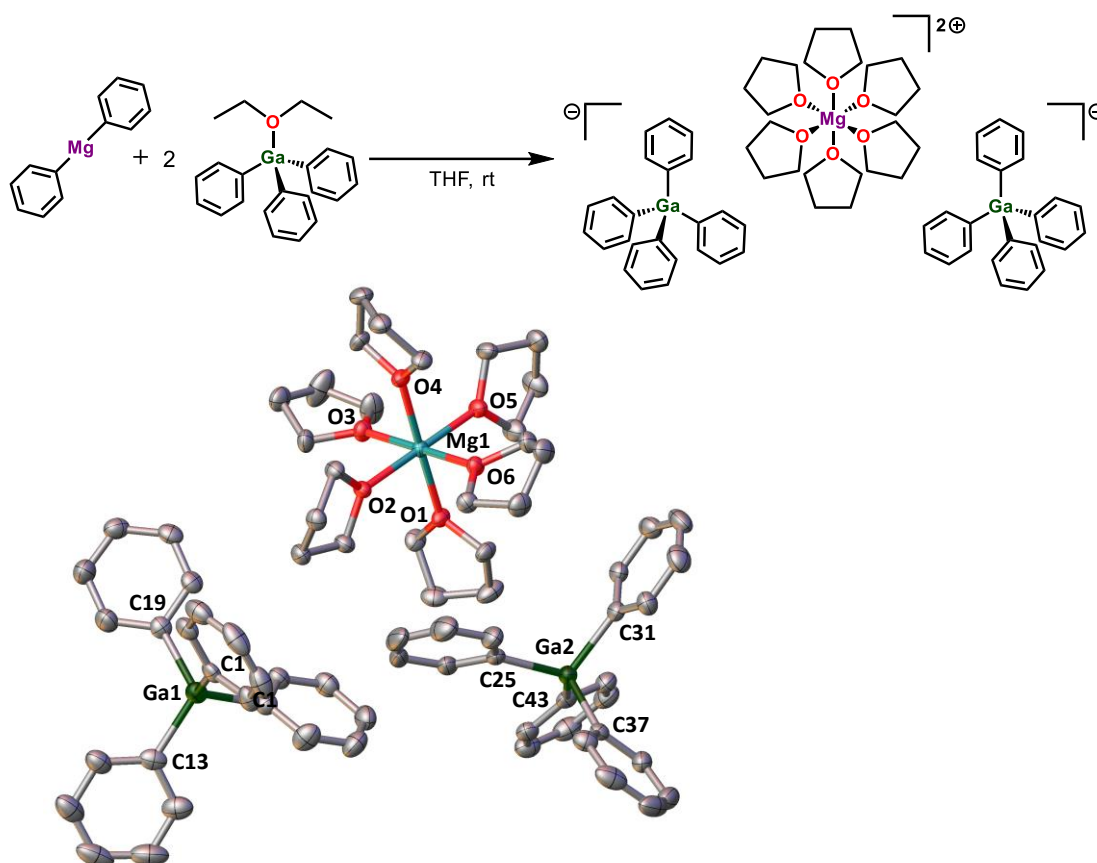


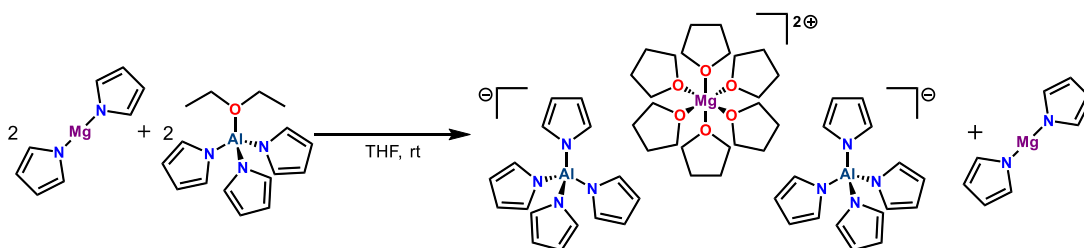
Figure 4.12: Scheme of the preparation (top) and molecular structure (bottom) of **24** $2[\text{Ga}(\text{Ph})_4]^- [\text{Mg} \cdot 6\text{THF}]^{2+}$. Hydrogen atoms and disorder present on one of the THF units are omitted for clarity. Thermal ellipsoids are drawn at the 50 % probability level. Selected bond distances (Å) and angles (°): Ga-C 2.023; Mg-O 2.1011; C-Ga-C 109.43; O-Mg-O_{cis} 90.00; O-Mg-O_{trans} 178.79. Atoms which do not carry a numerical label represent average parameter values.

To summarize this section, changing the aluminium anion for a zinc anion gave the formation of a solid which can be dissolved upon heating in THF but no characterisation of this solid was achieved. Changing the metal of the anion from Al to Ga did not improve the solubility and according to the crystal structure of these compounds their bond distances and angles are almost identical, giving them similar physical properties. The change to a metal also belonging to group 13 was maybe too subtle.

4.2.6. Synthesis of 1+:1- separated ion pair chloro-free magnesium aluminates

The second idea to improve the solubility of chloro-free magnesium aluminate compounds was to reduce the cationic moiety charge from 2+ to 1+ as already observed in the soluble chloromagnesium aluminate compounds previously studied, such as $[\text{AlCl}_{4-n}\text{Et}_n]^- [\text{Mg}_2\text{Cl}_3 \cdot 6\text{THF}]^+$.

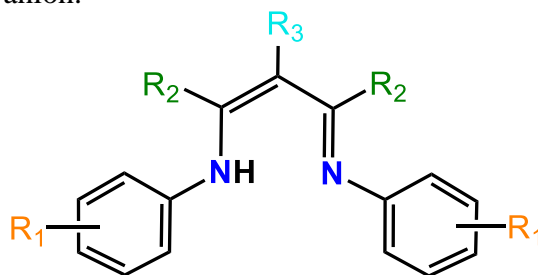
The first evident reaction was to react $\text{Mg}(\text{pyrrolyl})_2$ and $\text{Al}(\text{pyrrolyl})_3$ in a 1:1 ratio to ideally generate $[\text{Al}(\text{pyrrolyl})_4]^- [\text{Mg}(\text{pyrrolyl}) \cdot n\text{THF}]^+$. The result of this reaction was a redistribution to form compound **19** ($2[\text{Al}(\text{pyrrolyl})_4]^- [\text{Mg} \cdot 6\text{THF}]^{2+}$) instead. It seems that the pyrrolyl group remaining on the Mg cation is too labile or destabilises the cation, favouring the formation of the naked magnesium dication instead (Scheme 4.8).



Scheme 4.8: 1:1 reaction between $\text{Mg}(\text{pyrrolyl})_2$ and $\text{Al}(\text{pyrrolyl})_3$.

To prevent a redistribution occurring, we thought of making a heteroleptic magnesium compound $\text{MgR}(\text{pyrrolyl})$, where R is a group which prefers to stay on the Mg atom instead of being transmetallated to the Al atom in the presence of $\text{Al}(\text{pyrrolyl})_3$. Such a desired feature was thought to be accessible by using β -diketimine ligands such as DippNacnacH ($\text{DippNacnac} = \text{Ar}^*\text{NC}(\text{Me})\text{CHC}(\text{Me})\text{NAr}^*$; $\text{Ar}^* = 2,6\text{-}i\text{Pr}_2\text{-C}_6\text{H}_3$). With presence of a secondary amine site combined with an N donor atom, the ligand can clamp to the Mg atom as a bidentate ligand, avoiding redistribution through Schlenk type equilibrium (Scheme 4.9). This coupled with its tuneable bulk at the R_1 position would prevent the transmetallation onto the Al metal centre. β -diketimine ligands can also be tuned using different substituents at the R_2 and R_3 positions, offering different electronic properties.^{49–52} Moreover, Al has only one “vacant coordination site” which

is a key point for choosing a bidentate ligand since it shouldn't form any interaction with the aluminium anion.



Scheme 4.9: Generic β -diketimine molecule and its tuneable sites.

The starting material $[\text{DippNacnac}]\text{Mg}(\text{pyrrolyl})$ was synthesised by first preparing $[\text{DippNacnac}]\text{Mg}(\text{Bu})$ according to the literature method, then adding 1 equivalent of pyrrole.⁴⁵ X-ray quality crystals corresponding to $[\text{DippNacnac}]\text{Mg}(\text{pyrrolyl})\cdot\text{THF}$, **25** were obtained from a concentrated solution in THF; Yield : 80 % (Figure 4.13).

The structure of **25** displays a monomeric arrangement with a four coordinated Mg bisamide complex in a distorted tetrahedral geometry ($\tau_4 = 0.806$). ^1H and ^{13}C NMR spectroscopy in d_8 -THF shows that the two signals of the pyrrolyl are close to each other (5.73 and 5.91 ppm) but also largely shifted upfield compared to $\text{Mg}(\text{pyrrolyl})_2\cdot 4\text{THF}$ (5.99 and 6.68 ppm).

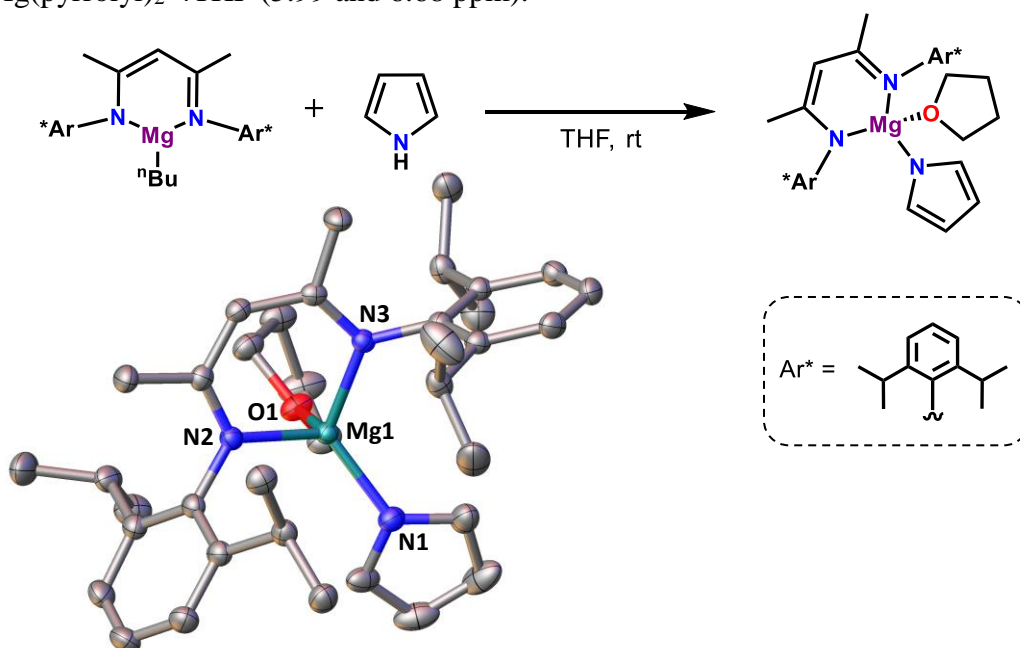


Figure 4.13: Scheme of the preparation (top) and molecular structure (bottom) of **25** $[\text{DippNacnac}]\text{Mg}(\text{pyrrolyl})\cdot\text{THF}$. Hydrogen atoms are omitted for clarity. Thermal ellipsoids are drawn at the 50 % probability level. Selected bond distances (\AA) and angles ($^\circ$): Mg1-N1 2.0039(11); Mg1-N2 2.0355(10); Mg1-N3 2.0286(10); Mg1-O1 2.0226(9); O1-Mg1-N1 100.95(4); N1-Mg1-N2 123.08(4); N1-Mg1-N3 123.24(4); O1-Mg1-N2 105.55(4); O1-Mg1-N3 107.54(4); N2-Mg1-N3 95.01(4).

Adding a solution of $\text{Al}(\text{pyrrolyl})_3\cdot\text{OEt}_2$ to a solution of **25** in THF in a 1:1 ratio gave a clear solution, the solvent system was changed to THF:hexane to obtain a slightly cloudy mixture. After filtration and a few days at $-20\text{ }^\circ\text{C}$ X-ray quality crystals were formed in a 50 % yield, characterised as $[\text{Al}(\text{pyrrolyl})_4]^- [[^{\text{Dipp}}\text{Nacnac}]\text{Mg}\cdot 2\text{THF}]^+$, **26** (Figure 4.14).

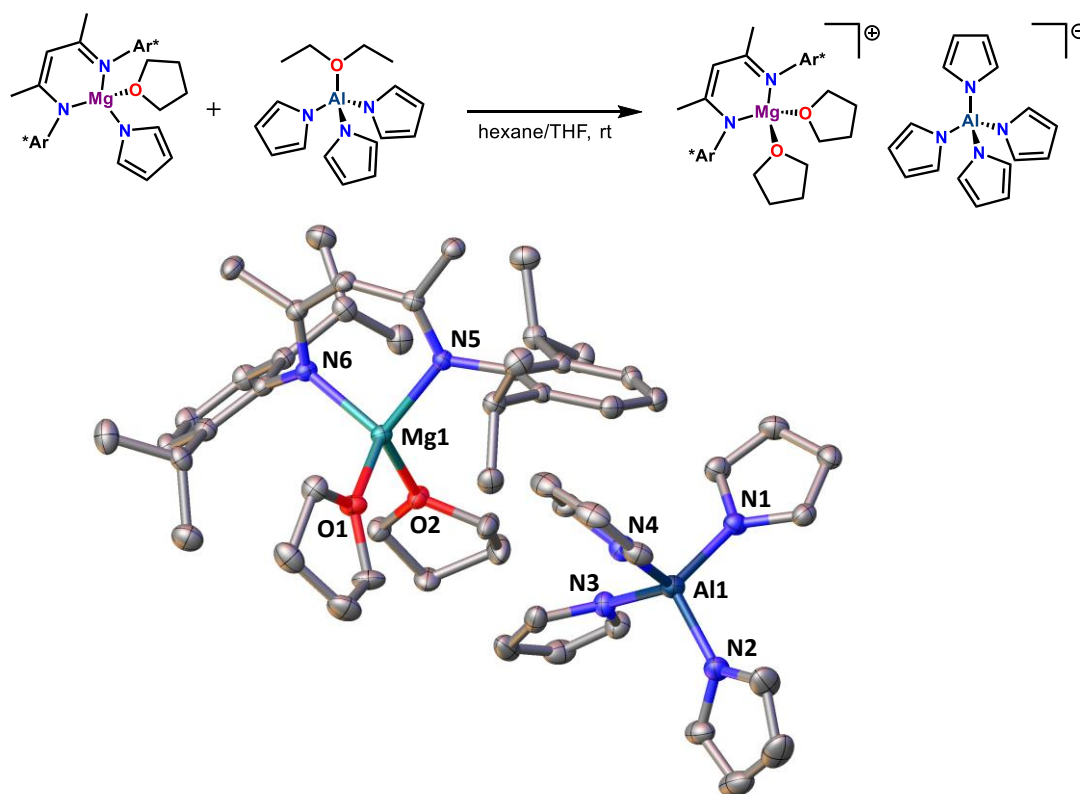


Figure 4.14: Scheme of the preparation (top) and molecular structure (bottom) of **26** $[\text{Al}(\text{pyrrolyl})_4]^- [[^{\text{Dipp}}\text{Nacnac}]\text{Mg}\cdot 2\text{THF}]^+$. Hydrogen atoms and disorder on both THF units and one pyrrole group are omitted for clarity. Thermal ellipsoids are drawn at the 30 % probability level. Selected bond distances (Å) and angles ($^\circ$): Al-N 1.851; Mg-O 1.9875; Mg-N 2.0147; N-Al-N 109.42; O1-Mg1-O2 99.37(7); O-Mg-N 115.55; N5-Mg1-N6 96.41(7). Atoms which do not carry a numerical label represent average parameter values.

Compound **26** is a chloro-free magnesium aluminate and the first example of an Mg cation with the $^{\text{Dipp}}\text{Nacnac}$ ligand clamping the Mg atom and two THF molecules filling the empty coordination sites, the Mg atom adopts a reduced distorted tetrahedral geometry ($\tau_4 = 0.879$) compared to **25**. ^1H , ^{13}C and ^{27}Al NMR spectroscopy in C_6D_6 shows the presence of the $[\text{Al}(\text{pyrrolyl})_4]^-$ anion with resonances for the pyrrolyl groups matching with the ^1H NMR spectrum of **16** ($[\text{Al}(\text{pyrrolyl})_4]^- [\text{Li}\cdot 4\text{THF}]^+$). ^{27}Al

NMR spectrum confirms presence of highly symmetric $[\text{Al}(\text{pyrrolyl})_4]^-$ by displaying a well-defined peak at 98.15 ppm.

The most exciting feature of compound **26** is its high solubility, not only in THF but also in less polar solvents such as toluene and benzene. At last a pursued compound of our own design shows suitable solubility and can be taken to the next step to study the viability of such a compound as an electrolyte in a MIB. The reduction of the cation moiety charge from 2+ to 1+ seems to have successfully improved the solubility of the magnesium aluminate. One can argue that the DippNacnac ligand is a large organic moiety and groups such as the Dipp fragments could influence the solubility properties as well. Yet as the fairly large ethereal TMEA ligand didn't seem to have any impact on the solubility, the implication of the DippNacnac on the solubility is uncertain. To dwell on this argument the use of analogous ligands without the large Dipp units, such as tBuNacnac or even *N,N,N'*-Trimethylethylenediamine, could also be studied.

To extend this work and continue the series started with the comparison between pyrrolyl and phenyl groups, the attempt to make the phenyl version of **26** was also undertaken. $[\text{DippNacnac}]\text{Mg}(\text{Ph})\cdot\text{THF}$, **27**, was easily synthesised and characterised by X-ray crystallography by reacting MgPh_2 and DippNacnacH in a 1:1 ratio to form a solution in THF in a 76 % yield (Figure 4.15). After 1h reflux and concentration of the solution a crop of colourless crystals resulted. Addition of AlPh_3 to a solution of **27** in THF gave no crystalline material. By analysing the reaction mixture via ^1H NMR analysis it was not clear if the transmetallation of the phenyl group from **27** to the aluminium reagent occurs as the resonances of the phenyl group attached to the Mg atom overlaps with the Dipp signals. The ^{27}Al NMR spectrum is more indicative and displays a sharp signal at 132.97 ppm corresponding to the $[\text{Al}(\text{Ph})_4]^-$ anion according to the literature.²⁸ Crystalline side-product $[[\text{DippNacnac}]\text{Mg}(\text{OH})\cdot\text{THF}]_2$ formed by hydrolysis of **27** was obtained following a few attempts. Hydrolysis reaction is common for analogous alkyl compounds, but it was not observed with compound **25** most likely due to the presence of a stronger Mg-N compared to an Mg-C bond.

Having proposed an easy synthetic route to access the targeted chloro-free magnesium aluminate compound **25**, the next following step is to find out if it is electrochemically active. The addition of a β -diketiminato ligand to a rechargeable battery electrolyte is

still unstudied and the effects it might have on the reversible deposition of Mg unpredictable.

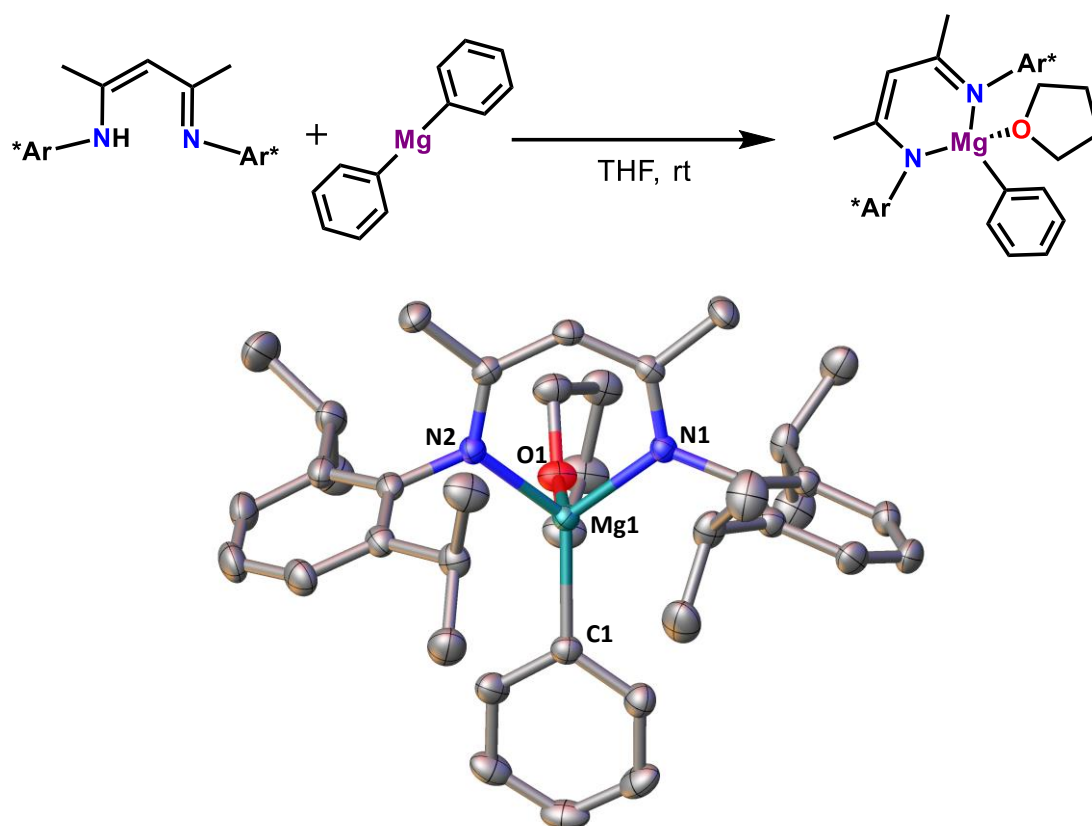


Figure 4.15: Scheme of the preparation (top) and molecular structure (bottom) of **27** [$^{Dipp}Nacnac$]Mg(Ph)·THF. Hydrogen atoms are omitted for clarity. Thermal ellipsoids are drawn at the 50 % probability level. Selected bond distances (Å) and angles (°): Mg1-C1 2.1201(13); Mg1-N 2.0480(10); Mg1-O1 2.0603(9); C1-Mg1-O1 99.40(4); C-Mg-N 125.99; O-Mg-N 104.11(4); N1-Mg1-N2 94.15(4). Atoms which do not carry a numerical label represent average parameter values.

4.3. Electrochemistry of chloro-free magnesium aluminates

This section presents the experimental results of a rechargeable magnesium battery using the newly synthesised and characterised chloro-free magnesium aluminate compounds as electrolytes. The battery system used is almost identical to the system used in Chapter 3, where a polished magnesium sheet is used as the anode and the Chevrel phase (Mo_6S_8) as the cathode. The solvent of choice is THF when the magnesium aluminate's solubility allows it, DMSO is used otherwise. The work has also been extended with mixtures of ionic liquid/THF which displays compelling

dissolution properties for compounds such as **19** and **21** ($2[\text{Al}(\text{pyrrolyl})_4]^- [\text{Mg}\cdot 6\text{THF}]^{2+}$ and $2[\text{Al}(\text{Ph})_4]^- [\text{Mg}\cdot 6\text{THF}]^{2+}$). So far, most of the few chloride free electrolytes show high overpotential, very sluggish intercalation kinetics and capacity loss when a Mg^{2+} naked cation such as $[\text{Mg}\cdot 6\text{THF}]^{2+}$ is involved. For the magnesocene based electrolyte (MgCp_2), the low ionic conductivity of this compound makes it a weak electrolyte and its small electrochemical window (oxidative stability of 1.8 V) limits its application with current higher voltage cathodes. Finally, the magnesium borohydride based electrolytes suffer high overpotentials, low current density and low coulombic efficiency.

4.3.1. Battery behaviour using “naked magnesium” aluminate compounds in DMSO as electrolyte

To date no MIB was attempted with an electrolytic solution in DMSO. The nearest study was carried out by Hong and Lee with the use of dialkyl sulfones as the solvent of choice for the simple electrolyte MgCl_2 .⁵³ The high melting point of these sulfones, the lowest is 29-33°C for dipropylsulfone (DPS), requires the addition of THF as a co-solvent in order to be lowered. The active species were isolated and characterised by X-ray in both DPS exclusively and DPS:THF (1:1) mixture. In bulk DPS the MgCl_2 forms the magnesium magnesiate contacted ion pair $\text{Mg}_2\text{Cl}_4\cdot 4\text{DPS}$ with one Mg atom solvated by four DPSO molecules and joined to an MgCl_2 molecule by two bridging chlorides atoms (Figure **4.16 a**). In a DPS:THF mixture the active species was identified as a magnesium magnesiate separated ion pair with a “naked magnesium” dication solvated by six DPS $[\text{Mg}\cdot 6\text{DPS}]^{2+}$ and two $[\text{MgCl}_3\cdot \text{THF}]^-$ counter anions (Figure **4.16 b**).

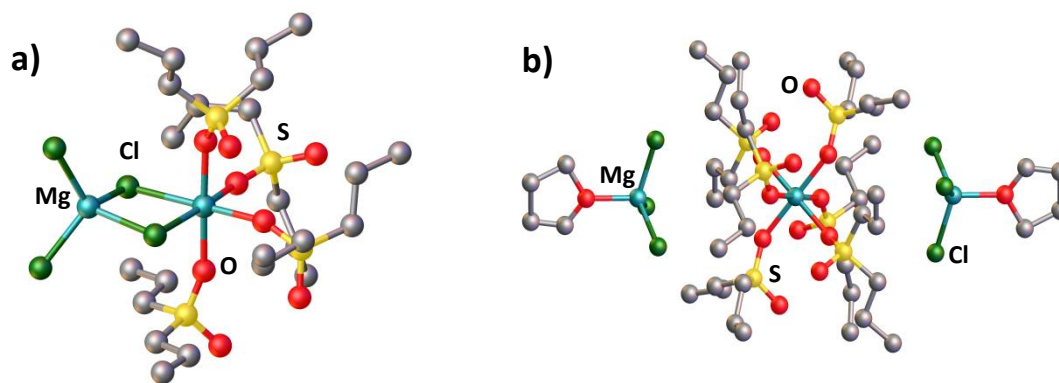
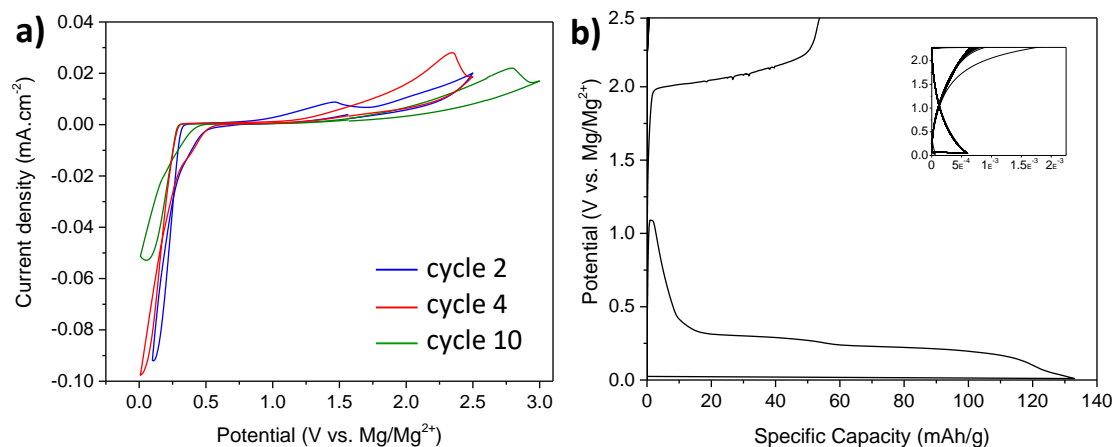


Figure 4.16: Molecular structure of **a)** Mg₂Cl₄·4DPS and **b)** 2[MgCl₃·THF]⁻ [Mg·6DPS]²⁺.

Only the battery performance using MgCl₂ in the DPS:THF mixture was studied due to the higher conductivity emanating from the separated ionic pair structure. In their system the battery displays good reversible Mg deposition and oxidative stability. Even though the ¹H and ²⁷Al NMR spectrum of **19** and **21** support a separated ion pair, attempts to crystallise either compounds in a mixture of DMSO/THF was not successful and only formed insoluble suspensions. Cyclic voltammetry of a saturated solution of **19** in THF did not show any redox activity, suggesting that an undetectable amount of **19** went into solution (Chapter 6, Section 6.2.7, Graph 6.6).



Graph 4.1: **a)** CV cycles, 0.1 mV/s, and **b)** typical charge/discharge profiles for a rechargeable battery with 0.35 M solution of **19** in DMSO, a Mg anode and an Mo₆S₈ cathode. Inset shows subsequent charge/discharge profiles at very low specific capacity.

Graph **4.1a** shows the cyclic voltamogram of a $\text{Mg}^0/\text{Mo}_6\text{S}_8$ battery cell using a 0.35 M solution of **19** in DMSO over 10 cycles. A noticeable reduction peak can be observed near 0 V, however only a small bump appears during the oxidation phase which is not proportional to the reduction peak. The oxidation peak observed at 1.46 V in cycle 2 shifts to higher voltages during the following cycles before “disappearing” beyond the 2.5 V maximum applied voltage. A new oxidation peak can be eventually obtained when the running voltage is increased to 3.0 V before it disappears over time. This behaviour could be seen as a possible passivation of the Mg electrode through a reaction involving the electrolyte occurring during the battery cycling. Graph **4.1 b**) displays the result of the galvanostatic experiment of the same battery system. It agrees with the CV, where the reduction peak is represented by the intercalation of Mg^{2+} ions in the Chevrel phase reaching its maximum theoretical specific capacity (128 mA.h/g). The observed overpotential displayed by the battery is however very large, over 2 V, and the unusual presence of a drop in potential before intercalating normally has no explanation. The battery recharges to less than half its specific capacity (50 mA.h/g) but no reintercalation occurs after the charge (Graph **4.1b** inset 2). It is not clear if the shutdown of the battery performance is induced by the structure of **19** not being compatible with the redox reactions in the battery mechanism or by the DMSO as the solvent of choice which has a high polarity which is sometimes linked to formation of passivating insoluble material onto the electrodes.

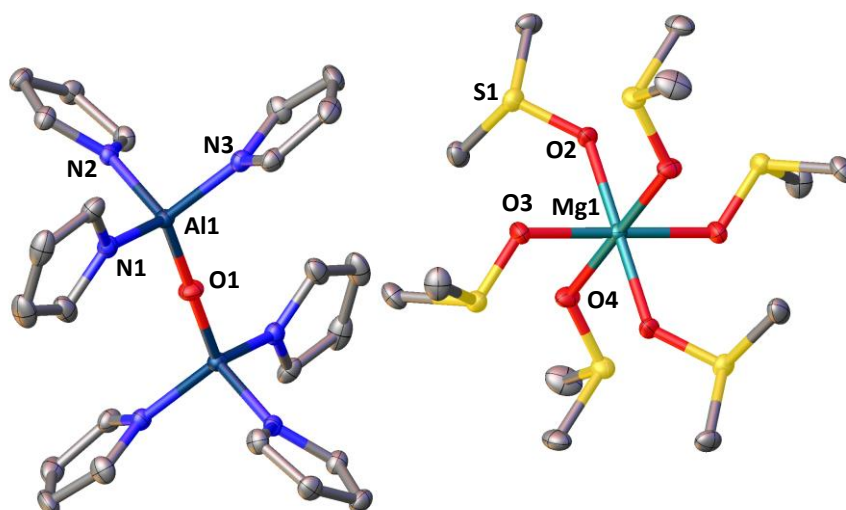
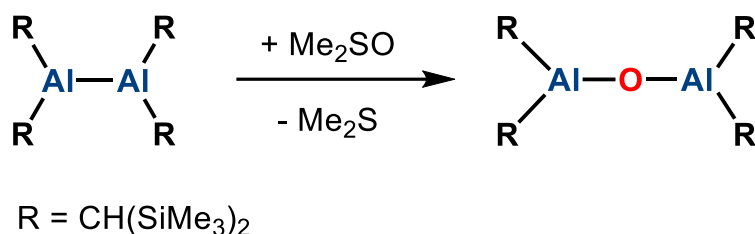


Figure 4.17: Molecular structure of $[(\text{Al}(\text{pyrrolyl})_3)_2\text{O}]^{2-} [\text{Mg}\cdot 6\text{DMSO}]^{2+}$, **28**. Thermal ellipsoids are drawn at the 50 % probability level. Selected bond distances (Å) and angles ($^\circ$): Al1-O1 1.6853; Al-N 1.873; Mg-O 2.071; Al-O-Al 180.00; O-Al-N 112.35; N-Al-N 106.43; O-Mg-O_{cis} 89.76; O-Mg-O_{trans} 180.00. Atoms which do not carry a numerical label represent average parameter values.

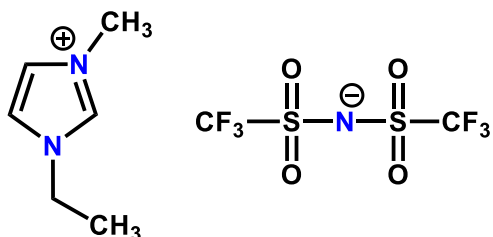
After a few weeks a few crystals formed from the solution of **19** in DMSO in the glove box, by mean of X-ray crystallographic the molecular structure was characterised as $[(\text{Al}(\text{pyrrolyl})_3)_2\text{O}]^{2-} [\text{Mg}\cdot 6\text{DMSO}]^{2+}$, **28**. Compound **28** is a separated ion pair composed of the naked dication $[\text{Mg}\cdot 6\text{DMSO}]^{2+}$ and the dianion $[(\text{Al}(\text{pyrrolyl})_3)_2\text{O}]^{2-}$ (Figure 4.17). The hexasolvated cation $[\text{Mg}\cdot 6\text{DMSO}]^{2+}$ was previously observed in the literature (4 entries in the CCDC) and adopts an octahedral geometry. Compared to $[\text{Mg}\cdot 6\text{THF}]^{2+}$ the Mg-O bonds are slightly shorter (2.071 and 2.1035 Å respectively) which is not totally unexpected as DMSO has stronger coordination properties than THF.⁵⁴ The dianion $[(\text{Al}(\text{pyrrolyl})_3)_2\text{O}]^{2-}$ possesses two $\text{Al}(\text{pyrrolyl})_3$ moieties bridged by an oxygen. Compound **28** crystallises as a monomer where the oxygen atom lies on a crystallographic inversion centre leading to a linear Al-O-Al bond angle. The Al-O bonds are very short (1.6853 Å), according to literature, it is a consequence of the participation of π interactions ($\rho_{\pi-p\pi}$, or $n-\sigma^*$). This type of compound was previously observed in the literature, with the example of the work done by Heckel et al. and the synthesis of tetraalkyldialuminumoxane $\text{R}_2\text{Al}-\text{O}-\text{AlR}_2$ ($\text{R} = \text{CH}(\text{SiMe}_3)_2$) by reacting a dialuminium compound with DMSO, inducing cleavage of the S=O bond (Scheme 4.10).⁵⁵



Scheme 4.10: Synthesis of $\text{R}_2\text{Al}-\text{O}-\text{AlR}_2$.

If in our situation the O insertion occurred through a similar pathway, it would mean that compound **19** is a reducing reagent of similar reactivity to the dialuminum reagent. However the presence of the Al-Al bond in the compounds used by Heckel et al. is suspected to proffer a much stronger reducing nature than **19**, challenging the likelihood of this pathway. The other plausible explanation could be double deprotonation of water molecules remaining in DMSO, as it known to be highly hygroscopic. Although it is possible, the double deprotonation of water is a challenging reaction hence the ability of compound **19** to exhibit such a reactivity is unlikely.

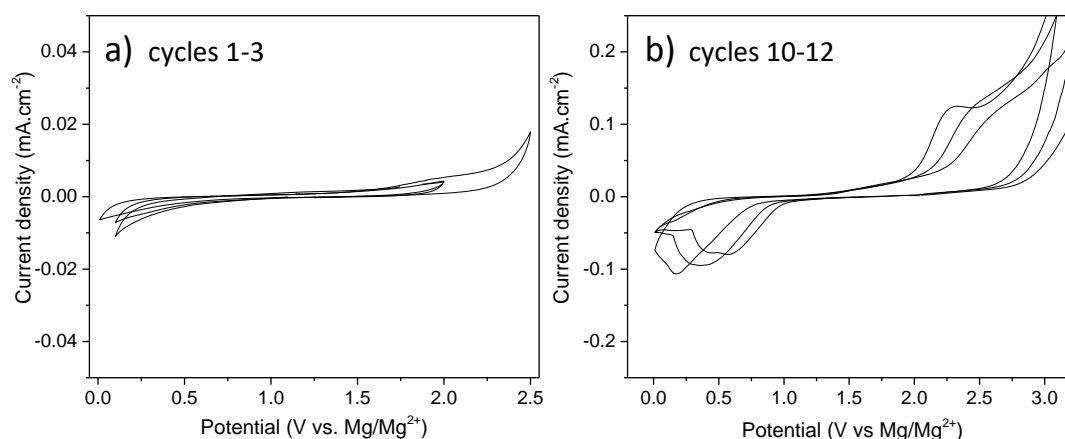
Zhang et al. used an ionic liquid : THF (IL:THF) mixture as their electrolytic solvent system with their “naked magnesium” but still chloro-containing electrolyte $2[\text{AlCl}_4]^- [\text{Mg}\cdot 6\text{THF}]^{2+}$. Similar work was attempted with compound **19** and a very similar ionic liquid (1-Butyl-1-methylpyrrolidinium bis(trifluoromethanesulfonyl)imide) to the one used in this thesis, 1-Ethyl-3-methylimidazolium bis(trifluoromethylsulfonyl)imide (EMIM-TFSI, Scheme 4.11).⁴⁰



Scheme 4.11: Molecule of EMIM TFSI..

4.3.2. Battery behaviour of “naked magnesium” aluminate compounds in IL : THF

Compound **19** dissolves well in a 1:1 mixture of EMIM-TFSI : THF providing a 0.35 M solution. The electrolytic performance of this solution was not improved by the change of solvent system where the first few cycles of the CV between 0 – 2.5 V shows no redox activity (Graph 4.2a). Over time and after increasing the voltage to 3.5 V a reduction peak appears around 0.2 V and shifts to higher voltage in the following cycles. An oxidation peak also appears at 2.3 V exhibiting a large overpotential corresponding to a battery with a low cell voltage efficiency (Graph 4.2b). The oxidation peak also appears to increase.



Graph 4.2: CVs of a rechargeable battery with 0.35 M solution of **19** in EMIM-TFSI : THF mixture, a Mg anode and an Mo₆S₈ cathode. **a)** cycles 1 to 3 **b)** cycles 10 to 12, 0.1 mV/s.

It is not entirely clear if these observed peaks correspond to a redox reaction involving compound **19** or a reaction involving the ionic liquid instead. In the literature there is still a lot of debate on whether ILs are actually effective in Mg system batteries. Conflicting results can be found in recent research as some apparently successful reversible Mg deposition was observed using ILs such as PP13-TFSI or BMIM-BF₄^{56,57} were shown not to be reproducible.^{58,59} The reason behind the deactivating nature of ILs was not established and was only related to side-reactions between imidazolium salts with magnesium, or from water still remaining in small quantities in ILs after a difficult drying process. Both proposed reasons would eventually lead to the formation of passivating layers. A solid crystalline material was observed in the sample vial. The structure was elucidated by X-ray crystallography as Mg(TFSI)₂·4THF, **29**, but the quality of the data being too low due to twinning means the parameters of the molecule can't be discussed. However this structure gives some insight into what could be responsible for the deactivating properties of ILs. Whereas compound **19** possesses a separated ion pair motif which is often responsible for the high ionic conductivity nature of a solution, compound **29** was formed by complexation of the Mg cation with the TFSI anions of the IL, losing the benefits of the ion pair motif of compound **29**. In some studies conducted using Mg(TFSI)₂ as an electrolyte for Mg rechargeable batteries, it was shown that pure Mg(TFSI)₂ dissolved in ethereal solvents, displays poor electrochemical performances.⁶⁰ Eventually the

electrochemical performance were improved by addition of MgCl_2 to a solution of $\text{Mg}(\text{TFSI})_2$, this option would defeat the purpose in the case of our study where the chloride atoms are undesired.

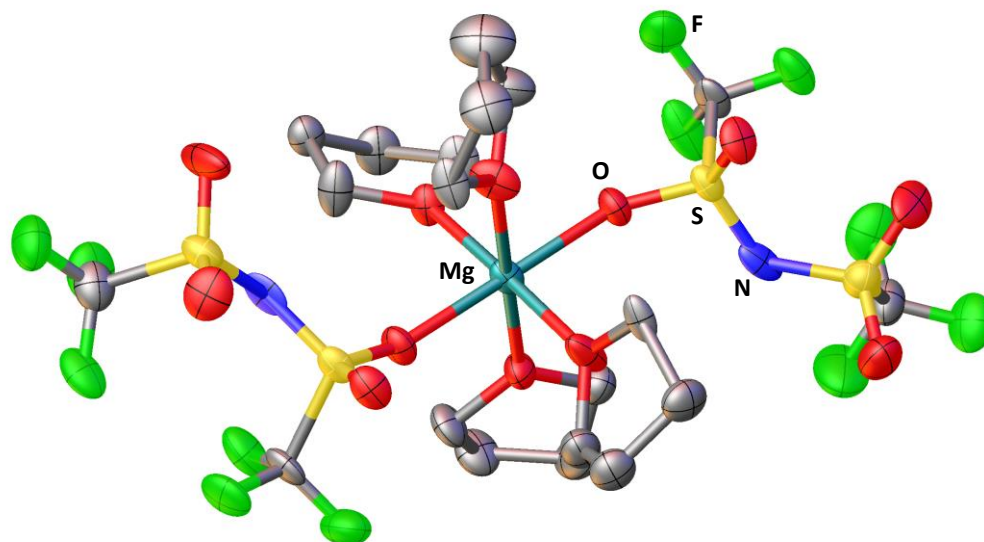
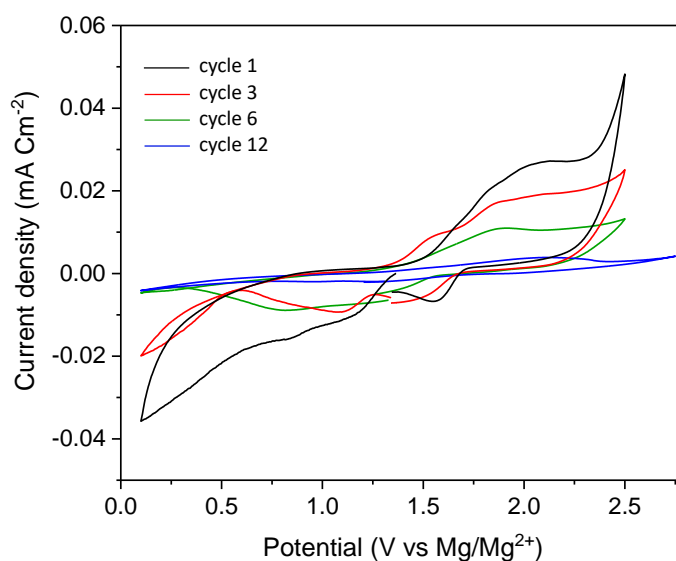


Figure 4.18: Molecular structure of $\text{Mg}(\text{TFSI})_2 \cdot 2\text{THF}$, **29**. Thermal ellipsoids are drawn at the 50 % probability level. The quality of the structure is low, allowing us to use as proof of connectivity.

4.3.3. $[\text{Al}(\text{pyrrolyl})_4]^-$ $[[\text{DippNacnac}]\text{Mg} \cdot 2\text{THF}]^+$ as a rechargeable magnesium battery electrolyte

Compound **26** is soluble in THF, toluene and other longer chained ethers such as glymes, making an interesting comparison with other magnesium aluminate electrolytes. The preliminary experiments run on a battery using a solution of **26** in THF are not very promising as the CV displays a redox process occurring only with a very low current density, confirmed by the galvanostatic cycling experiment where a low specific capacity is observed (Graph 4.3). The inactivity of compound **26** could be coming from multiple sources, and due to its novelty it is not straightforward to propose a solution to this problem. A more obvious factor could be the chelating ability of the β -diketiminato ligand being too strong to release the Mg atom for intercalation. Tuning of the ligand to decrease its grip on the Mg atom, for example replace the coordinating N atom for an O or S atom instead, might be interesting to study. Another

issue could originate from the presence of the pyrrolyl groups which are known to easily polymerise when a high voltage is applied.



Graph 4.3: CVs of for a rechargeable battery with 0.35 M solution of **26** in THF, a Mg anode and an Mo₆S₈ cathode, 0.1 mV/s.

4.4. Conclusion and future work

This chapter showed how difficult the development of novel chloro-free electrolytes is. The pathway to such valued compounds is hindered by the design of a simple, cheap procedure; the compounds undesired physical properties and their capability to reversibly deposit Mg.

Early attempts to synthesise targeted compound $2[\text{Al}(\text{pyrrolyl})_4]^- [\text{Mg}\cdot 6\text{THF}]^{2+}$ using metal hydride chemistry ended up in failure due to the formation of uncharacterisable solids. Another facile route was sought, and using a simple transmetallation reaction which shows that two small groups, such as pyrrolyl or phenyl, can be transferred from a homoleptic magnesium starting material to a homoleptic group 13 reagent, here aluminium and gallium. This reaction also forms an insoluble solid, but quality crystals can be grown if the transmetallation reaction is done by slow diffusion of a solution of one reagent to a solution of the other. Only DMSO and ILs:THF mixtures allowed solubilisation of these compounds, but the electrochemistry displayed in such systems was not successful.

The insolubility was overcome by altering $2[\text{Al}(\text{pyrrolyl})_4]^- [\text{Mg}\cdot 6\text{THF}]^{2+}$ using the $[\text{DippNacnac}]$ ligand which allowed formation of a Mg centred monocation, reducing the charges involved and lowering the attraction between the ions. Such a compound characterised as $[\text{Al}(\text{pyrrolyl})_4]^- [[\text{DippNacnac}]\text{Mg}\cdot 2\text{THF}]^+$ is soluble in a variety of polar and non-polar solvents, but preliminary results show very small reversible Mg deposition. We are optimistic that by tuning the molecule and especially using a more flexible ligand there is still a possibility to promote the intercalation of the Mg ions within a battery electrode.

In the near future it would be ideal to successfully synthesise a soluble, chloro-free magnesium aluminate compound which allows reversible deposition in a magnesium battery system. According to the literature, similar boronate and aluminate compounds with CF_3 substituents on the boron anion ($[\text{B}(\text{hfip})_4]^-$ or $[\text{BArF}]^-$, where hfip is tetrakis(hexafluoroisopropoxy) and BArF is tetrakis(3,5-bis(trifluoromethyl)-phenyl)borate) display an improved solubility and exhibit a good electrochemical activity as electrolyte for rechargeable Mg battery.^{61,62} The presence of fluoride atoms in these compounds could be responsible for the enhanced solubility; hence it would be interesting to see if changing the phenyl groups in compound **21** for pentafluorobenzene groups affects the solubility of these types of compounds. In addition to organofluorine containing electrolytes, the presence of the inorganic anion PF_6^- as the counter anion of $[\text{Mg}\cdot \text{CH}_3\text{CN}]^{2+}$ which also displays good solubility.¹³ If the presence of F atoms does not improve the solubility, the addition of a substituent to the phenyl groups could also be studied, but making sure that the bulk the substituent added does not destabilise the tetraarylaluminate anion.

- 1 J. Muldoon, C. B. Bucur and T. Gregory, *Angew. Chem. Int. Ed.*, 2017, **56**, 2064–2084.
- 2 R. E. Doe, R. Han, J. Hwang, A. J. Gmitter, I. Shterenberg, H. D. Yoo, N. Pour and D. Aurbach, *Chem. Commun.*, 2014, **50**, 243–245.
- 3 C. J. Barile, E. C. Barile, K. R. Zavadil, R. G. Nuzzo and A. A. Gewirth, *J. Phys. Chem. C*, 2014, **118**, 27623–27630.
- 4 K. A. See, K. W. Chapman, L. Zhu, K. M. Wiaderek, O. J. Borkiewicz, C. J. Barile, P. J. Chupas and A. A. Gewirth, *J. Am. Chem. Soc.*, 2016, **138**, 328–337.
- 5 G. Vardar, J. G. Smith, T. Thompson, K. Inagaki, J. Naruse, H. Hiramatsu, A. E. S. Sleightholme, J. Sakamoto, D. J. Siegel and C. W. Monroe, *Chem. Mater.*, 2016, **28**, 7629–7637.
- 6 Q. Li, J. Chen, L. Fan, X. Kong and Y. Lu, *Green Energy Environ.*, 2016, **1**, 18–42.
- 7 J. Muldoon, C. B. Bucur, A. G. Oliver, T. Sugimoto, M. Matsui, H. S. Kim, G. D. Allred, J. Zajicek and Y. Kotani, *Energy Environ. Sci.*, 2012, **5**, 5941–5950.
- 8 J. Song, E. Sahadeo, M. Noked and S. B. Lee, *J. Phys. Chem. Lett.*, 2016, **7**, 1736–1749.
- 9 H. D. Yoo, I. Shterenberg, Y. Gofer, G. Gershinsky, N. Pour and D. Aurbach, *Energy Environ. Sci.*, 2013, **6**, 2265–2279.
- 10 E. Roedern, R.-S. Kühnel, A. Remhof and C. Battaglia, *Sci. Rep.*, 2017, **7**, 1–6.
- 11 T. J. Carter, R. Mohtadi, T. S. Arthur, F. Mizuno, R. Zhang, S. Shirai and J. W. Kampf, *Angew. Chem. Int. Ed.*, 2014, **53**, 3173–3177.
- 12 O. Tutusaus, R. Mohtadi, T. S. Arthur, F. Mizuno, E. G. Nelson and Y. V. Sevryugina, *Angew. Chem. Int. Ed.*, 2015, **54**, 7900–7904.
- 13 E. N. Keyzer, H. F. J. Glass, Z. Liu, P. M. Bayley, S. E. Dutton, C. P. Grey and D. S. Wright, *J. Am. Chem. Soc.*, 2016, **138**, 8682–8685.
- 14 R. Schwarz, M. Pejic, P. Fischer, M. Marinaro, L. Jörissen and M. Wachtler, *Angew. Chem. Int. Ed.*, 2016, **55**, 14958–14962.
- 15 J. Zhu, Y. Guo, J. Yang, Y. Nuli, F. Zhang, J. Wang and S. I. Hirano, *J. Power Sources*, 2014, **248**, 690–694.
- 16 C. B. Bucur, T. Gregory, A. G. Oliver and J. Muldoon, *J. Phys. Chem. Lett.*, 2015, **6**, 3578–3591.
- 17 A. D. Bond, R. A. Layfield, J. A. MacAllister, M. McPartlin, J. M. Rawson and

- D. S. Wright, *Chem. Commun.*, 2001, 1956–1957.
- 18 M. Visseaux, P. Zinck, M. Terrier, A. Mortreux and P. Roussel, *J. Alloys Compd.*, 2008, **451**, 352–357.
- 19 D. R. Armstrong, M. J. Duer, M. G. Davidson, D. Moncrieff, C. A. Russell, C. Stourton, A. Steiner, D. Stalke and D. S. Wright, *Organometallics*, 1997, **16**, 3340–3351.
- 20 E. Rijnberg, J. T. B. H. Jastrzebski, J. Boersma, H. Kooijman, A. L. Spek and G. van Koten, *J. Organomet. Chem.*, 1997, **541**, 181–185.
- 21 K. Hensen, A. Lemke, T. Stumpf, M. Bolte, H. Fleischer, C. R. Pulham, R. O. Gould and S. Harris, *Inorg. Chem.*, 1999, **38**, 4700–4704.
- 22 R. J. Less, L. K. Allen, A. Steiner and D. S. Wright, *Dalton Trans.*, 2015, **44**, 4141–4147.
- 23 N. Pour, Y. Gofer, D. T. Major and D. Aurbach, *J. Am. Chem. Soc.*, 2011, **133**, 6270–6278.
- 24 C. A. Zechmann, T. J. Boyle, M. A. Rodriguez and R. A. Kemp, *Polyhedron*, 2000, **19**, 2557–2564.
- 25 E. C. Ashby, R. D. Schwartz and B. D. James, *Inorg. Chem.*, 1970, **9**, 325–332.
- 26 H. Nöth, M. Schmidt and A. Treit, *Chem. Ber.*, 1995, **128**, 999–1006.
- 27 M. Fichtner and O. Fuhr, *J. Alloys Compd.*, 2002, **345**, 286–296.
- 28 S. Kriek, H. Görls and M. Westerhausen, *Organometallics*, 2008, **27**, 5052–5057.
- 29 M. Barber, D. Liptak and J. P. Oliver, *Organometallics*, 1982, **10**, 1307–1311.
- 30 A. F. M. Maqsudur Rahman, K. F. Siddiqui and J. P. Oliver, *J. Organomet. Chem.*, 1987, **319**, 161–166.
- 31 A. W. Aplett and A. R. Barron, *J. Crystallogr. Spectrosc. Res.*, 1993, **23**, 529–532.
- 32 L. Rosch, G. Altnau, C. Kruger and Y. H. Tsay, *Z. Naturforsch. B*, 1983, **38**, 34–41.
- 33 C. J. Carmalt, J. D. Mileham, A. J. P. White, D. J. Williams and S. Rushworth, *Polyhedron*, 2003, **22**, 2655–2660.
- 34 L. Hubener, H.-W. Lerner and M. Bolte, *Acta Crystallogr. Sect. E Struct. Reports Online*, 2003, **59**, m929–m930.
- 35 L. Yang, D. R. Powell and R. P. Houser, *Dalton Trans.*, 2007, 955–964.

- 36 M. Gartner, R. Fischer, J. Langer, H. Görls, D. Walther and M. Westerhausen, *Inorg. Chem.*, 2007, **46**, 5118–5124.
- 37 C. Loh, C. Glock, S. Ziemann, H. Görls, S. Krieck and M. Westerhausen, *Zeitschrift für Naturforsch. B*, 2013, **68b**, 518–532.
- 38 X. Zheng, U. Englert, G. E. Herberich and J. Rosenplänter, *Inorg. Chem.*, 2000, **39**, 5579–5585.
- 39 D. C. Bradley, M. B. Hursthouse, A. A. Ibrahim, K. M. A. Malik, M. Motevalli, R. Moseler, H. Powell, J. D. Runnacles and A. C. Sullivan, *Polyhedron*, 1990, **9**, 2959–2964.
- 40 W. Li, S. Cheng, J. Wang, Y. Qiu, Z. Zheng, H. Lin, S. Nanda, Q. Ma, Y. Xu, F. Ye, M. Liu, L. Zhou and Y. Zhang, *Angew. Chem. Int. Ed.*, 2016, **55**, 6516–6520.
- 41 J. Langer, S. Krieck, H. Görls, G. Kreisel, W. Seidel and M. Westerhausen, *New J. Chem.*, 2010, **34**, 1667–1677.
- 42 A. Koch, S. Krieck, H. Görls and M. Westerhausen, *Organometallics*, 2017, **36**, 994–1000.
- 43 P. R. Markies, G. Schat, O. S. Akkerman, F. Bickelhaupt, W. J. J. Smeets, P. van der Sluis and A. L. Spek, *J. Organomet. Chem.*, 1990, **393**, 315–331.
- 44 M. M. Andrianarison, M. C. Ellerby, I. B. Gorrell, P. B. Hitchcock, J. D. Smith and D. R. Stanley, *J. Chem. Soc., Dalton Trans.*, 1996, 211–217.
- 45 S. E. Baillie, V. L. Blair, T. D. Bradley, W. Clegg, J. Cowan, R. W. Harrington, A. Hernán-Gómez, A. R. Kennedy, Z. Livingstone and E. Hevia, *Chem. Sci.*, 2013, **4**, 1895–1905.
- 46 T. D. Blümke, W. Clegg, P. García-Alvarez, A. R. Kennedy, K. Koszinowski, M. D. McCall, L. Russo and E. Hevia, *Chem. Sci.*, 2014, **5**, 3552–3562.
- 47 L. C. H. Maddock, T. Cadenbach, A. R. Kennedy, I. Borilovic, G. Aromí and E. Hevia, *Inorg. Chem.*, 2015, **54**, 9201–9210.
- 48 J. F. Malone and W. S. McDonald, *J. Chem. Soc. A*, 1970, 3362–3367.
- 49 N. A. Eckert, E. M. Bones, R. J. Lachicotte and P. L. Holland, *Inorg. Chem.*, 2003, **42**, 1720–1725.
- 50 C. Chen, S. M. Bellows and P. L. Holland, *Dalton Trans.*, 2015, **44**, 16654–16670.
- 51 S. J. Bonyhady, C. Jones, S. Nembenna, A. Stasch, A. J. Edwards and G. J. McIntyre, *Chem. Eur. J.*, 2010, **16**, 938–955.
- 52 M. Arrowsmith, B. Maitland, G. Kociok-Köhn, A. Stasch, C. Jones and M. S. Hill,

- Inorg. Chem.*, 2014, **53**, 10543–10552.
- 53 S. J. Kang, S. C. Lim, H. Kim, J. W. Heo, S. Hwang, M. Jang, D. Yang, S. T. Hong and H. Lee, *Chem. Mater.*, 2017, **29**, 3174–3180.
- 54 A. Jaenschke, J. Paap and U. Behrens, *Organometallics*, 2003, **22**, 1167–1169.
- 55 W. Uhl, M. Koch, W. Hiller and M. Heckel, *Angew. Chem. Int. Ed.*, 1995, **34**, 989–990.
- 56 Y. NuLi, J. Yang and P. Wang, *Appl. Surf. Sci.*, 2006, **252**, 8086–8090.
- 57 Z. Feng, Y. NuLi, J. Wang and J. Yang, *J. Electrochem. Soc.*, 2006, **153**, C689–C693.
- 58 N. Amir, Y. Vestfrid, O. Chusid, Y. Gofer and D. Aurbach, *J. Power Sources*, 2007, **174**, 1234–1240.
- 59 G. T. Cheek, W. E. O’Grady, S. Z. El Abedin, E. M. Moustafa and F. Endres, *J. Electrochem. Soc.*, 2008, **155**, D91–D95.
- 60 I. Shterenberg, M. Salama, H. D. Yoo, Y. Gofer, J.-B. Park, Y.-K. Sun and D. Aurbach, *J. Electrochem. Soc.*, 2015, **162**, A7118–A7128.
- 61 J. Muldoon, C. B. Bucur, A. G. Oliver, J. Zajicek, G. D. Allred and W. C. Boggess, *Energy Environ. Sci.*, 2013, **6**, 482–487.
- 62 Z. Zhao-Karger, M. E. Gil Bardaji, O. Fuhr and M. Fichtner, *J. Mater. Chem. A*, 2017, **5**, 10815–10820.

Chapter 5: Conclusion and Future Work

5.1. Conclusion

The development of new, viable electrolytes for rechargeable magnesium batteries is not widespread focus for leading research groups in the area of renewable energy. Instead MIB maintain some controversy, and extensively target the updated development of already existing lithium ion batteries, aiming to boost their current performances while reviewing their deficiencies. It was acknowledged that “the electrochemical behaviour of Mg^{2+} is different from Li^+ in regards to all battery compartments”,¹ in other words the need to put aside what is known in LIBs and discover from scratch how rechargeable magnesium batteries function. In the last five years a clearer future for magnesium battery could be envisioned and with this an increasing number of research groups are developing an interest in the topic.

In this thesis it was decided to explore the development of these electrolytes from a more synthetically rational approach, and propose new routes to make novel electrolytes related the already successful electrolytes exposed in recent breakthroughs. According to the literature, the synthesis, characterisation and purification of these electrolytes is challenging and the customised designing of a targeted compound exigent. Hence we were confident that our synthetic knowledge would counter-balance our deficiency in the energy sector knowledge.

The first contribution was to propose a new, easy synthetic method to make the widely successful magnesium aluminate electrolytes $[\text{AlR}_n\text{Cl}_{4-n}]^- [\text{Mg}_2\text{Cl}_3 \cdot 6\text{THF}]^+$ (R = alkyl, aryl, amide, alkoxide). This was undertaken after the method proposed by the literature was unsuccessful when using bulky R groups. Instead the organic group was attached to the Al atom prior addition of the Mg source. Subsequently, the idea to be able to tune the constitution of the magnesium cation was appealing since so far only the alteration of the anion was achieved. This prowess was easily achieved by the incorporation of a variety of Lewis donor ligands during the reaction, namely THF, MeTHF, TMEDA and Me₆TREN. Depending on the ligand and more precisely its bulk and denticity, the cation exclusively was altered to a trinuclear species, $[\text{Mg}_3\text{Cl}_5 \cdot 6\text{MeTHF}]^+$ (**5**) and $[\text{Mg}_3\text{Cl}_5 \cdot 3\text{TMEDA}]^+$ (**7**) or a mononuclear species $[\text{MgCl} \cdot \text{Me}_6\text{TREN}]^+$ (**9**), significantly different from the typically observed dinuclear species $[\text{Mg}_2\text{Cl}_3 \cdot 6\text{THF}]^+$ (**1**). All compounds possess the same aluminium anion

$[(\text{Dipp})(\text{SiMe}_3)\text{NAlCl}_3]^-$ and were isolated in high purity by crystallisation and characterised in the solid state by means of X-Ray crystallography. After tackling the challenges of synthesis and purification, the full characterisation and identification of the potential electroactive species in solution was undertaken. After uninformative results obtained with Raman spectroscopy, our efforts were focused on the use of ESI-MS. This technique allowed us observe different dynamic equilibria, occurring whether a compound possessing the dinuclear, trinuclear or mononuclear cation aggregate was present. A solution of the isolated dinuclear compound displayed an equilibrium between mono-, di- and trinuclear cation. In the case of a solution of the isolated trinuclear compound, the equilibrium is almost exclusively shifted toward the higher cation aggregates whereas for the case of the isolated mononuclear compound, the equilibrium is shifted toward the lower cation aggregates.

The next logical step was to study these compounds as electrolytes and observe the effect the different cation aggregate has in the battery performances. All of them showed electrolytic activity, but unfortunately early decomposition of the electrolyte during the charge prevented us from performing full electrochemical experiments on these compounds. The first major difference between them was the highly enhanced oxidative stability of **9** which exceed 3 V, whereas **1** and **5** decomposed at voltages below 2 V. This is quite an achievement and the presence of Me_6TREN is believed to be responsible for the high oxidative stability. Despite the low stability of **1** and **5**, preliminary experiments show a difference in the battery performances between the three aggregations. Compared to the widely studied dinuclear cation, the trinuclear cation gives a very low capacity which recovers slowly and the mononuclear cation gives a high overpotential and a modest capacity, although both properties recover with conditioning. To study the origin of the small electrochemical window of **1** and **5**, different series were prepared using a variety of amines on the aluminium, all possessing different steric and electronic properties. So far the study suggests, a combination of both properties and currently hence it is still unclear what features promote the oxidative stability. With a wider screening of amido groups it would be possible to show a more general trend.

Having participated in advances in the study of the chlorinated magnesium aluminate, the synthetic electrolyte design was taken a step further and aimed to tackle the

corrosive properties caused by the presence of chloride atoms. Here a simple transmetallation pathway was proposed to form the sought-after naked magnesium dication $[\text{Mg}\cdot 6\text{THF}]^{2+}$ countered by two $[\text{AlR}_4]^-$ (R = pyrrolyl or Ph) anions. So far all the synthesised and characterised compounds with the naked cation are insoluble in THF and other ethereal solvents. Using these compounds as electrolytes with DMSO or ionic liquids, the only solvents promoting solubility, did not display reversible Mg deposition. In order to tackle the solubility issue, the charges involved within the separated ion pair were reduced from +2/2(-1) to +1/-1 as observed in the chlorinated magnesium aluminate. This was achieved by placing a β -diketimine ligand on the Mg atom, ultimately generating $[\text{Al}(\text{pyrrolyl})_4]^- [(\text{DippNacnac})\text{Mg}\cdot 2\text{THF}]^+$ which is highly soluble in THF. Unfortunately, this compound was not electrolytically active in a battery system, and the DippNacnac ligand is believed to be holding too tightly to the Mg atom to release it.

5.2. Future work

A future work section for each chapter was already carried out at the end of the corresponding chapter. Instead this section introduces preliminary results to what could be considered as the start of a new chapter.

So far magnesium “ate complexes” were restricted to magnesium aluminates and magnesium borates. Considering the abundance of the elements, aluminium has a large advantage over boron, especially regarding the economical and sustainable aspect of the projected manufactured compounds. One study mentioned the electrochemical inactivity of a $\text{MgCl}_2 : \text{GaCl}_3$ mixture in DME and THF but no further studies were performed on gallium based electrolytes.² Regarding the economical and abundance aspect, gallium does not compete with aluminium but is extremely close to boron. As we are highly interested in synthesising, characterising and isolating our compounds in order to study their structures before using them as electrolytes, we decided to investigate the production of new magnesium gallate compounds. First the gallium equivalent of the MACC electrolyte was attempted by adding a THF solution of GaCl_3 to a THF solution of MgCl_2 in a 1:2 ratio. This resulted in the formation of a precipitate which redissolved when heating gently using a hairdryer, yielding a crop of crystals

upon cooling. Single crystal X-ray diffraction identified the product of the reaction as $[\text{GaCl}_4]^- [\text{MgCl} \cdot 5\text{THF}]^+$ (**30**) (Figure 5.1).

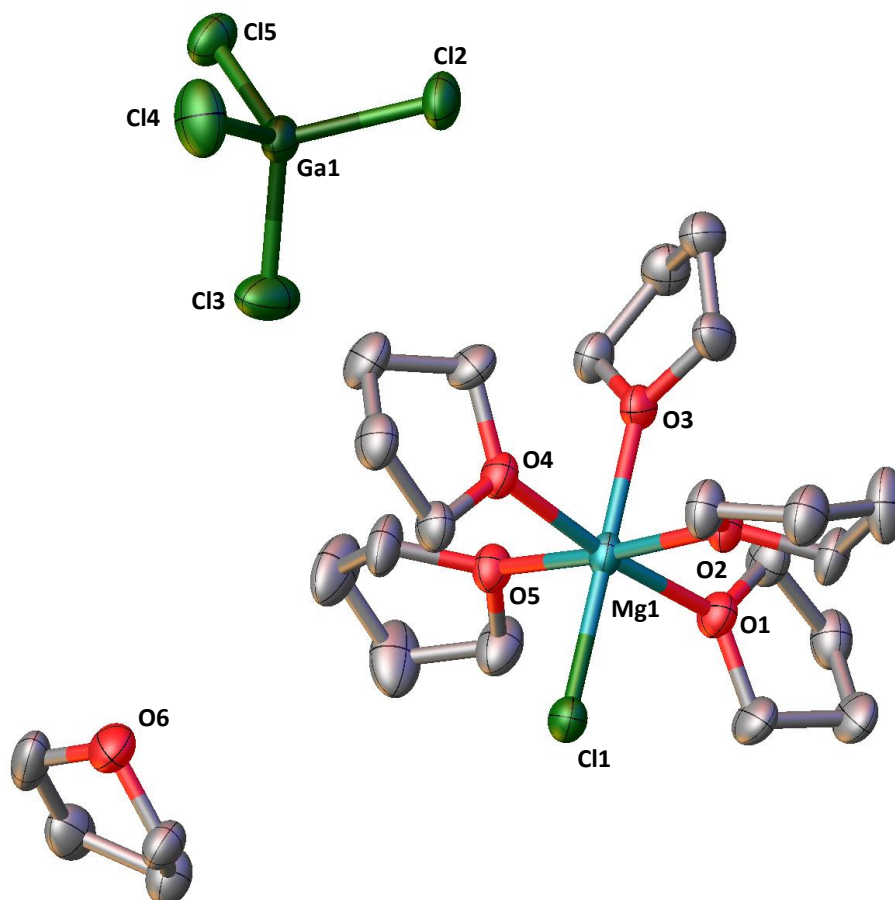


Figure 5.1: Molecular structure of $[\text{GaCl}_4]^- [\text{MgCl} \cdot 5\text{THF}]^+$, **30**. Hydrogen atoms are omitted for clarity. Thermal ellipsoids are drawn at the 50 % probability level. Selected bond distances (Å) and angles (°): Mg1-Cl1 2.3878(14); Mg-O 2.121; Ga-Cl 2.1660; Cl-Mg-O_{ax} 179.70(9); Cl-Mg-O_{eq} 93.31; Cl-Ga-Cl 109.64. Atoms which do not carry a numerical label represent average parameter values.

Compound **30** possess the exact same motif as the magnesium aluminate $[\text{AlCl}_4]^- [\text{MgCl} \cdot 5\text{THF}]^+$ characterised by Aurbach et al.,³ where only the Ga-Cl and Al-Cl bond distances differ (2.1660 and 2.071 Å respectively) as expected. $[\text{AlCl}_4]^- [\text{MgCl} \cdot 5\text{THF}]^+$ was shown to be poorly soluble in THF, consequently no electrochemical experiments were tested using this compound as electrolyte. Similar physical properties are observed with compound **30**, whose solubility in THF seems not good enough to use it as electrolyte. A test will still be attempted in order to witness any type of activity, even at low electrolytic concentrations. The MACC electrolyte

possesses the dinuclear cation $[\text{Mg}_2\text{Cl}_3 \cdot 6\text{THF}]^+$ which seems to increase the solubility of the compound and is thought responsible for the electrolytic properties displayed in a rechargeable magnesium battery. With gallium, the dinuclear cation was not observed even after attempting to obtain further crystals from the solution compound **30** crystallised from. The known active dinuclear cation is possibly not favoured when replacing $[\text{AlCl}_4]^-$ by $[\text{GaCl}_4]^-$ hence explaining the absence of electrochemical response reported by Gewirth et al.²

Moving on to another successful magnesium aluminate analogue, the same procedure for preparing the APC electrolyte $[\text{AlPh}_4]^- [\text{Mg}_2\text{Cl}_3 \cdot 6\text{THF}]^+$ was repeated with GaCl_3 . To a solution of GaCl_3 in THF, two equivalents of a solution of PhMgCl in THF was added leading to a white precipitate identified as MgCl_2 . After filtration of the precipitate and slow diffusion of hexane more colourless crystals were obtained and characterised by X-ray as $[\text{GaPh}_4]^- [\text{Mg}_2\text{Cl}_3 \cdot 6\text{THF}]^+$, **31**, (Figure 5.2).

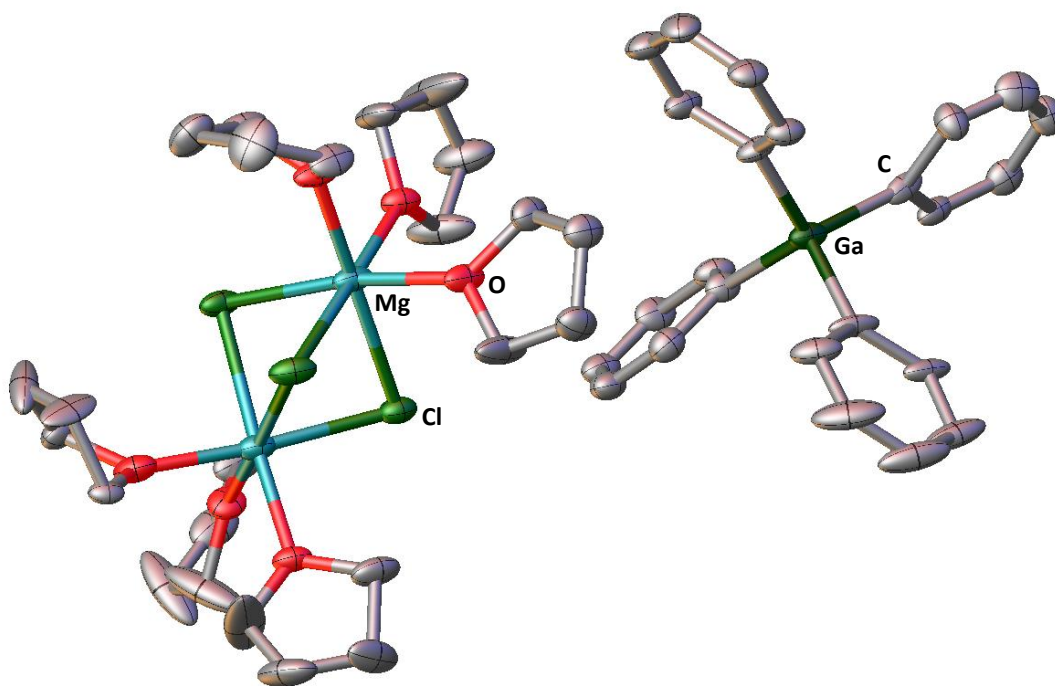


Figure 5.2: Molecular structure of $[\text{GaPh}_4]^- [\text{Mg}_2\text{Cl}_3 \cdot 6\text{THF}]^+$, **31**. Hydrogen atoms are omitted for clarity. Thermal ellipsoids are drawn at the 20 % probability level.

Compound **31** possesses the same separated ion pair motif as the APC electrolyte, where the Al atom was replaced by a Ga atom. The parameters of compound **31** can't

be discussed due to the low quality of the data. The electrolytic qualities of this compound were not yet tested, if it allows reversible deposition of Mg this would add a new class of compounds as potential rechargeable magnesium battery electrolytes.

- 1 J. Song, E. Sahadeo, M. Noked and S. B. Lee, *J. Phys. Chem. Lett.*, 2016, **7**, 1736–1749.
- 2 C. J. Barile, R. G. Nuzzo and A. A. Gewirth, *J. Phys. Chem. C*, 2015, **119**, 13524–13534.
- 3 N. Pour, Y. Gofer, D. T. Major and D. Aurbach, *J. Am. Chem. Soc.*, 2011, **133**, 6270–6278.

Chapter 6: Experimental Section

This final chapter contains the experimental procedures which have been executed during this project. In complement to the detailed procedure for each reaction, general techniques employed will be summarized and the apparatus type and model used thorough this research included.

6.1. General techniques

6.1.1. Schlenk techniques

During this project, all reactants and products were considered as air- and moisture-sensitive compounds to a certain degree. Therefore, the synthetic work was routinely carried out using standard Schlenk techniques through a Schlenk line procuring an oxygen and moisture free medium (Figure 6.1).

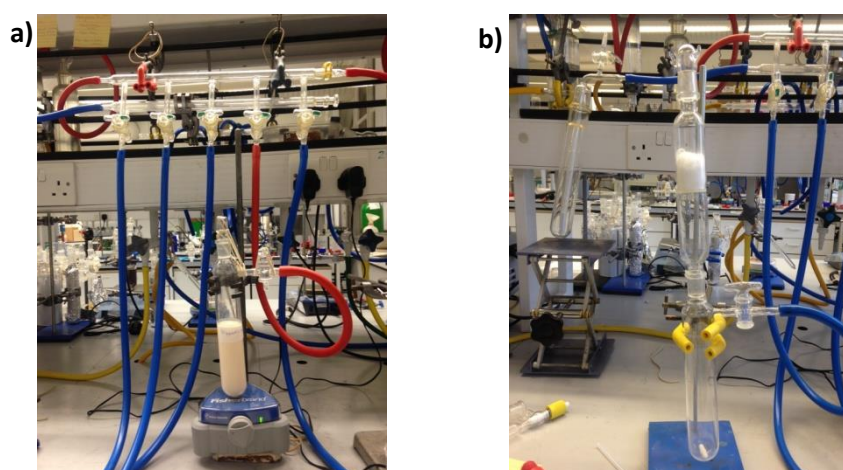


Figure 6.1: a) Photo of a standard Schlenk line; b) photo of a Schlenk flask with a filter stick.

A Schlenk line is constituted of a multi-junction two way tap manifold containing two independent paths; one linked to a vacuum pump; and the other one connected to a dried argon source. Using tubing the junctions can be connected to the commonly used Schlenk flasks, and by altering the two way tap the vessel can be subjected to either vacuum or argon gas. The vacuum is used to evacuate the flask of moisture and present gases prior to use, but also to evaporate present solvents which are collected using a liquid nitrogen cooled trap placed between the manifold and the pump. The argon is used to refill the vessel with an inert atmosphere where reagent additions can be

performed. The pressure within the line is regulated by oil bubblers which gives an idea of the argon flow at the entrance of the line, then releases the argon at the end so that there is no build-up of pressure.

6.1.2. Use of a glove box

The manipulation of the solids, reactants or products, such as yield determination of products, weighing starting materials, NMR sample preparation or simple storage were all carried out using a glove box in order to prevent decomposition of sensitive products or prevent moisture contamination of hygroscopic starting materials (Figure 6.2).



Figure 6.2: Photo of a typical research glove box.

The transfer of items in and out of the glove box is made through one of the ports situated on the right hand side. From outside the glove box, by placing the desired items in the port (note that air sensitive compounds must be placed in a sealed vial under vacuum) and applying vacuum for a satisfactory time to remove presence of air and moisture, the items can be safely transferred inside the glove box after refilling the port. From inside the box, the port must have been previously evacuated properly before taking any items outside.

6.1.3. Solvent purification

The solvents used for any reactions in this project were distilled over nitrogen in the presence of sodium; the communal solvents stills for diethyl ether, THF, hexane and toluene also contain benzophenone as a colour indicator of the solvents dryness.¹ An intense blue ketyl radical is observed when the sodium reacts with the benzophenone which is very sensitive to oxygen and water. If the solvent is exposed to air for too long a period or if the distillation system is refilled with too much new solvent (KOH containing solvents are used to refill the still to pre-dry them), the colour turns to a brown-yellow solution indicating that the solvent is not dry enough to use. Personally distilled solvents are kept in a previously evacuated Schlenk flask in the presence of microwave activated 4 Å molecular sieves.

The solvents are added to Schlenk flask, whose stopper was replaced by a Subaseal[®] (septum), using steel long needles and glass syringes previously flushed several times with argon.

6.2. Synthetic protocols

6.2.1. General experimental

TMEDA, PMDETA, tris[2-(2-methoxyethoxy)ethyl]amine, MeTHF, DME, aniline precursors (DippNH₂, DmpNH₂, PhNH₂), TMPH, HMDSH, pyrrole and iodobenzene were distilled over CaH₂ and stored over 4 Å molecular sieves prior to use. Air free reagents such as ⁿBuLi, ⁿBuMgCl, ⁿBu₂Mg, PhMgCl, GaCl₃ and TMSCl were purchased from Sigma Aldrich and used as received. Reagents used for the synthesis of Me₆TREN were used as received by the provider. NacnacH was synthesised according to the literature.² AlCl₃ was sublimed and stored in a glove box. NMR spectra were recorded on a Bruker AVANCE 400 NMR spectrometer, operating at 400.13 MHz for ¹H, 100.62 MHz for ¹³C, 155.5 MHz for ⁷Li and 104.2 MHz for ²⁷Al. All ¹³C spectra were proton decoupled. ¹H and ¹³C spectra were referenced to the appropriate solvent resonances. Elemental analyses were carried out on a Perkin-Elmer 2400 elemental analyser.

6.2.2. Preparation of starting materials

6.2.2.1. Synthesis of DippNHSiMe₃, DmpNHSiMe₃ and PhNHSiMe₃

ⁿBuLi (18.8 mL, 30.0 mmol, 1.6 M in hexane) was added to a solution of [2,6-diisopropylaniline (5.316 mL, 30.0 mmol); 2,6-dimethylaniline (3.66 mL, 30.0 mmol); or aniline (2.74 mL, 30 mmol)] in hexane (15 mL) at 0°C to form a white suspension. The mixture was stirred at room temperature for 3 h, after which time the suspending solid was filtered, dried under vacuum and weighed in the glove box. The solid (30.0 mmol) was transferred into a Schlenk flask and dissolved in diethyl ether (70 mL). Me₃SiCl (3.65 mL, 30.0 mmol) was slowly added at 0°C to form a white suspension. After 3 h the suspension was filtered off and the solvent of the slightly yellow filtrate was removed *in vacuo* to obtain an orange oil. Microwave-activated 4 Å molecular sieves were added to the oil which was used for the following reactions without further purification.

DippNHSiMe₃: Yield: 6.96 g (93 %). ¹H NMR (400 MHz, 298K, C₆D₆): δ = 7.09 (m, 3H, CH, Dipp Ar), 3.45 (sept., 2H, CH, ⁱPr), 2.01 (s, 1H, NH), 1.20 (d, 12H, CH₃, ⁱPr), 0.11 (s, 9H, SiMe₃); ¹³C NMR (100.6 MHz, 298K, C₆D₆): δ = 144.5 (C_{quaternary}, Dipp Ar), 139.7 (C_{quaternary}, Dipp Ar), 124.2 (CH, Dipp Ar), 123.3 (CH, Dipp Ar), 28.4 (CH, ⁱPr), 23.9 (CH₃, ⁱPr), 0.9 (SiMe₃); ¹H NMR (400 MHz, 298K, d₈-THF): δ = 7.01 (t, 2H, *m*-CH, Dipp Ar), 6.93 (d, 1H, *p*-CH, Dipp Ar), 3.51 (sept., 2H, CH, ⁱPr), 2.88 (s, 1H, NH), 1.17 (d, 12H, CH₃, ⁱPr), 0.11 (s, 9H, SiMe₃); ¹³C NMR (100.6 MHz, 298K, d₈-THF): δ = 145.5 (C_{quaternary}, Dipp Ar), 140.6 (C_{quaternary}, Dipp Ar), 124.3 (CH, Dipp Ar), 123.4 (CH, Dipp Ar), 28.9 (CH, ⁱPr), 24.1 (CH₃, ⁱPr), 1.0 (SiMe₃).

DmpNHSiMe₃: Yield: 4.97 g (86 %). ¹H NMR (400 MHz, 298K, C₆D₆): δ = 7.00 (d, 2H, *m*-CH, Ar), 6.86 (t, 1H, *p*-CH, Ar), 2.16 (s, 6H, CH₃), 2.10 (s, 1H, NH), 0.07 (s, 9H, SiMe₃); ¹³C NMR (400 MHz, 298K, C₆D₆): δ = 143.8 (C_{quaternary}, Dmp Ar), 131.9 (C_{quaternary}, Dmp Ar), 128.7 (CH, Dmp Ar), 122.2 (CH, Dmp Ar), 19.99 (CH₃), 1.2 (SiMe₃).

PhNHSiMe₃: Yield: 4.22 g (90 %) ¹H NMR (400 MHz, 298K, C₆D₆): δ = 7.12 (m, 2H, *m*-CH, Ar), 6.75 (m, 1H, *p*-CH, Ar), 6.57 (m, 2H, *o*-CH Ar), 3.04 (s, 1H, NH), 0.11 (s, 9H, SiMe₃); ¹³C NMR (400 MHz, 298K, C₆D₆): δ = 147.7 (C_{quaternary}, Ph), 129.6 (CH, Ph), 118.1 (CH, Ph), 116.6 (CH, Ph), 0.0 (SiMe₃).

5.2.2.2. Synthesis of Me₆TREN

At room atmosphere, aqueous formaldehyde (49.0 mL, 660 mmol, 37 wt%) was added to a solution of tris[2-aminoethyl]amine (3.00 mL, 19.9 mmol) and acetic acid (125 mL) in acetonitrile (600 mL) and allowed to stir for 1 h. Subsequently, the reaction mixture was cooled to 0 °C and sodium borohydride (10.0 g, 13.4 mmol) was slowly added. After 48 h stirring, all solvents were removed using a rotary evaporator and the residue was made strongly basic using aqueous sodium hydroxide (3 M) followed by three extractions with dichloromethane. The extracts were combined, dried with magnesium sulphate and the solvent removed by rotary evaporation. The residue was dissolved in pentane, filtered, and the filtrate reduced to dryness to give a pale yellow oil (4.17 g, 90%). ¹H NMR (400 MHz, 298K, C₆D₆): δ = 2.62 (m, 6H, CH₂NMe₂), 2.36 (m, 6H, NCH₂CH₂NMe₂), 2.11 (s, 18H, NCH₃); ¹³C NMR (400 MHz, 298K, C₆D₆): δ = 58.8 (NCH₂), 54.0 (NCH₂), 46.1 (NCH₃). The synthesis was adapted from the literature.³

6.2.3. Preparation of products

6.2.3.1. Synthesis of 1: [(Dipp)(SiMe₃)NAlCl₃]⁻ [Mg₂Cl₃·6THF]⁺; 2: [(Dmp)(SiMe₃)NAlCl₃]⁻ [Mg₂Cl₃·6THF]⁺; 3: [(Ph)(SiMe₃)NAlCl₃]⁻ [Mg₂Cl₃·6THF]⁺ and 4: [(TMP)AlCl₃]⁻ [Mg₂Cl₃·6THF]⁺

ⁿBuLi (2.5 mL, 4.0 mmol, 1.6 M in hexane) was added to a solution of [DippNHSiMe₃ (0.72 mL, 4.0 mmol); DmpNHSiMe₃ (0.72 mL, 4.0 mmol); PhNHSiMe₃ (0.68 mL, 4.0 mmol); TMPH (0.66 mL, 4.0 mmol)] in diethyl ether (10 mL) and the reaction mixture was stirred at room temperature for 20 min to give a light yellow solution. This solution was then transferred by syringe to a solution of AlCl₃ (0.532 g, 4.0 mmol) in diethyl ether (10 mL) to form a colourless suspension (LiCl) and the reaction mixture was stirred for 2h at room temperature. The suspension was filtered and the diethyl ether removed *in vacuo* and replaced by THF (10 mL). ⁿBuMgCl (2.0 mL, 4.0 mmol, 2.0 M in THF) was added to the solution and this was left to stir for 2h at room temperature. Colourless crystals were obtained overnight after slow diffusion of hexane.

[(Dipp)(SiMe₃)AlCl₃]⁻ [Mg₂Cl₃·6THF]⁺ : Yield: 1.70 g (44 % of 50% possible). Elemental analysis (%) for C₃₉H₇₄O₆Mg₂Cl₆NSiAl: calcd: C 48.32, H 7.69, N, 1.44; found: C 48.26, H 7.56, N 1.39; ¹H NMR (400 MHz, 298K, C₆D₆): δ = 7.09 (m, 3H, CH, Dipp Ar), 3.90 (sept., 2H, CH, ⁱPr), 3.63 (s, 24H, THF, broad), 1.41 (s, 24H, THF broad), 1.33 (d, 6H, CH₃, ⁱPr), 1.31 (d, 6H, CH₃, ⁱPr), 0.35 (s, 9H, SiMe₃); ¹³C NMR (100.6 MHz, 298K, C₆D₆): δ = 144.3 (C_{quaternary}, Dipp Ar), 121.1 (CH, Ar), 65.4 (THF), 27.6 (THF), 25.2 (CH, ⁱPr), 22.9 and 22.6 (CH₃, ⁱPr), 0.0 (SiMe₃); ²⁷Al NMR (104.2 MHz, 298K, C₆D₆): δ = 97.0 (broad); ¹H NMR (400 MHz, 298K, d⁸-THF): δ = 6.83 (d, 2H, *m*-CH, Dipp Ar), 6.36 (t, 1H, *p*-CH, Dipp Ar), 3.88 (sept., 2H, CH, ⁱPr), 3.61 (t, 24H, THF), 1.77 (t, 24H, THF), 1.13 (m, 12H, CH₃, ⁱPr), 0.04 (s, 9H, SiMe₃); ¹³C NMR (100.6 MHz, 298K, d⁸-THF): δ = 147.4 (C_{quaternary}, Dipp Ar), 123.0 (CH, Dipp Ar), 122.2 (CH, Dipp Ar), 68.2 (THF), 27.8 (CH, ⁱPr), 26.3 (THF), 26.1 and 25.2 (CH₃, ⁱPr), 3.1 (SiMe₃); ²⁷Al NMR (104.2 MHz, 298K, d⁸-THF): δ = 100.0 (broad).

[(Dmp)(SiMe₃)AlCl₃]⁻ [Mg₂Cl₃·6THF]⁺ : Yield: 1.51 g (42 % of 50% possible); ¹H NMR (400 MHz, 298K, C₆D₆): δ = 6.96 (d, 2H, *m*-CH, Dmp Ar), 6.81 (t, 1H, *p*-CH, Dmp Ar), 3.63 (s, 24H, THF, broad), 2.42 (s, 6H, Ar-CH₃), 1.41 (s, 24H, THF, broad), 0.38 (s, 9H, SiMe₃). ¹³C NMR (100.6 MHz, 298K, C₆D₆): δ = 147.7 (C_{quaternary}, Dmp Ar), 136.7 (C_{quaternary}, Dmp Ar), 128.5 (CH, Dmp Ar), 122.9 (CH, Dmp Ar), 69.4 (THF), 25.3 (THF), 20.7 (CH₃, Dmp), 2.5 (SiMe₃); ²⁷Al NMR (104.2 MHz, 298K, C₆D₆): δ = 98.0 (broad).

[(Ph)(SiMe₃)AlCl₃]⁻ [Mg₂Cl₃·6THF]⁺ : Yield: 1.32 g (38 % of 50 % possible); ¹H NMR (400 MHz, 298K, d⁸-THF): δ = 6.99 (m, 2H, *m*-CH, Ph), 6.62 (m, 2H, *o*-CH, Ph), 6.53 (m, 1H, *p*-CH, Ph), 3.61 (m, 24H, THF), 1.76 (m, 24H, THF), 0.21 (s, 9H, SiMe₃); ¹³C NMR (100.6 MHz, 298K, d⁸-THF): δ = 129.7 (C_{quaternary}, Ph), 129.3 (CH, Ph), 117.3 (CH, Ph), 116.6 (CH, Ph), 68.0 (THF), 26.1 (THF), -0.1 (SiMe₃); ²⁷Al NMR (104.2 MHz, 298K, d⁸-THF): δ = 76.8 (broad).

[(TMP)AlCl₃]⁻ [Mg₂Cl₃·6THF]⁺ : Yield: 1.02 g (30 % of 50% possible); ¹H NMR (400 MHz, 298K, C₆D₆): δ = 3.64 (t, 24H, THF), 1.63 (m, 2H, CH₂), 1.55 (s, 12H, CH₃), 2.42 (t, 4H, CH₂), 1.29 (24H, THF broad). ¹³C NMR (100.6 MHz, 298K, d⁸-THF): δ = 68.0 (THF), 42.6 (C_{quaternary}, TMP), 33.9 (CH₃, TMP), 32.0 (CH₂, TMP), 26.1 (THF), 25.3 (CH₂, TMP); ²⁷Al NMR (104.2 MHz, 298K, C₆D₆): δ = 97.0 (broad).

6.2.3.2. Synthesis of 5: $[(\text{Dipp})(\text{SiMe}_3)\text{NAlCl}_3]^- [\text{Mg}_3\text{Cl}_5\cdot 6\text{MeTHF}]^+$; 6 $[(\text{Dmp})(\text{SiMe}_3)\text{NAlCl}_3]^- [\text{Mg}_3\text{Cl}_5\cdot 6\text{MeTHF}]^+$

The same procedure for the synthesis of **1** was adopted but with MeTHF as the solvent. ${}^n\text{BuMgCl}$ (0.5 M in MeTHF) was pre-prepared from ${}^n\text{BuCl}$ and Mg, standardized and used in this reaction.

$[(\text{Dipp})(\text{SiMe}_3)\text{NAlCl}_3]^- [\text{Mg}_3\text{Cl}_5\cdot 6\text{MeTHF}]^+$: Yield: 1.43 g (31% of 33% possible). Elemental analysis (%) for $\text{C}_{45}\text{H}_{86}\text{O}_6\text{Mg}_3\text{Cl}_8\text{NSiAl}$: calculated: C 47.05, H 7.55, N, 1.22; found: C 47.04, H 7.55, N 1.79. ${}^1\text{H NMR}$ (400 MHz, 298K, C_6D_6): $\delta = 7.10$ (m, 3H, CH, Dipp Ar), 3.88 (m, 2H, CH, ${}^i\text{Pr}$), 3.77 (m, 12H, CH_aO and CH_cO , MeTHF), 3.56 (m, 6H, CH_bO , MeTHF), 1.46-1.63 (m, 18H, CH_{2d} and CH_f , MeTHF), 1.39-1.32 (m, 12H, CH_3 , ${}^i\text{Pr}$), 1.15 (d, 18H, CH_3 , MeTHF), 1.11 (m, 6H, CH_e , MeTHF), 0.34 (s, 9H, SiMe_3); ${}^{13}\text{C NMR}$ (100.6 MHz, 298K, C_6D_6): $\delta = 147.0$ ($\text{C}_{\text{quaternary}}$, Dipp Ar), 146.7 (C-N, Dipp Ar), 124.2 (CH, Dipp Ar), 75.1 (CH, MeTHF), 72.2 (OCH₂, MeTHF), 67.6 (CH₂O, MeTHF), 33.3 (CH₂, MeTHF), 25.4 (CH, ${}^i\text{Pr}$), 25.1 (CH₂, MeTHF), (21.2 (CH₃, MeTHF), 2.7 (SiMe_3); ${}^1\text{H NMR}$ (400 MHz, 298K, $\text{d}_8\text{-THF}$): $\delta = 6.84$ (d, 2H, $m\text{-CH}$, Dipp Ar), 6.87 (t, 1H, $p\text{-CH}$, Dipp Ar), 3.89 (m, 2H, CH, ${}^i\text{Pr}$), 3.78-3.81 (m, 12H, CH_aO and CH_cO , MeTHF), 3.57 (m, 6H, CH_bO , MeTHF), 1.92-1.82 (m, 18H, CH_{2d} and CH_f , MeTHF), 1.33 (m, 6H, CH_e , MeTHF), 1.13 (m, 30H, CH_3 of ${}^i\text{Pr}$ and $\text{CH}_{3(g)}$ of MeTHF), 0.05 (s, 9H, SiMe_3); ${}^{13}\text{C NMR}$ (100.6 MHz, 298K, $\text{d}_8\text{-THF}$): $\delta = 147.4$ ($\text{C}_{\text{quaternary}}$, Dipp Ar), 123.0 (CH, Dipp Ar), 122.2 (CH, Dipp Ar), 75.6 (CH₂O, MeTHF), 68.0 (CH₂O, MeTHF), 33.9 (CH₂, MeTHF), 27.8 (CH, ${}^i\text{Pr}$), 26.6 (CH₂, MeTHF), 26.1 and 25.2 (CH₃, ${}^i\text{Pr}$), 21.3 (CH₃, MeTHF), 3.1 (SiMe_3). ${}^{27}\text{Al NMR}$ (104.2 MHz, 298K, $\text{d}_8\text{-THF}$): $\delta = 98.0$ (broad).

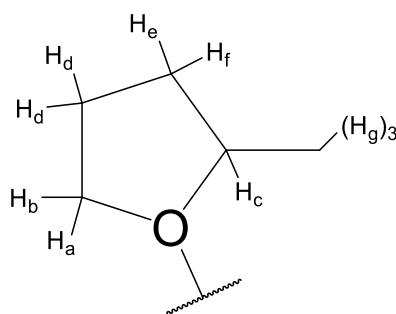


Figure 6.3: Molecule of MeTHF and its proton assigned for ${}^1\text{H NMR}$ shifts.

[(Dmp)(SiMe₃)AlCl₃]⁻ [Mg₃Cl₅·6MeTHF]⁺: Yield: 1.40 (32 % of 33% possible). ¹H NMR (400 MHz, 298K, C₆D₆): δ = 6.97 (d, 2H, *m*-CH, Dmp Ar), 6.83 (t, 1H, *p*-CH, Dmp Ar), 3.77 (m, 12H, CH_aO and CH_cO, MeTHF), 3.56 (m, 6H, CH_bO, MeTHF), 2.43 (s, 6H, Me, Dmp) 1.46-1.61 (m, 18H, CH_{2d} and CH_f, MeTHF), 1.15 (d, 18H, CH₃, MeTHF), 1.11 (m, 4H, CH_e, MeTHF), 0.38 (s, 9H, SiMe₃); ¹³C NMR (100.6 MHz, 298K, C₆D₆): δ = 147.6 (C_{quaternary}, Dmp Ar), 136.8 (C_{quaternary}, Dmp Ar), 128.6 (CH, Dmp Ar), 122.9 (CH, Dmp Ar), 75.5 (CH₂O, MeTHF), 67.7 (CH₂O, MeTHF), 33.4 (CH₂, MeTHF), 26.1 (CH₂, MeTHF), 21.3 (CH₃, MeTHF), 20.8 (CH₃, Dmp), 2.6 (SiMe₃); ²⁷Al NMR (104.2 MHz, 298K, C₆D₆): δ = 98.0 (broad).

6.2.3.3. Synthesis of 7: [(Dipp)(SiMe₃)AlCl₃]⁻ [Mg₃Cl₅·3TMEDA]⁺

A solution of **1** (0.969 g, 1.0 mmol) in THF (5 mL) was prepared and TMEDA (0.3 mL, 2.0 mmol) was added, giving a colourless solution. After stirring for 2 hours, toluene was slowly added until a slight suspension was noticed. This was heated to reform a solution and slowly cooled in a Dewar flask of hot water to give colourless crystals. Yield: 0.20 g (21% of 67% possible). Elemental analysis (%) for C₃₃H₇₄Mg₃Cl₈N₇SiAl: calculated: C 40.42, H 7.61, N, 10.00; found: C 40.05, H 7.64, N 9.87. ¹H NMR (400 MHz, 298K, d₈-THF): δ = 6.85 (d, 2H, *m*-CH, Dipp Ar), 6.75 (t, 1H, *p*-CH, Dipp Ar), 3.88 (sept., 2H, CH, ⁱPr), 2.38 (s, 12H, CH₂, TMEDA), 2.25 (s, 36H, CH₃, TMEDA), 1.14 (t, 12H, CH₃, ⁱPr), 0.04 (s, 9H, SiMe₃); ¹³C NMR (100.6 MHz, 298K, d₈-THF): δ = 147.6 (C_{quaternary}, Dipp Ar), 123.0 (CH, Dipp Ar), 122.3 (CH, Dipp Ar), 58.4 (CH₂, TMEDA), 47.0 (CH₃, TMEDA), 27.9 (CH, ⁱPr), 26.2 (CH₃, ⁱPr), 3.1 (SiMe₃); ²⁷Al NMR (104.2 MHz, 298K, d₈-THF): δ = 107.2 (broad).

6.2.3.4. Synthesis of 8: MgCl₂·PMDETA

A solution of **1** (0.969 g, 1.0 mmol) in THF (5 mL) was prepared and PMDETA (0.43 mL, 2.0 mmol) was added, giving the formation of a precipitate after a few seconds. Heating the mixture with a heat gun dissolved the precipitate to form a clear solution. Slowly cooling down the solution in a Dewar flask of hot water afforded a crop of colourless crystals. Yield: 0.187 g (70%). No suitable NMR spectroscopy was obtained due to the low solubility of the complex in most deuterated solvents.

6.2.3.5. Synthesis of 9: [(Dipp)(SiMe₃)AlCl₃]⁻ [MgCl·Me₆TREN]⁺, 10: [(Dmp)(SiMe₃)AlCl₃]⁻ [MgCl·Me₆TREN]⁺, 11: [(Ph)(SiMe₃)AlCl₃]⁻ [MgCl·Me₆TREN]⁺ and 12: [(HMDS)AlCl₃]⁻ [MgCl·Me₆TREN]⁺

The same procedures for the synthesis of **1**, **2** and **3** were adopted but with Me₆TREN (1.04 mL, 4.0 mmol) added prior to the ⁿBuMgCl solution. The THF solution was filtered to remove a small amount of colourless precipitate which formed upon stirring. Colourless crystals were obtained by slow diffusion of diethyl ether.

[(Dipp)(SiMe₃)AlCl₃]⁻ [MgCl·Me₆TREN]⁺: Yield: 1.76 g (65 %). Elemental analysis (%) for C₂₇H₅₆MgCl₄N₅SiAl: calcd: C 48.26, H 8.40, N, 10.42; found: C 48.29, H 8.37, N 10.04. ¹H NMR (400 MHz, 298K, C₆D₆): δ = 7.24 (d, 2H, *m*-CH, Dipp Ar), 7.10 (t, 1H, *p*-CH, Dipp Ar), 4.45 (sept., 2H, CH, ⁱPr), 2.30 (t, 6H, CH₂, Me₆TREN), 1.96 (t, 6H, CH₂, Me₆TREN), 1.82 (s, 18H, CH₃, Me₆TREN), 1.64 (d, 6H, CH₃, ⁱPr), 1.53 (d, 6H, CH₃, ⁱPr), 0.64 (s, 9H, SiMe₃); ¹³C NMR (100.6 MHz, 298K, C₆D₆): δ = 147.5 (C_{quaternary}, Dipp Ar), 146.7 (C_{quaternary}, Dipp Ar), 123.3 (CH, Dipp Ar), 123.0 (CH, Dipp Ar), 55.4 (CH₂, Me₆TREN), 49.3 (CH₂, Me₆TREN), 45.1 (CH₃, Me₆TREN), 27.9 (CH, ⁱPr), 26.5 (CH₃, ⁱPr), 25.2 (CH₃, ⁱPr), 3.4 (SiMe₃); ²⁷Al NMR (104.2 MHz, 298K, C₆D₆): δ = 77.1 (s, broad); ¹H NMR (400 MHz, 298K, d₈-THF): δ = 6.88 (d, 2H, *m*-CH, Dipp Ar), 6.77 (t, 1H, *p*-CH, Dipp Ar), 3.88 (sept, 2H, CH, ⁱPr), 2.92 (t, 6H, CH₂, Me₆TREN), 2.79 (t, 6H, CH₂, Me₆TREN), 2.49 (s, 18H, CH₃, Me₆TREN), 1.15 (d, 6H, CH₃, ⁱPr), 1.14 (d, 6H, CH₃, ⁱPr), 0.05 (s, 9H, SiMe₃); ¹³C NMR (100.6 MHz, 298K, d₈-THF): δ = 147.4 (C_{quaternary}, Dipp Ar), 147.2 (C_{quaternary}, Dipp Ar), 123.0 (CH, Dipp Ar), 122.3 (CH, Dipp Ar), 56.1 (CH₂, Me₆TREN), 50.1 (CH₂, Me₆TREN), 45.8 (CH₃, Me₆TREN), 27.7 (CH, ⁱPr), 26.1 (CH₃, ⁱPr), 24.9 (CH₃, ⁱPr), 2.9 (SiMe₃).

[(Dmp)(SiMe₃)AlCl₃]⁻ [MgCl·Me₆TREN]⁺: Yield: 1.57 g (63 %). ¹H NMR (400 MHz, 298K, C₆D₆): δ = 7.36 (t, 1H, *p*-CH, Dmp Ar), 6.92 (m, 2H, *m*-CH, Dmp Ar), 2.85 (s, 6H, CH₃, Dmp), 2.3 (t, 6H, CH₂, Me₆TREN), 1.90 (t, 6H, CH₂, Me₆TREN), 1.77 (s, 18H, CH₃, Me₆TREN), 0.63 (s, 9H, SiMe₃); ¹³C NMR (100.6 MHz, 298K, C₆D₆): δ = 137.6 (C_{quaternary}, Dmp Ar), 128.0 (CH, Dmp Ar), 121.7 (CH, Dmp Ar), 55.5 (CH₂, Me₆TREN), 49.4 (CH₂, Me₆TREN), 45.2 (CH₃, Me₆TREN), 21.4 (CH, Me), 3.2 (SiMe₃); ²⁷Al NMR (104.2 MHz, 298K, C₆D₆): δ = 67.6 (s, broad).

[(Ph)(SiMe₃)AlCl₃]⁻ [MgCl·Me₆TREN]⁺: Yield: 1.63 (69 %). **¹H NMR (400 MHz, 298K, C₆D₆)**: δ = 7.50 (m, 2H, *o*-CH, Ph), 7.21 (m, 2H, *m*-CH, Ph), 7.21 (m, 1H, *p*-CH, Ph), 2.44 (t, 6H, CH₂, Me₆TREN), 2.03 (t, 6H, CH₂, Me₆TREN), 1.85 (s, 18H, CH₃, Me₆TREN), 0.63 (s, 9H, SiMe₃). **¹³C NMR (100.6 MHz, 298K, C₆D₆)**: δ = 129.8 (CH, Ph), 120.8 (CH, Ph), 119.8 (CH, Ph), 55.3 (CH₂, Me₆TREN), 49.2 (CH₂, Me₆TREN), 45.0 (CH₃, Me₆TREN), 2.6 (SiMe₃); **²⁷Al NMR (104.2 MHz, 298K, C₆D₆)**: δ = 85.2 (s, broad).

[(HMDS)AlCl₃]⁻ [MgCl·Me₆TREN]⁺: A single crystal was obtained and used for the X-ray characterisation. No solid material was recovered for NMR spectroscopy characterisation.

6.2.3.6. Synthesis of 14: [(Dipp)(SiMe₃)AlCl₃]⁻ [Li·4THF]⁺

ⁿBuLi (2.5 mL, 4.0 mmol, 1.6 M in hexane) was added to a solution of DippNHSiMe₃ (0.72 mL, 4.0 mmol) in 10 mL of diethyl ether and the reaction mixture was stirred at room temperature for 20 min to give a light yellow solution. This solution was then transferred by syringe to a solution of AlCl₃ (0.532 g, 4.0 mmol) in diethyl ether (10 mL) to form a colourless suspension (LiCl) and the reaction mixture was stirred for 2h at room temperature. The solvent was removed *in vacuo* and replaced by a 5:1 mixture of hexane:THF, a crop of crystals was obtained at -70 °C. Yield: 0.756 g (56 %). **¹H NMR (400 MHz, 298K, C₆D₆)**: δ = 7.09 (m, 3H, CH, Dipp Ar), 3.91 (sept., 2H, CH, ⁱPr), 3.59 (s, 16H, THF, broad), 1.41 (s, 16H, THF broad), 1.33 (d, 6H, CH₃, ⁱPr), 1.31 (d, 6H, CH₃, ⁱPr), 0.35 (s, 9H, SiMe₃); **¹³C NMR (100.6 MHz, 298K, C₆D₆)**: δ = 147.0 (C_{quaternary}, Dipp Ar), 124.1 (CH, Dipp Ar), 67.9 (THF), 27.8 (THF), 25.9 (CH, ⁱPr), 25.5 (CH₃, ⁱPr), 25.3 (CH₃, ⁱPr), 2.6 (SiMe₃); **⁷Li NMR (155.5 MHz, 298K, C₆D₆)**: δ = -3.2. Due to the low solubility of this compound in C₆D₆, one CH (Dipp Ar) and one C_{quaternary} (DippAr) ¹³C NMR resonances belonging to the aromatic group could not be observed.

6.2.3.7. Synthesis of 15: [(Dipp)(SiMe₃)AlCl₃]⁻ [Li·3DME]⁺

ⁿBuLi (2.5 mL, 4.0 mmol, 1.6 M in hexane) was added to a solution of DippNHSiMe₃ (0.72 mL, 4.0 mmol) in 10 mL of diethyl ether and the reaction mixture was stirred at room temperature for 20 min to give a light yellow solution. This solution

was then transferred by syringe to a solution of AlCl_3 (0.532 g, 4.0 mmol) in diethyl ether (10 mL) to form a colourless suspension (LiCl) and the reaction mixture was stirred for 2h at room temperature. The solvent was removed *in vacuo* and replaced by DME and $^n\text{BuMgCl}$ was added to the reaction. Addition of 10 mL of hexane and cooling down to 4 °C afforded colourless crystals. Yield: 1.300 g (49%). **^1H NMR (400 MHz, C_6D_6):** δ = 7.25 (d, 2H, *m*-CH, Dipp Ar), 7.12 (t, 1H, *p*-CH, Dipp Ar), 4.47 (sept., 2H, CH, ^iPr), 3.28 (s, 18H, DME), 3.13 (s, 12H, DME), 1.66 (d, 6H, CH_3 , ^iPr), 1.52 (d, 6H, CH_3 , ^iPr), 0.65 (s, 9H, SiMe_3); **^{13}C NMR (100.6 MHz, C_6D_6):** δ = 147.6 ($\text{C}_{\text{quaternary}}$, Dipp Ar), 146.9 ($\text{C}_{\text{quaternary}}$, Dipp Ar), 123.4 (CH, Dipp Ar), 122.9 (CH, Dipp Ar), 71.8 (OCH_3 , DME), 59.0 (CH_2O , DME), 28.0 (CH, ^iPr), 26.4 (CH_3 , ^iPr), 25.3 (CH_3 , ^iPr), 3.4 (SiMe_3). **^7Li NMR (155.5 MHz, C_6D_6):** δ = -0.6.

6.2.3.8. Synthesis of 16: $[\text{Al}(\text{pyrrolyl})_4]^- [\text{Li}\cdot 4\text{THF}]^+$

A solution of LiAlH_4 (0.5 mL, 1.0 mmol, 2.0 M in THF) was added to 5 mL of THF for dilution, then pyrrole (0.28 mL, 4.0 mmol) was added drop wise at 0 °C. After the full amount of pyrrole was added and the effervescence caused by the evolution of H_2 was finished the reaction mixture was stirred at room temperature for 2h. A small amount of toluene was added and the mixture was placed in a fridge, a crop of crystal was obtained after a couple of days. Yield : 0.343g (60 %).

^1H NMR (400 MHz, C_6D_6): δ = 7.25 (t, 8H, NCH, pyrrolyl), 6.52 (t, 8H, β -CH, pyrrolyl), 3.16 (m, 16H, THF), 1.30 (m, 16H, THF); **^{13}C NMR (100.6 MHz, C_6D_6):** δ = 126.3 (NCH, pyrrolyl), 109.3 (β -CH; pyrrolyl), 68.1 (THF), 25.5 (THF); **^7Li NMR (155.5 MHz, C_6D_6):** δ = -3.3 (s); **^{27}Al NMR (104.2 MHz, C_6D_6):** δ = 98.1 (s).

6.2.3.9. Synthesis of 17: $\text{Al}(\text{pyrrolyl})_3\text{-OEt}_2$

$^n\text{BuLi}$ (3.75 mL, 6.0 mmol, 1.6 M in hexane) was added to a solution of pyrrole (0.42 mL, 6.0 mmol) in 15 mL of diethyl ether to form a yellow precipitate and the reaction mixture was stirred for 30 min at room temperature. AlCl_3 (0.266 g, 2.0 mmol) was added to the reaction mixture at 0 °C and stirred at room temperature for 3h to

form two layer mixtures, one dark brown layer with a white precipitate and one colourless. The diethyl ether was then removed in vacuo and replaced by 30 mL of toluene to give a brown solution with a white precipitate. The solid was filtered off and the remaining solution concentrated. Crystalline blocks grow from a toluene:hexane mixture with a drop of Et₂O at -18 °C. Yield: 0.386 g (65%).

¹H NMR (400 MHz, 298K, C₆D₆): δ = 7.05 (t, 6H, NCH, pyrrolyl), 6.65 (t, 6H, β-CH, pyrrolyl), 3.11 (q, 4H, CH₂, Et₂O), 0.35 (t, 6H, CH₃, Et₂O); **¹³C NMR (100.6 MHz, 298K, C₆D₆):** δ = 125.2 (NCH, pyrrolyl), 111.8 (β-CH; pyrrolyl), 70.0 (Et₂O), 12.8 (Et₂O).

6.2.3.10. Synthesis of 18: Mg(pyrrolyl)₂·4THF

ⁿBu₂Mg (1.0 mL, 1.0 mmol, 1 M in heptanes) was added to a solution of pyrrole (0.14 mL, 2.0 mmol) in 10 mL of THF to form a colourless solution. After stirring for 2h at room temperature a small amount of THF was removed under vacuum until a solid appears. The solid was easily dissolved upon gentle heating, by slowly cooling down the reaction mixture to room temperature, a crop of crystals was obtained. Yield: 0.258 g (60 %).

¹H NMR (400 MHz, 298K, C₆D₆): δ = 7.15 (broad s, 4H, NCH, pyrrolyl), 6.87 (t, 6H, β-CH, pyrrolyl), 3.38 (broad m, 16H, THF), 1.25 (m, 16H, THF); **¹H NMR (400 MHz, 298K, d₈-THF):** δ = 6.68 (t, 4H, NCH, pyrrolyl), 5.99 (t, 4H, β-CH, pyrrolyl), 3.61 (m, 16H, THF), 1.77 (m, 16H, THF), **¹³C NMR (100.6 MHz, 298K, d₈-THF):** δ = 125.5 (NCH, pyrrolyl), 106.8 (β-CH; pyrrolyl), 68.0 (THF), 26.1 (THF).

6.2.3.11. Synthesis of 19: 2[Al(pyrrolyl)₄]⁻ [Mg·6THF]²⁺

A solution of **17** (0.598 g, 2.0 mmol) in THF was added to a solution of **18** (0.444 g, 1 mmol) in THF. The addition was made very slowly in such a way that the solution of **17** lies on top of the solution of **18**, slowly diffusing overnight and forming large light brown crystals. Yield: 0.986 g (95 %).

¹H NMR (400 MHz, 298K, d₆-DMSO): δ = 6.65 (broad s, 16 H, NCH, pyrrolyl), 6.08 (broad s, 2H, β-CH, pyrrolyl), 3.60 (m, 24H, THF), 1.76 (m, 24H, THF); **¹³C NMR (100.6 MHz, 298K, d₆-DMSO):** δ = 124.7 (d, NCH, pyrrolyl), 108.6 (d, β-CH;

pyrrolyl), 67.0 (THF), 25.1 (THF); ^{27}Al NMR (MHz 104.2, 298K, $\text{d}_6\text{-DMSO}$): $\delta = 97.4$ (s).

6.2.3.12. Synthesis of 20: $2[\text{Al}(\text{pyrrolyl})_4]^- [\text{Mg}\cdot\text{L}_1]^{2+}$

Ligand L_1 (0.32 mL, 1 mmol) was added to a solution of **18** (0.444 g, 1 mmol) in THF, resulting in a colourless solution. A solution of **17** (0.598 g, 2.0 mmol) in THF was added in such a way that it lies on top of the solution of **18** and L_1 , slowly diffusing overnight forming small light brown crystals. Yield: 0.836 g (90 %).

^1H NMR (400 MHz, 298K, $\text{d}_6\text{-DMSO}$): $\delta = 6.65$ (s broad, 16H, NCH, pyrrolyl), 6.09 (s broad, 16H, $\beta\text{-CH}$, pyrrolyl), 3.48 (m, 6H CH_3OCH_2 , L_1), 3.43 (m, 12H, CH_2OCH_2 , L_1), 3.24 (s, 9H, OCH_3 , L_1), 2.66 (t, 6H, NCH_2 , L_1); ^{13}C NMR (100.6 MHz, 298K, $\text{d}_6\text{-DMSO}$): $\delta = 124.8$ (d, NCH, pyrrolyl), 108.6 (d, $\beta\text{-CH}$; pyrrolyl), 71.3 (CH_2OCH_2 , L_1), 69.5 (CH_3OCH_2 , L_1), 69.3 (CH_2OCH_2 , L_1), 58.1 (OCH_3 , L_1), 54.2 (NCH_2 , L_1); ^{27}Al NMR (MHz 104.2, 298K, $\text{d}_6\text{-DMSO}$): $\delta = 97.4$ (s).

6.2.3.13. Synthesis of 21: $2[\text{Al}(\text{Ph})_4]^- [\text{Mg}\cdot 6\text{THF}]^{2+}$

A solution of $\text{AlPh}_3\cdot\text{OEt}_2$ (0.664 g, 2.0 mmol) in THF was added to a solution of $\text{MgPh}_2\cdot 2\text{THF}$ (0.322g, 1 mmol) in THF. The addition was made very slowly in such a way that the solution of AlPh_3 lies on top of the solution of MgPh_2 slowly diffusing overnight, forming large colourless crystals. Yield: 1.082 g (96 %).

^1H NMR (400 MHz, 298K, $\text{d}_6\text{-DMSO}$): $\delta = 7.57$ (m broad, 16H, *o*-CH, Ph), 7.03 (m, 24H, *m*-CH and *p*-CH, Ph), 3.60 (m, 24H, THF), 1.76 (m, 24H, THF); ^{13}C NMR (100.6 MHz, 298K, $\text{d}_6\text{-DMSO}$): $\delta = 138.4$ (d, $\text{C}_{\text{quaternary}}$, Ph), 125.8 (m, 2CH, Ph), 124.5 (CH, Ph), 67.0 (THF), 25.1 (THF); ^{27}Al NMR (MHz 104.2, 298K, $\text{d}_6\text{-DMSO}$): $\delta = 132.6$ (s).

6.2.3.14. Synthesis of 23: $\text{GaPh}_3\cdot\text{OEt}_2$

A solution of PhLi (0.5 g, 6.0 mmol) in 15 mL of Et_2O was added to a solution of GaCl_3 (0.35 g, 2.0 mmol) in 10 mL Et_2O to form a white precipitate. After the filtration of the precipitate the remaining colourless solution was concentrated *in vacuo*

until a solid appears. The solid was redissolved after gentle heating and a crop of colourless crystals was obtained by slow cooling. Yield: 0.53 g (71 %).

¹H NMR (400 MHz, 298K, C₆D₆): δ = 7.94 (d, 6H, *o*-CH, Ph), 7.38 (t, 6H, *m*-CH, Ph), 7.31 (t, 3H, *p*-CH, Ph), 3.29 (t, 4H, CH₂, Et₂O), 0.56 (t, 6H, CH₃, Et₂O); **¹³C NMR (100.6 MHz, 298K, C₆D₆):** δ = 147.0 (*C*_{quaternary}, Ph), 137.9 (CH, Ph), 128.4 (CH, Ph), 128.1 (CH, Ph), 65.8 (Et₂O), 13.6 (Et₂O).

6.2.3.15. Synthesis of 24: 2[Ga(Ph)₄]⁻ [Mg·6THF]²⁺

A solution of GaPh₃·OEt₂ (0.749 g, 2.0 mmol) in THF was added to a solution of MgPh₂·2THF (0.322g, 1 mmol) in THF. The addition was made very slowly in such a way that the solution of GaPh₃ lies on top of the solution of MgPh₂ slowly diffusing overnight, forming large colourless crystals. Yield 1.204 g (84%).

¹H NMR (400 MHz, 298K, d₆-DMSO): δ = 7.54 (broad m, 16H, *o*-CH, Ph), 7.08 (t, 16H, *m*-CH, Ph), 7.01 (t, 8H, *p*-CH, Ph), 3.61 (m, 24H, THF), 1.77 (m, 24H, THF). **¹³C NMR (100.6 MHz, 298K, d₆-DMSO):** δ = 139.1 (d, *C*_{quaternary}, Ph), 126.2 (m, 2CH, Ph), 124.8 (CH, Ph), 67.1 (THF), 25.1 (THF);

6.2.3.16. Synthesis of 25: [DippNacnac]Mg(pyrrolyl)·THF

ⁿBu₂Mg (5 mL, 5.0 mmol, 1 M in heptanes) was added to a solution of NacnacH (2.08 g, 5.0 mmol) in 15 mL of THF. After leaving the reaction mixture to stir at room temperature for 1.5 h pyrrole (0.35 mL, 5.0 mmol) was added to the solution and an exothermic reaction occurs. Within 1 h a solid was obtained, redissolving it by gently heating and slowly cooling at room temperature afforded colourless crystals. Yield: 2.350 g (80%).

¹H NMR (400 MHz, 298K, C₆D₆): δ = 7.17 (broad m, 6H, CH, Ar*), 6.60 (t, 2H, NCH, pyrrolyl), 6.48 (t, 2H, β -CH, pyrrolyl), 4.87 (s, 1H, CH, Nacnac), 3.37 (broad s, 2H, CH, ⁱPr), 3.30 (m, 4H, THF), 3.16 (broad s, 2H, CH, ⁱPr), 1.70 (s, 6H, C-CH₃, Nacnac), 1.20 (d, 12H, CH₃, ⁱPr), 1.10 (d, 12H, CH₃, ⁱPr), 1.05 (m, 4H, THF) ; **¹³C NMR (100.6 MHz, 298K, C₆D₆):** δ = 169.4 (C-CH₃, Nacnac), 145.0 (*C*_{quaternary}, Ar*), 125.8 (CH, Ar*), 125.7 (NCH, pyrrolyl), 124.7 (CH, Ar*), 123.4 (*C*_{quaternary}, Ar*), 108.3 (β -CH, pyrrolyl), 94.5 (CH, Nacnac), 69.9 (THF), 28.3 (CH, ⁱPr), 25.1 (CH₃,

¹Pr), 24.6 (THF), 24.5(CH₃, ⁱPr), 24.0 (C-CH₃, Nacnac); **¹H NMR (400 MHz, 298K, d₈-THF)**: δ = 7.14 (m, 6H, CH, Ar*), 5.91 (t, 2H, NCH, pyrrolyl), 5.74 (t, 2H, β-CH, pyrrolyl), 4.96 (s, 1H, CH, Nacnac), 4.33 (sept, 2H, CH, ⁱPr), 3.61 (m, 4H, THF), 1.77 (m, 2H, THF), 1.75 (s, 6H, CH₃, Nacnac), 1.17 (d, 12H, CH₃, ⁱPr), 1.01 (d, 12H, CH₃, ⁱPr); **¹³C NMR (100.6 MHz, 298K, d₈-THF)**: δ = 170.0 (CH, Ar*), 145.5 (C-CH₃, Nacnac), 143.3, (C_{quarternary}, Ar*), 125.9 (NCH, pyrrolyl), 125.7 (C_{quarternary}, Ar*), 124.3 (CH, Ar*), 107.5 (β-CH, pyrrolyl), 94.8 (CH, Nacnac), 68.2 (THF), 28.9 (CH, ⁱPr), 24.8 (CH₃, ⁱPr), 24.6 (CH₃, ⁱPr), 24.2 (C-CH₃, Nacnac).

6.2.3.17. Synthesis of 26: [Al(pyrrolyl)₄]⁻ [(^{Dipp}Nacnac)Mg·2THF]⁺

A solution of **17** (0.84g, 2.8 mmol) in THF was added to a solution of [^{Dipp}Nacnac]Mg(pyrrolyl)·THF (1.64 g, 2.8 mmol) in 10 mL of THF. The reaction mixture was stirred for 2 h at room temperature. The solvent was removed *in vacuo* and 15 mL of hexane was added to form a slightly hazy solution. After filtration the filtrate was placed at -20 °C to form colourless crystals. Yield 1.25 g (50%)

¹H NMR (400 MHz, 298K, C₆D₆): δ = 7.16 (broad s, 8H, NCH, pyrrolyl), 7.17 (m, 4H, CH, Ar*), 7.07 (m, 2H, CH, Ar*), 6.50 (broad s, 8H, β-CH, pyrrolyl), 4.71 (s, 1H, CH, Nacnac), 3.12 (m, 8H, THF), 2.73 (m, 4H, CH, ⁱPr), 1.49 (s, 6H, C-CH₃, Nacnac), 1.20 (m, 8H, THF), 1.08 (d, 12H, ⁱPr), 1.02 (d, 12H, ⁱPr); **¹³C NMR (100.6 MHz, 298K, C₆D₆)**: δ = 171.4 (C-CH₃, Nacnac), 143.1 (C_{quarternary}, Ar*), 142.0 (CH, Ar*), 126.9 (C_{quarternary}, Ar*), 126.1 (NCH, pyrrolyl), 124.6 (CH, Ar*), 109.3 (β-CH, pyrrolyl), 94.3 (CH, Nacnac), 71.3 (THF), 28.4 (CH, ⁱPr), 25.3 (THF), 25.0 (CH₃, ⁱPr), 24.1 (CH₃, ⁱPr), 24.0 (C-CH₃, Nacnac). **²⁷Al NMR (MHz 104.2, 298K, C₆D₆)**: δ = 98.1 (s).

6.2.3.18. Synthesis of 27: [^{Dipp}Nacnac]Mg(Ph)·THF

MgPh₂·4THF (1.3 g, 2.9 mmol) was added to a solution of NacnacH (1.31 g, 3.0 mmol) in 15 mL of THF. The resulting solution was refluxed for two hours, after cooling down the reaction mixture the volume of THF was reduced until a precipitate appeared. Redissolving the precipitate and slow cooling afforded a crop of crystals. Yield: 1.3 g (76 %).

¹H NMR (400 MHz, 298K, C₆D₆): δ = 7.45 (m, 1H, *p*-CH, Ph), 7.19 (m broad, 6H, CH, Ar*), 7.06 (m, 4H, *o*- and *m*-CH, Ph), 4.86 (s, 1H, CH, Nacnac), 3.55 (m, 4H, THF), 3.30 (m, 4H, CH, ⁱPr), 1.71 (s, 6H, CH₃, Nacnac), 1.29 (m, 4H, THF), 1.21 (d, 12H, CH₃, ⁱPr), 1.11(d, 12H, CH₃, ⁱPr); **¹³C NMR (100.6 MHz, 298K, C₆D₆):** δ = 169.6 (C-CH₃, Nacnac), 165.4 (C_{quaternary}, Ph), 145.8 (C_{quaternary}, Ar*), 142.8 (CH, Ar*), 140.9 (CH, Ph), 126.4 (CH, Ph), 125.6 (CH, Ar*), 125.4 (CH, Ph), 124.2 (CH, Ar*), 95.0 (CH, Nacnac), 71.6 (THF), 28.4 (CH, ⁱPr), 25.5 (THF), 25.1 (CH₃, ⁱPr), 24.5 (CH₃, ⁱPr), 24.2 (C-CH₃, Nacnac).

6.2.4. Raman spectroscopy

All the measurements were performed using a Renishaw inVia Raman microscope using flame sealed glass capillaries filled with either 0.1 M solutions of the corresponding compound in THF or MeTHF, or filled with a fine powder of the corresponding compound.

6.2.5. Electrospray ionisation mass-spectroscopy

Sample solutions were transferred into a gas-tight syringe and injected into the ESI source of a quadrupole-ion trap mass spectrometer (HCT, Bruker Daltonik) at a flow rate of 8 $\mu\text{L min}^{-1}$. The ESI source was operated at an ESI voltage of ± 3000 V and with nitrogen as nebulizer gas (5 L min^{-1} flow rate) and drying gas (0.7 bar backing pressure). Mild conditions identical to those reported previously were chosen to prevent unwanted decomposition processes during the ESI process and the ion transfer into the quadrupole ion trap (drying gas at 60 °C, low potential differences along the flight path of the ions).^{4,5} The helium-filled quadrupole ion trap (estimated pressure $p(\text{He}) \approx 2$ mTorr) was typically operated at a trap drive of 40, which permits the efficient detection of ions of medium m/z ratios. Typically, ESI mass spectra for m/z 50 – 1000 were recorded, but it was checked that no ions of considerable signal intensity were present at higher m/z ratios. For gas-phase fragmentation experiments, ions of interest were mass-selected with isolation widths of 1 - 12 u (centered at the given m/z ratios), subjected to excitation voltages of amplitudes of V_{exc} , and allowed to collide with the helium gas. The given assignments are based on the observed m/z

ratios, isotope patterns, and results of the gas-phase fragmentation experiments. For controlling the HCT instrument and the simulation of ion patterns, the Compass software package (Bruker Daltonik) was used.

6.2.5. Electrochemistry

6.2.5.1. Battery cell

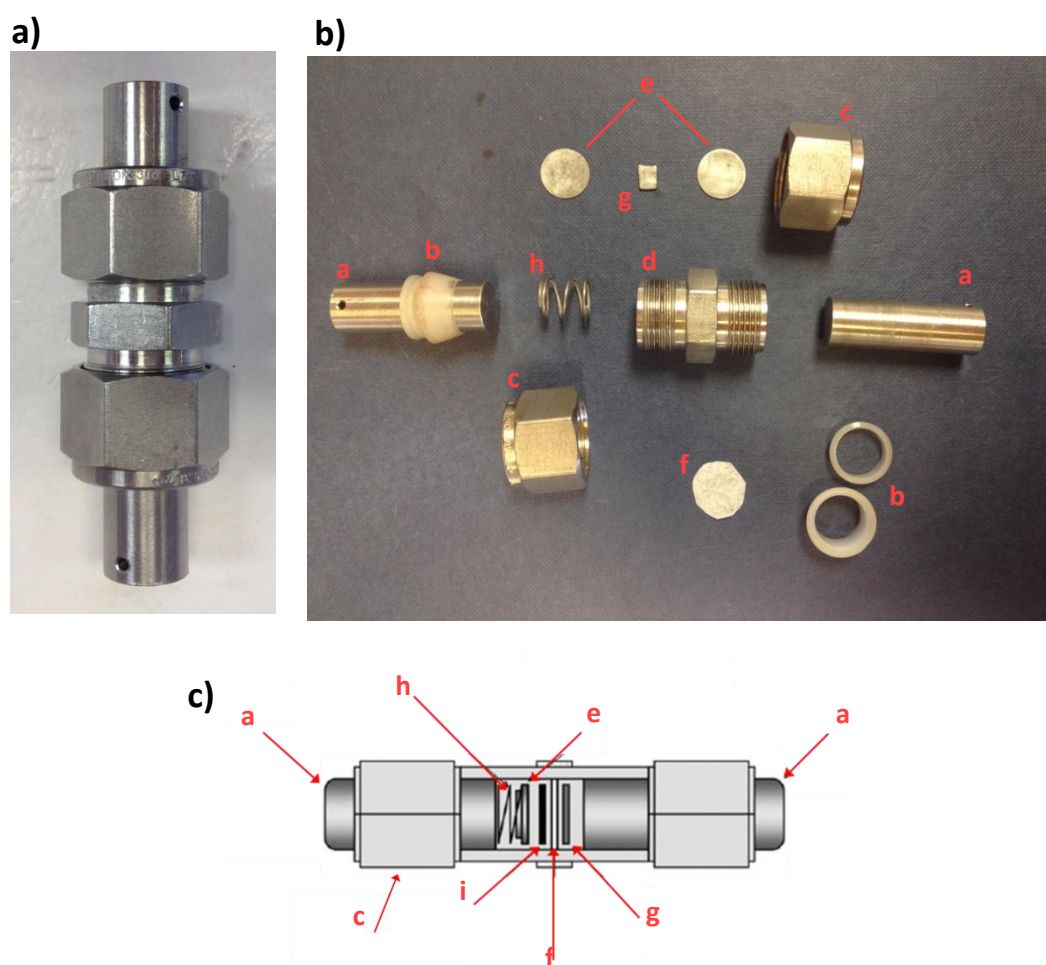


Figure 6.4: a) Image of an assembled Swagelok battery cell; b) image of a dismantled Swagelok battery cell; c) scheme of a Swagelok battery cell. a: electrode bolt, b: joint, c: tightening nut, d: cylinder body, e: current collector, f: glass fibre separator, g: Mg sheet, h: spring, i: cathode material.

The battery cells used for the experimental electrochemical measurements of the electrolytes performance in this study were Swagelok cells as shown in the example displayed in Figure 6.4. The parts of the cell are made of stainless steel apart for the current collectors which are made of Inconel 625, an alloy resistant to the corrosive

nature of the chlorinated electrolytes. The battery cell is itself half built outside the glove box by tightly assembling parts **a**, **b**, **c** and **d**. A current collector **e** is then introduced and a known amount of a cathode material pellet **i** is gently positioned on the current collector and all the parts are placed in the glove box. A cut, dry glass fibre separator **f** is placed above the cathode material and approximately 10 drops of a freshly prepared electrolyte solution were added onto it to soak the fibre. A polished piece of Mg sheet **g** is placed on the soaked fibre, followed by another current collector, a spring **h** and the battery is finally tightly closed using the second set of parts **a**, **b**, **c** and **d**.

6.2.5.2. Electrochemical measurements

In this study the cathode material of choice was the Chevrel Phase Mo_6S_8 , synthesised following a previously reported method.⁶ The Mo_6S_8 -carbon composite was prepared by homogeneously mixing Chevrel Phase, carbon black and polytetrafluoroethylene (PTFE) in a 75:15:10 ratio. Both cyclic voltammetry and galvanostatic cycling measurements were performed at room temperature on a battery cell system introduced above and using a BioLogic potentiostat.

6.2.7. X-ray crystallography

Crystallographic data were collected on Oxford Diffraction instruments with Mo and Cu $K\alpha$ radiation. Structures were solved using *SHELXS-97*,⁷ and refined on F^2 against all independent reflections by the full-matrix least-squares method using the *SHELXL-97*⁷ or OLEX 2 programs.⁸ All non-hydrogen atoms were refined using anisotropic thermal parameters. Appropriate bond length restraints were applied to the C–C, C–O and C–N distances involved in the disordered groups.

6.2.7.1. Selected crystallographic and refinement parameters

Compound	1	3	4	5
Empirical Formula	C ₃₉ H ₇₄ AlCl ₆ Mg ₂ NO ₆ Si	C ₃₃ H ₆₂ AlCl ₆ Mg ₂ NO ₆ Si	C ₃₃ H ₆₆ AlCl ₆ Mg ₂ NO ₆	C ₄₅ H ₈₆ AlCl ₈ Mg ₃ NO ₆ Si
Mol. Weight	969.42	885.22	861.20	1148.79
Crystal System	Monoclinic	Triclinic	Monoclinic	Monoclinic
Space Group	P2 ₁ /n	P-1	P2 ₁ /c	P2 ₁ /n
a (Å)	19.5415(9)	11.1043(10)	16.8190(3)	13.3260(3)
b (Å)	13.8802(5)	12.3802(11)	13.0920(3)	14.1674(3)
c (Å)	19.5602(8)	17.3992(9)	19.0920(4)	32.6193(8)
α (°)	90	97.746(6)	90	90
β (°)	110.428(5)	107.622(6)	104.809(2)	95.436(2)
γ (°)	90	95.568(8)	90	90
Volume (Å ³)	4971.9(4)	2234.7(3)	4339.67(16)	6130.7(2)
Z	4	2	4	4
λ Å	0.71073	1.54184	0.71073	0.71073
μ mm ⁻¹	0.454	4.551	0.485	0.473
Refls. Collected	54746	22111	49393	59048
Refls. Unique	12079	7127	10321	14559
R _{int}	0.0392	0.1313	0.0313	0.0387
Goodness of fit	1.052	0.960	1.068	1.081
R[>2σ(I)]	0.0406	0.0851	0.0377	0.0699
wR ₂	0.0897	0.2094	0.0814	0.1586

Compound	7	8	9	10
Empirical Formula	C ₃₃ H ₇₄ AlCl ₈ Mg ₃ N ₇ Si	C ₉ H ₂₃ Cl ₂ MgN ₃	C ₂₇ H ₅₆ AlCl ₄ MgN ₅ Si	C ₂₃ H ₄₈ AlCl ₄ MgN ₅ Si
Mol. Weight	980.61	268.51	671.96	615.85
Crystal System	Monoclinic	Monoclinic	Monoclinic	Monoclinic
Space Group	P2 ₁ /c	P2 ₁ /c	P2 ₁ /n	Pc
a (Å)	19.692(2)	8.3278(4)	17.4285(12)	9.1112(2)
b (Å)	16.2309(12)	29.5439(14)	13.2180(7)	12.4080(4)
c (Å)	16.9709(15)	11.9786(5)	17.5260(12)	14.2740(4)
α (°)	90	90	90	90
β (°)	107.610(11)	101.773(5)	114.337(8)	91.619(3)
γ (°)	90	90	90	90
Volume (Å ³)	5170.0(9)	2885.2(2)	3678.7(5)	1613.06(8)
Z	4	8	4	2
λ Å	0.71073	0.71073	0.71073	0.71073
μ mm ⁻¹	0.543	0.471	0.420	0.472
Refls. Collected	28175	15977	40914	12218
Refls. Unique	11753	6762	7220	6834
Rint	(twinned)	0.0218	0.1136	0.0204
Goodness of fit	0.720	1.045	1.022	1.043
R[>2σ(I)]	0.0494	0.0356	0.0586	0.0306
wR2	0.0961	0.0722	0.0959	0.0653

Compound	11	12	15	16
Empirical Formula	C ₂₁ H ₄₄ AlCl ₄ MgN ₅ Si	C ₁₈ H ₄₈ AlCl ₄ MgN ₅ Si ₂	C ₂₇ H ₅₆ AlCl ₃ LiNO ₆ Si	C ₃₂ H ₄₈ AlLiN ₄ O ₄
Mol. Weight	587.79	583.88	659.11	586.98
Crystal System	Monoclinic	Monoclinic	Orthorhombic	Triclinic
Space Group	P2 ₁	P2 ₁ /c	Pca2 ₁	P-1
a (Å)	9.6189(2)	9.3865(3)	18.8747(5)	10.2257(6)
b (Å)	13.7073(3)	23.6370(6)	10.3113(3)	10.2624(9)
c (Å)	12.3672(2)	14.6538(4)	19.0910(5)	16.3057(13)
α (°)	90	90	90	83.238(7)
β (°)	99.646(2)	101.839(3)	90	83.297(6)
γ (°)	90	90	90	89.696(7)
Volume (Å ³)	1607.55(6)	3182.06(16)	3715.55(17)	1687.5(2)
Z	2	4	4	2
λ Å	1.54184	1.54184	1.54184	0.71073
μ mm ⁻¹	4.297	4.682	3.055	0.099
Refls. Collected	12441	29459	15589	18215
Refls. Unique	5905	6318	6417	6.541
Rint	0.0417	0.0822	0.0327	0.0345
Goodness of fit	1.084	1.026	1.038	1.049
R[>2σ(I)]	0.0411	0.0445	0.0414	0.0833
wR2	0.1189	0.1219	0.1028	0.2192

Compound	17	18	19	20
Empirical Formula	C ₁₆ H ₂₂ AlN ₃ O	C ₂₄ H ₄₀ MgN ₂ O ₄	C ₅₆ H ₈₀ Al ₂ MgN ₈ O ₆	C ₄₇ H ₆₅ Al ₂ MgN ₉ O ₆
Mol. Weight	299.35	444.90	1039.58	930.37
Crystal System	Monoclinic	Monoclinic	Triclinic	Tetragonal
Space Group	P2 ₁ /c	P2 ₁ /c	P-1	P4 ₁
a (Å)	11.0633(14)	8.3479(4)	10.8032(3)	16.7670(1)
b (Å)	7.7845(10)	13.7143(6)	11.9767(4)	16.7670(1)
c (Å)	19.436(3)	10.6931(5)	12.7662(4)	34.7742(5)
α (°)	90	90	115.388(3)	90
β (°)	101.884(12)	91.795(4)	94.776(2)	90
γ (°)	90	90	105.796(2)	90
Volume (Å ³)	1638.0(4)	1223.61(10)	1397.40(8)	9776.15(16)
Z	4	2	1	8
λ Å	0.71073	0.71073	1.54184	1.54174
μ mm ⁻¹	0.126	0.104	1.026	1.121
Refls. Collected	17300	11231	26892	47293
Refls. Unique	3515	2907	5539	14805
R _{int}	00830	0.0317	0.0233	0.0350
Goodness of fit	1.034	1.048	1.040	1.140
R[<i>I</i> >2σ(<i>I</i>)]	0.0586	0.0538	0.0409	0.1007
wR ₂	0.0966	0.1280	0.1083	0.2471

Compound	21	22	23	24
Empirical Formula	C ₇₂ H ₈₈ Al ₂ MgO ₆	C ₁₅ H ₃₀ AlN ₃	C ₂₂ H ₂₅ GaO	C ₇₂ H ₈₈ Ga ₂ MgO ₆
Mol. Weight	1127.69	279.41	375.17	1213.25
Crystal System	Monoclinic	Triclinic	Monoclinic	Monoclinic
Space Group	P2 ₁ /c	P-1	P2 ₁ /c	P2 ₁ /c
a (Å)	18.7709(5)	8.5714(4)	12.2499(2)	18.8395(9)
b (Å)	13.0019(3)	8.7903(3)	7.4542(1)	13.0587(6)
c (Å)	25.8666(7)	10.9473(4)	21.2085(3)	25.9481(15)
α (°)	90	94.980(3)	90	90
β (°)	91.115(2)	90.678(3)	100.416(1)	91.321(5)
γ (°)	90	107.797(4)	90	90
Volume (Å ³)	6311.7(3)	781.74(5)	1904.70(5)	6382.0(6)
Z	4	2	4	4
λ Å	1.54184	1.54174	1.54184	0.71073
μ mm ⁻¹	0.913	1.051	1.993	0.905
Refls. Collected	35631	13397	12719	49400
Refls. Unique	12426	3095	3757	14739
R _{int}	0.0473	0.0238	0.0324	0.0703
Goodness of fit	1.008	1.069	1.045	1.037
R[<i>I</i> >2σ(<i>I</i>)]	0.0524	0.0377	0.0281	0.0468
wR2	0.1135	0.1004	0.0764	0.1009

Compound	25	26	27	28
Empirical Formula	C ₃₇ H ₅₃ MgN ₃ O	C ₅₃ H ₇₃ AlMgN ₆ O ₂	C ₃₉ H ₅₄ MgN ₂ O	C ₃₆ H ₆₀ Al ₂ MgN ₆ O ₇ S ₆
Mol. Weight	580.16	877.50	591.18	959.58
Crystal System	Monoclinic	Monoclinic	Monoclinic	Triclinic
Space Group	P2 ₁ /n	C2/c	P2 ₁ /n	P-1
a (Å)	10.8131(14)	38.2698(12)	10.7108(2)	9.8395(19)
b (Å)	19.0170(3)	9.7287(3)	19.4049(3)	11.373(2)
c (Å)	17.3003(2)	27.2433(8)	17.7729(3)	11.600(2)
α (°)	90	90	90	70.151(17)
β (°)	105.9243(14)	92.726(3)	106.699(2)	79.320(16)
γ (°)	90	90	90	84.585(16)
Volume (Å ³)	3420.98(8)	10131.6(5)	3538.17(11)	1199.0(4)
Z	4	8	4	1
λ Å	1.54184	1.54184	0.71073	0.71073
μ mm ⁻¹	1.1263	0.812	0.081	0.385
Refls. Collected	28308	34237	53508	19328
Refls. Unique	6765	9984	8703	5396
R _{int}	0.0228	0.0711	0.0324	0.0713
Goodness of fit	1.057	1.011	1.045	1.026
R[<i>I</i> >2σ(<i>I</i>)]	0.402	0.0530	0.0423	0.0490
wR ₂	0.1087	0.1286	0.0965	0.0938

Compound	29	30	31
Empirical Formula	C ₂₀ H ₃₂ F ₁₂ MgN ₂ O ₁₂ S ₄	C ₂₄ H ₄₈ Cl ₅ GaMgO ₆	C ₄₈ H ₆₈ Cl ₃ GaMg ₂ NO ₆
Mol. Weight	873.02	703.94	965.71
Crystal System	Triclinic	Triclinic	Monoclinic
Space Group	P-1	P-1	P2 ₁ /c
a (Å)	10.4822(15)	10.7358(5)	16.5741(9)
b (Å)	10.6866(16)	12.7971(9)	16.2904(9)
c (Å)	16.890(2)	13.3800(7)	18.4085(10)
α (°)	75.280(12)	63.072(7)	90
β (°)	71.931(12)	89.490(4)	90.923(5)
γ (°)	76.009(12)	89.770(5)	90
Volume (Å ³)	1712.1(4)	1638.87(19)	4969.6(5)
Z	2	2	4
λ Å	0.71073	1.54184	0.71073
μ mm ⁻¹	0.419	5.371	0.785
Refls. Collected	10729	14469	24943
Refls. Unique	10729	11168	13010
R _{int}	Merged	Merged	0.953
Goodness of fit	1.016	1.007	1.093
R[<i>I</i> >2σ(<i>I</i>)]	0.1082	0.0723	0.1126
wR ₂	0.3001	0.2113	0.2208

6.2.8. Appendix

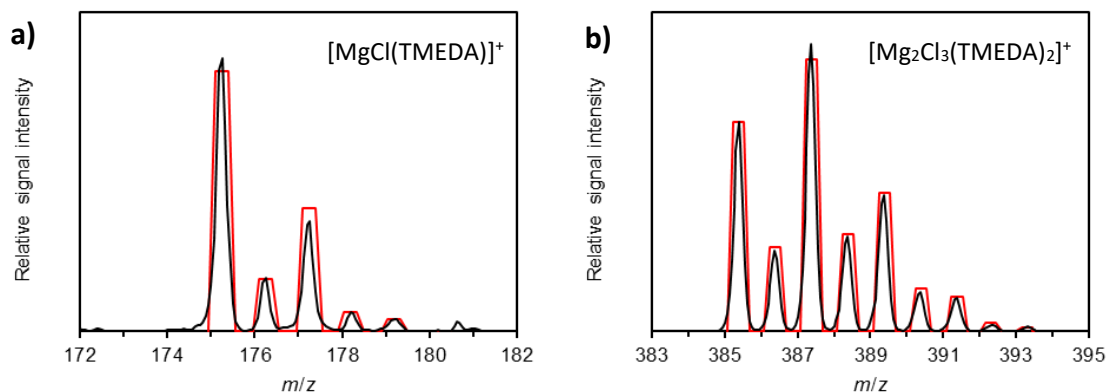


Figure 6.5: a) Comparison of observed (black) and simulated (red) isotope pattern of $[\text{MgCl}(\text{TMEDA})]^+$; b) comparison of observed (black) and simulated (red) isotope pattern of $[\text{Mg}_2\text{Cl}_3(\text{TMEDA})_2]^+$.

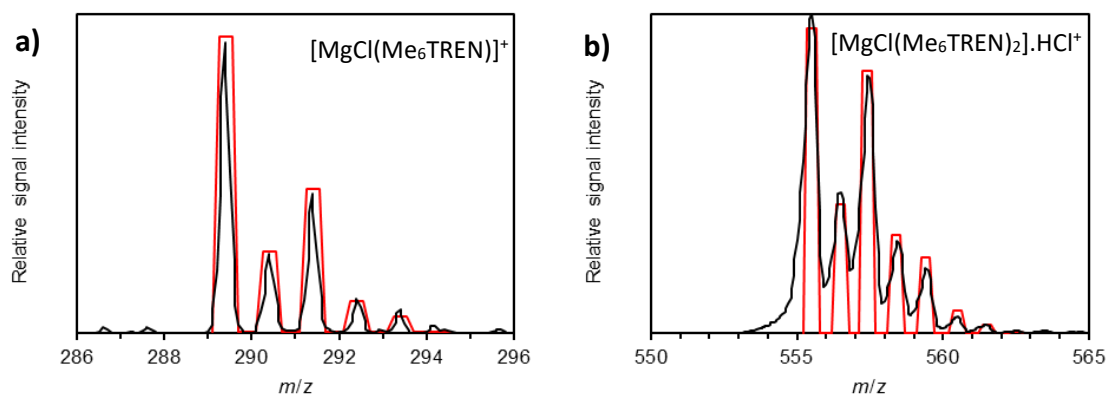
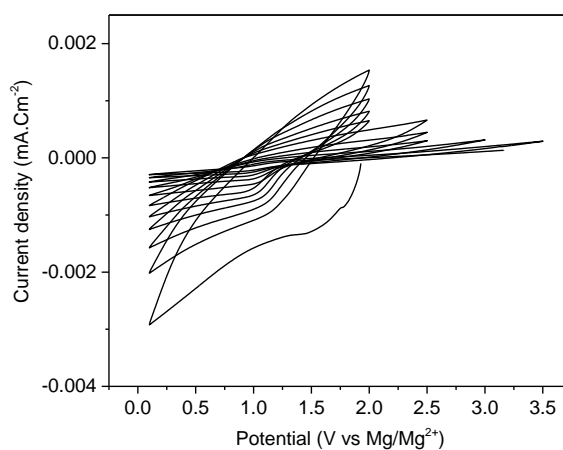


Figure 6.6: a) Comparison of observed (black) and simulated (red) isotope pattern of $[\text{MgCl}(\text{Me}_6\text{TREN})]^+$; b) comparison of observed (black) and simulated (red) isotope pattern of $[\text{MgCl}(\text{Me}_6\text{TREN})_2]\cdot\text{HCl}^+$.



Graph 6.6: a) CV cycles, 0.1 mV/s, of a rechargeable battery with a saturated solution of **19** in THF, a Mg anode and an Mo_6S_8 cathode.

- 1 D. F. Shriver and M. A. Drezdson, *The manipulation of air-sensitive compounds*, Wiley, 1986.
- 2 M. Stender, R. J. Wright, B. E. Eichler, J. Prust, M. M. Olmstead, H. W. Roesky and P. P. Power, *J. Chem. Soc. Dalton Trans.*, 2001, 3465–3469.
- 3 G. J. P. Britovsek, J. England and A. J. P. White, *Inorg. Chem.*, 2005, **44**, 8125–8134.
- 4 K. Koszinowski, *J. Am. Chem. Soc.*, 2010, **132**, 6032–6040.
- 5 A. Putau and K. Koszinowski, *Organometallics*, 2010, **29**, 3593–3601.
- 6 E. Lancry, E. Levi, A. Mitelman, S. Malovany and D. Aurbach, *J. Solid State Chem.*, 2006, **179**, 1879–1882.
- 7 G. M. Sheldrick, *Acta Crystallogr. Sect. A Found. Crystallogr.*, 2008, **64**, 112–122.
- 8 O. V Dolomanov, L. J. Bourhis, R. J. Gildea, J. A. K. Howard and H. Puschmann, *J. Appl. Cryst.*, 2009, **42**, 339–341.